ALFRED-WEGENER-INSTITUT
HELMHOLTZ-ZENTRUM FÜR POLAR- UND MEERESFORSCHUNG

718
2018

Berichte
zur Polar- und Meeresforschung

Reports on Polar and Marine Research

The Expedition PS111 of the Research POLARSTERN to the southern Weddell Sea in 2018

Edited by
Michael Schröder
with contributions of the participants

HELMHOLTZ GEMEINSCHAFT

Die Berichte zur Polar- und Meeresforschung werden vom Alfred-Wegener-Institut, Helmholtz-Zentrum für Polar- und Meeresforschung (AWI) in Bremerhaven, Deutschland, in Fortsetzung der vormaligen Berichte zur Polarforschung herausgegeben. Sie erscheinen in unregelmäßiger Abfolge.

Die Berichte zur Polar- und Meeresforschung enthalten Darstellungen und Ergebnisse der vom AWI selbst oder mit seiner Unterstützung durchgeführten Forschungsarbeiten in den Polargebieten und in den Meeren.

Die Publikationen umfassen Expeditionsberichte der vom AWI betriebenen Schiffe, Flugzeuge und Stationen, Forschungsergebnisse (inkl. Dissertationen) des Instituts und des Archivs für deutsche Polarforschung, sowie Abstracts und Proceedings von nationalen und internationalen Tagungen und Workshops des AWI.

Die Beiträge geben nicht notwendigerweise die Auffassung des AWI wider.

Herausgeber
Dr. Horst Bornemann

Redaktionelle Bearbeitung und Layout
Birgit Reimann

Alfred-Wegener-Institut
Helmholtz-Zentrum für Polar- und Meeresforschung
Am Handelshafen 12
27570 Bremerhaven
Germany

www.awi.de
www.reports.awi.de

The Reports on Polar and Marine Research are issued by the Alfred Wegener Institute, Helmholtz Centre for Polar and Marine Research (AWI) in Bremerhaven, Germany, succeeding the former Reports on Polar Research. They are published at irregular intervals.

The Reports on Polar and Marine Research contain presentations and results of research activities in polar regions and in the seas either carried out by the AWI or with its support.

Publications comprise expedition reports of the ships, aircrafts, and stations operated by the AWI, research results (incl. dissertations) of the Institute and the Archiv für deutsche Polarforschung, as well as abstracts and proceedings of national and international conferences and workshops of the AWI.

The papers contained in the Reports do not necessarily reflect the opinion of the AWI.

Editor
Dr. Horst Bornemann

Editorial editing and layout
Birgit Reimann

Alfred-Wegener-Institut
Helmholtz-Zentrum für Polar- und Meeresforschung
Am Handelshafen 12
27570 Bremerhaven
Germany

www.awi.de
www.reports.awi.de

Titel: Abendstimmung mit Seerauch im Bereich starker Neueisbildung vor dem Filchner-Ronne Schelfeis (Foto: Michael Schröder, Alfred-Wegener-Institut, 24.02.2018, 21:25 Ortszeit bei -18°C Lufttemperatur)

Cover: Afterglow and sea smoke in the leads of new ice formation in the vicinity of the Filchner-Ronne Ice Shelf (Photo: Michael Schröder, Alfred Wegener Institute, 24.02.2018, 21:25 LT at -18°C air temperature)

The Expedition PS111 of the Research Vessel POLARSTERN to the southern Weddell Sea in 2018

Edited by
Michael Schröder
with contributions of the participants

Please cite or link this publication using the identifiers
http://hdl.handle.net/10013/epic.fc15cdcc-d16a-4074-b855-38a963799dde and
https://doi.org/10.2312/BzPM_0718_2018

ISSN 1866-3192

PS111

(ANT-XXXIII/2)

FROST

19 January 2018 - 14 March 2018

Cape Town – Punta Arenas

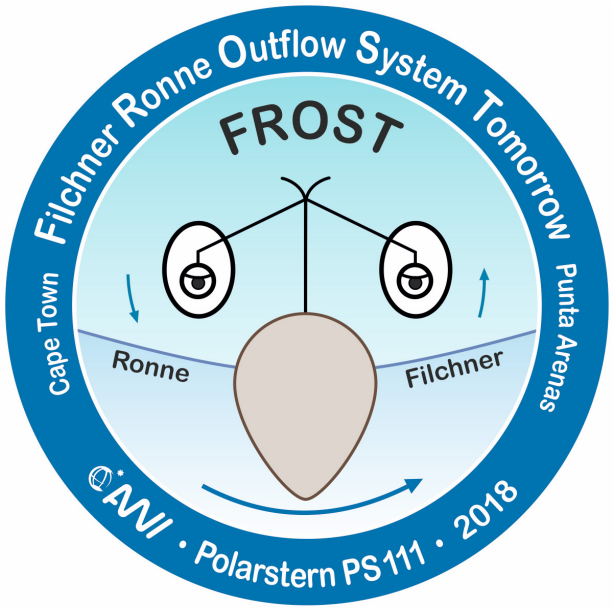

Chief scientist
Michael Schröder

Coordinator
Rainer Knust

Contents

1. ÜBERBLICK UND FAHRTVERLAUF

Michael Schröder AWI

Am 19. Januar 2018 lief *Polarstern* mit 53 Wissenschaftlern und 44 Mann Besatzung zur Expedition PS111 von Kapstadt mit Kurs in Richtung *Neumayer-Station III* aus. Durch das Aufkommen starker Winde am Kap kam es zu einem vorzeitigen Auslaufen, kurz bevor der Hafen geschlossen wurde. Auf dem Weg nach Süden wurde kurzfristig im Gebiet von Maud Rise ein minimales Messprogramm zur Beobachtung der seit September 2017 aufgetretenen Weddell-Polynia eingeschoben. Dieses Phänomen, das seit 1976 erstmalig wieder aufgetreten ist, wurde mit Hilfe von ARGO floats verschiedener Institutionen und einer 'underway' CTD beprobt. Zur Anbindung dieser Messungen an bestehende Datensätze wurden außerdem drei tiefe CTD-Stationen zum Vergleich durchgeführt.

Die Eissituation vor *Neumayer III* erlaubte es, die Entladearbeiten innerhalb von zwei Tagen abzuschließen, so dass es am 30.01. zügig zu einer ersten Station vor Austasen weiterging, die besonders für die Biologen an Bord von Interesse war.

Die erste Station im eigentlichen Einsatzgebiet, dem Filchner-Ronne-Schelf, war dann der erfolgreiche Austausch einer seit vier Jahren dort liegenden Akustikverankerung. Von hier ging es weiter auf 76° S, wo drei weitere Strommesserverankerungen aus dem Jahr 2016 getauscht wurden. Eine erste Auswertung der Daten zeigt, dass alle Messinstrumente erfolgreich gemessen haben und es somit bereits vierjährige Zeitreihen vom Osthang des Filchner-Grabens mit seinen Einschüben von wärmeren Wassermassen gibt. Ein kurzer hydrographischer Schnitt über den östlichen Hang wurde als Ergänzung zu den Verankerungsdaten gefahren und am 06.02. beendet. Zu diesem Zeitpunkt wurde anhand der Eissituation im Filchner-Ronne-Gebiet beschlossen, zunächst das Gebiet vor dem Ronne-Schelfeis zu beproben. Über den nördlichen Weg im Bereich der Filchner-Schwelle, wo wiederum drei Verankerungen für die norwegischen Kollegen ausgebracht wurden, ging es westlich am Eisberg A23A vorbei nach Süden. Zu diesem Zeitpunkt wurden auch die übermittelten, hochauflösenden Terra SAR X Aufnahmen immer wichtiger, um die effektivste Strecke nach Süden durch das dichter werdende Meereis zu nehmen. Am 09.02. hatten wir dann die erste hydrographische Station direkt vor dem Ronne-Schelfeis. Neben den üblichen Geräten wie CTD, Bongo und Multinetz wurde zum ersten Mal das ALR1 AUV der britischen Kollegen eingesetzt, das bis etwa 20 km in die Schelfeiskaverne fuhr und nach 24 Std. am gleichen Ort wieder aufgenommen werden konnte. Danach wurde der Schnitt in westliche Richtung bis in den Ronne-Trog fortgesetzt, wo allerdings dichte Eismassen verhinderten, dieses Becken auch in nördlicher Richtung weiter zu vermessen und zu beproben. Dafür konnten auf dem Rückweg Messungen entlang der westlichen Begrenzung der Festeiszunge vor Berkner Island durchgeführt werden, bei der besonders ein ROV Einsatz direkt an der Schelfeiskante interessant war. Hier wurde eine große Anzahl von Eisplättchen in der Wassersäule und direkt am Schelfeis 'angeklebt' beobachtet, die bis 142 m Tiefe reichte. Dies ging einher mit konstant tiefen Meerwassertemperaturen von -2.1 °C. Die Ursache für die massive Plättcheneisbildung an der Schelfeiskante an dieser Stelle muss noch erforscht werden, deutet jedoch auf einen bevorzugten Ausstrom von Eisschelfwasser hin. Mit dem

EM-Bird, einem elektromagnetischen Eisdickensensor, wurde die Festeisnase auf mehreren Flügen vom Hubschrauber aus vermessen. Nebenher gab es mehrere lange Eisstationen, bei den die Meereisphysiker die Eigenschaften von Schneeauflage und Meereis mit den unterschiedlichsten Messinstrumenten beprobt haben.

Am 14.02. wurde dann das Ronne-Schelfeis wieder in Richtung Norden verlassen. Nach einer Station direkt an der NW-Ecke von A23A wurde nach einem Eiserkundungsflug beschlossen, direkt nach Osten auf etwa 76°S zu versuchen, den Filchner-Graben zu queren. Dies gelang wie bei den anderen hydrographischen Schnitten mit einer engen Stationsdichte (< 15 nm).

An dieser Stelle ist es die erste Realisation einer vollständigen Überquerung des Grabens in einem sonst von dichtem Meereis bedecktem Gebiet. Danach wurde versucht, die Polynia vor dem Filchner-Schelfeis zu beproben, was vier Tage später in Angriff genommen wurde. Während dieser Zeit öffnete sich die Ostseite der Festeisnase vor Berkner, so dass die Entscheidung leicht fiel, auch hier entlang Profile zu fahren. Diese gingen bis auf 8 nm an die, von der Westseite zuvor gemachten Stationen heran, so dass es jetzt einen durchgehenden Schnitt von 61° W bis 35°30’ W entlang des gesamten Filchner-Ronne-Schelfeises gibt. Dies gelang *Polarstern* im Filchner-Gebiet zuletzt 1986 vor Abbruch der großen Eisberge, von denen A23A der letzte verbliebene Rest ist. Am Westhang des Filchner-Grabens wurden dann auch die tiefsten Temperaturen auf dieser Reise im Kern des Eisschelfwassers mit -2,29°C gemessen. Bei Rückkehr nach Osten in die Filchner-Polynia wurde dann eine zweite Messreihe des ALR1 AUV’s geplant, die diesmal sowohl das vorgelagerte Festeis (22 nm) als auch eine Schelfeiskaverne (6,5 nm) zum Ziel hatte. Bei heftiger Neueisbildung wurde das AUV dann planmäßig nach 48 Stunden sicher geborgen. Die sich ändernden Eisbedingungen zwangen uns nun, uns nach Norden in den Bereich der Filchner-Schwelle zu begeben, um dort bei etwa 75°S einen Schnitt zu wiederholen, der bereits bei den *Polarstern* Expeditionen PS82 (2014) und PS96 (2016) durchgeführt wurde. Auch dieser konnte mit geringem Stationsabstand von <10 nm bei 17 Stationen abgeschlossen werden. Allerdings wurde nach Westen hin das Meereis immer dichter, so dass hier bei etwa 37°W abgebrochen wurde. Die Bergung einer zweiten Akustikverankerung weiter nördlich in diesem Bereich musste auch aufgegeben werden, so dass ihre Nachfolgeverankerung in ein Gebiet mit moderateren Eisbedingungen weiter östlich verlegt wurde. Das Aussetzen dieser Verankerung gelang dort problemlos und so konnten wir pünktlich und vereinbarungsgemäß zur Beladung zweier Pistenbullies und diverser anderer Güter einen Anlegepunkt in einem schmalen Inlet an der ansonsten hohen Schelfeiskante vor *Halley Station VI* finden. Sehr gutes Wetter ermöglichte den Abschluss der Arbeiten innerhalb eines Tages und so verließen wir *Halley* am 02.03. abends Richtung Antarktische Halbinsel. Bedingt durch den Ausfall des Versorgers *Ernest Shackleton* wurden wir außerdem gebeten, zusätzlich 16 britische Kollegen bis Punta Arenas mitzunehmen, was durch enges Zusammenrücken und Freimachen von Kabinen und die Hilfsbereitschaft aller Teilnehmer auch problemlos gelang.

PS111 ging nach 9.125 nm, davon 4.294 nm im Forschungsgebiet, insgesamt 148 Stationen mit 261 casts am 14. März in Punta Arenas sehr erfolgreich zu Ende.

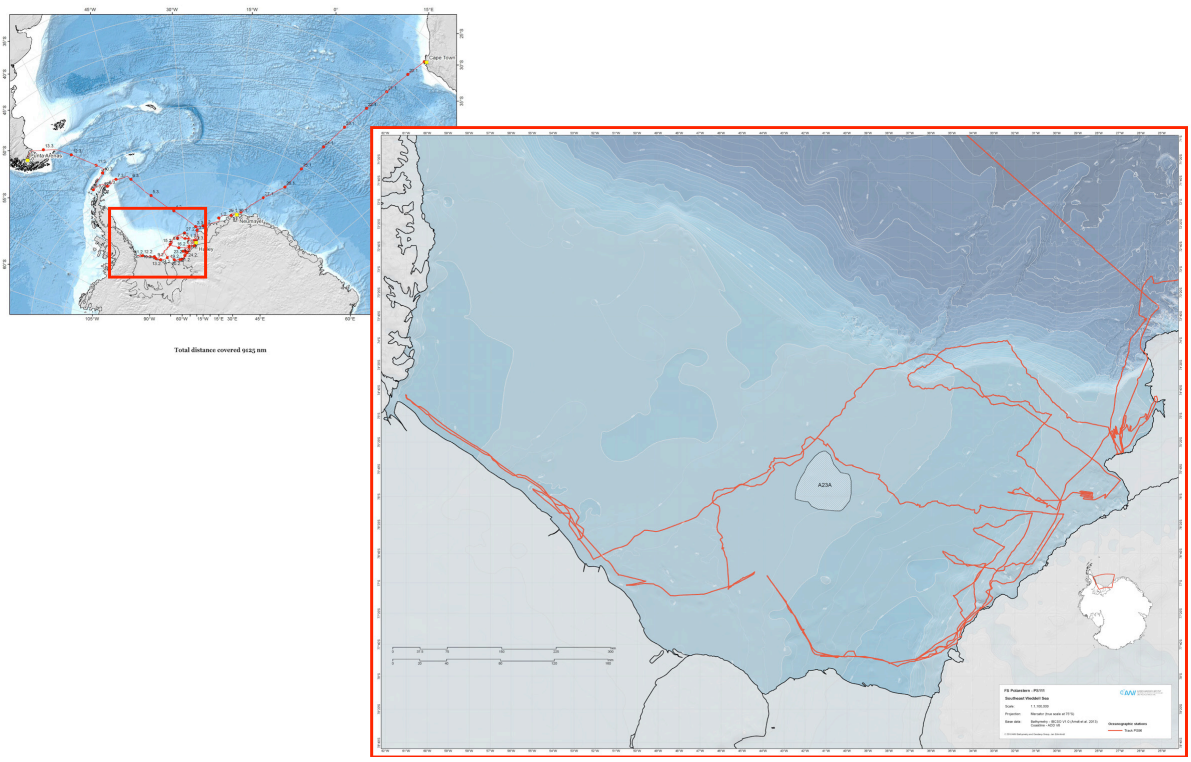

Abb. 1: Fahrtverlauf (oben) und Haupt-Arbeitsgebiet während der Expedition PS111. Siehe https://doi.pangaea.de/10.1594/PANGAEA.890602 für eine Darstellung des master tracks in Verbindung mit der Stationsliste.

Fig. 1.1: Cruise track (above) and main working area during PS111. See https://doi.pangaea.de/10.1594/PANGAEA.890602 to display the master track in conjunction with the list of stations.

SUMMARY AND ITINERARY

On 19th of January 2018 *Polarstern* left Cape Town with 53 scientists and 44 crew in direction to *Neumayer Station III*. Due to increasing winds in the harbour the departure was earlier than planned, just before the harbor had to be closed. On our way southward a short programme was conducted in the region of Maud Rise to investigate the area of the Weddell Sea Polynia, a phenomenon that has occurred again since September 2017 after 40 years. This was done by means of ARGO floats of different institutions and an 'underway' CTD. For comparison with recent datasets three deep CTD casts where done in addition.

The ice situation in front of *Neumayer III* enabled the supply of goods within two day. On January 30, we left in the direction to Austasen where the biologists were interested in a benthic repeat station.

The first station in the area of the main interests, the Filchner-Ronne shelf, was the successful exchange of an acoustic mooring, which was deployed 4 years ago. From here we sailed to 76°S, where 3 current meter moorings were replaced which now provide 4 year long time

series to monitor the inflow of warm waters on the eastern flank of the Filchner Trough. In addition a short hydrographic section on the eastern slope was done to imbed the mooring data in a wider context. It ended on February 6. The ice situation in the Filchner-Ronne area at that time let us decide to begin our measurements along the Ronne Ice Shelf. Along the northern route three Norwegian moorings at the Filchner sill were deployed. From here on the western side of iceberg A23A to the south high resolution Terra SAR X images were used to find the most effective way through the increasing concentration of sea ice. On February 9, we began our hydrographic section along the ice edge. Together with the usual instruments like CTD, Bongo and Multinet the first launch of the British ALR1 AUV was performed, which was guided the first 20 km of the ice shelf cavity. It was safely recovered after 24 hours at the predetermined position. From here we went further to the west into the Ronne Trough where large thick ice floes avoid measurements in the northern part of the trough. On our way back we were able to work on the western edge of the fast ice tongue in front of Berkner Island. Here a ROV station direct in front of the shelf Ice was of great interest which showed ice platelets attached to the vertical ice edge up to a depth of 142 m. The accompanying CTD profile showed constant temperatures of -2.1°C as a straight lone over the whole water column. At the same time helicopter flights with an electromagnetic ice thickness sensor (EM-Bird) were done to investigate the thickness of the fast ice tongue. Besides, a multitude of ice stations were done by the ice physicists, to measure snow and ice properties with a variety of instruments.

On the 14th of February we left the Ronne polynya to the north. During a station at the northwest corner of A23A an ice reconnaissance flight showed a possibility for the ship to make a west-east section along 76°S across the Filchner Trough. This was highly successful with a station spacing of less than 15 nm as on other hydrographic sections. Here, this was the first complete hydrographic traverse of the Filchner depression in an area otherwise packed with heavy sea ice. After 4 days the Filchner polynya was in our focus. At the same time the eastern edge of the Berkner fast ice tongue opened up, so that we took the chance to take profiles up to a distance of 8 nm to our easternmost point of our Ronne section. This results in a continuous hydrographic section from 61°W to 35°30'W in front of the complete Filchner-Ronne Ice Shelf. This was last done by *Polarstern* in 1986, before the break-up of the large icebergs from Filchner. A23A is still the remnant of this event. On the western flank of the Filchner Trough, the lowest temperatures with -2.29°C were reported during that cruise. They coincide with the core of the ice shelf water. On our way back within the polynya a second launch of the ALR1 AUV was done, which led below 22 nm of fast ice as far as 12 km into the cavity of the Filchner Ice Shelf. After 48 hours the AUV was safely recovered in a polynya with heavy new ice formation. The changing ice conditions in the south force us to leave the area to the north to repeat a section along the Filchner sill at 75°S, which was already done by *Polarstern* in PS82 (2014) and PS96 (2016). On 17 stations with a spacing of less than 10 nm this work had to be stopped near 37° W due to heavy sea ice conditions.

Also, the recovery of another acoustic mooring further north was impossible, so that the replacement mooring was placed further east in an area of moderate ice conditions.

The deployment there was successful so that we could reach *Halley Station VI* in time to load two Pistenbullies and other equipment as agreed. Because of the absolutely fine weather we could finish this work in days time and left *Halley* in the evening of 02nd March.

Due to the cancellation of the second call of *Ernest Shackleton* we were asked to take 16 British colleagues to the port of Punta Arenas. This could be achieved without any problems by the making available of cabins and the cooperation of all scientists.

PS111 very successfully ended after 9,125 nm, of this 4,294 nm within the area of scientific interest, 148 stations with 261 casts on 14th of March in Punta Arenas.

2. WEATHER CONDITIONS DURING PS111

Tobias Schaaf[1], Christian Rohleder[1] [1]DWD

On 19th January 2018 *Polarstern* departed from the summery Cape Town with a strong to stormy Southeastern. Due to the Captains' request the departure took place a couple of hours earlier and right on time to prevent closure of the harbor due to strong winds. The expedition PS111 to Antarctica began. The supply of the research station *Neumayer III* and atmospheric, oceanographic, ice and biological science was scheduled over the next 8 weeks. Weather along the transit to *Neumayer III* turned out to be favourable. Instead of storms frequently observed between latitudes 40 to 60 S, the offset of a westerly drift came right on time to set up weak lows and highs to be passed by *Polarstern* with not a handful of days with strong wind events until Atka Bay. Furthermore, *Polarstern* was relatively late in the southern hemispheric summer season and the ice situation in the Atka-Bay was favourable, too. By the late 28th of January *Polarstern* arrived at the southern ice port of Atka Bay. The adjacent supply was carried out under fair and calm weather which was caused by a ridge extending from the Antarctic Plateau to the central Dronning Maud Land. Some expedition participants used the stay for a short visit of the research station.

On the late 30th of January *Polarstern* left Atka-Bay and headed along the ice shelf southwestwards to the Weddell Sea. In the meantime, a subtropical ridge extended to the northern Weddell Sea and induced a high in place over the eastern and northern Weddell Sea portions for a couple of days. In advantage of the high *Polarstern* passed Austasen, Drescher and the Riiser-Larsenisen under relatively calm, but partly cloudy boundary layer conditions. At the beginning of February the high moved to western portions of the Weddell Sea and made room for a South-Atlantic trough to extend southwards to Coats Land. A resulting southerly flow from Filchner Ice Shelf pushed dry air to the ship and caused a couple of sunny days for *Polarstern*. Furthermore, satellite imagery revealed increasingly opening polynyas in front of Ronne and Filchner Ice Shelves. With a medium-range forecast showing no significant signatures for sustained winds from north to northeast near the polynyas the decision was made on 6th February to head along a 400 nm route to the Ronne Ice Shelf and investigate along the polynya. On the transit and in the vicinity of the large iceberg A23A it was conspicuous how cloud basis subsided over regions of dense ice concentrations. Finally clouds grounded on the morning of the 8th of February and caused poor visibility temporarily. With the arrival at the Ronne Ice Shelf on the 9th of February cold winds from the ice shelf caused dense steam fog at the Ronne polynya, which prevented any flight operations. *Polarstern* followed the ice shelf edge until the Ronne Trough, where on the one hand fair weather within a local high developed, on the other hand high ice concentration led to retreat. As *Polarstern* headed back towards Berkner Island cold winds from the ice shelf caused significantly dropping temps on the 12th of February. Measurements revealed -23.7°C at the mast and a windchill of -51°C. On the 14th of February, however, less cold air was pushed to the ship by a low travelling across the Weddell Sea to the Ronne Ice Shelf. Ongoing snowfall and poor visibility occurred, respectively. At the wake of the low cold air advection and upper level subsidence caused improving weather conditions in the course of the 15th of February. *Polarstern* had already left the polynya of the Ronne Ice Shelf and sailed around the iceberg A23A to the Filchner side (Fig. 2.1).

On the 17th of February and approximately at Vahsel-Bay (named after the Captain of barque *Deutschland* 1911/1912) medium range forecast revealed for the next couple of days once again quite persistent southerly winds between quasi-stationary pressure systems, namely a low over Coats Land and a high over the Antarctic Peninsula. The decision was quickly made to head into the Filchner polynya, as it was widely opening up under these wind conditions. Surprisingly the polynya opened up as far as to the sill of the Ronne Ice Shelf and made possible to investigate along the polynya in an area not being accessible for a couple of years, latest 1993, but back then without science. Due to the southerly winds *Polarstern* became again influenced by cold air from the ice shelf, and on the morning of the 21st of February the record low temperatures of PS111 were recorded with -28.2°C air temperature and a windchill of -51°C. Steam fog rose frequently and new ice formed widespread – it left no doubt it was a signal of the ending southern hemispheric season and time to move on and out of the polynya soon. But due to the ongoing southerly winds at the polynya an Autonomous Underwater Vehicle (AUV) was deployed for its 48 hour solo effort beneath the ice shelf. Meanwhile *Polarstern* headed out of the polynya and into the influence of a mesoscale low near the coast of Coats Land, which caused weather to worsen with low clouds. Flight operations were suspended, respectively. Heading back to the polynya and recovering the AUV successfully on the late 23rd of February *Polarstern* sailed 150 nm northward to the eastern Weddell Sea to do an East-West transect with multiple water sampling stations and moorings between 75°S to 74°S latitude. An upper level trough passed eastwards. It caused a decent snowfall event. Accordingly, on the early 25th of February was covered by a few centimeters of fresh powder. The following day dense sea ice led to reorganize the science schedule and head back to less concentrated ice conditions at the Halley polynya. The resulting fair weather conditions at the wake of the aforementioned upper level trough were used for a long flight operation within the framework of sea ice science and exploring ice conditions for routing.

On the 1st of March a strong wind event at the southern flank of a low moving across the Halley polynya northward took place, but was followed by easing winds and fair weather on the 2nd of March right on time to welcome crew members of the *British Antarctic Survey Station Halley VI* for their trip to Punta Arenas/Chile on board of *Polarstern*. Afterwards course was set to the Trinity Peninsula and via the Antarctic Sound, the South-Shetland Islands and Drake Passage to Punta Arenas. The zonal frontal boundary happened to be extended far north leading to a storm track over the northern Drake Passage portions, which caused fair weather and mainly moderate winds around the South-Shetland Islands. By the time of traversing the Drake Passage the frontal boundary became meridional displaced with a strong ridge extending from the Falkland Islands to the Weddell Sea, which then blocked any storm approaching the Drake Passage eastward. Accordingly, lows rather moved southwards from Chile to the Antarctic Peninsula. Conditions turned out to be slightly below average along the traverse with strong to stormy heading winds and 3.5 m significant wave height. In the morning of the 14th of March *Polarstern* safely arrived at Punta Arenas.

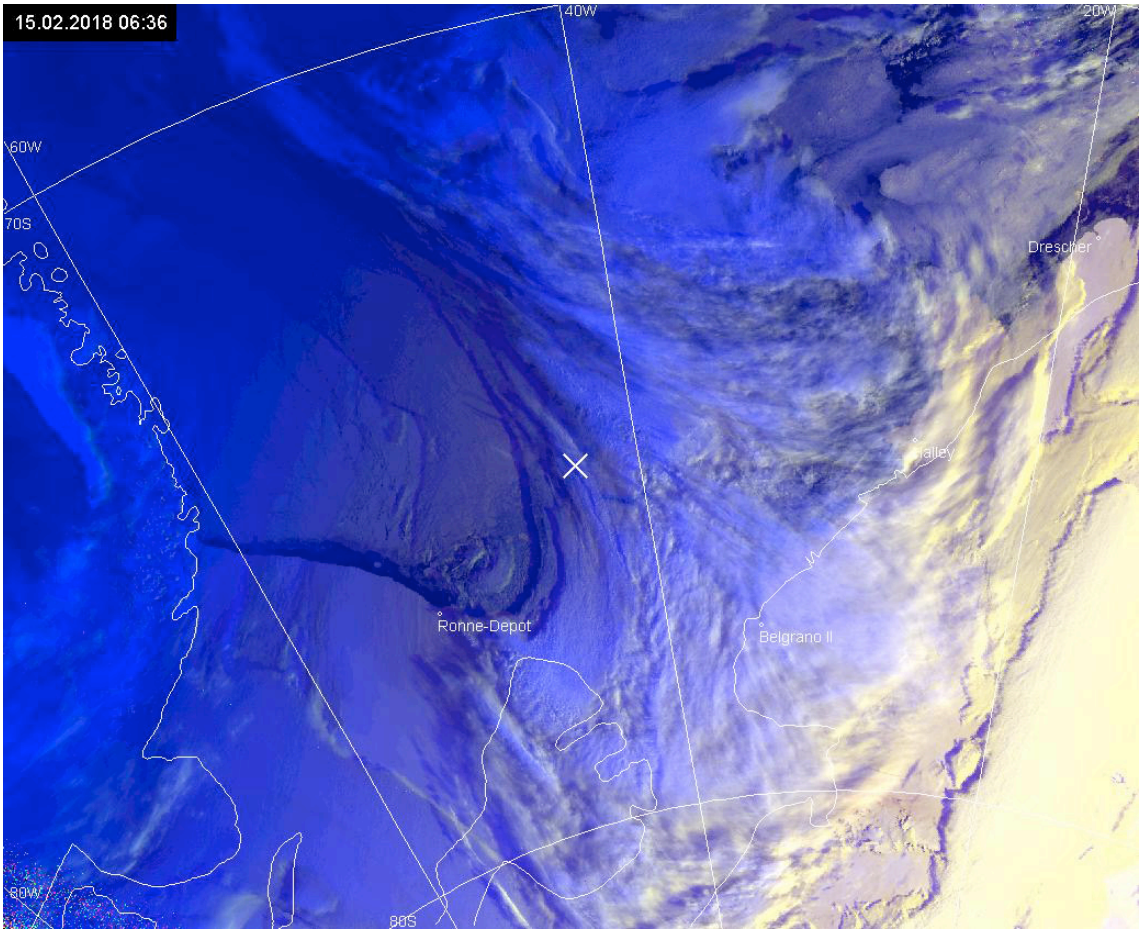

Fig. 2.1: A RGB-Satellite image of NOAA polar orbiting satellite received on the 15th of February 06:36 UTC on board Polarstern. The image shows the southern Weddell Sea and in particular the Ronne Shelf Ice with its polynya and adjacent sea ice. Berkner Island is in the lower center and the white cross marks the position of Polarstern. The center of a low is visible nearby Ronne-Depot and Berkner Island with its front stretching northward to Polarstern.

3. OCEANOGRAPHIC CONDITIONS AND DISTRIBUTION OF OXYGEN ISOTOPES AND OCEANIC TRACE GASES OFF FILCHNER-RONNE ICE SHELF, SOUTHERN WEDDELL SEA

Hartmut H. Hellmer[1], Markus Janout[1], Andreas Wisotzki[1], Svein Østerhus[3], Clara Stolle[1], Johanna Geilen[1], Yannick Kern[3,1], Jürgen Sültenfuß[2], Pia Sültenfuß[2], Fanny Wischnewski[2], Michael Schröder[1]

[1]AWI
[2]Uni Bremen
[3]Uni Bergen

Grant-No. AWI_PS111_00

Background

Long-term observations of the flow of dense waters from the area of formation to the World Ocean abyss, and the return flow of warm waters, are central to climate research. For the Weddell Sea, an important component of this system entails monitoring the formation of High Salinity Shelf Water (HSSW) on the continental shelf north of Ronne Ice Shelf, the transformation to Ice Shelf Water (ISW) beneath the floating Filchner-Ronne Ice Shelf, and the transport of ISW overflowing the shelf break and descending to the deep Weddell Sea. Equally important is the return flow of warm water towards the Filchner-Ronne Ice Shelf (FRIS).

The Filchner Trough in the southeastern Weddell Sea is the main conduit for northward flowing Ice Shelf Water, defined by temperatures below the surface freezing point. ISW originates from HSSW and carries the basal melt water of the FRIS. The ISW pathway within the trough varies on seasonal scales with flow out of the Filchner Ice Shelf cavity occurring on the western slope only during late summer/early fall. On its way to the continental shelf break, ISW encounters a seasonal inflow of Modified Warm Deep Water (MWDW), flowing along the eastern slope of the trough towards the ice shelf front (Ryan et al., 2017). ISW dominates at the trough's sill where mixing with open ocean waters forms the deep and bottom waters of the Weddell Sea, the former being the precursor of Antarctic Bottom Water and thus one of the main contributors to the lower branch of the global thermohaline circulation (Foldvik et al., 2004). Projections based on the output of our coupled sea ice–ocean-ice shelf models indicate that in the near future the density of HSSW and, thus, of ISW at the Filchner Trough sill might decrease such that unmodified Warm Deep Water (WDW) can enter the trough and penetrate into the deep FRIS cavity (Hellmer et al., 2012). The presence of WDW underneath FRIS is bound to cause a dramatic increase in basal melting. The latter changes the ice shelf thickness, reduces the buttressing effect of bottom topography and ultimately influences the dynamics of the ice streams draining the West and East Antarctic Ice Sheets. The resulting freshwater input will have a profound impact on the structure of the shelf water column, the sea ice cover, the formation of deep and bottom waters, and the melting at the base of ice shelves located downstream (Timmermann & Hellmer, 2013).

The actual amount of ice shelf basal melting, its variability and possible future trend yet have to be determined. To assess basal melt rates by measurements and to determine the impact on (a) composition and formation rate of Weddell Sea Deep and Bottom Water and (b) the global ocean circulation, more tracer observations are needed. A useful tool to identify and quantify melt water is the oceanic measurement of the low-solubility and stable noble gases helium

and neon (Schlosser 1986). Atmospheric air with a constant composition of these noble gases is trapped in the ice matrix during its formation. Due to the enhanced hydrostatic pressure at the base of the shelf ice, these gases are completely dissolved in the water, when the ice melts from below. This leads to an excess of ^{4}He = 1060 % and Ne = 770 % in pure glacial melt water (Hohmann et al., 2002). Frontal and surface glacial as well as sea ice melt water equilibrate quickly and do not lead to any noble gas excess. With an accuracy of 0.5 % for He measurements performed at the IUP Bremen, basal melt water fractions of 0.05 % are detectable.

Anthropogenic transient trace gases (chlorofluorocarbons, CFCs) allow for estimating the time scales of the transport and the renewal and ventilation of inner oceanic water masses. As CFCs enter the ocean by gas exchange with the atmosphere, their evolution is determined on first order by the temporal increase in the atmosphere and subsequently by entrainment and advection in the ocean interior. Combining CFC based time scales with noble gas and multi-parameter analysis allows to assess basal melt rates and the glacial melt water induced water mass transformation rates (Huhn et al., 2008).

This expedition supports the operation of a long-term observatory, named S2, at the Filchner Trough sill as part of a cooperation between AWI and Uni Research, Bergen. Established in 1977, the S2 observatory is one of the longest existing oceanographic time series from Antarctica, situated at a key site for monitoring the ISW overflow. In addition, PS111 is closely connected to the ongoing monitoring of hydrographic properties underneath the Filchner Ice Shelf in the framework of the Filchner Ice Shelf Project (FISP). The fieldwork is designed to extend existing data sets, necessary for (a) the build-up of a reference data set to identify changes on the southern Weddell Sea continental shelf and within the ice shelf/sheet system, expected to occur due to climate change, and (b) the initialization and validation of our coupled ice shelf - ice sheet models.

General objectives

- Determine the temporal variability of the hydrography and tracer distribution on the southern Weddell Sea continental shelf, in particular the Filchner Trough, with regard to shelf water characteristics, basal melt water pathways, and Modified Warm Deep Water inflow.
- Monitor the Ice Shelf Water flow toward the deep Weddell Sea and its contribution to Weddell Sea Bottom Water formation.
- To produce an improved estimate of glacial melt water inventories and basal melting rates for the Filchner-Ronne Ice Shelf to be able to address temporal trends.
- Specify the physical properties controlling the flow across the Filchner Trough sill.
- Provide a comprehensive data set for numerical model initialisation and validation of coupled ocean-ice shelf-ice sheet models.

Specific objectives

- Determine the course of the coastal current in the south-eastern Weddell Sea and the characteristics and temporal variability of MWDW flowing towards the Filchner Ice Shelf front.
- Re-visit the Ronne Ice Shelf front for a new snapshot of the characteristics of MWDW (Hugh Trough) and HSSW (Ronne Trough), the spatial distribution, and spreading paths on the southern continental shelf.

- Determine basal melt water inventories and subglacial meltwater drainage using the stable noble gas isotopes [3He, 4He, Ne].
- Identify transit time scales and formation rates of Weddell Sea Bottom Water using transient trace gases [CFCs and SF6].

Work at sea - Physical Oceanography

On our way to *Neumayer Station III*, north of 60°S, we deployed 4 ARVOR floats for the BSH, Hamburg, Germany, as contribution to the Argo Float Programme (by writing all four still provide reliable records). Starting at 60°S (Fig. 3.1), we collected 23 CTD profiles (40 km spacing) using an under-way CTD (UCTD) to detect possible remnants of deep ocean convection in the water column, caused by the appearance of a large Weddell Polynya during the previous winter. The UCTD system is operated from the back of the ship at regular cruising speed and consists of a free falling CTD probe that is connected to a winch through a thin spectra line and recovered after each cast. The UCTD sensors manufactured by Seabird measure temperature, pressure, and conductivity at 16 Hz with accuracies of 0.004°C and 0.002-0.005 S m^{-1} for temperature and conductivity, respectively. In addition, we conducted 3 full-depth CTD stations, where we also deployed APEX floats – and the fourth between the last two stations - for the University of Washington, Seattle, USA.

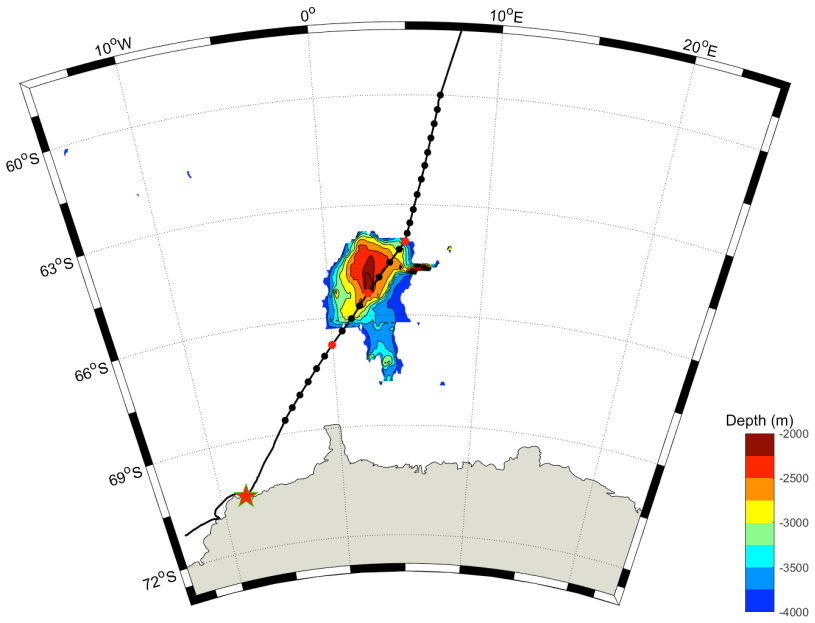

Fig. 3.1: Station map of UCTD-launches (black dots) and three CTD casts (red dots) on our way from Cape Town to Neumayer Station III (red star) focused on the region of Maud Rise. Depth is contoured between 2,000 m and 4,000 m.

In total 129 ship-borne CTD profiles were taken during PS111 (Fig. 3.2 - details of all stations are provided in Table 3.1) using a Seabird 911+ CTD (SN 937) attached to a carousel (SBE32, SN 718) with 24 Niskin bottles of 12 liter capacity. The system included (a) two sensor pairs for conductivity (SBE4, SN 3590, SN 3570) and temperature (SBE 3, SN 5112, SN 5115), (b) one high precision pressure sensor Digiquartz 410K-134 (SN 937), (c) one oxygen sensor (SBE43, SN 1834), (d) one transmissometer (Wetlab C-Star, SN 1198), (e) one fluorimeter (Wetlab FLRTD, SN 1853), and (f) one altimeter (Benthos PSA-916, SN 47768). Additionally,

an upward and downward looking ADCP (LADCP Workhorse Monitor WHM 300 SN 23292, SN 23293) was fixed to the carousel.

Tab. 3.1: Detailed CTD-station list of PS111

Station	Cast	Date	Time	Latitude	Longitude	Water-depth [m]	Pressure max [dbar]
PS111_09	2	2018-01-26	07:26:00	64°00.024’ S	05°00.108’ E	3849	608
PS111_09	3	2018-01-26	09:46:52	63°59.988’ S	04°59.994’ E	3849	3874
PS111_10	2	2018-01-26	21:22:44	65°23.118’ S	02°34.026’ E	2092	2144
PS111_12	2	2018-01-27	09:00:04	66°44.328’ S	00°02.322’ W	4698	4753
PS111_14	1	2018-01-31	08:25:23	70°56.418’ S	10°32.448’ W	280	101
PS111_14	5	2018-01-31	13:01:12	70°56.640’ S	10°31.596’ W	280	264
PS111_16	1	2018-02-01	22:07:36	72°23.046’ S	17°49.026’ W	1419	1395
PS111_17	1	2018-02-03	00:18:35	73°42.000’ S	25°43.986’ W	3244	507
PS111_17	2	2018-02-03	01:44:02	73°41.970’ S	25°43.884’ W	3241	103
PS111_17	4	2018-02-03	04:00:56	73°42.018’ S	25°43.428’ W	3219	3228
PS111_18	1	2018-02-04	10:47:31	76°09.474’ S	30°00.846’ W	410	394
PS111_19	3	2018-02-05	09:41:54	76°05.250’ S	30°27.300’ W	461	445
PS111_20	3	2018-02-05	07:05:07	76°02.712’ S	30°59.862’ W	472	454
PS111_21	3	2018-02-04	19:35:10	75°57.588’ S	31°28.212’ W	595	576
PS111_22	1	2018-02-04	21:30:43	75°54.090’ S	31°45.510’ W	723	701
PS111_23	1	2018-02-04	23:37:30	75°57.174’ S	32°02.628’ W	747	725
PS111_24	1	2018-02-05	02:42:51	75°56.892’ S	32°19.650’ W	770	745
PS111_25	1	2018-02-05	05:43:10	75°59.928’ S	31°13.998’ W	477	476
PS111_26	1	2018-02-05	08:30:41	76°04.158’ S	30°44.766’ W	462	445
PS111_27	3	2018-02-05	18:44:24	75°57.288’ S	29°04.926’ W	426	410
PS111_28	1	2018-02-05	20:32:22	75°58.506’ S	28°24.996’ W	356	344
PS111_29	1	2018-02-06	06:22:46	75°58.380’ S	27°40.872’ W	402	395
PS111_31	1	2018-02-06	21:29:23	75°48.324’ S	26°58.200’ W	318	306
PS111_32	1	2018-02-07	09:05:34	74°51.618’ S	31°48.906’ W	637	615
PS111_33	1	2018-02-07	11:49:42	74°50.604’ S	32°31.104’ W	595	574
PS111_34	1	2018-02-07	14:36:15	74°51.510’ S	33°00.954’ W	592	572
PS111_35	2	2018-02-09	09:33:20	76°43.902’ S	52°03.438’ W	295	290
PS111_36	1	2018-02-09	12:54:50	76°30.360’ S	52°48.888’ W	404	389
PS111_37	2	2018-02-09	15:15:03	76°28.980’ S	52°38.226’ W	382	380
PS111_38	1	2018-02-10	02:34:46	76°11.868’ S	53°40.728’ W	459	442
PS111_39	1	2018-02-10	05:31:32	75°58.938’ S	54°40.056’ W	505	485
PS111_40	3	2018-02-10	09:22:02	76°00.060’ S	54°14.400’ W	513	102
PS111_42	3	2018-02-10	20:37:05	76°08.682’ S	53°21.396’ W	493	477
PS111_43	1	2018-02-11	02:27:52	75°46.038’ S	55°40.290’ W	474	457
PS111_44	1	2018-02-11	04:57:01	75°36.030’ S	56°34.734’ W	363	347
PS111_45	1	2018-02-11	06:29:30	75°31.074’ S	56°56.016’ W	445	428
PS111_46	1	2018-02-11	10:00:14	75°15.966’ S	58°35.322’ W	627	606
PS111_47	1	2018-02-11	13:17:52	74°59.010’ S	60°00.096’ W	661	640

Station	Cast	Date	Time	Latitude	Longitude	Water-depth [m]	Pressure max [dbar]
PS111_48	1	2018-02-11	17:25:27	74°48.030’ S	60°47.940’ W	648	624
PS111_49	1	2018-02-11	20:57:02	74°43.914’ S	61°01.554’ W	633	614
PS111_50	1	2018-02-12	06:43:20	74°53.010’ S	60°19.704’ W	660	639
PS111_51	1	2018-02-12	10:39:14	75°08.910’ S	59°04.728’ W	628	607
PS111_52	1	2018-02-12	14:16:13	75°22.734’ S	57°44.616’ W	555	536
PS111_53	1	2018-02-12	23:26:33	76°01.554’ S	54°07.236’ W	497	479
PS111_55	1	2018-02-13	08:42:34	76°54.486’ S	50°53.916’ W	289	280
PS111_56	1	2018-02-13	10:59:25	76°58.728’ S	49°35.124’ W	230	220
PS111_57	3	2018-02-13	17:29:19	77°01.452’ S	50°30.324’ W	288	274
PS111_58	1	2018-02-13	21:41:13	77°08.448’ S	48°24.108’ W	251	240
PS111_59	1	2018-02-14	00:37:14	77°07.488’ S	46°52.218’ W	268	254
PS111_60	1	2018-02-14	04:30:05	77°01.200’ S	45°23.820’ W	322	316
PS111_61	1	2018-02-14	07:43:46	76°52.584’ S	44°23.820’ W	357	343
PS111_62	1	2018-02-14	14:03:52	77°04.110’ S	45°39.000’ W	312	299
PS111_63	1	2018-02-15	13:16:48	75°20.568’ S	41°06.396’ W	369	355
PS111_64	2	2018-02-16	01:23:24	75°37.200’ S	39°43.698’ W	370	369
PS111_65	1	2018-02-16	05:21:21	75°43.872’ S	38°34.722’ W	394	393
PS111_66	1	2018-02-16	09:53:07	75°58.632’ S	37°45.768’ W	516	498
PS111_67	1	2018-02-16	13:21:17	76°05.586’ S	36°38.046’ W	680	659
PS111_68	1	2018-02-16	16:26:18	76°03.312’ S	35°42.756’ W	747	723
PS111_69	1	2018-02-16	20:52:13	76°06.300’ S	34°39.264’ W	766	743
PS111_70	1	2018-02-17	00:55:13	76°07.422’ S	33°39.954’ W	790	766
PS111_71	1	2018-02-17	04:54:26	76°08.946’ S	32°40.110’ W	797	772
PS111_72	1	2018-02-17	08:58:41	76°10.290’ S	31°39.786’ W	540	524
PS111_73	1	2018-02-17	11:24:15	76°11.700’ S	30°40.440’ W	447	431
PS111_74	1	2018-02-17	13:29:07	76°12.816’ S	29°40.554’ W	387	370
PS111_75	1	2018-02-17	20:47:47	76°46.980’ S	31°09.696’ W	460	446
PS111_76	1	2018-02-17	23:00:54	76°46.572’ S	32°05.976’ W	248	237
PS111_77	1	2018-02-18	01:23:56	76°50.088’ S	33°02.226’ W	439	425
PS111_78	1	2018-02-18	03:26:19	76°47.994’ S	33°57.126’ W	740	721
PS111_79	1	2018-02-18	05:43:22	76°46.698’ S	34°53.526’ W	971	945
PS111_80	1	2018-02-18	08:11:43	76°38.706’ S	35°25.848’ W	932	908
PS111_81	1	2018-02-18	13:27:53	76°47.550’ S	34°19.476’ W	879	856
PS111_82	1	2018-02-18	15:46:16	76°46.920’ S	33°23.046’ W	556	539
PS111_83	1	2018-02-18	20:06:26	77°08.460’ S	34°55.722’ W	680	692
PS111_84	1	2018-02-18	23:15:15	77°12.774’ S	34°43.902’ W	550	531
PS111_85	1	2018-02-19	00:42:57	77°18.498’ S	34°31.152’ W	453	435
PS111_86	1	2018-02-19	02:26:10	77°25.026’ S	34°19.896’ W	167	155
PS111_87	1	2018-02-19	07:23:12	77°44.976’ S	35°30.636’ W	377	374
PS111_88	1	2018-02-19	08:38:05	77°47.700’ S	36°00.822’ W	574	551
PS111_89	1	2018-02-19	10:41:58	77°49.248’ S	36°25.326’ W	808	783
PS111_90	1	2018-02-19	12:18:29	77°50.688’ S	36°46.746’ W	1120	1109

Station	Cast	Date	Time	Latitude	Longitude	Water-depth [m]	Pressure max [dbar]
PS111_91	1	2018-02-19	13:57:43	77°51.852’ S	37°12.720’ W	1121	1093
PS111_92	3	2018-02-19	17:12:07	77°53.880’ S	37°35.190’ W	1155	1125
PS111_93	1	2018-02-19	19:29:59	77°49.656’ S	38°20.208’ W	1198	1166
PS111_94	1	2018-02-19	21:45:46	77°47.664’ S	39°09.714’ W	1123	1092
PS111_95	1	2018-02-20	00:04:09	77°47.694’ S	40°00.384’ W	966	939
PS111_96	1	2018-02-20	02:03:06	77°47.436’ S	40°50.706’ W	888	860
PS111_97	1	2018-02-20	03:33:58	77°47.514’ S	41°15.264’ W	842	816
PS111_98	1	2018-02-20	07:20:39	77°47.370’ S	40°27.690’ W	926	899
PS111_99	1	2018-02-20	13:22:47	77°30.576’ S	42°02.970’ W	604	583
PS111_100	1	2018-02-20	16:50:22	77°12.258’ S	42°54.084’ W	473	454
PS111_101	1	2018-02-20	19:43:22	76°55.254’ S	43°48.384’ W	397	383
PS111_102	1	2018-02-20	21:44:25	77°04.206’ S	43°20.496’ W	428	429
PS111_103	1	2018-02-21	00:52:48	77°21.642’ S	42°29.070’ W	557	537
PS111_104	1	2018-02-21	03:54:35	77°41.076’ S	41°41.922’ W	726	701
PS111_105	1	2018-02-21	08:16:42	77°47.388’ S	39°34.848’ W	1062	1033
PS111_106	1	2018-02-21	10:31:15	77°48.846’ S	38°45.498’ W	1182	1151
PS111_107	1	2018-02-21	12:44:27	77°52.074’ S	37°59.016’ W	1198	1167
PS111_109	1	2018-02-22	01:14:37	77°42.642’ S	35°14.130’ W	461	443
PS111_110	1	2018-02-22	06:55:56	77°06.792’ S	33°56.220’ W	391	391
PS111_111	1	2018-02-22	08:44:09	77°00.564’ S	33°56.970’ W	453	436
PS111_112	1	2018-02-22	14:02:02	76°35.280’ S	32°30.036’ W	478	460
PS111_113	1	2018-02-22	15:36:33	76°31.098’ S	33°02.598’ W	716	693
PS111_114	1	2018-02-22	18:12:48	76°23.244’ S	33°58.356’ W	839	817
PS111_115	1	2018-02-22	23:37:27	76°17.034’ S	32°18.600’ W	700	701
PS111_116	1	2018-02-23	03:33:00	76°11.910’ S	31°09.990’ W	474	454
PS111_117	2	2018-02-23	17:02:05	77°34.968’ S	34°32.976’ W	161	153
PS111_119	1	2018-02-24	22:10:11	75°46.878’ S	30°44.844’ W	464	447
PS111_120	1	2018-02-25	00:29:14	75°38.358’ S	31°14.292’ W	626	608
PS111_121	1	2018-02-25	03:01:10	75°29.940’ S	31°54.024’ W	757	733
PS111_122	1	2018-02-25	09:22:08	74°59.250’ S	30°15.606’ W	421	418
PS111_123	1	2018-02-25	13:32:40	74°56.688’ S	30°59.160’ W	566	550
PS111_124	1	2018-02-25	16:13:33	74°48.348’ S	31°31.386’ W	604	585
PS111_125	1	2018-02-25	18:50:13	74°47.862’ S	32°15.690’ W	616	595
PS111_126	1	2018-02-25	21:05:30	74°44.286’ S	32°45.936’ W	595	577
PS111_127	1	2018-02-26	01:58:47	74°45.534’ S	33°31.956’ W	591	570
PS111_128	1	2018-02-26	04:08:48	74°38.676’ S	34°20.004’ W	553	535
PS111_129	1	2018-02-26	06:21:34	74°39.918’ S	35°04.170’ W	506	488
PS111_130	1	2018-02-26	09:53:32	74°38.886’ S	35°52.584’ W	439	423
PS111_131	1	2018-02-26	12:43:40	74°37.044’ S	36°55.374’ W	387	373
PS111_132	1	2018-02-27	12:03:56	74°00.528’ S	32°25.410’ W	1800	1773
PS111_133	1	2018-02-28	03:59:05	75°01.242’ S	29°27.636’ W	408	390
PS111_134	1	2018-02-28	05:47:25	75°04.854’ S	28°53.100’ W	405	388

Station	Cast	Date	Time	Latitude	Longitude	Water-depth [m]	Pressure max [dbar]
PS111_135	1	2018-02-28	07:32:50	75°06.456' S	28°16.806' W	466	468
PS111_136	1	2018-02-28	09:30:08	75°08.730' S	27°32.706' W	388	397
PS111_137	2	2018-02-28	18:25:49	75°28.152' S	27°06.780' W	260	247
PS111_138	1	2018-02-28	22:29:12	75°07.770' S	26°02.664' W	400	385
PS111_140	1	2018-03-01	11:26:49	75°07.962' S	26°37.938' W	341	325
PS111_141	2	2018-03-01	17:39:10	75°27.822' S	26°55.134' W	235	222
PS111_147	1	2018-03-06	18:42:32	63°35.226' S	48°44.658' W	3342	3335

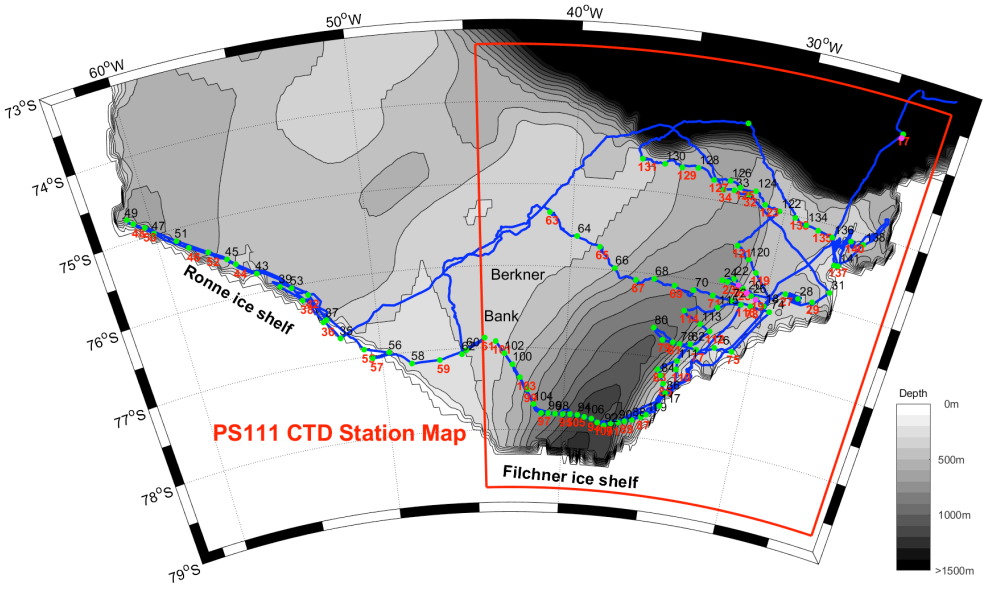

Fig. 3.2: Station map of all CTD casts (green dots) south of 73°S. Change between black and red colored station numbers introduced for better visibility. The blue line represents the cruise track. The red line surrounds the Filchner Trough area, enlarged in Fig. 3.5.

Calibration of the conductivity and temperature sensors was performed prior to the cruise at Seabird Electronics. The accuracy of the temperature sensors amounts to 2 mK. The readings for the pressure sensor are better than 1dbar. Conductivity was corrected using salinity measurements from water samples. IAPSO Standard Seawater from the P-series P160 (K15 = 0.99983, practical salinity 34.993) was used. A total of 71 water samples were measured using an Optimare Precision Salinometer (OPS SN 006). Based on the water sample correction, salinity was measured to an accuracy of 0.002 (Fig. 3.3). The salinity still has to be corrected at home after recalibration of the sensors at the manufacturer.

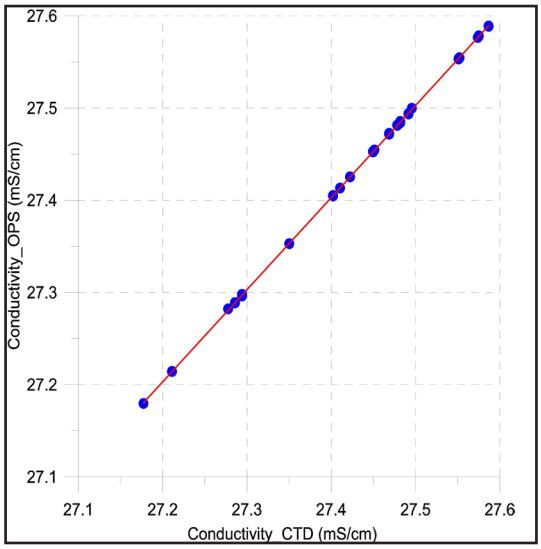

Fig. 3.3: Conductivity in mS/cm of water samples measured with OPS compared to the CTD primary conductivity sensor in mS/cm

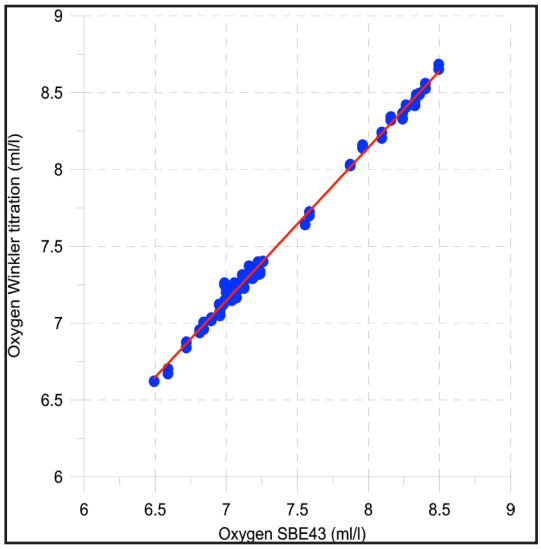

Fig. 3.4: Oxygen in ml/l of water samples measured by the Winkler method compared to the CTD oxygen sensor (SBE43) values in ml/l

At 120 stations, a total of 720 samples from the Niskin bottles were filled in 30 ml vials for post-cruise $\delta^{18}O$-analysis at the University of Hokkaido, Sapporo, Japan and in 120 ml flasks for oxygen correction with the Winkler method using a Dissolved Oxygen Analyzer (DOA, SIS-Kiel type). A total of 130 water samples were measured revealing that the sensor measured dissolved oxygen to an accuracy of 0.02 ml/l (Fig. 3.4).

To supply the ship with surface temperature and salinity values, the ship's SBE 21/ SBE 38 thermosalinograph was used at 11-m depth in the keel. The instrument was controlled by taking water samples which were measured on board with the same salinometer type as for the CTD.

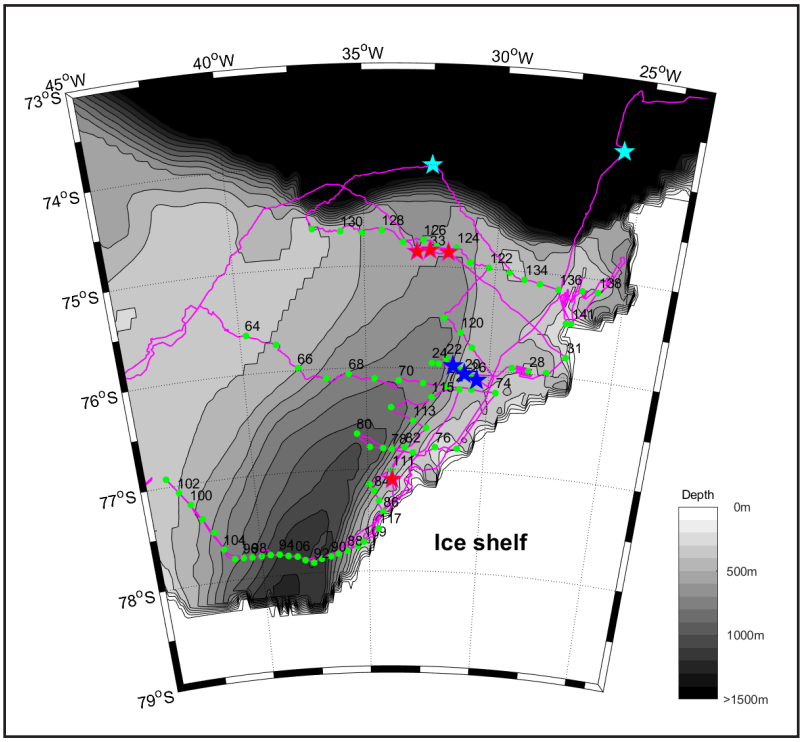

Fig. 3.5: Station map of all CTD casts (green dots labeled with station number) in the Filchner Trough region bounded to the west by Berkner Bank. The cruise track corresponds to the purple line. Stars mark the mooring positions of AWI (blue) and Uni Research, Bergen (red). The most southern stations follow the fast ice/ice shelf edge not included in the used land mask.

In total 8 moorings have been deployed and 4 recovered (Table 3.2). The two deep ocean moorings (light blue stars in Fig. 3.5) serve as sound sources for the navigation of ARGO floats in the southern Weddell Sea (RAFOS), additionally equipped with a receiver for whale sounds and one MicroCat (SBE37). At position 73.72 °S, 25.77 °W we were able to redeploy the mooring. Due to heavy sea ice conditions at the second deep site, the new deployment had to be shifted to the east to 74°S, 32.37 °W. The three AWI moorings along 76 °S on the eastern flank of the Filchner Trough (dark blue stars in Fig. 3.5) have been replaced the third time with the first launch in 2014 (PS82) and replaced during PS96 in 2016. Each mooring consists of (from the bottom up) an anchor stone (500 kg), two releasers, acoustic current meter (Nortek), MicroCat (SBE37), four temperature data loggers (SBE56), MicroCat (SBE37), current meter (Nortek), and floatation (Fig. 3.6).

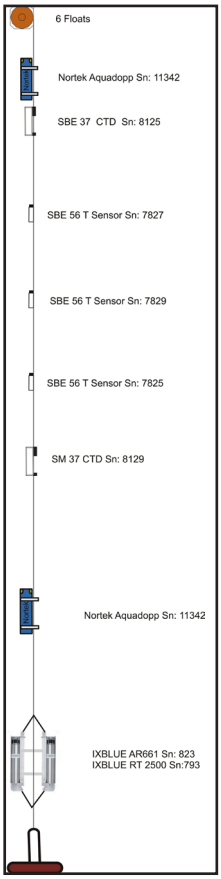

Fig. 3.6: Detailed schematic of mooring AWI252-3 deployed on the eastern slope of the Filchner Trough at 76°S in 470-m deep waters (Fig. 3.5)

As part of the cooperation with Uni Research, Bergen (S. Østerhus), three moorings were deployed at roughly 75°S, slightly south of the Filchner Trough sill. Together with a mooring deployed in February 2017, the S2 observatory now consists of four sub-surface instrumented moorings, carrying sensors for current velocity, temperature, salinity, and dissolved oxygen to monitor the exchange of water masses between the Filchner Trough and the deep ocean (red stars in Fig. 3.5). In addition, two LoTUS buoys were deployed at the Ronne Ice Shelf edge and the eastern flank of the Filchner Trough. Both are sampling ambient water temperature at hourly intervals. A timer is set to release the buoy from the anchor weight on 2 February 2023. As they surface, they will transmit the data using Iridium Short Burst Data (SBD). The LoTUS system, developed at KTH, Stockholm, Sweden, is an expendable, bottom-landing sensor tailored for long-time sampling of bottom temperature. The buoy is rugged, small, and light with a 250-mm diameter pressure hull of polystyrene rated for 2,000-m depth. The buoy weight is about 3 kg excluding, connected to an anchor weight by means of a 1.5-m long rope.

Tab. 3.2: List of deployed and recovered moorings during PS111

Mooring	Station	Date Time	Latitude	Longitude	Depth [m]	Comment
AWI 255-1	PS111_17-6	2018-02-03 11:37:11	73°43.112‘ S	025°49.565‘ W	3232.5	recovered
AWI 255-2	PS111_17-7	2018-02-03 16:42:24	73°43.224‘ S	025°46.498‘ W	3212.1	deployed
AWI 252-2	PS111_19-2	2018-02-04 13:19:40	76°05.484‘ S	030°27.677‘ W	465.1	recovered
AWI 253-2	PS111_20-2	2018-02-04 15:28:33	76°02.664‘ S	030°59.077‘ W	468.4	recovered
AWI 254-2	PS111_21-1	2018-02-04 17:20:22	75°57.397‘ S	031°27.913‘ W	594.6	recovered
AWI 254-3	PS111_21-2	2018-02-04 18:55:43	75°57.680‘ S	031°28.846‘ W	596.4	deployed
AWI 252-3	PS111_19-6	2018-02-05 11:34:29	76°05.463‘ S	030°28.198‘ W	467.1	deployed
AWI 253-3	PS111_20-4	2018-02-05 13:10:06	76°02.789‘ S	031°00.624‘ W	473.3	deployed
S2-2018-E	PS111_32-2	2018-02-07 10:06:24	74°51.331‘ S	031°49.980‘ W	636.6	deployed
S2-2018-C	PS111_33-2	2018-02-07 12:54:50	74°50.169‘ S	032°30.721‘ W	598.7	deployed
S2-2018-W	PS111_34-2	2018-02-07 15:29:59	74°51.190‘ S	033°00.020‘ W	595.8	deployed

Mooring	Station	Date Time	Latitude	Longitude	Depth [m]	Comment
LoTUS SN:46	PS111_54-1	2018-02-13 03:48:13	76°20.138‘ S	053°00.528‘ W	497.2	deployed
LoTUS SN:45	PS111_110-3	2018-02-22 07:38:51	77°06.706‘ S	033°56.186‘ W	404.1	deployed
AWI256-2	PS111_132-3	2018-02-27 16:27:06	73°59.973‘ S	032°22.089‘ W	1823.7	deployed

Work at sea - Tracer Oceanography

About 500 water samples for noble gases (^{3}He, ^{4}He, and Ne) and CFC-12 plus SF_6 have been retrieved with the CTD-water-sampler (Niskin bottles) system on regular hydrographic stations. The bottles were closed by stainless steel springs instead of rubber springs. Due to the high volatility and very low concentrations in the water we took our samples first (i.e., before oxygen, salinity, CO_2, and others sampling). For one noble-gas sample we need 1.5 liter (incl. rinsing), for CFCs we need 0.5 liter (incl. rinsing). Water samples for helium isotopes and neon are stored in 40 ml gas tight copper tubes, clamped of at both sides. The noble gas samples are to be analyzed at the IUP Bremen noble gas mass spectrometry lab. Water samples for CFC-12/SF_6 measurements are stored in 100 ml glass ampoules, sealed off after a headspace of pure nitrogen were injected. The CFC-12/SF_6 samples will be analyzed in the CFC-laboratory again at the IUP Bremen. 40 samples were taken in the vicinity of Maud Rise and 120 samples at shallow stations along the Ronne Ice Shelf front. The remaining samples were obtained from three sections crossing the Filchner Trough (Fig. 3.5).

Preliminary results - Physical Oceanography

The hydrographic activities in the Weddell Sea during PS111 can be split into three sub-regions: (a) Transit to *Neumayer Station III* and Maud Rise, (b) Filchner Trough, and (c) Ronne Ice Shelf front (Figs 3.1 & 3.2). Work in the vicinity of Maud Rise (a) was added to the original station plan to detect possible remnants of deep ocean convection in the water column, caused by the appearance of a large Weddell Polynya during the previous winter. Activities in (b), covering the ocean from the Filchner Ice Shelf front to the sill of the Filchner Trough (Fig. 3.2), allows for a detailed analysis of the highly variable (in space and time), globally relevant, and climate sensitive hydrography in this area. After many years of unsuccessful try, work in (c) was aimed to get a new snapshot of the hydrographic conditions along the Ronne Ice Shelf front, supposed to be the formation region of HSSW, which fuels melting at the base of Filchner-Ronne Ice Shelf. To serve Marine Geology, sampling the isotopes iron, neodymium, and lead in Weddell Sea Bottom Water, one CTD profile was taken at the position of former station 253 of the Brazilian cruise ARXVIII in 2,000 near the tip of the Antarctic Peninsula.

Surface properties measured with the ship’s thermosalinograph from Cape Town to Neumayer Station III crossing Maud Rise

Changes in surface temperature and salinity along the cruise track were recorded using the ship’s thermosalinograph at 11-m depth. The data shows the latitudinal frontal structure of the Antarctic Circumpolar Current and the influence of Maud Rise (Fig. 3.6). Some fronts coincide with drastic temperature and salinity changes especially the Subtropical Fronts (NSTF, SSTF) and the Subantarctic Front (SAF). Others show smaller variations at the surface as they are characterized by property changes at deeper levels such as the Polar Front (PF). The variability of the fronts as well as the possible influence of the polynya of the previous winter becomes obvious when comparing the records from 2016 (PS96) and 2018 (PS111). The Weddell Front (WF) moved about 1° further north certainly caused by higher surface salinities to both sides of Maud Rise (MR). The salinity increase coincides with higher – up to 3°C - surface temperatures, both indicative for the upwelling of deeper waters (Fig. 3.7).

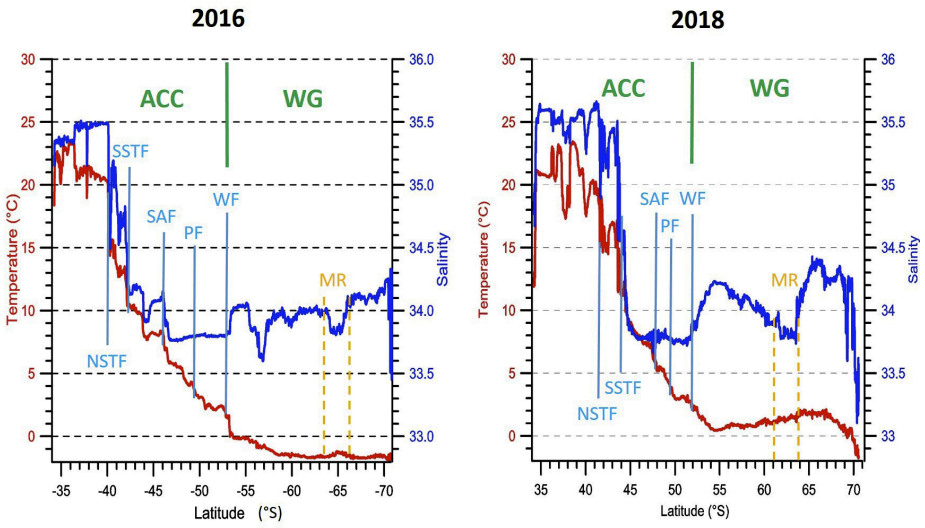

Fig. 3.7: Comparison of thermosalinograph transects from Cape Town to Neumayer Station III in 2016 (PS96) and 2018 (PS111). ACC: Antarctic Circumpolar Current, WG: Weddell Gyre , NSTF: Northern Subtropical Front, SSTF: Southern Subtropical Front, SAF: Subantarctic Front, PF: Polar Front, WF: Weddell Front, and MR: Maud Rise.

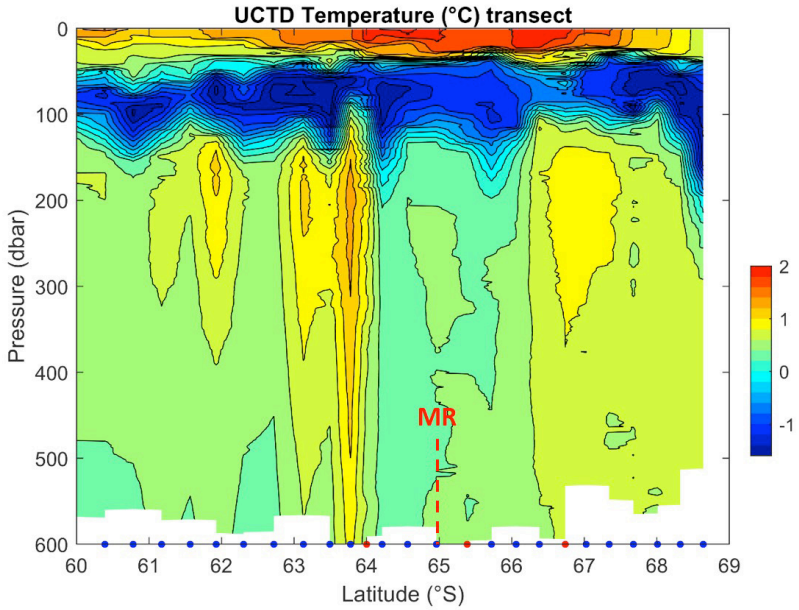

Fig. 3.8: Underway-CTD temperature section from 60°S to Atka Bay (Fig. 3.1). Maximum depth changes due to differences in rope length and sinking velocity. The three ship-CTD stations are marked as red dots. MR: Maud Rise.

The salinity minimum between 61°S and 64°S, which has the same value but shifted to the north in 2018, is surrounded by the two branches of the southern, westward flowing limb of the Weddell Gyre (Fig. 3.7). The U-CTD temperature section clearly identifies the two cores as heat sources with the northern branch consisting of two cores of which the one close to MR is more pronounced and the warmest. This heat influenced the temperature of the Winter Water layer (50 – 120 m) and might also be responsible for the higher surface temperatures because of an early melting of the sea ice cover and, thus, earlier heating by solar radiation. The section, however, does not show any remnants of deep ocean convection as observed by Gordon (1978), possibly due to a ship track too far to the east. This might be confirmed by the data of the profiling APEX floats of University of Washington once available.

Filchner Trough

From the many stations we conducted across the Filchner Trough (Fig. 3.5), in the following we shortly discuss the CTD-section at 76°S, the latitude of our moorings. The temperature maximum (< -1.57°C) on the eastern slope of the Filchner Trough corresponds to the inflow of MWDW (Fig. 3.9) as described in more detail by Ryan et al. (2017). The temperature maximum (< -1.12°C) at 200-m depth to the west seems to be a remnant of warmer MWDW observed at 75°S on the western slope of the Filchner Trough sill (Foldvik et al., 1985). Ice Shelf Water (ISW) with temperatures below -2°C occupies the water column below 300-m depth, flowing northward towards the Filchner Trough sill. The temperature distribution indicates several plumes at different depth with the coldest ISW (< -2.1°C) located on the trough's western slope. Within a thin (~100 m) thick bottom layer temperatures rise above -2°C and salinity reaches the maximum of 34.67, both characterize HSSW which might descend directly from Berkner Bank (Fig. 3.2) into the trough. A careful analysis, including all our sections across the Filchner Trough (Fig. 3.5) and the mooring data of additional two years, now spanning the period from 2014 to 2018, is necessary to illustrate the complex hydrographic structure in the trough and its spatial and temporal variability.

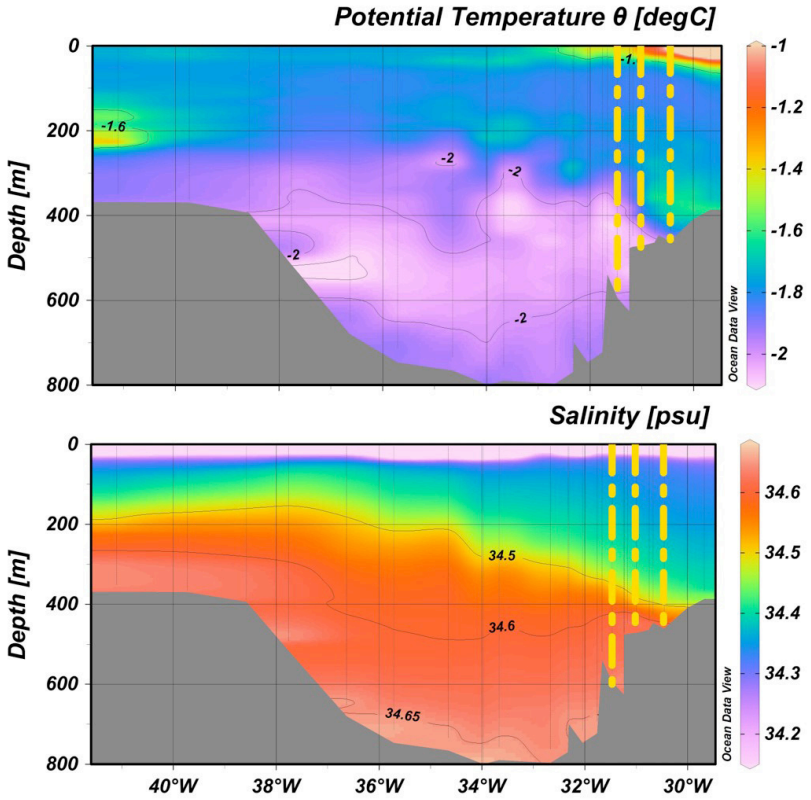

Fig. 3.9: Sections of potential temperature (upper panel) and salinity (lower panel) across the Filchner Trough at roughly 76°S (Fig. 3.5). Vertical lines mark CTD (thin grey) and mooring (dash-dotted orange) positions.

Filchner-Ronne Ice Shelf Front

The hydrographic section along the FRIS front is unique, because for the first time CTD stations from Ronne Trough (61°W) to the southeastern corner of the Filchner Trough (35°30' W) have been completed at such high resolution within less than two weeks. I.e., the variability we see in the water mass characteristics is solely based on spatial variability and tides, which are quite strong at the front of Ronne Ice Shelf. Below a fresh surface layer at surface freezing point, thicker to the east due to the coastal current, three water masses dominate the water

column: MWDW, HSSW, and ISW (Fig. 3.10). MWDW reaches the Ronne front at 52°W with a maximum temperature of -1.48°C and, thus, represents the warmest water with access to the ice shelf cavity (Fig. 3.10 – upper panel). The core on the eastern slope of the Filchner Trough, though warmer (-1.14°C), is too shallow to enter the Filchner cavity. HSSW dominates the western portion of the section (Ronne Trough) with salinity continuously increasing towards the west (Fig. 3.10 – lower panel). A maximum salinity of 34.85 was measured at station #49 close to the Antarctic Peninsula. The ISW above the HSSW represents an outflow related to the western sub-ice shelf circulation (Nicholls et al., 2009). Below 400-m depth, the Filchner Trough is completely filled with various types of ISW, which differ in temperature. The lowest temperature of -2.25°C is found on the trough's western slope. Temperature and salinity both increase with depth and to the east, possibly related to a return flow of ISW from the Filchner Trough sill (Nicholls et al., 2009). Traces of ISW also exist on the eastern slope of Berkner Bank, which might indicate a separate, shallow outflow at this location and a possible source for ice platelets observed on the ROV mission close to the ice shelf front (Chapter 13).

In summary, this data together with the data from the sub-Filchner moorings and the sections across the Filchner Trough in combination with numerical models will certainly foster our understanding of the spatial and temporal variability of the Filchner Ice Shelf system and its sensitivity to present and future environmental conditions.

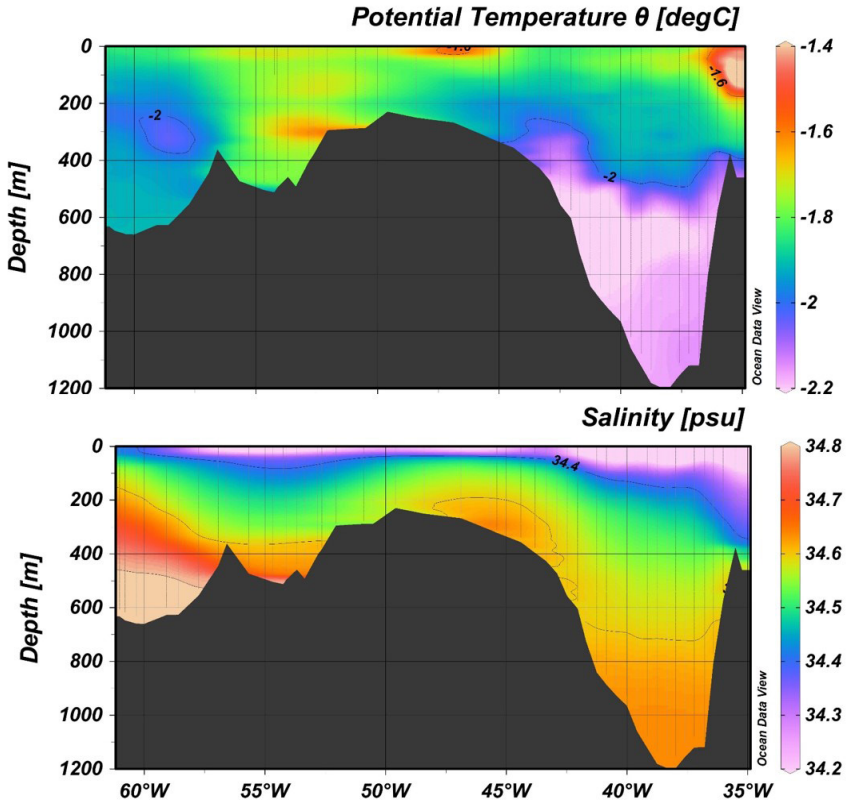

Fig. 3.10: Sections of potential temperature (upper panel) and salinity (lower panel) along the Filchner-Ronne Ice Shelf front (Fig. 3.2). Vertical lines (thin grey) mark CTD-station positions.

Expected results - Tracer Oceanography

The tracer samples from the vicinity of Maud Rise (Fig. 3.1) will allow to study the influence on the gas exchange induced by the Weddell Polynya during September/October 2017. We expect to compare tracer data from this cruise with former CFC and noble gas data to see changes in the ventilated water masses.

The major goal of this project is to study the flow of water masses into and out of the Filchner-Ronne Ice Shelf cavity and estimate the amount of basal melting. As we collected surface samples from 50 stations just in front of both ice shelves (Fig. 3.2), we are now able to study in detail the gas saturation for the transient gases CFC-12 and SF_6. The ratio of SF_6/CFC-12 allows to derive the age of young waters formed on the continental shelf with a resolution of 2 years or better (atmospheric CFC-12 concentration is nearly stable and SF_6 is increasing by about 3 % per year). Therefore, we need to know the initial conditions at the surface. For the first time, SF_6/CFC-samples of ventilated waters in front of the Ronne Ice Shelf at its western most location have been acquired. In addition, this large set of samples will provide reliable information on He and Ne concentrations and He isotope ratios of the ventilated surface waters in front of Ronne Ice Shelf, all needed to quantify the input conditions.

About 50 noble gas samples were retrieved from layers in the water column with potential temperatures below -2.0°C, indicating a dominance of ISW. It will be interesting to quantify the content of glacial melt water on the different sections across the Filchner Trough. The ratios of He/Ne and $^3He/^4He$ in water samples from below the Filchner Ice Shelf (Huhn et al., 2018) can be used to identify the gas contribution from continental ice, which slides on the bedrock and melts near the grounding line. The high data coverage might provide the opportunity to detect this type of melt water in the ISW of the Filchner Trough. The $^3He/^4He$ ratio also identifies the non-ventilated contributions of WDW in all water masses. A correlation to salinity is expected.

Data management

All oceanographic data sets either have been calibrated on board or will after return of the sensors from the manufacturer at the Alfred Wegener Institute. After quality control, they will be published in peer-reviewed journals and be stored in the PANGAEA Data Publisher for Earth & Environmental Science for public use.

All gas tracer data will be made public on the PANGAEA data base as soon as available (approximately one year after the cruise), carefully quality controlled, and published in a peer reviewed journal. Our cooperation partners will receive the data as soon as the final data set is available.

References

Foldvik A, Gammelsrød T & Tørresen T (1985) Circulation and water masses on the southern Weddell Sea shelf. In: Oceanology of the Antarctic Continental Shelf ed. Jacobs SS, Antarctic Research Series, 43, 5-20, American Geophysical Union, Washington, DC.

Foldvik A, Gammelsrød T, Østerhus S, Fahrbach E, Rohardt G, Schröder M, Nicholls KW, Padman L & Woodgate RA (2004) Ice shelf water overflow and bottom water formation in the southern Weddell Sea. J. Geophys. Res. Oceans, 109 (C2), C02015, doi:10.1029/2003JC002008.

Gordon AL (1978) Deep Antarctic convection west of Maud Rise. J. Phys. Oceanogr., 8, 600-612.

Hellmer HH, Kauker F, Timmermann R, Determann J & Rae J (2012) Twenty-first-century warming of a large Antarctic ice-shelf cavity by a redirected coastal current. Nature, 485, 5-8, doi:10.1038/nature11064.

Hohmann R, Schlosser P, Jacobs SS, Ludin A & Weppernig R (2002) Excess helium and neon in the southeast Pacific. Tracers for glacial meltwater. J. Geophys. Res. Oceans, 107 (C11), doi. 10.1029/2000JC000378.#

Huhn O, Hellmer HH, Rhein M, Roether W, Rodehacke C, Schodlok & Schröder M (2008) Evidence of deep and bottom water formation in the western Weddell Sea. Deep-Sea Research II, 55/8-9, pp. 1098-1116, doi:10.1016/j.dsr2.2007.12.015.

Huhn O, Hattermann T, Davis PED, Dunker E, Hellmer HH, Østerhus S, Rhein M, Schröder M, Sültenfuß J & Nicholls KW (2018) Basal melt and freezing rates from first noble gas samples beneath an ice shelf. Submitted to Geophys. Res. Lett.

Nicholls KW, Østerhus S, Makinson K, Gammelsrød T & Fahrbach E (2009) Ice-ocean processes over the continental shelf of the Southern Weddell Sea, Antarctica: A review. Reviews of Geophysics, 47 (3), 1-23, doi:10.1029/2007RG000250.

Ryan S, Hattermann T, Darelius E & Schröder M (2017) Seasonal cycle of hydrography on the eastern shelf of the Filchner Trough, Weddell Sea, Antarctica. J. Geophys. Res. Oceans, 122, 6437-6453, doi:10.1002/2017JC012916.

Schlosser P (1986) Helium: A new tracer in Antarctic oceanography. Nature, 321, 233-235.

Timmermann R & Hellmer HH (2013) Southern Ocean warming and increased ice shelf basal melting in the twenty-first and twenty-second centuries based on coupled ice-ocean finite-element modelling. Ocean Dynamics, 63 (9-10), 1011-1026, doi:10.1007/s10236-013-0642-0.

4. PROJECT ISO-ARC: ISOTOPE SIGNATURE OF WATER VAPOUR OVER THE SOUTHERN ATLANTIC OCEAN

Martin Werner[1], [1]AWI
not on board: Jean-Louis Bonne[1], Melanie Behrens[1], Sepp Kipfstuhl[1], Hanno Meyer[1], Benjamin Rabe[1]

Grant-No. AWI_PS111_00

Objectives

Within the project Iso-Arc, funded by AWI's strategy fond, water vapour and its isotopic signature ($H_2{}^{18}O$ and HDO) have been continuously measured on board of *Polarstern* since mid-2015. These measurements are accompanied by daily surface water sampling. In combination with corresponding water isotope measurements at *Neumayer Station III* (since early 2017) and paired with complementing climate simulations, an integrated analyses of model results and measurements will allow a quantitative assessment of the South Atlantic water cycle, its isotopic variations and imprint in Antarctic ice core records.

Work at sea

Vapour isotope measurements on board of *Polarstern* are performed by a light-weighted cavity-ring-down spectrometer (CRDS, built by *Picarro Inc.*). The CRDS system runs continuously and autonomously and requires only a few minutes of daily maintenance.

During the first twelve days of PS111 (ANT-XXXIII/2), additional maintenance, measurements and data analyses were carried out, focussing on the following aspects:

- The *Labview* software package, which enables the controlling of all relevant valves and conducts the automatic calibration measurements as a daily routine, was overhauled and improved. This task included an update of the *Labview* runtime engine to its latest revision as well as several changes of the flow control routines.
- For the first time since the installation of the instrument, the so-called humidity-response function of the *Picarro* CRDS was determined *in-situ* for two different water standards. The retrieved functions are comparable to the ones measured on several past occasions in Bremerhaven, while *Polarstern* was in dock. The results thus nicely confirm the applied calibration routines, used so far, and rule out any potential difference between performed *in-situ* and *ex-situ* calibrations.
- So far, data analyses have focussed on the $\delta^{18}O$ and dD signal in water vapour in the Atlantic realm. During P111 (ANT-XXXIII/2), a first analyses of the measured concentration of $H_2{}^{17}O$ in vapour was performed. Preliminary results indicate that the

so-called O-17 excess signal over the open ocean varies in a substantially different manner with latitude than the Deuterium excess signal. A combination of both signals might enable to separate the influence of sea surface temperatures and near-surface relative humidity on the initial isotopic composition of marine water vapour in future analyses.

- A planned in-depth *in-situ* analyses of the isotope variability in sea ice covered regions was hampered by the very low sea ice coverage during this first part of PS111 (ANT-XXXIII/2). During the travel from Cape Town to Atka Bay, *Polarstern* was in suitable ice conditions on the very last day, only. Further analyses of the influence of sea ice coverage on the isotope signal in water vapour will therefore be performed after the full leg of PS111 (ANT-XXXIII/2), when more suitable isotope measurements are available.

Preliminary results

From our work at sea, we will get a first assessment on the quality of the performed $H_2{}^{17}O$ measurements in vapour and its potential future utilization. The observation of isotopic changes in partly or fully covered sea ice areas will help to evaluate its current modelling approach.

Data management

All humidity and isotope data of this project will be uploaded to the PANGAEA database after processing and post-operative calibration. Unrestricted access to the data will be granted within 2-3 years, pending analysis and publication.

5. SHIP-BASED WIND LIDAR MEASUREMENTS OF THE ANTARCTIC BOUNDARY LAYER (SWIANT)

Fabian Reiser[1], Frank Schnaase[1,2], [1]Uni Trier
Günther Heinemann[1] (not on board) [2]AWI

Grant-No. AWI_PS111_00
DFG grant No: HE 2740/22

Objectives

The representation of the atmospheric boundary layer (ABL) in the Antarctic is a major challenge for numerical weather forecast models and regional climate models. Reference data sets are rare, particularly over the ocean areas. Standard measurements on research vessels yield near-surface observations and one or two radiosonde launches per day. The group of the University of Trier will perform measurements of vertical and horizontal profiles of wind, turbulence and aerosols. We will use a wind lidar, which is a programmable scanner and can operate with a maximum range of 10 km. Radiosondes launched from *Polarstern* will be used for comparisons of the wind profiles. The data will be used for the verification of simulations using a high-resolution regional climate model and for process studies. The project was endorsed by the Polar Prediction Project (PPP) as a valuable contribution to the Year of Polar Prediction (YOPP).

Work at sea

We use a scanning wind lidar, which measures wind profiles in the ABL with a high vertical resolution (15 m) and a high temporal resolution (15 min). The wind lidar can operate with a maximum range of 10 km. The used lidar is a programmable scanner, which enables vertical scans in all directions. The main scan patterns are the vertical azimuth display (VAD), the range-height indicator (RHI) and horizontal scans with fixed azimuth (STARE). The VAD is used for the determination of wind profiles above the lidar. The STARE mode is used at two or three azimuth angles, which are adjusted to the heading of the ship and the wind direction. The RHI mode is generally applied together with the STARE mode and at the same azimuth angles to obtain cross-sections. This allows for measurements of e.g. the internal boundary layer at the sea ice edge or ice shelf front. Since the lidar is not mounted on a stabilized platform, the ship's heading, roll and pitch angles are recorded using an Attitude Heading Reference System (AHRS), an external GPS and data from the ship's navigation system.

Continuous sampling of vertical profiles will be performed during the cruise. For intensive observation periods during the cruise, RHI and horizontal scans will be performed additionally yielding cross-sections of the ABL. Of particular interest are katabatic winds at Coats Land, the flow in the area of iceberg A23A, the internal boundary layer over the Ronne polynya and over sea ice leads. Radiosondes launched from *Polarstern* will be used for comparisons of the wind profiles (Heinemann and Zentek, 2016).

Preliminary (expected) results

The lidar was operated between 28 January 2018 and 03 March 2018. During this cruise, the lidar was deployed at the port side of *Polarstern* as seen in Fig. 5.1.

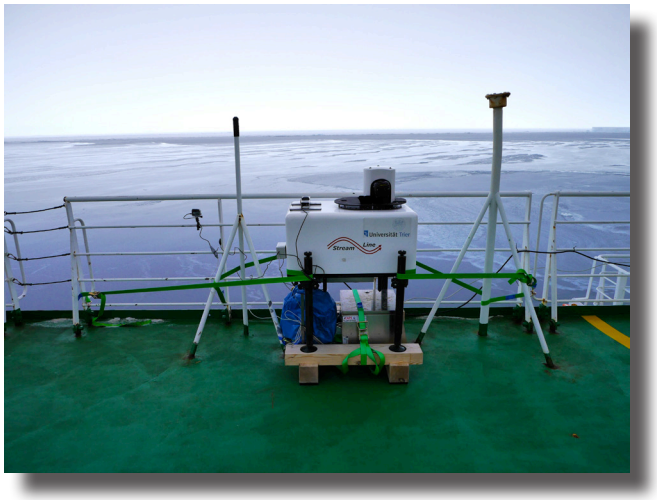

Fig. 5.1: Lidar on the port side

Vertical profiles from the VAD as well as vertical slices of the atmosphere from the dual RHI are continuously acquired. Fig. 5.2 gives an overview of the statistics of the different scanning modes per day. Vertical profiles retrieved form VAD and Wind Profiles pose the largest proportion of measurements. RHIs as well as horizontal stares were performed at lower frequencies depending on the actual weather and ice situation. Such scanning modes are more suitable for stations where *Polarstern* remains at a specific location for a certain time. The only dedicated station was possible in the lee of iceberg A23A on 15 February 2018 between 18:00 and 20:35 UTC. In total, 28Gb of data were acquired whereby the focus was set on vertical and horizontal profiles of the atmosphere. During stations of *Polarstern* the scanning modes were extended by longer stares.

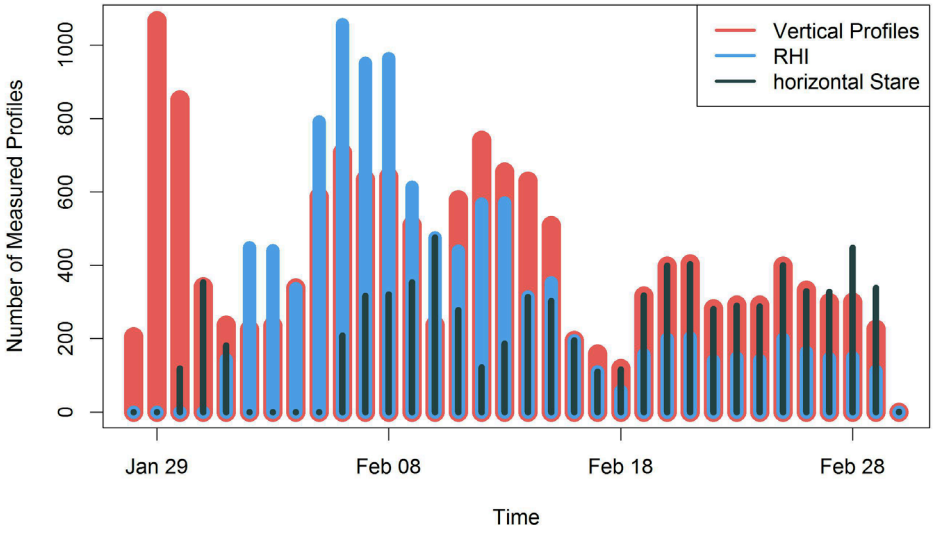

Fig. 5.2: Overview over the different scanning modes per day during FROST

As an overview of the data availability Fig. 5.3 shows the complete time series covered by the measurements of the lidar. Due to low concentrations of particles in the ABL data gaps in the time series occur. A preliminary quality check excludes such measurements since the signal-to-noise ratio is insufficient. The vertical range is also limited to the height of the atmospheric boundary layer or clouds.

During the station at iceberg A23A low clouds were present. The overall signal-to-noise ratio was sufficient in particular for the horizontal scans. Different modes were performed e.g. dual horizontal RHI together with stares (scan at a fixed azimuth) for longer periods of time (up to 1 minute). Vertical profiles of the atmosphere were also carried out. The data depicted in Fig. 5.3 show the temporal evolution of the vertical wind field of the respective day. As winds decrease, the wind direction changes also. A shear (change of wind direction with increasing height) within the vertical profile between 10 and 12 UTC can be seen.

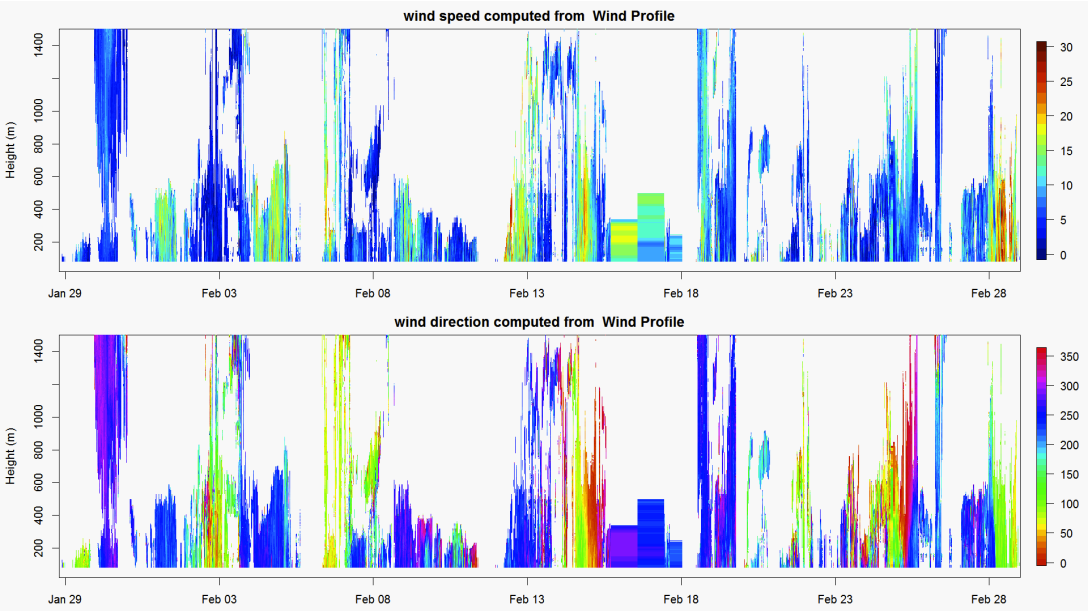

Fig. 5.3: Overview over the complete measuring period with vertical wind speed in the upper panel and the respective horizontal wind direction in the lower panel

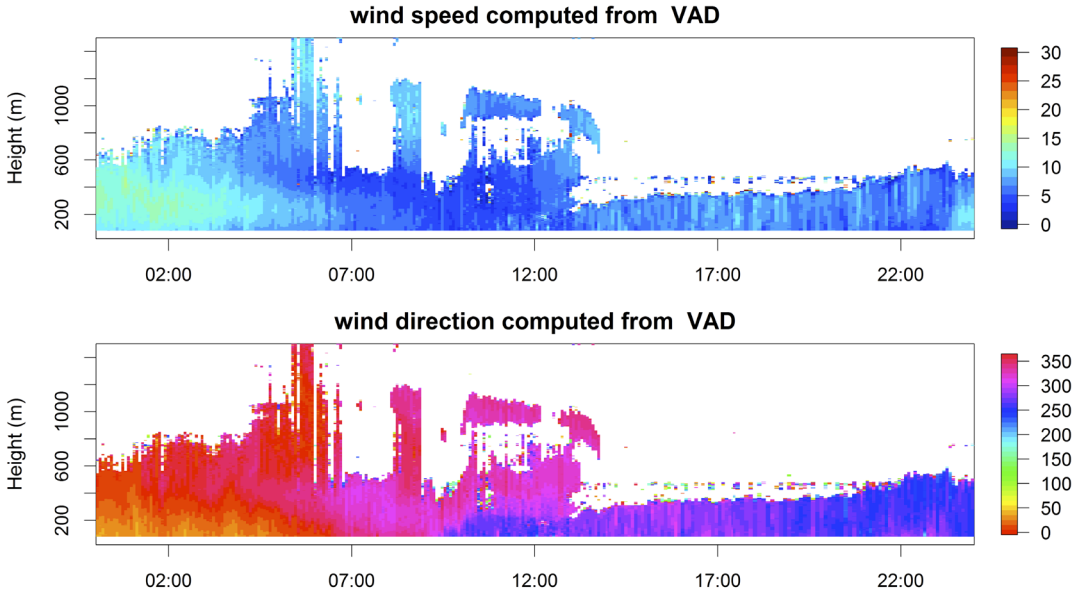

Fig: 5.4: Vertical profiles of the horizontal wind speed and direction as derived from VAD at iceberg A23A (15 February 2018)

Data management

All lidar data obtained during the cruise will be stored on a laptop and USB disks of the participants. After the cruise, all lidar data will be stored at data servers of the University of Trier. The processed data will be stored in the PANGAEA data base.

References

Heinemann G, Zentek R (2016) Measurements of the atmospheric boundary layer using a wind lidar. In: The Expedition PS96 of the Research Vessel POLARSTERN to the southern Weddell Sea in 2015/2016 (ed. M. Schröder). Reports on Polar and Marine Research 700, Alfred-Wegener-Institute for Polar and Marine Research, Bremerhaven, Germany, 148pp. http://doi.pangaea.de/10013/epic.48157.d001.

6. SEA ICE PHYSICS

Stefanie Arndt[1], Nicolas Angelo Stoll[1],
Ricarda Winkelmann[2], Ronja Reese[2],
Marcus Huntemann[3,1]
not on board: Christian Haas[1], Dirk Notz[4],
Marcel Nicolaus[1], Mario Hoppmann[1],
Ignatius Rigor[5], Petra Heil[6]

[1]AWI
[2]PIK Potsdam
[3]Uni Bremen
[4]MPI Hamburg
[5]University of Washington, Applied Physics Laboratory (APL)
[6]Australian Antarctic Division (AAD)

Grant-No. AWI_PS111_00

Objectives

Sea ice and snow are key variables in the global climate system. Through their manifold interactions with the atmosphere (e.g. the ice-albedo feedback) and the ocean (e.g. freshwater budgets during melt and formation), they have strong impacts on global circulation patterns extending far beyond the polar regions. The year-around snow-cover on the ice dramatically alters these exchange processes. Therefore, seasonal transitions, and corresponding freezing and melting events, strongly affect snow properties and its volume with effects such as surface flooding, superimposed ice formation, and extensive snow metamorphism (Arndt et al., 2016; Eicken et al., 1994; Haas et al., 2001; Nicolaus et al., 2009). Given the increasing role of remote sensing observations for sea-ice research, snow cover properties become even more important, since they dominate most retrieval algorithms and data interpretation (Cavalieri et al., 2012; Kern and Ozsoy-Çiçek, 2016; Kern et al., 2016; Ricker et al., 2014; Schwegmann et al., 2015).

Much of the direct impact of sea ice on the underlying ocean is related to the release and storage of salt during sea-ice growth and melt. The release of salt from sea ice occurs generally only through gravity drainage during winter and, if air temperatures rise sufficiently to allow for substantial surface melting, through flushing with fresh water during summer (Notz and Worster, 2009). Because of the low air temperatures, the latter process is all but absent in the Antarctic, and gravity drainage is by far the most dominant process for the release of salt from sea ice. In recent years, we have come a long way in understanding (Notz and Worster, 2009), measuring (Notz et al., 2005) and simulating (Griewank and Notz, 2013) gravity drainage. Particularly for the Weddell Sea, strong progress has been made in monitoring and comparing sea-ice data. However, in order to understand the interaction of the sea-ice with the upper ocean and its role for ocean dynamics in general, *in-situ* measurements of the distribution of salt in sea ice are necessary.

Moreover, the variability of Antarctic sea ice, regarding sea-ice extent, concentration, and season duration, is significantly spatially heterogeneous (Kwok et al., 2017; Lee et al., 2017; Parkinson and Cavalieri, 2012; Stammerjohn et al., 2012; Turner et al., 2014). It is therefore necessary to study not only the seasonal and inter-annual evolution of sea ice, but to describe in particular the regional variability of key variables, such as sea-ice thickness, snow depth, and sea-ice drift (ECVs).

To achieve this, the Seasonal Snow and sea-ice Studies (SeaSonS) program performed sea-ice thickness and snow depth surveys, deployments of autonomous stations (buoys), and

along-track ice observations from the bridge during PS111 (FROST). In addition, we obtained physical properties of the sea ice and its snow cover during all ice stations. Those measurements covered different spatial and temporal scales, allowing an advanced understanding of the status and importance of Antarctic sea ice, with respect to its interactions in the climate system.

The data gained from this study will help to investigate the seasonal and interannual variability of sea-ice thickness, snow depth, sea-ice drift and deformation in the Weddell Sea close and in the Filchner Outflow System complementary to those done during PS82 (ANT-XXIX/9) during austral summer 2013/14, PS96 (ANT-XXX/2) during austral summer 2014/15, and PS96 during austral summer 2015/16.

Tab. 6.1: PANGAEA labels as used for sea-ice physics measurements during PS111

PANGAEA label	Description
Ship based	
ICEOBS	Ice Observations from ship bridge (along track)
Ice station	
SPIT	Snow pit
SMP	SnowMicroPen
SDMP	Snow depth measured with Magna Probe (SnowHydro)
GEM	Ground electromagnetic sounding (GEM-2, Geophex)
CORE	Sea-ice core
Buoys	
BUOY-IMB	Ice Mass Balance Buoy
BUOY-SNOW	Snow Depth Buoy
BUOY-SVP	Surface Velocity Profiler
BUOY-RAD	Spectral radiation station
HARP-SALT	Salt harp
HARP-OPTO	Opto harp
Helicopter based	
AEM	Airborne EM ice thickness profiler (EM-Bird)

Tab. 6.2: List of all sea-ice stations within the SeaSonS project during PS111. Explicit label names for each gear at the respective station are given in the following sub chapters

Station	Date	Time [UTC], start	Time [UTC], end	Gear	Latitude [min]	Longitude [min]
PS111_SIP_1	2018-02-03	14:25	15:32	AEM	-73.7215	-25.7838
PS111_SIP_2	2018-02-08	13:39	15:31	SPIT, SMP	-75.1063	-41.8088
PS111_SIP_3	2018-02-11	11:00	17:07	BUOY-SNOW, SPIT, SMP, SDMP, GEM, CORE	-74.9868	-59.6174

Station	Date	Time [UTC], start	Time [UTC], end	Gear	Latitude [min]	Longitude [min]
PS111_SIP_4	2018-02-13	12:14	14:27	AEM	-77.0250	-50.4900
PS111_SIP_5	2018-02-14	09:50	11:18	AEM	-76.8860	-44.4570
PS111_SIP_6	2018-02-14	13:25	13:43	AEM	-77.0683	-45.6483
PS111_SIP_7	2018-02-15	13:10	16:08	SPIT, SMP, CORE, SSAMP	-75.3471	-41.1960
PS111_SIP_8	2018-02-16	11:35	17:05	BUOY-SNOW, BUOY-IMB_ FLEX, BUOY-IMB, SPIT, SMP, SDMP, CORE	-75.9851	-36.4682
PS111_SIP_9	2018-02-16	17:30	18:30	BUOY-SVP(4)	-75.9851	-36.4682
PS111_SIP_10	2018-02-18	10:21	15:04	BUOY-SNOW, BUOY-IMB_ FLEX, SPIT, SMP, SDMP, CORE	-76.8608	-35.5544
PS111_SIP_11	2018-02-19	10:25	12:09	BUOY-SNOW, BUOY-IMB_ FLEX, CORE	-77.8410	-37.3072
PS111_SIP_12	2018-02-20	13:59	15:25	AEM	-77.5067	-42.0550
PS111_SIP_13	2018-02-20	15:52	17:02	AEM	-77.5250	-42.2683
PS111_SIP_14	2018-02-22	10:34	15:13	BUOY-SNOW, BUOY-IMB_ FLEX, SPIT, SDMP, GEM, CORE, SSAMP	-76.9319	-34.2749
PS111_SIP_15	2018-02-25	17:51	19:19	BUOY-SVP(3)	-74.7196	-32.5288
PS111_SIP_16	2018-02-26	17:17	22:42	BUOY-SNOW, BUOY-IMB_FLEX, BUOY-IMB, BUOY-RAD, HARP-SALT, HARP-OPTIC, CORE	-74.5614	-37.0124
PS111_SIP_17	2018-03-03	12:34	14:09	SPIT, SMP, SDMP	-72.8199	-27.6185

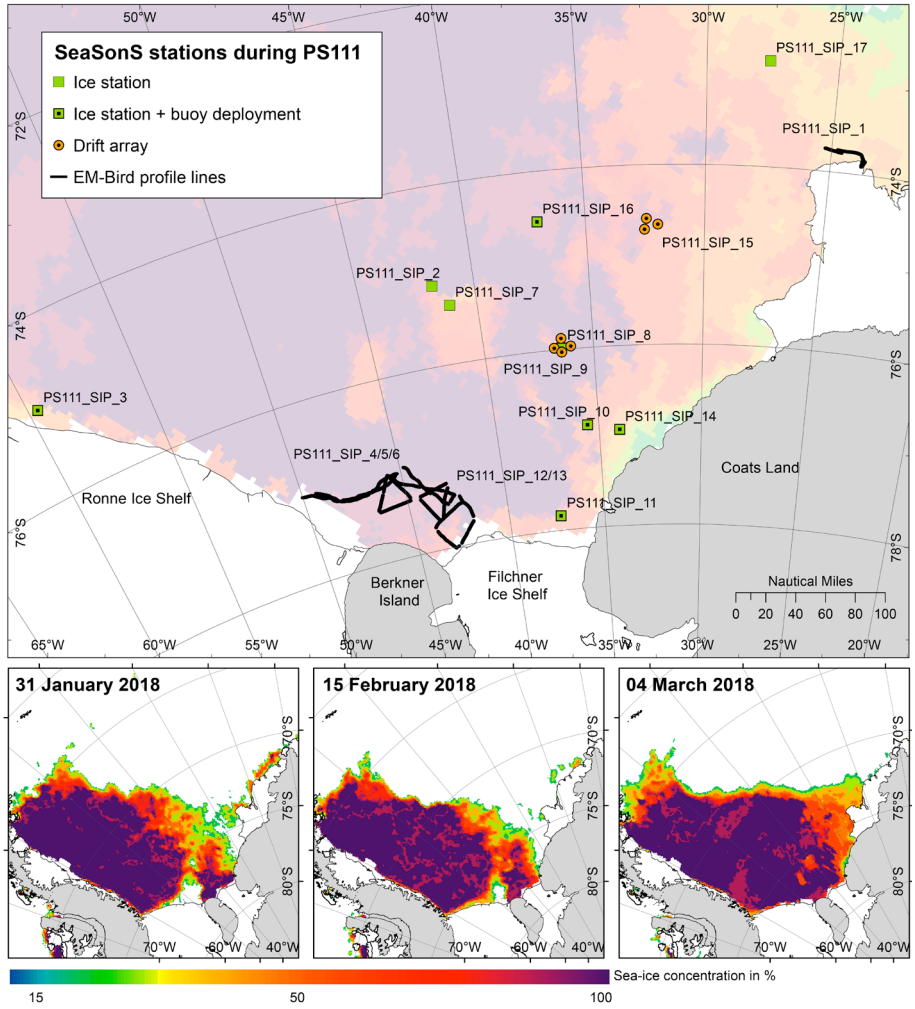

Fig. 6.1: Overview of all activities within the SeaSonS project during P111. The three bottom panels show the sea-ice concentration from AMSR2 for the three given dates during the expedition. Not shown here: Hourly observations of sea ice conditions along the cruise track.

6.1 Deployments of autonomous ice tethered platforms (buoys)

Objectives

The investigation of physical sea-ice and snow parameters during work on one ice floe can only give a snap-shot of the sea ice conditions. In order to obtain also information about the seasonal and inter-annual variability and evolution of the observed ice floes, we deploy autonomous ice tethered platforms (buoys), which measure the sea ice and snow characteristics also beyond the cruise. We use different kinds of buoys: Ice Mass Balance buoys (IMBs) deriving the sea ice growth; snow depth buoys measuring the snow accumulation over the course of the year; Surface Velocity Profilers (SVPs) providing information on the local oceanic and sea-ice drift; a radiation station measuring spectral incoming, reflected and transmitted shortwave radiation fluxes; salinity and optical harps measuring *in-situ* vertical profiles of salt, solid fraction, temperature and light during sea-ice growth and decline.

In addition, buoys are partly equipped with sensors measuring air and/or body temperature and sea level pressure. Combing all retrieved data, we will be able to enhance the understanding of sea-ice processes and feedback mechanisms in the ice-covered Weddell Sea.

Beyond the immediate value for our work, all SVP and Snow Buoys report their position together with measurements of surface temperature and atmospheric pressure directly into the Global Telecommunication System (GTS). Thus, this data may directly be used for weather prediction and numerical model applications.

Work at sea

Fig. 6.2 and Table 6.3 give an overview about all deployed autonomous ice tethered platforms (buoys) during PS111 in the Weddell Sea.

In total, we deployed six Snow Depth Buoys, seven Ice Mass Balance Buoys (IMBs), seven Surface Velocity Profilers (SVPs), one Radiation Station, two salt harps, and one opto harp.

In three cases, one Snow Depth Buoy and one IMB were deployed as combined sets on one floe (setup A). On one other ice floe, one Snow Depth Buoy was combined with two IMB systems (setup B). These combined sets were deployed in the ice-covered south-eastern Weddell Sea. Slightly further north, a super buoy station was built up consisting of one Snow Depth Buoy, two IMBs, one Radiation Station, two salt harps and one opto harp (setup C). In addition, one single Snow Depth Buoy was deployed in the south-western Weddell Sea in front of the Ronne Ice Shelf, close to the Antarctic Peninsula (setup D).

Moreover, two so-called drift arrays were deployed on the ice. The first drift array is consisting of 4 SVPs, surrounding setup B. The second one, consisting of 3 SVPs, was deployed independently from other autonomous platforms. The distance between each drifter in the respective drift array was initially between 5 and 10 nm.

As part of the outreach project “Adopt a buoy”, all Snow Depth and Ice-Mass balance Buoys were decorated with pictures painted by children from all over Germany.

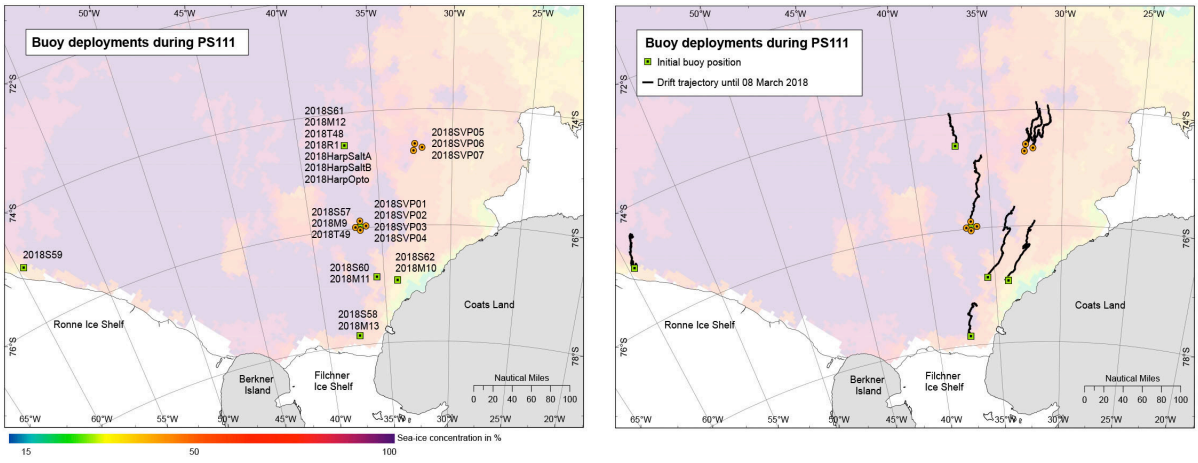

Fig. 6.2: Overview of (left) all deployed buoys and their initial position, and (right) their drift paths until 08 March 2018. Drift paths from 2018SVP01-04 are not shown due to limited data access.

Tab. 6.3: List of all deployed buoys with their initial deployment position and time. Buoy names are identical to their name in www.meereisportal.de, where all data and buoy information is available in real time.

Station	Label	Date	Time [UTC]	Name	IMEI	Latitude [min]	Longitude [min]
PS111_SIP_3-1	PS111_SIP_3-1_BUOY-SNOW	2018-02-11	11:00	2018S59	300234065261080	-74.9868	-59.6174
PS111_SIP_8-1	PS111_SIP_8-1_BUOY-SNOW	2018-02-16	12:30	2018S57	300234065169560	-75.9533	-36.4682
PS111_SIP_8-2	PS111_SIP_8-2_BUOY-IMB_FLEX	2018-02-16	13:40	2018M9	300025010917700	-75.9788	-36.4673
PS111_SIP_8-3	PS111_SIP_8-3_BUOY-IMB	2018-02-16	14:20	2018T49	300234064911160	-75.9769	-3.,4842
PS111_SIP_9-1	PS111_SIP_9-1_BUOY-SVP	2018-02-16	17:45	2018SVP1	300234062782450	-75.9802	-36.8087
PS111_SIP_9-2	PS111_SIP_9-2_BUOY-SVP	2018-02-16	17:56	2018SVP2	300234062781480	-75.9723	-36.0485
PS111_SIP_9-3	PS111_SIP_9-3_BUOY-SVP	2018-02-16	18:08	2018SVP3	300234062787470	-75.8782	-36.4592
PS111_SIP_9-4	PS111_SIP_9-4_BUOY-SVP	2018-02-16	18:20	2018SVP4	300234062786500	-76.0317	-36.4860
PS111_SIP_10-1	PS111_SIP_10-1_BUOY-SNOW	2018-02-18	11:20	2018S60	300234065268080	-76.8628	-35.5506
PS111_SIP_10-2	PS111_SIP_10-2_BUOY-IMB_ FLEX	2018-02-18	11:55	2018M11	300025010125200	-76.8609	-35.5544
PS111_SIP_11-1	PS111_SIP_11-1_BUOY-SNOW	2018-02-19	11:05	2018S58	300234065079570	-77.8410	-37.3072
PS111_SIP_11-2	PS111_SIP_11-2_BUOY-IMB_ FLEX	2018-02-19	11:45	2018M13	300025010024670	-77.8411	-37.3052
PS111_SIP_14-1	PS111_SIP_14-1_BUOY-SNOW	2018-02-22	11:25	2018S62	300234065061680	-76.9319	-34.2749
PS111_SIP_14-2	PS111_SIP_14-2_BUOY-IMB_ FLEX	2018-02-22	12:05	2018M10	300025010026310	-76.9296	-34.4372
PS111_SIP_15-1	PS111_SIP_15-1_BUOY-SVP	2018-02-25	18:29	2018SVP05	ACED-UT-0002	-74.7196	-32.5288
PS111_SIP_15-2	PS111_SIP_15-2_BUOY-SVP	2018-02-25	18:49	2018SVP06	ACED-UT-0001	-74.6646	-31.9632
PS111_SIP_15-3	PS111_SIP_15-3_BUOY-SVP	2018-02-25	19:04	2018SVP07	ACED-UT-0003	-74.5983	-32.4394
PS111_SIP_16_1	PS111_SIP_16_1_BUOY-SNOW	2018-02-26	18:08	2018S61	300234065267070	-74.5614	-37.0124
PS111_SIP_16_2	PS111_SIP_16_2_BUOY-RAD	2018-02-26	20:15	2018R1	300025060601480	-74.5530	-37.0160

Station	Label	Date	Time [UTC]	Name	IMEI	Latitude [min]	Longitude [min]
PS111_SIP_16_3	PS111_SIP_16_3_BUOY-IMB_FLEX	2018-02-26	20:52	2018M12	300025010023830	-74.5525	-37.0328
PS111_SIP_16_4	PS111_SIP_16_4_BUOY-IMB	2018-02-26	21:30	2018T48	300234064816350	-74.5503	-37.0467
PS111_SIP_16_5	PS111_SIP_16_5_HARP-SALT	2018-02-26	19:30	2018HarpSaltB	n.a.	-74.5614	-37.0124
PS111_SIP_16_6	PS111_SIP_16_6_HARP-SALT	2018-02-26	20:30	2018HarpSaltA	n.a.	-74.5614	-37.0124
PS111_SIP_16_7	PS111_SIP_16_7_HARP-OPTO	2018-02-26	21:30	2018HarpOpto	n.a.	-74.5614	-37.0124

Preliminary (expected) results

Snow Buoys and ice-mass balance buoys (IMB)

The Snow Depth Buoys measure the snow accumulation at four spots by sonar sensors whereas the main measuring device of the IMB is a thermistor string going through the ice into the water. By measuring the temperature and thermal conductivity every 2 cm, it is possible to identify the boundaries between ice and ocean, ice and snow and snow and air. Combining both data sets, information on snow depth changes, sea-ice growth and eventually estimates of flooding processes can be expected from the data.

Fig. 6.3 gives an example for snow accumulation of Snow Depth Buoy 2018S58 for the time period from 19 February to 04 March 2018. During this time, there are barely any changes in the snow cover and meteorological data visible. In the beginning of March, increasing temperature to about 0°C leads to a weak snowmelt of about 8 cm which is recognized similarly at all 4 sensors.

Sea-ice growth data from the IMBs will be only processed after the cruise. Finally, all data will be combined with findings of former deployments during PS82, PS89 and PS96 to enhance our understanding of temporal and spatial variability in snow accumulation, sea-ice growth and eventually flooding of Antarctic sea ice.

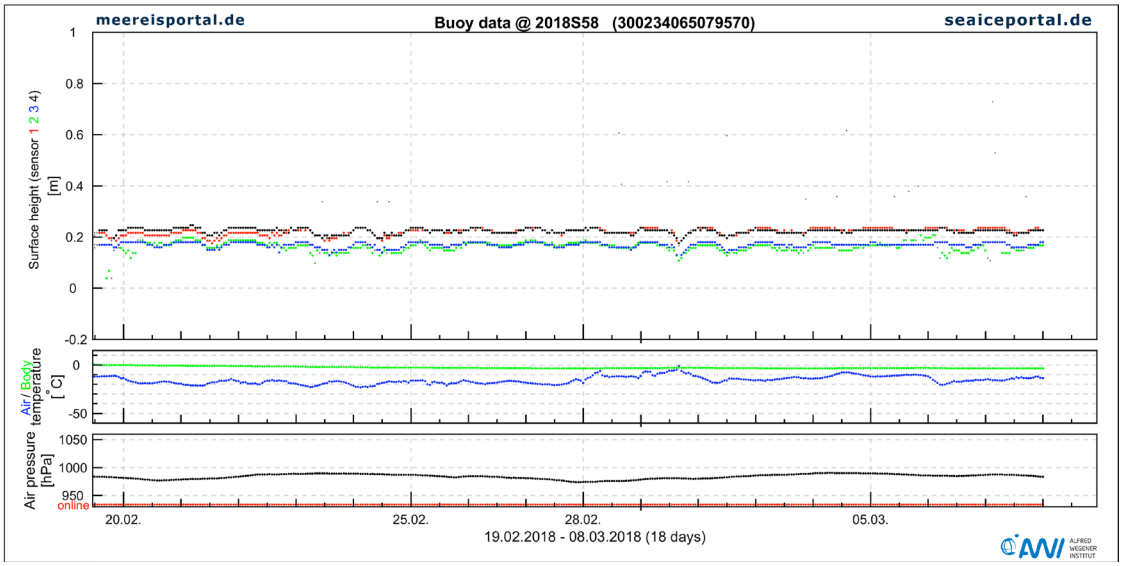

Fig. 6.3: Exemplary time series of snow accumulation along with respective meteorological conditions for Snow Buoy 2018S58, deployed on 19 February 2018

Radiation Station

The deployed radiation station consists of three irradiance sensors measuring spectral incoming, reflected and transmitted shortwave solar radiation in a wavelength range between 320 and 950 nm. Doing so, one sensor is mounted upward looking and one downward looking in a height of about 1 m above the snow. The third sensor is installed about 0.40 m below the ice (upward looking), close to the ice-water interface. By measuring the described three radiation fluxes, we can calculate seasonal spectral and broadband albedo and transmittance values for the sampled floe on its drift paths through the Weddell Sea.

Surface Velocity Profiler (SVP)

The SVP buoys will serve information on the sea-ice drift velocity and its seasonal behavior. As soon as the ice floe is melted, the SVPs will pass over to the ocean and will measure ocean currents at the ocean surface.

Fig. 6.4 shows the time series and histograms of drift velocities of the second drift array, consisting of three SVPs from 25 February to 8 March 2018. Although the buoys were deployed originally only 5 to 10 nm apart from each other, their drift pattern reveals differences in their actual drift velocities. Buoy 2018SVP05 shows overall the longest drift path of about 82 nm, compared to about 75 nm of both other SVPs. Therefore, 2018SVP shows highest drift velocities with a mean drift velocity of 0.16 m/s. That slightly different behavior of 2018SVP05 compared to 2018SVP06 and 2018SVP07 might be related to different floe sizes of the sampled floes: While 2018SVP05 was deployed on an ice floe with a diameter of 0.5-1 km, the ice floes of the other buoys measured about 1-2 km.

So far, none of the buoys in the drift array experienced a significant storm event in the area.

Over the next months, the buoys will record further data, which will be used to calculate the sea-ice drift and deformation variability throughout the Weddell basin.

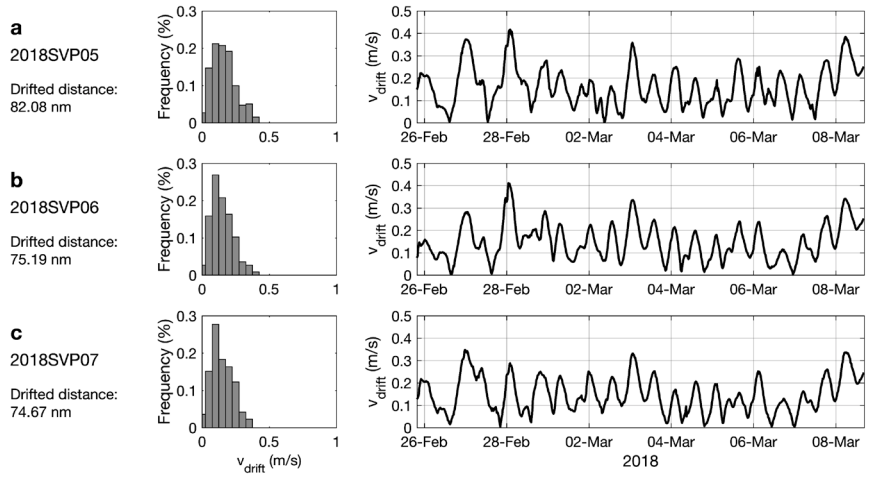

Fig. 6.4: Histograms and time series of drift velocities of Surface Velocity Profilers (SVPs) of the second drift array (2018SVP05-07) deployed on 25 February 2018

Salt and opto harps

The salinity and light harps, developed at Max-Planck-Institute for Meteorology in Hamburg, will measure *in-situ* vertical profiles of solid fraction, bulk salinity, temperature and light transmission in sea ice. They allow for a spatial resolution of 5 cm and take measurements every 6 hours. The data is transferred via Iridium satellite link.

Over the next months, the harps, which were deployed on an ice floe during station PS111_SIP_16, will record the ice floe´s growth and melt as it is drifting through the Weddell Sea. The aim of these measurements is to better understand how sea ice affects the salinity and temperature structure of the upper ocean through the process of brine rejection, and thus how sea ice drives or hinders the vertical transport of water in the Southern Ocean.

Data management

All buoy positions and raw data are available in near real time through the sea-ice portal www.meereisportal.de. At the end of their lifetime (end of transmission of data) all data will be finally processed and made available in PANGAEA. All SVP and Snow Buoys report their position and atmospheric pressure directly into the Global Telecommunication System (GTS). Furthermore, all data are exchanged with international partners through the International Program for Antarctic Buoys.

6.2 Sea-ice and snow transect measurements

Objectives

The thickness of Antarctic sea ice and its snow cover is one of the most important parameters in terms of total mass and energy balance, but sea-ice thickness datasets are sparse. In addition, there are rarely data sets that combine high-resolution thickness information and high spatial coverage. Therefore, snow depths and sea-ice thicknesses are measured simultaneously on transect lines on the ice floes.

The final data sets are used to class other conducted measurements on the floe in the general ice floe characteristics. Also, both sea-ice thickness and snow depth data will be used for validation of satellite remote sensing data products.

Work at sea

Total sea-ice thickness (sea-ice thickness plus snow depth) was measured on the ice during transect measurements with a ground-based multi-frequency electromagnetic induction instrument (GEM-2, Geophex Ltd.). The instrument was mounted on a modified plastic sled and pulled over the snow surface. A GPS-equipped Magna Probe (Snow Hydro, Fairbanks, AK, USA) was operated simultaneously in order to obtain snow depth along the GEM-2 tracks. Snow depth measurements were taken every 1.5 to 2.5 m along the track. Sea-ice thickness was then calculated as the difference of total sea-ice thickness and snow depth.

Due to technical issues with GEM-2, the instrument was used only at station PS111_SIP_14. However, snow transect lines were measured on 5 ice floes in total.

All transect measurements are summarized in Table 6.4.

Tab. 6.4: List of all snow and sea-ice transect measurements during PS111. Profile length indicates the respective number of measurement points per transect. Abbreviations (according to Table 6.1): SDMP – Snow depth measured with Magna Probe (snow depth transect), GEM – Ground electromagnetic sounding (sea-ice thickness transect).

Station	Label	Date	Time [UTC], start	Time [UTC], end	Lati-tude [min]	Longi-tude [min]	Profil length [n]	Mean snow/ice thickness [cm]
PS111_SIP_3-4	PS111_SIP_3-4_SDMP	2018-02-11	13:32	15:10	-59.9866	-59.6168	641	34
PS111_SIP_8-6	PS111_SIP_8-6_SDMP	2018-02-16	14:56	15:37	-75.9733	-36.4847	483	25
PS111_SIP_10-5	PS111_SIP_10-5_SDMP	2018-02-18	12:51	13:48	-75.8557	-35.5569	350	22
PS111_SIP_14-4	PS111_SIP_14-4_SDMP	2018-02-22	12:38	13:55	-76.9246	-34.2603	1126	21
PS111_SIP_14-5	PS111_SIP_14-5_GEM	2018-02-22	12:37	13:53	-76.9254	-34.2622	37572	114
PS111_SIP_17-3	PS111_SIP_17-3_SDMP	2018-03-03	12:50	13:48	-72.8207	-27.6233	282	88

Preliminary (expected) results

Fig. 6.5 shows the distribution function of all measured snow depth transects during PS111. Four profiles were sampled on first-year ice with a moderate ridge density of 10 to 15 %, while the last one (PS111_SIP_17) was sampled on a small fully ridged multi-year ice floe.

Analyzing the snow depth profiles on first-year ice floes shows a typical distribution function for the area: Strongest modes of snow depth are found between 20 and 40 cm with mean (median) values between 21 (19) and 34 (30) cm. However, due to the ridge structures on

the floes, maximum snow depths of up to 1 m are partly measured. In contrast, the sampled multi-year ice floe hardly shows any thin snow layers. Instead, the distribution function peaks at 1.20 cm (limited due to the probe length) with a median value of 1.00 m.

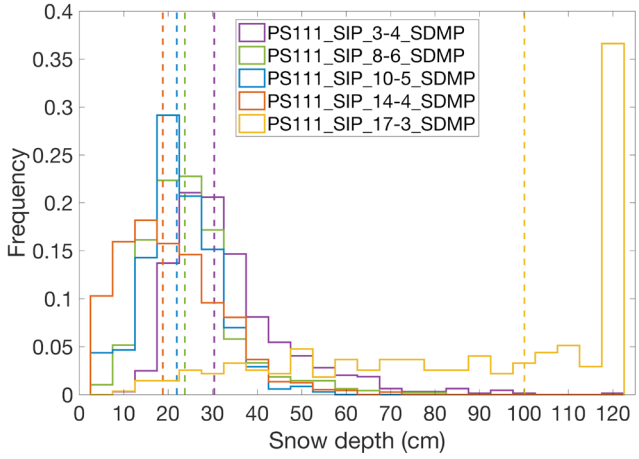

Fig. 6.5: Normalized histogram of all conducted snow depth transects. Vertical lines indicate the median snow depth for each transect, respectively.

Data management

The sea-ice thickness and snow depth transect data will be released following final processing after the cruise or depending on the completion of competing obligations (e.g. PhD projects), upon publication as soon as the data are available and quality-assessed. Data submission will be to the PANGAEA database.

6.3 Physical properties of sea ice

Objectives

With means of the newly developed salinity and light harps as well as sea-ice samples from several ice floes in the Weddell Sea, we aim to quantify characteristic salinity and temperature profiles in the ice and the upper ocean. The overall objective is to achieve a more comprehensive understanding of the salt and heat exchange between sea ice and the ocean.

Work at sea

The work on physical properties of sea ice was performed on seven of the sampled ice floes. It consists of two parts: 1) Ice cores provide important *in-situ* measurements of the temperature, salinity and density profiles of the ice floes. 2) The salinity and light harps allow us to obtain information about the evolution of these sea-ice properties from the observed ice floes over the upcoming months. In particular, the harps will record the seasonal changes in the salt distribution and light transfer in the ice and upper ocean. The measurements complement the data obtained from the other ice-tethered platforms.

Ice cores

A total of 15 ice cores was taken on seven different floes. At each ice core position, the air temperature 50 cm above the snow surface was measured and a snow temperature profile from the surface to the snow-ice interface was taken using a hand-held thermometer. The ice core was then retrieved with an ice corer of 10 cm diameter. The ice temperature profile was measured directly on the floe. The core was then sawn into separate disks of 5 cm thickness

each. In the laboratory on-board *Polarstern*, their salinity was measured and their density profile derived. An overview of all sampled ice cores is given in Table 6.5.

Tab. 6.5: Overview of all sampled ice cores. Possible conducted measurements are: temperature (T), salinity (S), and density (ρ). X indicates done measurements

Station	Label	Date	Time [UTC]	Latitude [min]	Longitude [min]	Ice thickness [cm]	Snow depth [cm]	Measurements		
								T	S	*p*
PS111_SIP_3-6	PS111_SIP_3-6_CORE01	2018-02-11	11:45	-74.9868	-59.6174	140	41	X	X	X
PS111_SIP_7-4	PS111_SIP_7-4_CORE01	2018-02-15	13:30	-75.3471	-41.1960	104	26	X	X	X
PS111_SIP_7-4	PS111_SIP_7-4_CORE02	2018-02-15	14:00	-75.3471	-41.1960	135	26	X	X	X
PS111_SIP_7-4	PS111_SIP_7-4_CORE03	2018-02-15	14:30	-75.3471	-41.1960	143	26	X	X	X
PS111_SIP_8-7	PS111_SIP_8-7_CORE01	2018-02-16	13:00	-75.9851	-36.4682	100	31	X	X	X
PS111_SIP_8-7	PS111_SIP_8-7_CORE02	2018-02-16	14:00	-75.9851	-36.4682	73	26	X	X	X
PS111_SIP_8-7	PS111_SIP_8-7_CORE03	2018-02-16	15:00	-75.9851	-36.4682	50	22	X	X	X
PS111_SIP_10-6	PS111_SIP_10-6_CORE01	2018-02-18	11:30	-76.8608	-35.5544	99	30	X	X	X
PS111_SIP_10-6	PS111_SIP_10-6_CORE02	2018-02-18	13:00	-76.8608	-35.5544	110	24	X	X	X
PS111_SIP_11-3	PS111_SIP_11-3_CORE01	2018-02-19	12:00	-77.8410	-37.3072	75	25	X	X	X
PS111_SIP_14-6	PS111_SIP_14-6_CORE01	2018-02-22	11:15	-76.9319	-34.2749	124.5	17	X	X	X
PS111_SIP_14-6	PS111_SIP_14-6_CORE02	2018-02-22	12:30	-76.9319	-34.2749	141	11	X	X	X
PS111_SIP_14-6	PS111_SIP_14-6_CORE03	2018-02-22	14:00	-76.9319	-34.2749	126.5	50	X	X	X
PS111_SIP_16-8	PS111_SIP_16-8_CORE01	2018-02-26	18:15	-74.5614	-37.0124	140	22		X	X
PS111_SIP_16-8	PS111_SIP_16-8_CORE02	2018-02-26	22:00	-74.5614	-37.0124	96	20		X	X

Salinity and light harps

Two salinity harps and one optical harp were deployed on an ice floe at 74°33.685’ S and 37°00.741’ W. The floe consisted of first-year ice, was more than a kilometer in diameter and about 1.4 m thick at the deployment location. The harps were placed approximately 10 meters apart. The salinity harps were vertically positioned in a way that one is frozen into the ice to about one third and the other to about two thirds of the respective ice thickness, so that the changes in salinity in the prevalent ice column as well as the upper ocean can be measured.

Preliminary (expected) results

The ice cores retrieved from seven different ice floes had a minimum ice thickness of 50 cm and a maximum ice thickness of 143 cm. Salinity profiles of different types were found, the most prominent being the S-type also found in previous samples from the Weddell Sea, with higher salinities near the ice surface, which has been associated with sea-water flooding and snow ice formation. An exemplary temperature and salinity profile is shown in Fig. 6.6.

These measurements are complemented by the ongoing measurements from the salinity and light harps. Over the next months, they will continue to record real-time vertical profiles of temperature, light transmission and conductivity from which we can derive changes in salinity in the ice as well as the upper ocean.

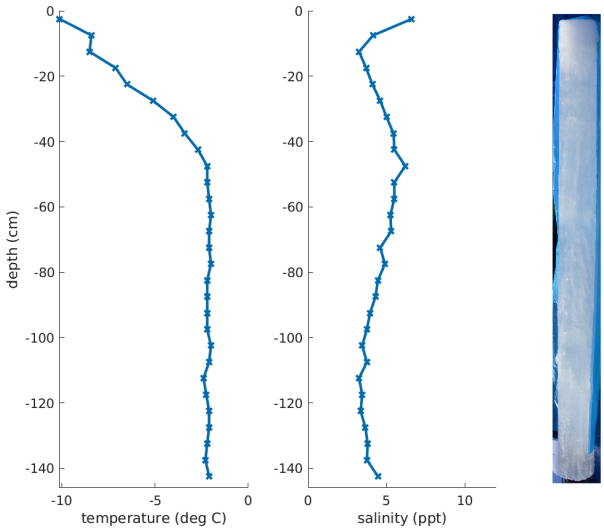

Fig. 6.6: Exemplary temperature and salinity profiles from sea-ice core retrieved on 22 February 2018 at station PS111_SIP_14

Data management

Data from the ice cores will be delivered to PANGAEA within two years after the cruise. At the end of their lifetime (end of transmission of data) all data from the salinity and optical harps will be finally processed and also made available in PANGAEA.

6.4 Physical properties of snow

Objectives

Physical snow properties are highly variable even on small horizontal scales. These spatial and temporal variations in the snow pack characteristics (e.g. temperature, density, stratigraphy) and its dimension have a crucial impact on the energy and mass budget of Antarctic sea ice. Therefore, the snow pack on different ice floes is characterized in detail.

Snow stratigraphy will be used as ground truth for the interpretation of retrieved snowmelt signatures from passive microwave data.

Work at sea

The work on physical snow properties was performed on six of the sampled ice floes. The work can be subdivided in two parts: Snow pits to describe essential physical snow parameters and its stratigraphy, and SnowMicroPen measurements deriving a high-resolution density profile of the prevalent snowpack.

Snow pits

Snow pit measurements were taken on the undisturbed shaded working wall of the snow pit. At first, the temperature was measured every 1 to 5 cm from the top (snow-air interface) to the bottom (snow-ice interface) with a hand-held thermometer (Testo). In a next step the different

layers in the snow pack and its stratigraphic parameters were described. For each layer the snow grain size and type (e.g. rounded crystals, facetted crystals, depth hoar) is determined by the magnifying glass and a 1-to-3-mm grid card. In addition, every layer was characterized by its hardness with the following categories: fist (F), 4 fingers (4F), 1 finger (1F), pencil (P), and knife (K). Afterwards, the density of each layer was measured volumetrically by removing a defined snow block with a density cutter of snow from each layer (density cutter weight: 155 g, volume: 100 ml) and weighting it with a spring scale. In addition, measurements of liquid water content (in Vol. %) were performed with a Snow Fork (Toikka, Finland) through the di-electrical properties of the snowpack. Snow Fork measurements were performed twice every 2 cm from the top to the bottom. Moreover, snow samples were taken from the bottom snow layer at three measurements sites for salinity measurements on board. At two sites, additional snow samples were taken from the top of the snowpack for later isotope analysis back at AWI, Bremerhaven.

Overall, 16 snow pits were analyzed on 6 different ice floes. Table 6.6 summarizes the explicit conducted measurements for each snow pit.

Tab. 6.6: Overview of all sampled snow pits. Possible conducted measurements are: temperature (T), density (ρ), stratigraphy (STR), liquid water content (LWC), and salinity (S). X indicates done measurements

Station	Label	Date	Time [UTC]	Latitude [min]	Longi-tude [min]	Snow depth [cm]	Measurements				
							T	*p*	STR	LWC	S
PS111_SIP_2-1	PS111_SIP_2-1_SPIT01	2018-02-08	14:25	-75.1063	-41.8088	51	X	X	X		
PS111_SIP_3-2	PS111_SIP_3-2_SPIT01	2018-02-11	13:15	-74.9868	-59.6174	33	X	X	X		
PS111_SIP_3-2	PS111_SIP_3-2_SPIT02	2018-02-11	14:30	-74.9851	-59.6106	50	X	X	X		
PS111_SIP_3-2	PS111_SIP_3-2_SPIT03	2018-02-11	15:25	-74.9839	-59.6018	38	X	X	X		
PS111_SIP_7-1	PS111_SIP_7-1_SPIT01	2018-02-15	13:36	-75.3471	-41.1960	26	X	X	X	X	
PS111_SIP_7-1	PS111_SIP_7-1_SPIT02	2018-02-15	14:20	-75.3452	-41.1774	14	X	X	X	X	
PS111_SIP_7-1	PS111_SIP_7-1_SPIT03	2018-02-15	14:52	-75.3438	-41.1641	21	X	X	X	X	
PS111_SIP_8-4	PS111_SIP_8-4_SPIT01	2018-02-16	14:49	-75.9713	-36.4672	21	X	X	X		X
PS111_SIP_8-4	PS111_SIP_8-4_SPIT02	2018-02-16	15:32	-75.9710	-36.4836	14	X	X	X		X
PS111_SIP_10-3	PS111_SIP_10-3_SPIT01	2018-02-18	12:28	-76.8575	-35.5574	16	X		X		
PS111_SIP_10-3	PS111_SIP_10-3_SPIT02	2018-02-18	13:12	-76.8497	-35.5542	25	X		X		
PS111_SIP_10-3	PS111_SIP_10-3_SPIT03	2018-02-18	13:45	-76.8488	-35.5543	26	X		X		
PS111_SIP_14-3	PS111_SIP_14-3_SPIT01	2018-02-22	12:35	-76.9238	-34.2591	15	X	X	X		
PS111_SIP_14-3	PS111_SIP_14-3_SPIT02	2018-02-22	13:08	-76.9212	-34.2519	24	X	X	X		X
PS111_SIP_14-3	PS111_SIP_14-3_SPIT03	2018-02-22	13:44	-76.9189	-34.2439	16	X	X	X	X	
PS111_SIP_17-1	PS111_SIP_17-1_SPIT01	2018-03-03	13:05	-72.8199	-27.6185	69	X	X	X		X

SnowMicroPen

The SnowMicroPen (SMP) is a high-resolution snow penetrometer. It measures the bonding force between snow grains, with high spatial resolution and high speed. During the measurement, the SMP is pressed down to the snow surface while the rod is driven into the snow pack. A piezoelectric force sensor measures penetration resistance as function of depth. The measured data is displayed on the controller and stored in binary format on a SD card.

During PS111 the SMP was used in two different ways. On the one hand, 4 to 7 SMP measurements were conducted close to each snow pit as reference measurement to the manual measurements. On the other hand, we performed transect measurements on straight lines with two measurements per 0.5 to 2 m.

An overview of all measurements is given in Table 6.7.

Tab. 6.7: Overview of all SMP measurements, subdivided into measurements close to snow pits (_SPIT) and on transect lines (_TRANS). Time and position indicate the starting point of the respective measurement sequence.

Station	Label	Date	Time [UTC]	Latitude [min]	Longi-tude [min]	Total casts [n]	Transect spacing
PS111_SIP_2-2	PS111_SIP_2-2_SMP_TRANS01	2018-02-08	14:19	-75.1064	-41.8093	19	0.5 m
PS111_SIP_2-2	PS111_SIP_2-2_SMP_SPIT01	2018-02-08	14:54	-75.1070	-41.8128	7	
PS111_SIP_3-3	PS111_SIP_3-3_SMP_TRANS01	2018-02-11	13:12	-74.9868	-59.6177	101	0.5 m
PS111_SIP_3-3	PS111_SIP_3-3_SMP_SPIT01	2018-02-11	14:28	-74.9851	-59.6107	6	
PS111_SIP_3-3	PS111_SIP_3-3_SMP_SPIT02	2018-02-11	15:28	-74.9838	-59.6014	5	
PS111_SIP_3-3	PS111_SIP_3-3_SMP_SPIT03	2018-02-11	15:56	-74.9835	-59.5954	6	
PS111_SIP_7-2	PS111_SIP_7-2_SMP_TRANS01	2018-02-15	13:42	-75.3469	-41.1928	46	2.0 m
PS111_SIP_7-2	PS111_SIP_7-2_SMP_SPIT01	2018-02-15	14:27	-75.3448	-41.1744	5	
PS111_SIP_7-2	PS111_SIP_7-2_SMP_SPIT02	2018-02-15	14:48	-75.3440	-41.1657	5	
PS111_SIP_7-2	PS111_SIP_7-2_SMP_SPIT03	2018-02-15	15:15	-75.3428	-41.1551	5	
PS111_SIP-8-5	PS111_SIP_8-5_SMP_TRANS01	2018-02-16	14:49	-75.9737	-36.4850	70	1.0 m
PS111_SIP-8-5	PS111_SIP_8-5_SMP_SPIT01	2018-02-16	15:29	-75.9711	-36.4837	5	
PS111_SIP-8-5	PS111_SIP_8-5_SMP_SPIT02	2018-02-16	15:36	-75.9707	-36.4834	5	
PS111_SIP_10-4	PS111_SIP_10-4_SMP_TRANS01	2018-02-18	12:20	-76.8581	-35.5570	85	2.0 m
PS111_SIP_10-4	PS111_SIP_10-4_SMP_SPIT01	2018-02-18	13:26	-76.8520	-35.5558	5	
PS111_SIP_10-4	PS111_SIP_10-4_SMP_SPIT02	2018-02-18	13:48	-76.8495	-35.5542	6	
PS111_SIP_10-4	PS111_SIP_10-4_SMP_SPIT03	2018-02-18	13:55	-76.8488	-35.5543	5	
PS111_SIP-17-2	PS111_SIP_17-2_SMP_SPIT01	2018-03-03	13:05	-72.8196	-27.6164	4	
PS111_SIP-17-2	PS111_SIP_17-2_SMP_TRANS01	2018-03-03	13:13	-72.8190	-27.6127	14	1.0 m

Preliminary (expected) results

Fig. 6.7 shows an example snow pit data set from station PS111_SIP_3. The snow pit was sampled in a representative area of the floe with a snow depth of 38 cm. The snow pack contained of 6 different layers (from top to bottom): thin wind slab crust (1), followed by a soft layer of rounded ice grains (2), a hard wind slab layer (3), again a soft layer of rounded ice grains (4), and a layer of fine-grained old snow (5). Finally, the bottom layer shows typical depth hoar structures (6). Throughout the sampled snowpack the grain sizes increase, which correlated with the strong temperature gradient from -6.9°C (30 cm) to -3.2°C (bottom). Due to clear sky conditions and associated high shortwave solar radiation fluxes, the layer below the crust is slightly heated up.

In addition to the traditional snow pit measurements, about 404 SnowMicroPen (SMP) measurements have been conducted. Those were done, on the one hand, close to all sampled snow pit sites (Fig. 6.7, gray lines), and, on the other hand, on transect lines with a spacing of 0.5 to 2 m. Therefore, Fig. 6.8 shows an extract of 10 SMP profiles (covering 10 m) from a 23-m transect line at station PS111_SIP_3. The measurement site of the transect was chosen

as representative for the ice floe with a homogenous surface appearance. Measurements were taken twice at every measurement point. During post-processing, corresponding measurement profiles were averaged. Even though, the measurement site was visually homogeneous, the internal structures differ significantly on the shown 10-m transect. While the snowpack is rather homogeneous between meter 6 and 10, an increased layering becomes obvious throughout the end of the profile line. This transect line is therefore an excellent example for small scale variabilities on vertical and horizontal scales in the snowpack on Antarctic sea ice.

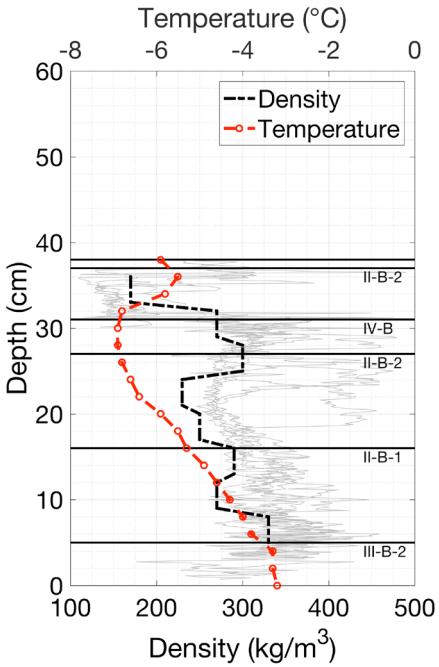

Fig. 6.7: Example of a snow pit analysis from station PS111_SIP_3_2_SPIT02. Temperature measurements are marked in red, density measurements with the density cutter in black, and density measurements with the SMP in gray. Horizontal lines indicate the different layer interfaces. Below the lines grain type classifications for the respective layer are given.

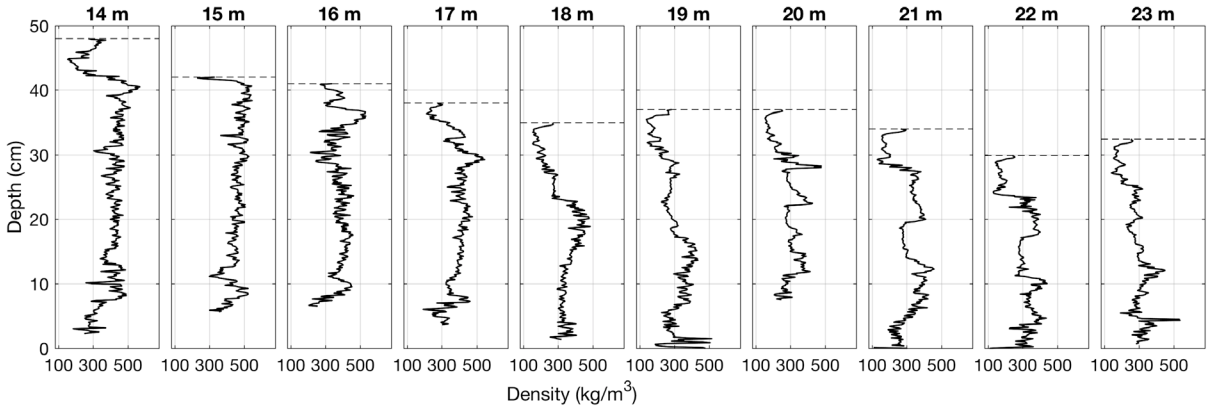

Fig. 6.8: Extract from a 23-m SMP transect line at station PS111_SIP_3-3_SMP. Plotted vertical profile lines are calculated mean values of two measurements per measurement point. Horizontal lines indicate the respective snow depth.

Data management

Data from all snow pit and SMP measurements will be delivered to PANGAEA within two years after the cruise.

6.5 Airborne ice thickness measurements

Objectives

Sea ice fastened to coasts, icebergs and ice shelves (fast ice) is of crucial importance for climate and ecosystems. At the same time, it is not represented in climate models and many processes affecting its energy- and mass balance are currently only poorly understood. Near Antarctic ice shelves, this landfast sea ice exhibits two unique characteristics that distinguish it from most other sea ice: On the one hand, ice platelets form and grow in super-cooled water, which originates from ice shelf cavities. The crystals accumulate beneath the solid sea-ice cover and are incorporated into the sea-ice fabric, contributing between 10 and 60 % to the mass of the land-fast sea ice around Antarctica. On the other hand, a thick and partly multi-year snow cover accumulates on the fast ice, altering the sea-ice surface and affecting the sea-ice energy and mass balance. However, sea-ice thickness of fast ice along the coast of the Weddell Sea is poorly investigated and only few observational data exist so far.

Therefore, we studied the extensive fast-ice tongue in front of Berkner Island, which is forming in the area since the late 1986, when the iceberg A23A grounded in the area. Results play a crucial role for the comprehensive understanding of interactions between the ice shelf, sea ice and ocean in the area.

Work at sea

We used the airborne multi-frequency electromagnetic (AEM) induction sounding system Orphan to measure total sea-ice thickness (ice thickness plus snow depth) by helicopter surveys. The 4-m long instrument, the EM-Bird, is towed on a 20-m long cable underneath the helicopter and measures the sea-ice thickness in a height of 10-15 m above the surface. A laser altimeter is integrated in the EM-Bird system, measuring the distance to the surface. Beside its role for sea ice thickness calculation, the laser data allows the calculation of surface roughness and accordingly ridge density and distribution.

We conducted one test flight in an inlet at the Stancomb-Wills-Ice Tongue. The main area of interest was the fast ice in front of Berkner Island. Here, we were able to perform in total 5 survey flights – three in the west and two in the east. Table 6.8 summarizes all conducted EM-Bird flights.

Tab. 6.8: Overview of all conducted EM-Bird flights. The position indicates the starting point of the respective profile flight.

Station	Label	Date	Time [UTC], start	Time [UTC], end	Latitude [min]	Longitude [min]	Profil length [km]	Comment
PS111_SIP_1-1	PS111_SIP_1-1_AEM	2018-02-03	14:25	15:32	-73.7214	-25.7838	76.5	Test flight
PS111_SIP_4-1	PS111_SIP_4-1_AEM	2018-02-13	12:14	14:27	-77.0250	-50.4900	310.7	Berkner Island
PS111_SIP_5-1	PS111_SIP_5-1_AEM	2018-02-14	09:50	11:18	-76.8860	-44.4570	166.0	Berkner Island
PS111_SIP_6-1	PS111_SIP_6-1_AEM	2018-02-14	13:25	13:43	-77.0683	-45.483	131.3	Berkner Island
PS111_SIP_12-1	PS111_SIP_12-1_AEM	2018-02-20	13:59	15:25	-77.5067	-42.0550	160.2	Berkner Island
PS111_SIP_13-1	PS111_SIP_13-1_AEM	2018-02-20	15:52	17:02	-77.5250	-42.2683	120.7	Berkner Island

Preliminary (expected) results

In total, we performed 5 survey flights with the EM-Bird at the fast-ice area in front of Berkner Island, covering a total length of 889 km. While three flights have been conducted from the western edge, two surveys focused on the eastern part.

Fig. 6.9 illustrates the measured total sea-ice thickness of all survey flights at the fast-ice area. The mean (median) thickness is calculated as 4.24 m (3.50 m). However, one can distinguish between three different regimes. (1) Along the ice edge (western part), a mixture of fast ice and slightly attached ice floes has been sampled. Therefore, this area shows the overall thinnest total ice thicknesses. (2) The central part of the fast ice tongue was quite rough and ridged from above. This is in line with estimated total ice thicknesses of up to 18 meters, while mean values are estimated between 6 and 8 meters. Thus, this area indicates the thickest ice of the surveyed fast-ice zone. (3) In front of the Filchner Ice Shelf, small cracks and leads gave hints of a dynamic regime related to new ice formation in the area. Also, the fast ice was comparably flat in that area. A derived total ice thickness of about 1 to 2 meters approves these observations.

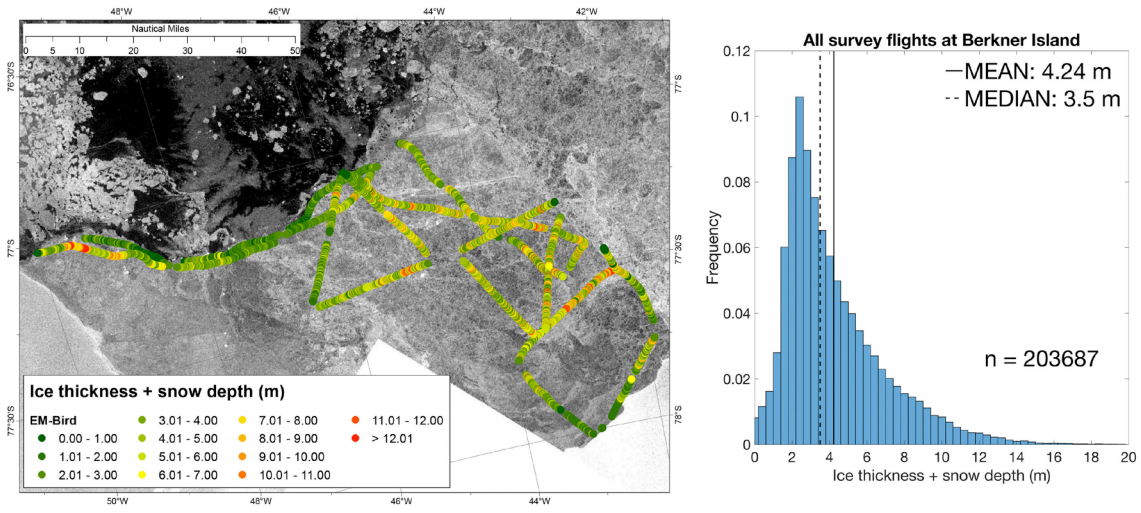

Fig. 6.9: (left) All EM-Bird survey transects color-coded with their fast-ice thickness (+ snow) in front of Berkner Island, and (b) the respective thickness distribution with the marked mean and median (ice+snow) thickness.

Data management

The sea-ice thickness data will be released following final processing after the cruise or depending on the completion of competing obligations (e.g. PhD projects), upon publication as soon as the data are available and quality-assessed. Data submission will be to the PANGAEA database.

6.6 Along track observations of sea ice conditions

Objectives

Over the last three decades, ship-based visual observations of the state of the sea ice and its snow cover have been performed over all seasons and serve the best-available observational data set of Antarctic sea ice. The recordings follow the Scientific Committee on Antarctic Research (SCAR) Antarctic Sea Ice Processes and Climate (ASPeCt) protocol and include information on sea-ice concentration, sea-ice thickness and snow depth as well as sea-ice type, surface topography and floe size. This data is combined with information about meteorological conditions as air temperature, wind speed and cloud coverage. This protocol is a useful method to obtain a broad range of characterization and documentation of different sea-ice states and specific features during the cruise.

Work at sea

Every full hour during steaming, sea-ice observations were carried out by trained scientists. The observations follow the ASPeCt protocol (Worby, 1999), with a software following the ASPeCt standard and being provided on a notebook on the ship's bridge. For every observation, pictures were taken in three different directions (portside, ahead, starboard).

Date, time and position of the observation were obtained from the DSHIP system, along with standard meteorological data (current sea temperature, air temperature, true wind speed, true wind direction, visibility). The characterization of the ice conditions was estimated by taking the average between observations to port side, ahead and to starboard side. Ice thicknesses of tilted floes were estimated by observing a stick attached to the ships starboard side.

Preliminary (expected) results

We performed hourly sea-ice observations as soon as we passed the first sea ice on 28 January 08:00 UTC at 70° 05.551'S/ 6° 50.894'W (close to Atka Bay). On the transit towards the Antarctic Peninsula, the ship the sea-ice zone on 04 March 2018 23 UTC at 69° 14.196' S/ 39° 27.138' W. Over the time period of 34 days, 472 individual observations were recorded. Sea-ice observations were skipped when the ship was stopped for station work (e.g. CTD, biology/ geology station) and supply and loading activities at the shelf ice edge (*Neumayer III, Halley VI*). Due to imited sight, ice observations are also skipped during civil twilight/nighttime.

Steaming towards the Antarctic Peninsula, we crossed again sea-ice covered areas. However, this area is not considered for further ice observations as it was not part of the main working area.

Fig. 6.10 summarizes all conducted sea-ice observations during PS111. The mean sea-ice concentration was calculated as 58.0 % with a mean sea-ice thickness of 0.48 m and 0.12 m snow on top. However, Fig. 6.10 indicates that new ice classes, especially Nilas, are the main contributors in all observed ice classes. Also, thin ice classes do correlate with areas of high sea-ice concentration. Excluding new ice classes (e.g. Nilas, Brash, …), the mean thickness of level first-year ice (FYI) is 0.75 m with 0.30 cm snow on top. Moreover, small areas of multi-year ice (MYI) are crossed, with a mean sea-ice thickness of 1.67 m and 0.51 m of snow on top. These results from level ice classes are in line with actually measured sea-ice and snow thicknesses on the sampled floes during the expedition.

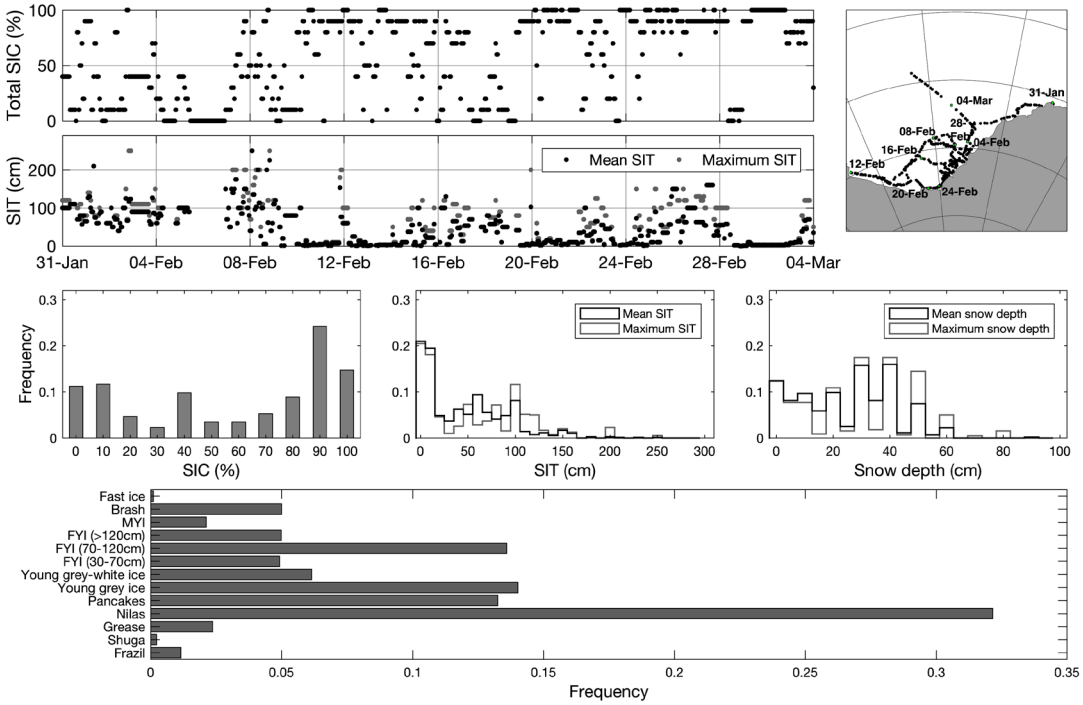

Fig. 6.10: Overview of all conducted sea-ice observations from the ship bridge. Total sea-ice concentration (SIC) displays the overall sea-ice concentration around the ship. Sea-ice thickness (SIT) and snow depth data are subdivided into calculated mean (black) and maximum values (gray) per ice observations. Bottom panel displays the overall sea-ice type distribution from all ice observations. Upper right panel displays all locations of ice observations. Green dots are in line with the date ticks of sea-ice concentration and thickness time series.

Data management

The visual sea-ice observations were already post-processed on board and will be published together with the taken pictures in PANGAEA within two months after the cruise.

6.7 Deployments of ocean drifters

Objectives

The Year of Polar Prediction (YOPP) has the mission to enable a significant improvement in environmental prediction capabilities for the polar regions and beyond, by coordinating a period of intensive observing, modelling, prediction, verification, user-engagement, and education activities. The YOPP core phase is from mid-2017 to mid-2019, flanked by a preparation and consolidation phase. In order to enhance the polar observing for prediction purpose, YOPP is concentrating observational efforts of Special Observing Periods (SOPs). For the Southern Ocean, the SOP is scheduled from 16 November 2018 to 15 February. The purpose of the SOPs is to enhance the routine observations in an attempt to close the gaps in the conventional polar observing systems for an extended period of time.

Therefore, we aim to deploy ocean drifters along the cruise track which are meant to stay in the area for at least a year and do therefore contribute to the SOP of the Southern Ocean.

Work at sea

Fig. 6.11 and Table 6.9 give an overview about all deployed ocean drifters (Surface Velocity Profilers, SVPs). The 10 ocean drifters have been deployed by throwing over board during steaming in mainly ice-free areas.

On our transit from Cape Town 6 of the ocean drifters have been deployed at 45°S, 52.5°S, 58.5°S, 60.5°S, 62°S, and 67°S. After leaving the main area if research again, four additional ocean drifters have been deployed between 37°W and 49°W with a spacing of 4° in longitude.

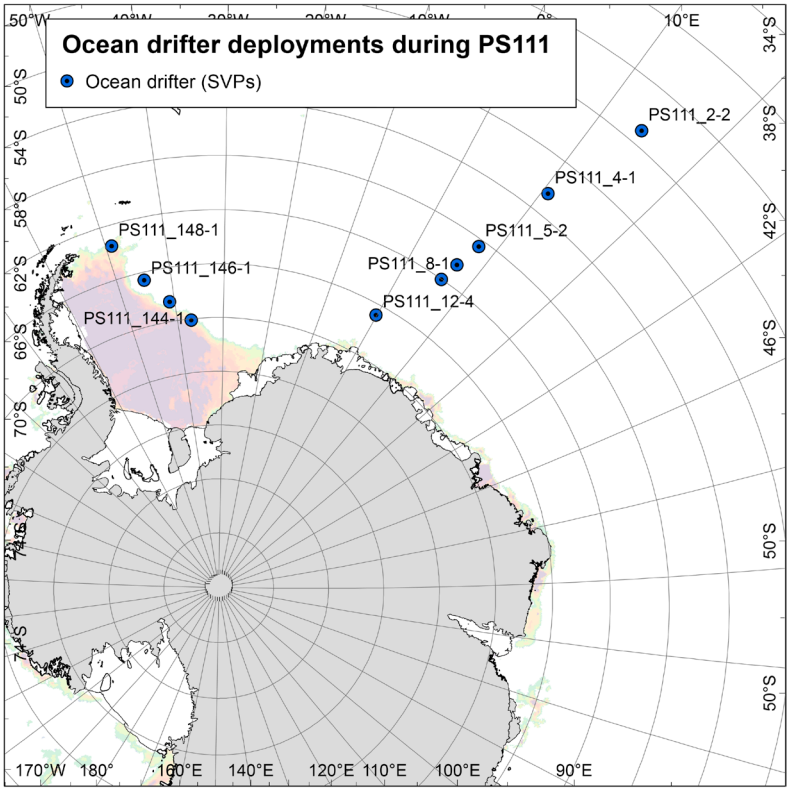

Fig. 6.11: Overview of all ocean drifters (Surface Velocity Profilers, SVPs) deployed by throwing over board during steaming

Preliminary (expected) results

All deployed ocean drifters report their position together with measurements of surface temperature and atmospheric pressure directly into the Global Telecommunication System (GTS). Thus, these data may directly be used for weather prediction and numerical model applications.

Data management

All buoys/drifters report their position and atmospheric pressure directly into the Global Telecommunication System (GTS). Furthermore, all data are exchanged with international partners through the International Program for Antarctic Buoys.

Tab. 6.9: List of all deployed ocean drifters with their initial deployment position and time.

Station	Label	Date	Time [UTC]	Name	IMEI	Latitude [min]	Longitude [min]
PS111_2-2	PS111_2-2_SVP_B	2018-01-23	01:05	2018_SVP_YOPP-SH_01	300234064824320	-44.9985	14.1178
PS111_4-1	PS111_4-1_SVP_B	2018-01-23	17:27	2018_SVP_YOPP-SH_02	300234064824310	-52.4994	10.6840
PS111_5-2	PS111_5-2_SVP_B	2018-01-25	01:55	2018_SVP_YOPP-SH_03	300234064824280	-58.5013	7.7416
PS111_7-1	PS111_7-1_SVP_B	2018-01-25	11:58	2018_SVP_YOPP-SH_04	300234064824070	-60.4989	6.7286
PS111_8-1	PS111_8-1_SVP_B	2018-01-25	19:38	2018_SVP_YOPP-SH_05	300234064824010	-62.0143	6.0925
PS111_12-4	PS111_12-4_SVP_B	2018-01-27	11:07	2018_SVP_YOPP-SH_06	300234064824360	-66.7767	-0.1152
PS111_143-1	PS111_143-1_SVP_B	2018-03-04	15:29	2018_SVP_YOPP_SH_07	300234063805020	-70.1065	-36.9990
PS111_144-1	PS111_144-1_SVP_B	2018-03-05	03:42	2018_SVP_YOPP_SH_08	300234063808050	-68.5341	-40.9997
PS111_146-1	PS111_146-1_SVP_B	2018-03-05	19:07	2018_SVP_YOPP_SH_09	300234063802040	-66.5818	-45.0073
PS111_148-1	PS111_148-1_SVP_B	2018-03-07	00:01	2018_SVP_YOPP_SH_10	300234063800040	-63.5199	-48.9753

References

Arndt S, Willmes S, Dierking W, Nicolaus M (2016) Timing and regional patterns of snowmelt on Antarctic sea ice from passive microwave satellite observations. Journal of Geophysical Research - Oceans, 121(8), 5916-5930, doi:10.1002/2015JC011504.

Cavalieri DJ, et al. (2012) A Comparison of Snow Depth on Sea Ice Retrievals Using Airborne Altimeters and an AMSR-E Simulator. IEEE Transactions on Geoscience and Remote Sensing, 50(8), 3027-3040, doi:10.1109/tgrs.2011.2180535.

Eicken H, Lange MA, Hubberten HW, Wadhams P (1994) Characteristics and distribution patterns of snow and meteoric ice in the Weddell Sea and their contribution to the mass balance of sea ice. Annales Geophysicae-Atmospheres Hydrospheres and Space Sciences, 12(1), 80-93, doi:10.1007/s00585-994-0080-x.

Griewank PJ, Notz D (2013) Insights into brine dynamics and sea ice desalination from a 1-d model study of gravity drainage. J. Geophys. Res., 118(7), 3370–3386, 10.1002/jgrc.20247.

Haas C, Thomas DN, Bareiss J (2001) Surface properties and processes of perennial Antarctic sea ice in summer. Journal of Glaciology, 47(159), 613-625, doi:10.3189/172756501781831864.

Kern S, Ozsoy-Çiçek B (2016) Satellite Remote Sensing of Snow Depth on Antarctic Sea Ice: An Inter-Comparison of Two Empirical Approaches. Remote Sensing, 8(6), 450, doi:10.3390/rs8060450.

Kern S, Ozsoy-Çiçek B, Worby AP (2016) Antarctic Sea-Ice Thickness Retrieval from ICESat: Inter-Comparison of Different Approaches. Remote Sensing, 8(7), 538, doi:10.3390/rs8070538.

Kwok R, Pang SS, Kacimi S (2017) Sea ice drift in the Southern Ocean: Regional patterns, variability, and trends. Elem Sci Anth, 5.

Lee SK, Volkov DL, Lopez H, Cheon WG, Gordon AL, Liu YY, Wanninkhof R (2017) Wind-driven ocean dynamics impact on the contrasting sea-ice trends around West Antarctica. Journal of Geophysical Research-Oceans, 122(5), 4413-4430, doi:10.1002/2016jc012416.

Nicolaus M, Haas C, Willmes S (2009) Evolution of first-year and second-year snow properties on sea ice in the Weddell Sea during spring-summer transition. Journal of Geophysical Research, 114(D17109), doi:10.1029/2008JD011227.

Notz D, Worster MG (2009) Desalination processes of sea ice revisited. J. Geophys. Res., 114, C05,006, doi: 10.1029/2008JC004885.

Notz D, Wettlaufer JS, Worster MG (2005) A non-destructive method for measuring the salinity and solid fraction of growing sea ice in situ. J. Glaciol., 51(172).

Parkinson, CL Cavalieri DJ (2012) Antarctic sea ice variability and trends, 1979-2010. Cryosphere, 6(4), 871-880, doi:10.5194/tc-6-871-2012.

Ricker R, Hendricks S, Helm V, Skourup V, Davidson M (2014) Sensitivity of CryoSat-2 Arctic sea-ice freeboard and thickness on radar-waveform interpretation. The Cryosphere, 8(4), 1607-1622.

Schwegmann S, Rinne E, Ricker R, Hendricks S, Helm V (2015) About the consistency between Envisat and CryoSat-2 radar freeboard retrieval over Antarctic sea ice. The Cryosphere Discuss., 9(5), 4893-4923, doi:10.5194/tcd-9-4893-2015.

Stammerjohn S, Massom R, Rind D, Martinson D (2012) Regions of rapid sea ice change: An inter-hemispheric seasonal comparison. Geophysical Research Letters, 39, doi:10.1029/2012gl050874.

Turner J, et al. (2014) Antarctic climate change and the environment: an update. Polar Rec, 50(3), 237-259, doi:10.1017/S0032247413000296.

Worby AP (1999) Observing operating in the Antarctic sea ice: A practical guide for conducting sea ice observations from vessels operating in the Antarctic pack ice.

7. ICE SHELVES IN A WARMING WORLD: FILCHNER ICE SHELF SYSTEM, ANTARCTICA

Adrian Jenkins[1], Stephen McPhail[2], Robert Templeton[2]

[1]BAS
[2]NOCS

Grant-No. AWI_PS111_00

Objectives

Ice shelves are the floating extensions of the Antarctic Ice Sheet that form where the ice is not thick enough to maintain contact with the seabed. They are sensitive to change both in the atmosphere above them and the ocean below. Any change can have far-reaching consequences because they regulate the flow of ice from the interior of the ice sheet (Alley et al., 2005), while their interaction with the ocean determines the fate of half the freshwater coming from the continent (Rignot et al., 2013). Temperatures that remain above freezing year-round and the enormous specific heat capacity of water make the ocean, through its role in melting ice from the underside of the ice shelves, the most significant agent of change. Understanding the processes that can deliver warmer ocean waters to the sub-ice-shelf environment is thus critical for projections of future ice loss from Antarctica and the resulting impacts on sea level and ocean circulation.

Critical to the transmission of an ocean warming signal beneath the ice are the currents that cross the ice front, a quasi-vertical wall of ice that extends up to ~500 m into the water. Since the currents experience planetary rotation and must conserve their angular momentum, they cannot readily cross such a step change in water column thickness. Thus the physical geometry puts a strong and as yet not fully understood constraint on the access of continental shelf waters to the sub-ice cavity. Early modelling studies suggested that complete isolation of the sub-ice cavity was possible (Determann & Gerdes, 1993), although that was probably an artefact of the simple model geometry, with more realistic setups showing inflows and outflows that vary in time (Jenkins et al., 2004). Nevertheless, recent observation and high-resolution modelling (Darelius et al., 2014) suggest a complex circulation near the Filchner Ice Front in which waters flowing north along the western coast of the sub-ice cavity turn along the ice front to exit the cavity at the eastern coast, while the currents immediately north of the ice front flow in the opposite sense, from east to west.

This project aimed to study that complex region near the ice front using an Autonomous Underwater Vehicle (AUV) to measure water properties and currents along a series of transects that cross the ice front, linking ship-based observations to the north with sub-ice observations in the south.

Work at sea

The AUV used for the study was one of the Autosub Long Range (ALR) vehicles that have been designed and built at the National Oceanography Centre Southampton. With an emphasis on long endurance, these vehicles carry a more limited instrument payload than other vehicles

in the Autosub fleet. For the PS111 work, ALR carried: a Seabird SBE-52 CTD, two Teledyne RDI 300 kHz ADCPs, one looking up and one looking down, and a Wetlabs ECO-FLNTU fluorometer/scatterometer that were all integrated into the central mission control and data storage systems. In addition, two free-running, internally-recording ancillary sensors were added: an RSI MicroRider microstructure probe, powered from the main ALR batteries, and an Idronaut OceanSeven 304 CTD, running on its own internal batteries. In this configuration, and running at a nominal speed of 0.65 m s^{-1}, ALR has an endurance of around 12 days, giving it a maximum range of around 650 km.

However, since these were to be the first under-ice deployments of ALR, we planned to run much shorter missions. Running beneath permanent ice cover, from a deployment and recovery point surrounded by moving pack ice, presents challenges beyond those encountered in open-water work. Once beneath the surface, safe resurfacing requires communication from the ship, from where ALR can be redirected, if necessary, to an area of ice-free water. An inability to surface means that the dead-reckoning navigation, based on magnetic compass heading and ADCP speed over ground, cannot be up-dated with GPS fixes, as it would be in normal operations. So for our PS111 missions we had to be confident that the dead-reckoning navigation would be sufficiently accurate to bring ALR close enough to the recovery waypoint that it would be within range of the acoustic telemetry system, required to direct it to the surface. In addition, the accuracy of the under-ice navigation, using the top-track speed from the upwards-looking ADCP, could not be properly tested until ALR had successfully tracked off a fixed upper surface.

On 2018-02-06, ALR successfully completed a 6 hour test mission (M45) in sheltered, open water of about 400 m depth near the Brunt Ice Shelf (Fig. 7.1). With all systems checked, ALR was ready for the first sub-ice science mission (M46), beneath Ronne Ice Shelf on 2018-02-09. The planned track ran along the western flank of Berkner Bank from a point 5 km north-east of the ice front to a point 20 km beneath the ice (Fig. 7.1). The location was chosen because a core of relatively warm Modified Weddell Deep Water is typically found along that part of the ice front. ALR was programmed to maintain a clearance of 80 m from the seabed on the way to and from the ice front, and to alternate between stretches of bottom tracking and top tracking 80 m below the ice base while beneath the ice shelf, giving periodic water column profiles. Critically, in this region of high tidal currents, M46 was timed to coincide with neap tides. Following the launch and dive, ALR was monitored for 4 hours before being sent on the 20-hour mission beneath the ice at around 18:30. Contact was re-established at around 15:00 on 2018-02-10 and ALR found to be only about 300 m from the recovery waypoint. Surfacing and recovery took about 1 hour.

A second mission beneath Ronne Ice Shelf was planned for 2018-02-11, in Ronne Depression. However, the narrowness of the shore lead and the thickening cover of new ice, coupled with the additional navigational uncertainty created by the deeper water column, entailing longer times out of both top track and bottom track ranges, presented significant challenges. In the absence of a complete analysis of ALR performance, particularly the top track navigation, the decision was taken to abort the mission. While ice conditions remained more favourable further to the east, by the time *Polarstern* was back in the wider shore lead the strength of the tidal currents was becoming a significant concern. That and the developing ice cover meant that no further missions were planned for Ronne Ice Shelf.

Nevertheless, following continued analysis of M46 data, an inspection of ice conditions in front of Filchner Ice Shelf, and a favourable weather forecast suggesting that the shore lead would stay open, albeit with a covering of new ice, the decision was taken to attempt the top priority mission beneath Filchner Ice Shelf (Fig. 7.1). The aim was to link the ice front observations with the FNE moorings beneath the ice shelf, but the fast ice in front of the ice shelf put the

mooring locations out of reach in the time available. The track was planned to start 3 km north of the fast ice edge and extend to a point 20 km beneath the ice shelf, following the eastern flank of Filchner Depression towards the site of mooring FNE1. That gave a total, each-way track length of 55 km and a nominal mission duration of 48 hours.

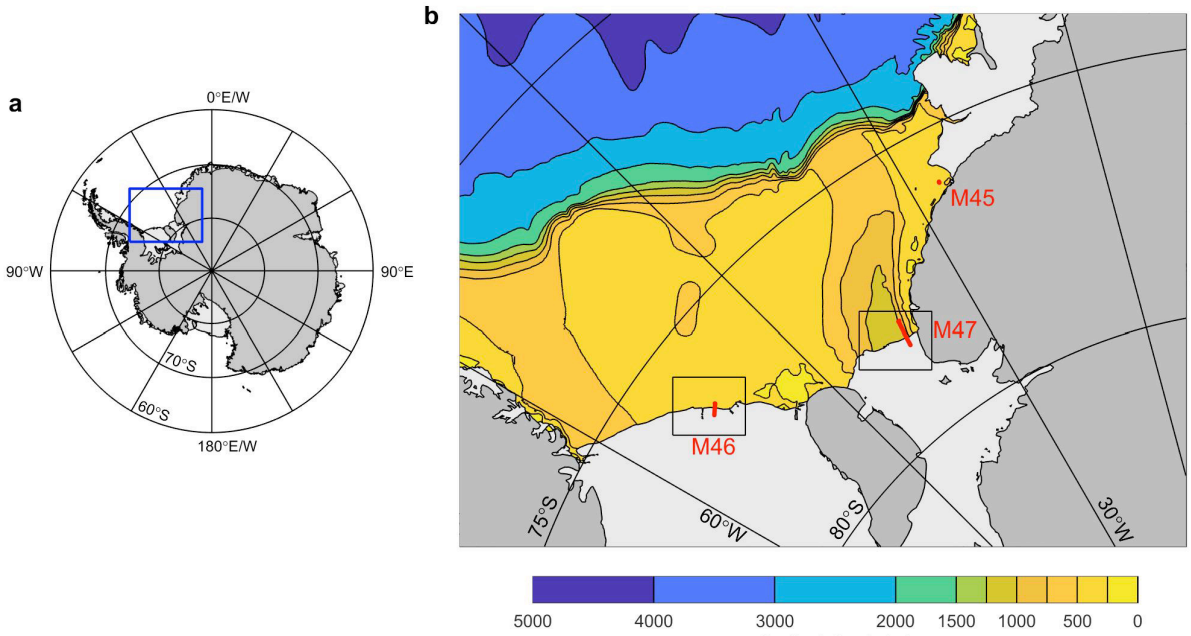

Fig. 7.1: (a) Map of Antarctica showing ice sheet (darker shading), ice shelves (lighter shading) and study area (outlined in blue). (b) Enlargement of study area showing bathymetry (Fretwell et al., 2013) and routes of ALR missions M45, M46 and M47. Boxes around M46 and M47 indicate the areas enlarged in Fig.s 7.2 and 7.3, respectively.

At around 17:30 on 2018-02-21, ALR was launched on M47 through a 150 m wide hole in the ice cover created by *Polarstern*. Following the dive, the 4-hour testing phase of the mission included an out and back run to 2 km distance from the ship to test the range of the acoustic telemetry and GAPS USBL tracking. If the working range of the tracking and telemetry systems had not been found to be significantly better than 1 km, the mission would have been aborted once ALR was back at the location of the ship. In the event, the telemetry range was found to be around 2 km, so following the completion of the 4-hour test, ALR was sent on its way for a 48 hour mission beneath the fast ice and ice shelf.

Returning to the recovery waypoint on 2018-02-23, *Polarstern* re-establised contact with ALR, located about 750 m from the waypoint, at around 21:00. The ship broke up the ice over the position of ALR and attempted to clear the broken ice away. Although the area of broken ice was ~1 km across, the ice free region was no more than a few hundred metres. ALR was brought to 200 m depth so that the ice could be cleared more effectively over its anticipated surfacing point. However, the difficulty of moving the ship in ice with the GAPS USBL system deployed through a moon pool and the slow drift of ALR in the currents necessitated a different approach. ALR was given a navigation offset to guide it to the open water beside the ship and then the signal to surface. The final recovery was hampered a little by the accumulation of new ice in the area cleared by *Polarstern*, but ALR was back on deck about 4 hours after the initial contact was made. The completion of M47 brought the ALR work on PS111 to a successful conclusion.

Preliminary (expected) results

Preliminary results from M46 are shown in Fig. 7.2. The launch site was close to the location of a Norwegian mooring, R2, which recorded between 1993 and 1995 (Foldvik et al., 2001), and a number of PS111 CTD stations. The warmest water encountered under the ice shelf was warmer than anything sampled along the ice front, although higher temperatures still were recorded on occasions at the R2 mooring site. The warm inflow is clearly highly variable, possibly because of eddying. The highest temperatures were recorded at different points on the outbound and return legs of the mission. That could reflect tidal displacement of the water mass or the movement of an eddy. The recorded currents give no clear indication of eddy activity, but there could yet be tidal contamination in the detided currents. Tidal currents were obtained from the CATS02.01 tidal model output (Padman et al., 2002) but because the ice front is displaced in the model domain, relative to its position at the time of PS111, there could be significant biases in the solutions.

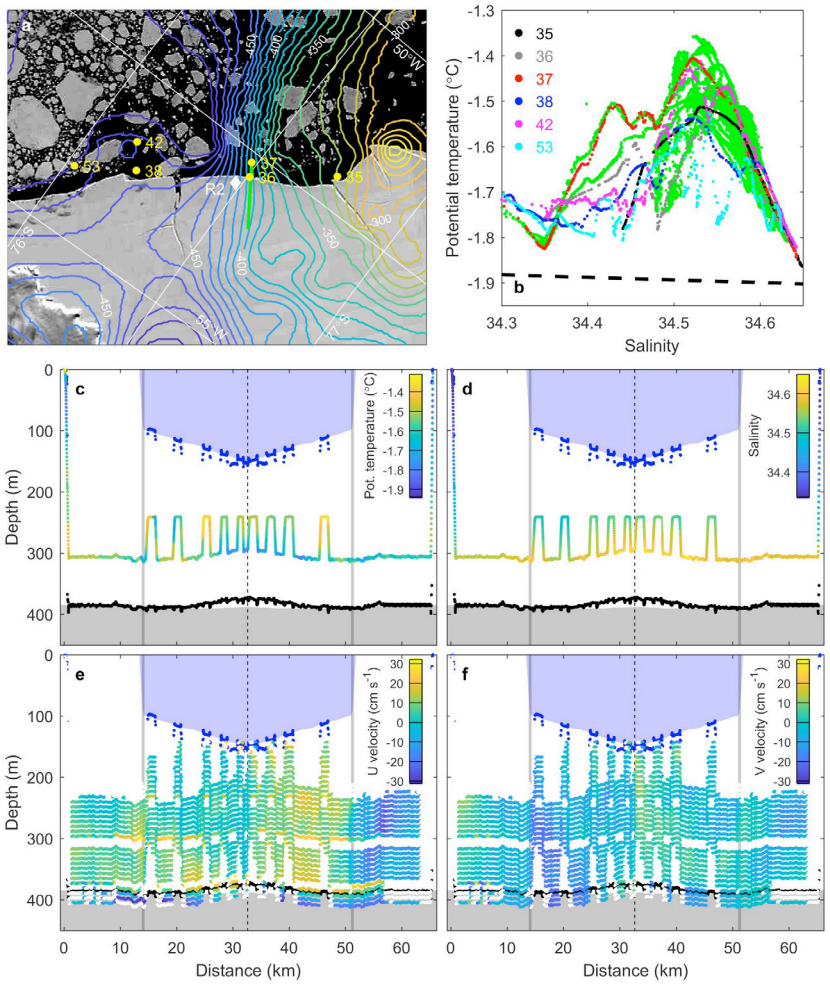

Fig. 7.2: (a) Modis image from 2018-02-08 overlain with contours of seabed elevation (m), track of ALR mission M46 (green), PS111 CTD stations (yellow circles, numbered) and R2 mooring (white diamond). (b) Potential temperature versus salinity diagram for data from ALR mission M46 (green) and PS111 CTD stations (colour-coded by station number). (c) Potential temperature, (d) salinity, (e) along-track and (f) across-track velocity components recorded along track of M46. Blue shading indicates the ice shelf and grey the seabed as extracted from BEDMAP2 grids (Fretwell et al. 2013). Blue and black dots indicate, respectively, ice base and seabed inferred from ALR ADCP range data. Grey, solid and black, dashed vertical lines show, respectively, where ALR crossed the ice front and turned at the farthest point. Along-track (U) and across-track (V) velocities are defined as positive in the direction of the distance axis and into the page, respectively.

Preliminary results from M47 are shown in Fig. 7.3. The launch site was close to a number of PS111 CTD stations and the turning point was about 25 km short of sub-ice-shelf mooring FNE1. Between the initial dive and the final resurfacing ALR sampled only Ice Shelf Water (ISW) with temperatures lower than -2.15°C. Two classes of ISW were found, with slightly different source waters. The deeper, slightly warmer class was also found at all the nearby ice front CTD stations. The lowest temperatures encountered in the cavity, near the ice shelf base, were also recorded at CTD stations to the east and west of the M47 track, but not at stations 89 and 90. Detided currents (with the caveat mentioned above) suggest that the coldest ISW was flowing towards the ice front and to the west. Currents recorded beneath the fast ice suggest that the deeper ISW was flowing into the cavity. Backscatter data from the upward-looking ADCP suggest that there may have been frazil ice crystals in the upper water column. The temperatures and salinities recorded at the depth of ALR would give supercooling *in-situ* about 60 m above its track.

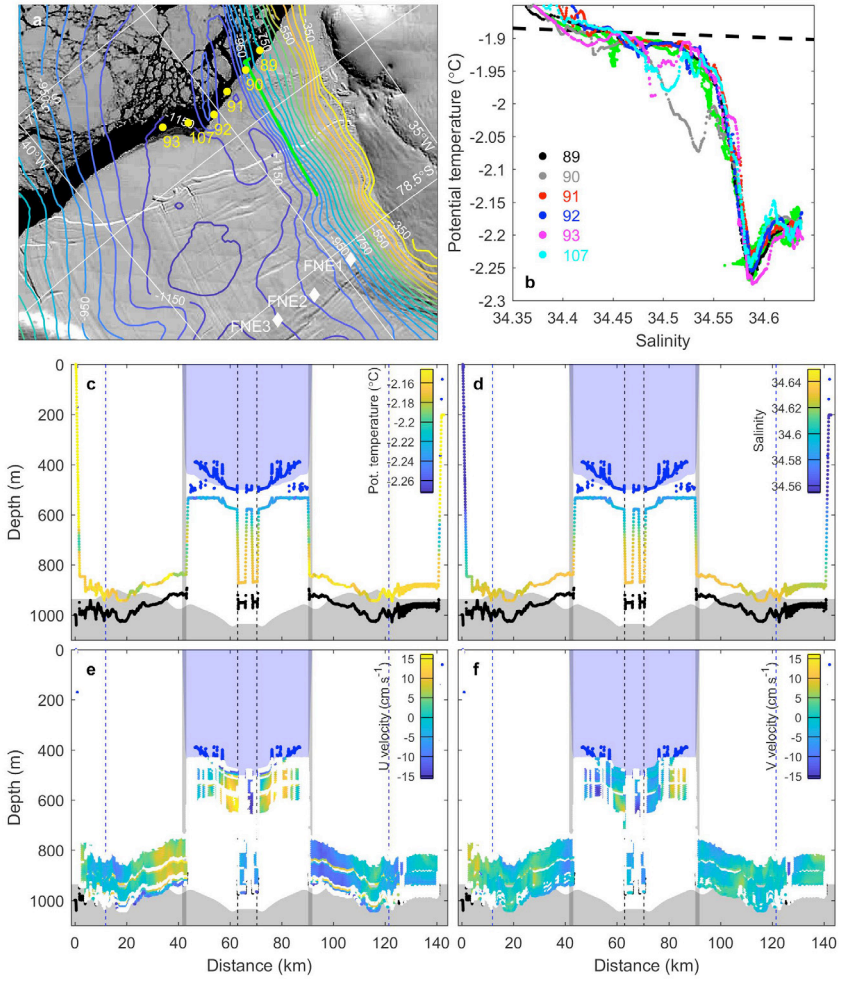

Fig. 7.3: (a) Modis image from 2018-02-20 overlain with contours of seabed elevation (m), track of ALR mission M47 (green), PS111 CTD stations (yellow circles, numbered) and sub-ice-shelf moorings (white diamonds). (b) Potential temperature versus salinity diagram for data from ALR mission M47 (green) and PS111 CTD stations (colour-coded by station number). (c) Potential temperature, (d) salinity, (e) along-track and (f) across-track velocity components recorded along track of M47. Blue shading indicates the ice shelf and grey the seabed as extracted from BEDMAP2 grids (Fretwell et al. 2013). Blue and black dots indicate, respectively, ice base and seabed inferred from ALR ADCP range data. Grey, solid and black, dashed vertical lines show, respectively, where ALR crossed the ice front and turned at the farthest point. Along-track (U) and across-track (V) velocities are defined as positive in the direction of the distance axis and into the page, respectively.

Following post-cruise recalibration of the sensors these data will be reprocessed. The results will then be used for processing of the microstructure data, only a small subset of which has been processed so far to check the operation of the sensors. The final datasets, when combined with the nearby PS111 ice front CTDs and the sub-ice and historical mooring data should give new insight into the processes by which warm water flows beneath Ronne Ice Shelf and into the exchange of ISW across the Filchner Ice Front.

Data management

The ALR work on PS111 produced about 5 Gbyte of navigation, control and sensor data, the largest part of which comprised the microstructure data. Multiple copies have been made and will be and shipped north via different routes. Initial processing and quality control was completed on *Polarstern*, while final processing, following post-cruise re-calibration of sensors, will be completed in the UK. Data will be archived at the British Oceanographic Data Centre, with unrestricted access after two years.

References

Alley RB, Clark PU, Huybrechts P, Joughin I (2005) Ice-sheet and sea-level changes. Science, 310, 456–460, doi: 10.1126/science.1114613.

Darelius E, Makinson K, Daae K, Fer I, Holland PR, Nicholls KW (2014) Hydrography and circulation in the Filchner Depression, Weddell Sea, Antarctica. Journal of Geophysical Research Oceans, 119, 5797–5814, doi: 10.1002/2014JC010225.

Determann J, Gerdes R (1993) Melting and freezing beneath ice shelves: implications from a three-dimensional ocean-circulation model. Annals of Glaciology, 20, 413–419.

Foldivk A, Gammelsrød T, Nygaard E, Østerhus S (2001) Current measurements near Ronne Ice Shelf: Implications for circulation and melting. Journal of Geophysical Research Oceans, 106, 4463–4477.

Fretwell P., et al. (2013) Bedmap2: improved ice bed, surface and thickness datasets for Antarctica. The Cryosphere, 7, 375–393.

Jenkins A, Holland DM, Nicholls KW, Schröder M, Østerhus S (2004) Seasonal ventilation of the cavity beneath Filchner-Ronne Ice Shelf simulated with an isopycnic coordinate ocean model. Journal of Geophysical Research Oceans, 109, C01024, doi: 10.1029/2001JC001086.

Padman, L, Fricker HA, Coleman R, Howard S, Erofeeva S (2002), A new tidal model for the Antarctic ice shelves and seas, Annals of Glaciology, 34, 247–254.

Rignot E, Jacobs S, Mouginot J, Scheuchl B (2013) Ice-shelf melting around Antarctica. Science, 341, 266–270, doi: 10.1126/science.1235798.

8. HYDROACOUSTICS

Jan Erik Arndt[1], Patricia Slabon[1], Anne Braakmann-Folgmann[1]

[1]AWI

Grant-No. AWI_PS111_00

Objectives

Knowledge of the seafloor morphology is essential basic information for various scientific disciplines of Antarctic research, i.e. marine geology, oceanography, biology and glaciology. Multibeam bathymetric surveys are the state-of-the-art technique to acquire high resolution seafloor data by insonifying a swath below a research vessel. In the southern Weddell Sea Embayment (WSE) multibeam acquisition has been carried out during several expeditions, predominantly as 'en route' measurements during transits but not as systematic surveys. Large data gaps still exist both in deep water and especially on the shallow continental shelf (Fig. 7.1). However, only detailed mapping of the seafloor morphology on the continental shelf can reveal glacial bedforms that can be used for reconstructing past grounded ice-sheet extent, flow pattern, bed conditions and style of retreat (e.g. Ó Cofaigh et al., 2008; Graham et al., 2009; Lavoie et al., 2015; Slabon et al., 2016; Arndt et al., 2017a). Therefore, these morphological features provide information on past ice sheet dynamics which is crucial for improving ice-sheet models (e.g. DeConto and Pollard, 2016).

Due to sparse data coverage in the remote southern WSE with its harsh ice conditions, its glacial history still remains poorly known. Hillenbrand et al. (2014) reviewed studies based on glacial-geological records in the study area and developed two alternative scenarios for the Last Glacial Maximum (LGM) ice sheet extent: 1) geomorphological and radiocarbon data suggest an ice sheet extension at least close to the shelf edge, 2) surface exposure age results from rock outcrops surrounding the Filchner-Ronne Ice Shelf show only minor thickening of ice and therefore suggest that ice did not ground in the deepest parts of the troughs. A recent investigation of new swath bathymetry, sub-bottom profiling data and sediment cores from the outer shelf part of Filchner Trough suggests that the trough was filled by a highly dynamic palaeo-ice stream that did not reach its maximum extent during the LGM but in the early Holocene (Arndt et al., 2017b). A possible mechanism for this behavior is the interplay of the West Antarctic Ice Sheet with the East Antarctic Ice Sheet in the hinterland that possibly alternatingly drained ice trough Filchner Trough. Pre-dominantly single track lines of multibeam data directly in front of the ice shelf in Ronne Trough and Hughes Trough revealed the presence of glacial lineations on the seafloor and, hence, streaming ice at some time in the past (Stolldorf et al., 2012). A more comprehensive image of glacial landforms and, hence, the past extent and dynamics of the ice in these troughs remains unresolved until new data is acquired. These observations highlight, that the LGM to Holocene glacial history in the study area is complex and still poorly known. More data is needed to better understand the past ice sheet system and the processes involved.

In addition to an improved knowledge on glacial landform distribution and therefore the past ice sheet evolution, the acquired data will refine future regional bathymetric compilations, i.e. new versions of the International Bathymetric Chart of the Southern Ocean (IBCSO) (Arndt et

al., 2013). These regional bathymetric models then will be used to update global bathymetric compilations like the General Bathymetric Chart of the Ocean (GEBCO) (Weatherall et al., 2015). Apart from these post-cruise products, the bathymetric data are also essential for other working groups on board to plan the deployment of gear and after sampling to set punctual information into relation to its surrounding environment.

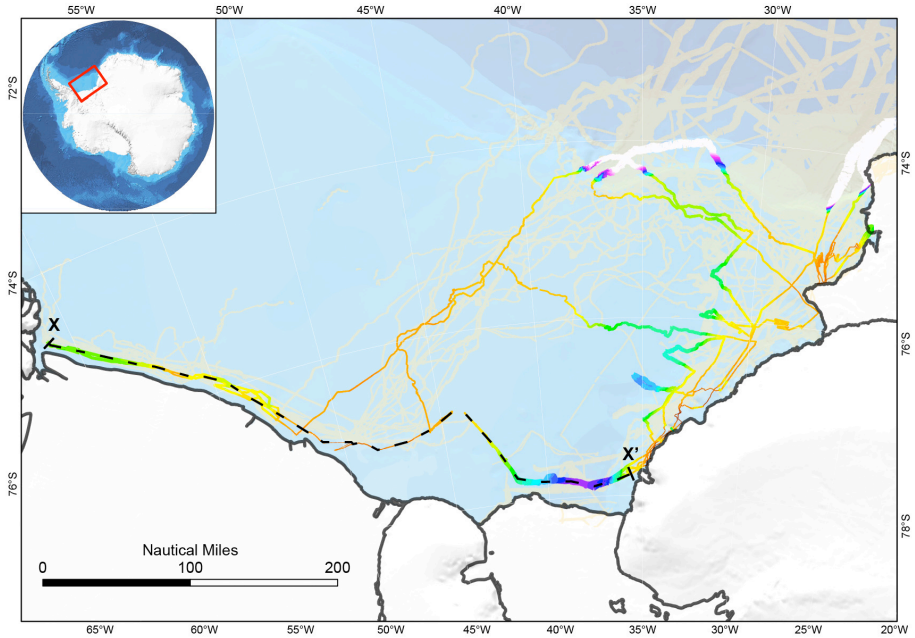

Fig. 8.1: Overview map of the research area showing color-coded collected multibeam bathymetry data, yellow semi-transparent area shows multibeam coverage available before PS111; the dashed line indicates the location of a cross-profile shown in Fig. 8.2.

Work at sea

The hull-mounted *Teledyne Reson Hydrosweep DS3* multibeam echosounding system (~16 kHz, up to 960 beams) had been used to collect swath bathymetric data. The system was controlled using the programme *Hydromap Control*. Live data visualisation was performed with the *Hypack 2016* software package. The data was stored in ASD format using the software *Parastore*. Subsequent data processing and preliminary cleaning was performed with the *CARIS Hips and Sips* software. For further data visualization, preparation of working maps, and track planning we used *ESRI ArcGIS*.

The *Teledyne Reson Parasound System DS3 (P70)* was used to collect sub-bottom profiling data. This system uses the parametric effect by transmitting two acoustic signals with slightly differing frequencies. During expedition PS111, 18 kHz were used as the Primary High Frequency and 4 kHz as the Secondary Low Frequency. The combined signal has a beam width of ~4.5°. The system was controlled using the program *Hydromap Control*. Live data visualization and data storage was performed with the *Parastore* software. Online prints from *Parastore* were used for later data visualization.

Data acquisition with both systems took place during all times of transit and was switched off during station time and in times when the ship was not moving for longer periods, e.g. when it was stuck in sea-ice. Before switching the systems back on, we conducted a Marine Mammal Watch for at least 15 min to secure that no marine mammal was within 100 m radius to the

ship. After the systems were switched off for more than 30 min the systems were started in a Whale Warning Mode. The systems were controlled in 24/7 shifts.

The acquired bathymetric and sub-bottom profiler data were directly investigated for seafloor features that are suitable targets for further geological investigation (see also chapter 14 – Marine Geology).

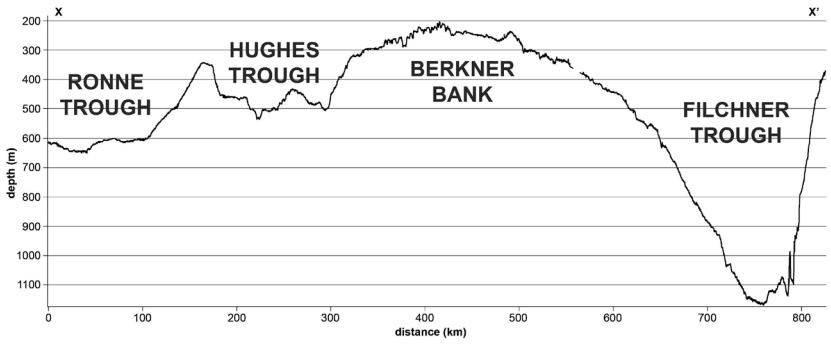

Fig. 8.2: Bathymetric cross-profile from Ronne Trough to Filchner Trough based on multibeam bathymetry acquired during PS111, for profile location see Fig. 8.1.

Preliminary (expected) results

The newly acquired swath bathymetry during PS111 covered an area of ~17,000 km² on the southern Weddell Sea embayment (Fig. 8.1). Due to favourable ice-conditions, it was possible for the first time to get a nearly complete cross-section of the Ronne, Hughes, and Filchner troughs with high-resolution swath bathymetry (Fig. 8.2). All acquired swath bathymetry data will be included in upcoming versions of IBCSO and subsequently GEBCO. Sub-bottom profiler data were acquired for more than 6000 km on the southern Weddell Sea continental shelf. Fig. 8.3 is a sample sub-bottom profiler image showing seafloor disturbed by grounded icebergs that eroded the seafloor and redeposited the sediments at their sides.

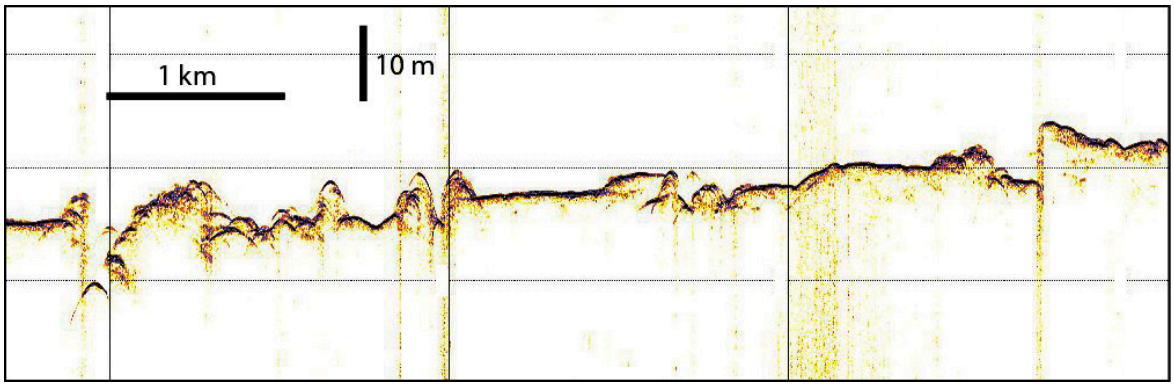

Fig. 8.2: Sample sub-bottom profiler data across a seafloor section covered by iceberg ploughmarks in outer Filchner Trough

The PS111 bathymetry revealed glacial landforms in all three major cross-shelf troughs, in smaller troughs off Luitpold Coast and in the Brunt Basin. The sub-bottom profiler data is showing the inner composition of the mapped landforms and reveals if they are draped by a sedimentary layer or not providing an indication of their formation chronology and post-formation environment. The glacial landforms were formed by the West Antarctic Ice Sheet in Ronne and Hughes Trough and by the East Antarctic Ice Sheet off Luitpold Coast and in the Brunt Basin. Filchner Trough is assumed to have been occupied by ice masses from both ice sheets depending on ice flow changes in the hinterland. These ice flow switches most probably are a result of different chronologic expansion and shrinking of the West Antarctic and East

Antarctic Ice Sheets. Therefore, we expect that the newly acquired data will help us improve our understanding of this dynamic ice sheet interaction. Thorough investigation of the PS111 hydroacoustic data will follow after its inclusion into a compilation of all available data that were acquired during the past decades on *Polarstern* and *RRS JC Ross* cruises acquired by AWI and BAS (Fig. 8.1). These results will then also be combined with results from sediment cores taken during PS111 and other cruises to constrain the sediment composition of these landforms and potentially constrain the time of landform formation and deglaciation (see also chapter 14 – Marine Geology).

Data management

All acquired bathymetric and sub-bottom profiler data will be stored in PANGAEA.

References

Arndt JE, Hillenbrand CD, Grobe H, Kuhn G, Wacker L (2017b) Evidence for a dynamic grounding line in outer Filchner Trough, Antarctica, until the early Holocene. Geology.

Arndt JE, Jokat W, Dorschel B (2017a) The last glaciation and deglaciation of the Northeast Greenland continental shelf revealed by hydro-acoustic data. Quaternary Science Reviews, 160, 45-56, doi:10.1016/j.quascirev.2017.01.018.

Arndt JE, Schenke HW, Jakobsson M, Nitsche FO, Buys G, Goleby B, Rebesco M, Bohoyo F, Hong J-K, Black J, Greku R, Udintsev G, Barrios F, Reynoso-Peralta W, Taisei M, Wigley R (2013) The International Bathymetric Chart of the Southern Ocean (IBCSO) Version 1.0 - A new bathymetric compilation covering circum-Antarctic waters. Geophysical Research Letters, 40, 3111-3117, doi:10.1002/grl.50413.

DeConto RM, Pollard D (2016) Contribution of Antarctica to past and future sea-level rise. Nature, 531, 591-597, doi:10.1038/nature17145.

Graham, A.G.C., Larter, R.D., Gohl, K., Hillenbrand, C.-D., Smith, J.A., Kuhn, G., 2009. Bedform signature of a West Antarctic palaeo-ice stream reveals a multi-temporal record of flow and substrate control. Quaternary Science Reviews, 28, 2774-2793, doi:10.1016/j.quascirev.2009.07.003.

Hillenbrand C-D, Bentley MJ, Stolldorf TD, Hein AS, Kuhn G, Graham AGC, Fogwill CJ, Kristoffersen Y, Smith JA, Anderson JB, Larter RD, Melles M, Hodgson DA, Mulvaney R, Sugden DE (2014) Reconstruction of changes in the Weddell Sea sector of the Antarctic Ice Sheet since the Last Glacial Maximum. Quaternary Science Reviews, 100, 111-136, doi:10.1016/j.quascirev.2013.07.020.

Lavoie C, Domack EW, Pettit EC, Scambos TA, Larter RD, Schenke HW, Yoo KC, Gutt J, Wellner J, Canals M, Anderson JB, Amblas D (2015) Configuration of the Northern Antarctic Peninsula Ice Sheet at LGM based on a new synthesis of seabed imagery. The Cryosphere, 9, 613-629, doi:10.5194/tc-9-613-2015.

Ó Cofaigh C, Dowdeswell JA, Evans J, Larter RD (2008) Geological constraints on Antarctic palaeo-ice-stream retreat. Earth Surface Processes and Landforms, 33, 513-525, doi:10.1002/esp.1669.

Slabon P, Dorschel B, Jokat W, Myklebust R, Hebbeln D, Gebhardt C (2016) Greenland ice sheet retreat history in the northeast Baffin Bay based on high-resolution bathymetry. Quaternary Science Reviews, 154, 182-198, doi:10.1016/j.quascirev.2016.10.022.

Stolldorf T, Schenke H-W, Anderson JB (2012) LGM ice sheet extent in the Weddell Sea: evidence for diachronous behavior of Antarctic Ice Sheets. Quaternary Science Reviews, 48, 20-31, doi:10.1016/j.quascirev.2012.05.017.

Weatherall P, Marks KM, Jakobsson M, Schmitt T, Tani S, Arndt JE, Rovere M, Chayes D, Ferrini V, Wigley R, (2015) A new digital bathymetric model of the world's oceans. Earth and Space Science, 2, doi:10.1002/2015ea000107.

9. FORAGING ECOLOGY OF ROSS AND WEDDELL SEALS IN THE WEDDELL SEA, ANTARCTICA

Marthán N. Bester[1], Mia Wege[1], [1]MRI
Horst Bornemann[2] [2]AWI

Grant-No. AWI_PS111_00

Objectives

The Ross seal (*Ommatophoca rossii*) is the least studied of Antarctic phocids (Bester & Hofmeyr, 2007; Southwell et al., 2008). In particular, estimating the circumpolar population status of the Ross seal has proved nigh impossible (Southwell et al., 2008; Bengtson et al., 2011). Their ranging behaviour is poorly known (Southwell et al., 2012) but they appear to forage beyond the pack-ice region outside of the breeding and moulting seasons (Blix & Nordøy, 1998, 2007; Arcalís-Planas et al., 2015), suggesting that they may be more pelagic rather than ice-loving (Nordøy & Blix, 2001; Arcalís-Planas et al., 2015). In this context, they are also described as “commuters” (Kooyman & Kooyman, 2009). Apart from the description of a few stomach contents and scats (Øritsland, 1977; Skinner & Klages ,1994), inferences from diving patterns (Bengtson & Stewart, 1997; Blix & Nordøy, 2007) and haulout data (Southwell et al., 2005) from only a few individuals, the diet and foraging behaviour of the Ross seal are largely unknown. As climate change is affecting the oceans (Levitus et al., 2000; Lyman et al., 2010, United Nations ,2017), it is widely anticipated that impacts on marine mammals will be mediated primarily via changes in prey distribution and abundance (Simmonds & Isaac, 2007; Siniff et al., 2008; Kovacs et al., 2012), which has management implications (Trathan & Agnew, 2010). Additionally, the physical environmental changes, including thinner and less extensive seasonal ice formation linked to increased water (and air) temperatures and ocean acidification will result in alterations to the forage base of marine mammals (Siniff et al., 2008). This presumably includes density and distributional shifts in their prey, as well as potential losses of some of their favoured prey species (Kovacs & Lydersen, 2008). This study therefore aimed to obtain a comprehensive picture of the Ross seal’s foraging activity in a three-dimensional environment and gain an understanding of seal behaviour in the context of both biological and physical parameters of the marine ecosystem (*cf*. Bowen, 1997) in the eastern and southwestern Weddell Sea, and in view of a proposed development of a Marine Protected Area (MPA) in the Weddell Sea (Teschke et al., 2013, 2016), managed by the Convention for the Conservation of Antarctic Marine Living Resources (CCAMLR). To this end, work carried out successfully from aboard SA *Agulhas II* along the east coast of the Weddell Sea in 2016 were continued towards the area around the Filchner Trough and the Filchner-Ronne Ice Shelves with RV *Polarstern* in 2018.

The project builds on earlier seal research initiatives of the South African National Antarctic Programme (SANAP) in the pack-ice off Dronning Maud Land (e.g. Condy, 1976; Skinner & Westlin-van Aarde, 1989; Bester & Skinner, 1991; Skinner & Klages, 1994; Bester & Odendaal, 2000; Bester et al., 2002), extend the pioneering work of Bengtson & Stewart (1997), Nordøy & Blix (2001, 2002) and Blix & Nordøy (2007), by continued use of technology such as Temperature and Depth Satellite Relay Data Loggers (SRDLs) (Boehme et al., 2009), stable-

isotope analyses (Rau et al., 1992; Aubail et al., 2011), and ship-board strip (Condy, 1977; Bester et al., 1995), and line-transect census studies (Bester & Odendaal, 2000; Bester et al., 2014) to characterise Ross seal distribution, diet and physical characteristics of the water column where they forage as a contribution to detailing the structure and function of the pack-ice ecosystem (Ackley et al., 2003) and beyond. Although inferring diet from diving behaviour, habitat use and stable isotope analyses from samples is indirect and circumstantial (Southwell et al., 2012), it will be enhanced by data from vomitus and opportunistic scat collections. Such a mix and match of various techniques is likely to improve our insight on ecosystem trophic dynamics in a spatial and temporal context.

In order to pursue alternative investigations should unfavourable sea ice conditions prevent access to Ross seals, we included a second sentinel species, the Weddell seal (*Leptonychotes weddellii*). Research on Weddell seals would extend the data collected during the earlier mission PS82 (2013/2014) and compliment the envisaged research on Ross seals. The reconciliation of data on the seals' diving behaviour with hydrographic features and available information on the occurrence and biomass of the seals' prey aims to contribute to the understanding of the upper trophic level interactions. Only five publications provide data on satellite-tracked Weddell seals within the Weddell Sea (Nicholls et al., 2008; Årthun et al., 2012; McIntyre et al., 2013; Böhme et al., 2016; Nachtsheim et al., in prep). Adult Weddell seal males should preferably be instrumented with satellite transmitters, as they are expected to remain in the investigation area throughout the year due to their "maritorial" behaviour.

Work at sea

Ross seals were investigated through deploying satellite-linked temperature-time-depth data loggers on them to measure diving and ranging behaviour of individuals (n = 2) and, through the use of stable isotope analyses on sampled blood, tissue, fur and whiskers, their diet. The corresponding investigation on Weddell seals (n = 5) extended the data set generated during PS82 (2013/2014) by deployments south of 77°S.

During PS111 we:

- deployed SPLASH10-309A satellite linked position, temperature time-depth recorders (Wildlife Computers, Redmond, USA) to determine horizontal movement, haul-out, diving behaviour and frequented water temperatures (n = 2, see Table 9.1),
- deployed SPOT-300s satellite position and temperature tags (Wildlife Computers, Redmond, USA) to determine horizontal movement, haul-out, and water temperatures to enlarge the satellite data pool for Weddell seal migration and diving behaviour (n = 5, see Table 9.1),
- collected whisker, hair, blood and tissue samples of Ross and Weddell seals (see Table 9.1)
- measured length and girth of each individual, and photographed with calibrated lenses to provide image data for post hoc calculation of the mass of each seal through photogrammetry (de Bruyn et al., 2009; see Table 9.1),
- collected associated oceanographic and meteorological data using the RV *Polarstern* on-board automated recording system DSHIP (WERUM, FRG),
- conducted ship-board detection surveys (Condy, 1977; Bester et al., 1995) to locate Ross seals (Table 9.2; Table 9.3) within an approximate distance of 400-500 m either side of the ship, and to broadly compare with results from ship-board strip surveys during earlier expeditions (e.g. Condy, 1976, 1977; Bester et al., 1995; Bester & Odendaal, 2000; Bester et al., 2017),

- used helicopter flights ahead of the RV *Polarstern* steaming direction within the pack-ice areas, preferably in the time slot 10:00 – 15:00 local apparent time (LAT), the most likely period during which the Ross seals are hauled out on the ice floes (Blix & Nordøy, 2007), to locate Ross and Weddell seals for temporary capture and instrumentation (see Table 9.4 and Fig. 9.1).

For instrumentation and biopsy sampling Ross seals were restrained physically (*c.f.* Arcalís-Planas, 2015) while Weddell seals were immobilized chemically with ketamine/xylazine combinations following the procedure as described in Bornemann et al. (1998) and Bornemann & Plötz (1993).

Tab. 9.1: Data on instrumentation of Ross and Weddell seals with satellite tags and sampling during PS111 (see at end of chapter).

Tab. 9.2: Data on ship-board and aerial Ross seal sightings during PS111

Obs. Nr.	Date	Time UTC]	Latitude	Longitude	Comment
1	2018-01-28	18:00	70°31.500'S	08°05.300'W	deployment
2	2018-01-31	23:00	71°06.743'S	13°39.208'W	deployment
3	2018-02-01		71°06.500'S	13°58.500'W	ice floe too small
4	2018-02-01		71°06.835'S	14°09.550'W	seal left ice floe
5	2018-02-01		71°07.600'S	14°13.900'W	seal left ice floe
6	2018-02-01	03:46	71°08.500'S	14°18.500'W	seal left ice floe
7	2018-02-01	04:57	71°15.114'S	14°32.055'W	seal left ice floe
8	2018-02-01	05:11	71°16.071'S	14°34.186'W	ice floe too small
9	2018-02-01	13:04	71°40.377'S	15°45.022'W	obs
10	2018-02-01	13:14	71°41.856'S	15°41.200'W	obs
11	2018-02-01	13:14	71°41.935'S	15°40.802'W	obs
12	2018-02-01	13:17	71°43.237'S	15°37.338'W	obs
13	2018-02-01	15:15	71°56.331'S	15°24.371'W	obs
14	2018-02-01	15:40			heli obs (flight 03)
16	2018-02-02	06:00	72°51.609'S	20°36.695'W	obs
17	2018-02-02	06:10	72°52.802'S	20°41.099'W	obs
19	2018-02-02	07:00	72°55.924'S	21°03.629'W	abondoned deployment
20	2018-02-02	08:35	72°57.300'S	21°03.600'W	obs
21	2018-02-02	18:50	72°08.264'S	25°36.097'W	obs
22	2018-02-02	21:25	73°19.629'S	25°57.955'W	obs
23	2018-02-03	14:24			heli obs (flight 04)
27	2018-02-08	12:09			heli obs (flight 06)

Tab. 9.3: Ship-board seal census observations during PS111

Date	Start Time [UTC]	End Time [UTC]	Latitude Start	Longitude Start	Latitude End	Longitude End
2018-01-28	10:00	17:00	70° 05.617’ S	006° 50.992’ W	70° 31.496’ S	008° 04.614’ W
2018-01-31	13:00	23:59	70° 56.644’ S	010° 31.599’ W	71° 06.656’ S	013° 39.596’ W
2018-02-01	00:00	07:00	71° 06.649’ S	013° 39.624’ W	71° 26.670’ S	015° 05.774’ W
2018-02-02	18:30	23:50	73° 07.166’ S	025° 34.266’ W	73° 41.974’ S	025° 44.079’ W
2018-02-02	03:00	06:00	72° 33.589’ S	018° 54.048’ W	72° 51.502’ S	020° 36.201’ W
2018-02-03	17:00	23:59	73° 43.277’ S	025° 45.946’ W	74° 31.652’ S	026° 59.464’ W
2018-02-04	00:00	06:00	74° 31.798’ S	026° 59.661’ W	75° 28.691’ S	028° 10.462’ W
2018-02-05	16:00	17:00	76° 02.805’ S	029° 44.875’ W	75° 57.241’ S	029° 08.162’ W
2018-02-07	15:45	23:59	74° 51.018’ S	033° 03.920’ W	74° 11.042’ S	036° 17.844’ W
2018-02-07	13:15	14:19	74° 50.190’ S	032° 31.151’ W	74° 51.507’ S	033° 00.964’ W
2018-02-07	10:00	11:30	74° 51.289’ S	031° 49.649’ W	74° 50.655’ S	032° 31.157’ W
2018-02-07	05:30	07:00	75° 06.544’ S	030° 32.538’ W	74° 59.233’ S	031° 08.706’ W
2018-02-08	00:00	21:00	74° 11.036’ S	036° 18.453’ W	75° 46.843’ S	044° 23.855’ W
2018-02-15	20:00	21:15	75° 22.001’ S	040° 58.130’ W	75° 23.665’ S	040° 48.329’ W
2018-02-15	10:46	12:56	75° 18.894’ S	041° 59.592’ W	75° 20.555’ S	041° 06.599’ W
2018-02-16	18:20	23:59	76° 03.093’ S	035° 42.051’ W	76° 08.727’ S	033° 39.415’ W
2018-02-16	14:09	16:15	76° 06.179’ S	036° 36.451’ W	76° 03.348’ S	035° 42.882’ W
2018-02-16	10:10	13:02	75° 58.583’ S	037° 45.973’ W	76° 05.683’ S	036° 38.210’ W
2018-02-16	02:00	08:30	75° 37.476’ S	039° 43.770’ W	75° 52.988’ S	038° 05.426’ W
2018-02-17	07:00	08:30	76° 08.692’ S	032° 40.386’ W	76° 10.339’ S	031° 42.783’ W
2018-02-17	02:55	04:25	76° 06.221’ S	033° 37.906’ W	76° 08.879’ S	032° 40.689’ W
2018-02-18	10:34	12:55	76° 38.415’ S	035° 25.490’ W	76° 47.203’ S	034° 22.043’ W
2018-02-18	06:00	07:40	76° 46.771’ S	034° 53.410’ W	76° 38.752’ S	035° 25.916’ W
2018-02-18	02:00	03:00	76° 49.968’ S	033° 15.737’ W	76° 47.882’ S	033° 56.730’ W
2018-02-19	13:00	13:28	77° 50.641’ S	036° 53.212’ W	77° 51.822’ S	037° 12.558’ W
2018-02-19	10:15	11:00	77° 49.233’ S	036° 25.349’ W	77° 49.262’ S	036° 25.274’ W
2018-02-19	09:30	10:05	77° 48.060’ S	036° 04.568’ W	77° 49.181’ S	036° 25.237’ W
2018-02-22	13:00	15:00	76° 40.084’ S	032° 50.511’ W	76° 32.193’ S	032° 56.251’ W
2018-02-22	10:30	12:15	77° 00.626’ S	033° 56.843’ W	76° 46.513’ S	033° 12.565’ W

Date	Start Time [UTC]	End Time [UTC]	Latitude Start	Longitude Start	Latitude End	Longitude End
2018-02-22	08:00	08:30	77° 03.997' S	033° 55.819' W	77° 00.573' S	033° 57.137' W
2018-02-22	05:45	07:00	77° 14.424' S	033° 54.439' W	77° 06.783' S	033° 56.183' W
2018-02-22	00:00	01:00	77° 42.944' S	035° 45.948' W	77° 42.621' S	035° 14.085' W
2018-02-25	06:00	23:59	75° 18.687' S	031° 14.558' W	74° 43.728' S	033° 03.107' W
2018-02-26	00:01	23:59	74° 43.758' S	033° 03.476' W	74° 27.365' S	037° 00.769' W
2018-02-27	06:00	23:00	74° 06.141' S	035° 01.132' W	74° 40.163' S	030° 38.025' W
2018-02-28	06:00	08:00	75° 04.912' S	028° 53.669' W	75° 06.514' S	028° 14.420' W
2018-03-01	06:00	08:00	74° 58.592' S	025° 37.951' W	75° 02.686' S	026° 03.513' W
2018-03-03	23:00	23:59	71° 57.675' S	030° 51.695' W	71° 51.385' S	031° 14.876' W
2018-03-03	07:00	20:00	73° 41.082' S	025° 32.275' W	72° 17.103' S	029° 44.268' W
2018-03-04	07:00	20:00	71° 03.695' S	033° 54.710' W	69° 36.508' S	038° 33.078' W
2018-03-06	07:00	17:00	64° 49.499' S	047° 16.492' W	63° 36.084' S	048° 46.390' W
2018-03-07	07:00	20:00	63° 28.543' S	051° 10.297' W	63° 21.112' S	054° 10.080' W

Tab. 9.4: Data on helicopter reconnaissance flights within pack and along fast ice areas to locate Ross and Weddell seals for instrumentation (see end of chapter)

Preliminary results

To obtain a comprehensive picture of the Ross seals' foraging activity in a three-dimensional environment it is necessary to understand seal behaviour in the context of both biological and physical parameters of the seals' marine environment in the Southern Ocean. The reconciliation of the obtained seal data with oceanographic data and the seasonal, inter-annual, and long-term changes in the marine habitat of seals will improve our understanding of the structure and dynamics of the Antarctic (and sub-Antarctic) marine ecosystem, contribute to the understanding of the status of Ross seal populations, and individual movements of Ross seals on a regional level. The comprehensive analysis and synthesis of biological and physical data perceivably could make an important contribution to determining relationships between hydrographic features, ocean currents, sea floor characteristics, prey dynamics, and the distribution and abundance of marine top predators. To this end we:

- investigated the ranging and diving behaviour of Ross seals in an area of high relative abundance in Atka Bay, off *Neumayer Station III*, and along the cruise track of the RV *Polarstern* past Kap Norvegica and along the Riiser-Larsen Ice Shelf into the deep Weddell Sea (see cruise track Fig. 9.1). Twenty Ross seals were encountered in the area bound by 26°W, 08°W (Table 9.2, Fig. 9.1C), and only two were instrumented. All other encounters were either during times when the ship was in transit (no stopping), or when ice floes were either too small for delivering personnel onto the ice, or the animals escaped into the sea before capture could be attempted. The tracks (Fig. 9.2A), diving

profiles (Fig. 9.3) and time spent at various temperatures within the water column (Fig. 9.4) over the first ~30 days after release are presented,

- collected biopsy, blood, hair, and whisker samples from the two animals, to research their diet through indirect (stable isotope analyses) means,
- compare their (and the other ice-breeding seal species') presence/absence along the cruise track of RV *Polarstern* with earlier ship-board surveys, to improve our knowledge of the way oceanographic conditions affect the rarest of the four true Antarctic species of seal breeding off the Princess Martha Coast, Dronning Maud Land (SA *Agulhas* II SANAE 55 expedition 2016), the Filchner Trough area (RV *Polarstern* PS111 expedition 2018), and deeper into the Weddell Sea towards the Filchner-Ronne Ice shelves, Antarctica, and
- extended the research on Weddell seals previously carried out during PS82 of the RV *Polarstern* to the southern Weddell Sea (Filchner Trough) in 2013/2014 (Bester et al., 2014, Bornemann et al., 2014) further into the Weddell Sea beyond 77°S by instrumenting individuals (n = 5) for satellite tracking (Fig. 9.2B) and whisker/fur sampling. Time spent at water temperatures within the water column (Fig. 9.4) during the first ~20 days after deployment are presented. Additionally, locations of Weddell seals within inlets observed during flights are shown in Fig. 9.5.

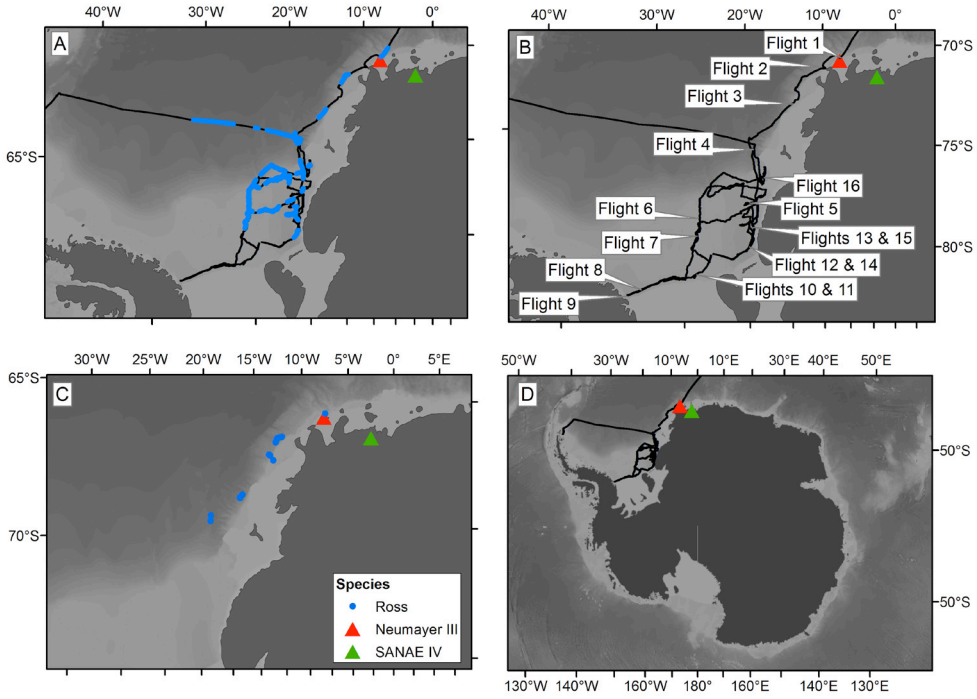

Fig. 9.1: A) PS111 Polarstern track (28 January - 8 March 2018) within the Weddell Sea shown with black and observation locations along the track are shown in blue. B) The locations of flights 1-16 along the Polarstern PS111 track. C) Sightings of Ross seals along the cruise track. D) The location of the PS111 Polarstern track within the Weddell Seal in relation to Antarctica. Background is Gebco 0.5 minute bathymetry.

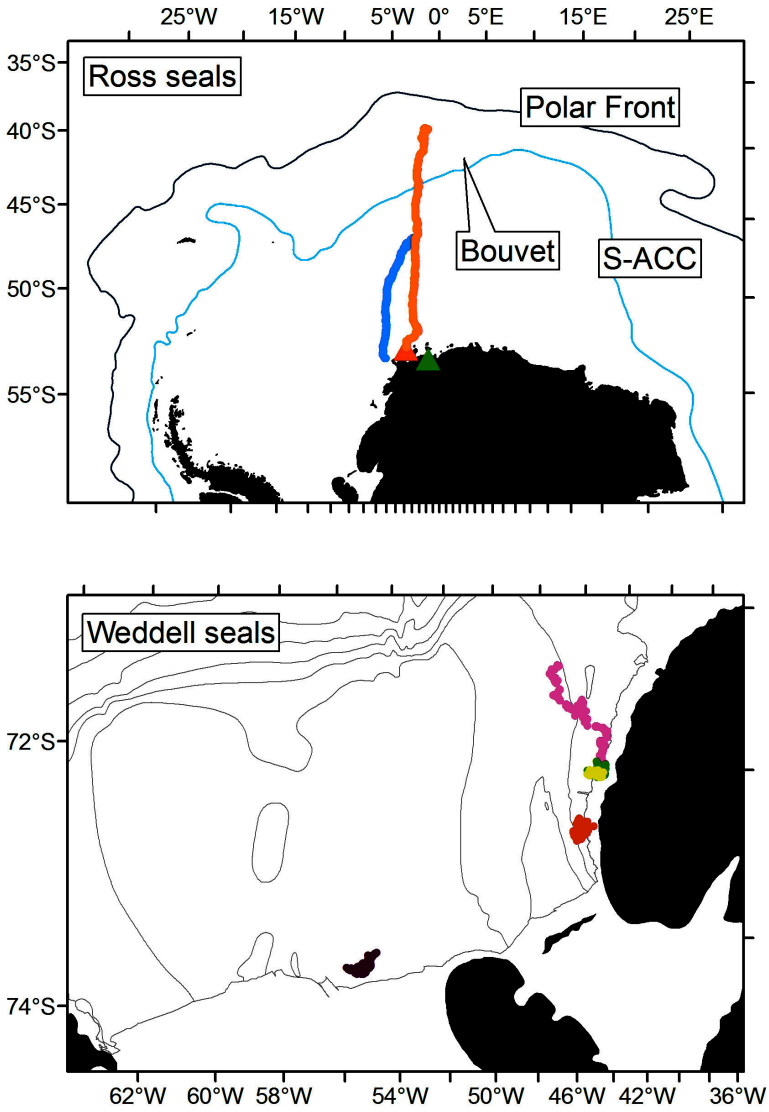

Fig. 9.2: A) At-sea locations of A) Ross seals (n=2) in relation to the Polar Front, Bouvet Island, and the southern boundary of the Antarctic Circumpolar Current (S-ACC) during the first ~30 days after deployment. B) At-sea locations of Weddell seals (n=5) during the first ~20 days after deployment. Different colours denote different individuals.

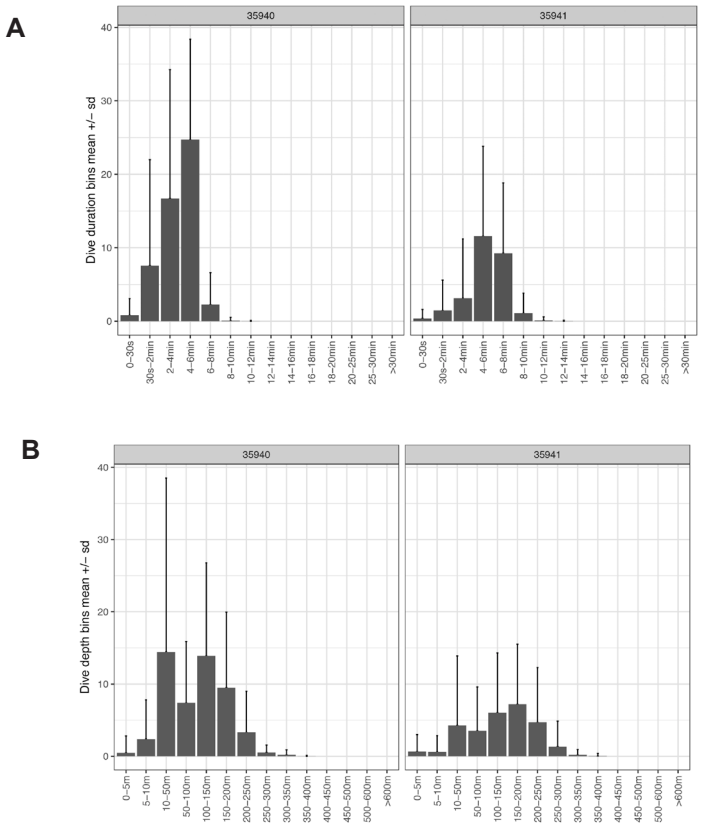

Fig. 9.3: Mean (± standard deviation) diving duration (A) and depth (B) within each of the histogram bins during the first ~30 days after deployment of the two instrumented Ross seals.

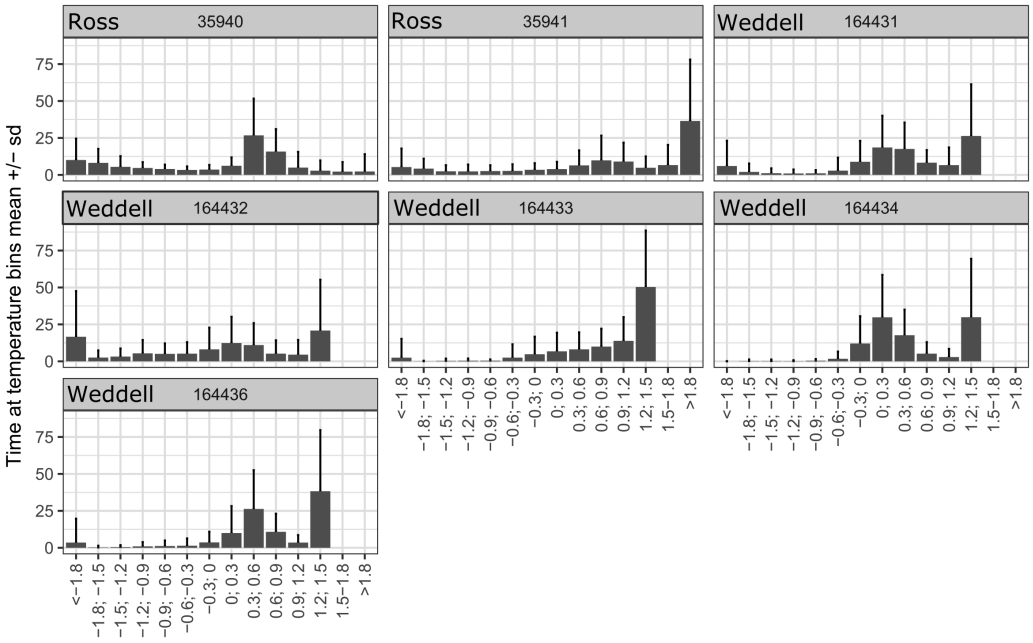

Fig. 9.4: Mean (± standard deviation) time spent at temperature within the water column for each of the histogram bins during the first ~20-30 days after deployment of the Ross (n=2) and Weddell seals (n=5).

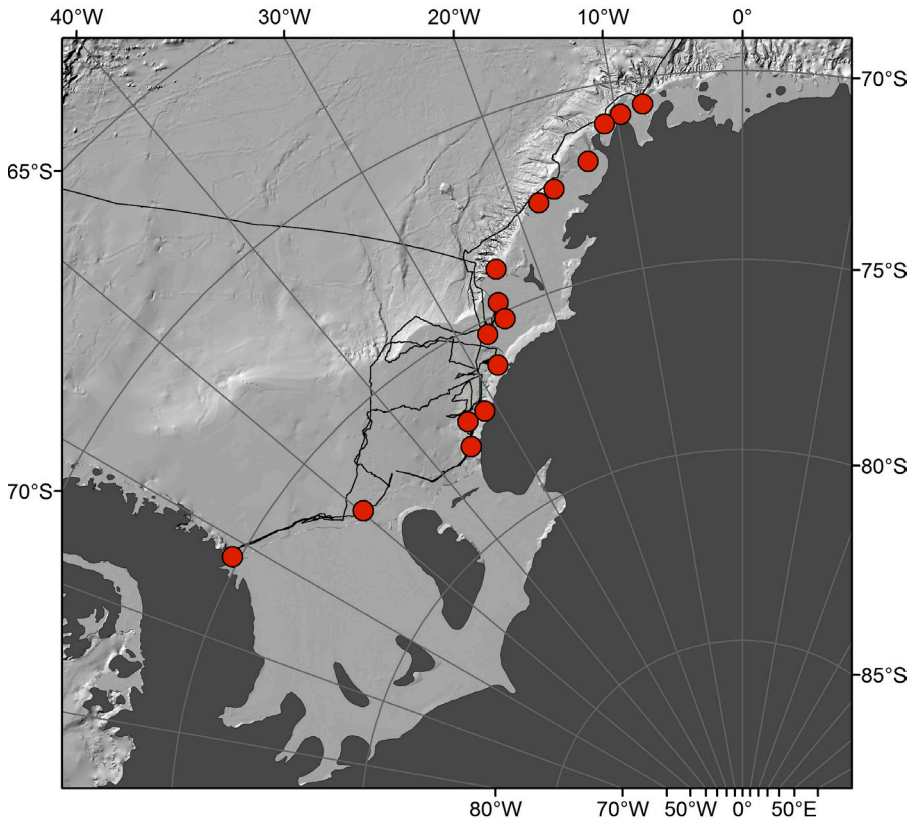

Fig. 9.5: Locations of Weddell seals observed within fast-ice inlets during the helicopter flights. The PS111 cruise track is shown in black.

Data management

Satellite linked SPLASH and SPOT tags (Wildlife Computers, Redmond, USA) transmit signals to the polar orbiting ARGOS satellites which relay received signals via the Centre de Localisations Satellites (CLS) in Toulouse, France, where the location data undergo a certain precision filtering algorithm before they are being harvested for further manufacturer-specific processing and cloud-based downloads. The latter is ensured weekly by FIELAX, Bremerhaven, Germany, for further post-processing and aggregation of data. The resulting primary data will be uploaded in PANGAEA following an established work-flow. The PANGAEA database contains a large set of circum-Antarctic oceanographic data relevant to the proposed project, and has already been extensively used for seal tracking data. All data and related meta-information will be made available in open access via the Data Publisher for Earth & Environmental Science PANGAEA (www.pangaea.de/) and will be attributed to a consistent project label denoted as “Marine Mammal Tracking” (MMT).

References

Ackley SF, Bengtson JL, Boveng P, Castellini M, Daly KL, Jacobs S, Kooyman GL, Laake J, Quetin L, Ross R, Siniff DB, Stewart BS, Stirling I, Torres JJ, Yochem PK (2003) A top-down, multidisciplinary study of the structure and function of the pack-ice ecosystem in the eastern Ross Sea, Antarctica. Polar Record, 39, 219-230.

Arcalís-Planas A, Sveegaard S, Karlsson O, Harding KC, Wahlin A, Harkonen T, Teilmann J (2015) Limited use of sea ice by the Ross seal (*Ommatophoca rossii*), in Amundsen Sea, Antarctica, using telemetry and remote sensing data. Polar Biology, 38, 445-461.

Aubail A, Teilmann J, Dietz R, Riget F, Harkonen T, Karlsson O, Rosing-Asvid A, Caurant F (2011) Investigation of mercury concentrations in fur of phocid seals using stable isotopes as tracers of trophic levels and geographical regions. Polar Biology, 34, 1411-1420.

Bengtson JL, Stewart BS (1997) Diving patterns of a Ross seal (*Ommatophoca rossii*) near the eastern coast of the Antarctic Peninsula. Polar Biology, 18, 214-218.

Bengtson, JL, Laake JL, Boveng P, Cameron MF, Stewart BS (2011) Distribution, density, and abundance of pack-ice seals in the Amundsen and Ross Seas, Antarctica. Deep-Sea Research Part II, 58, 1261-1276.

Bester MN, Ferguson JWH, Jonker FC (2002) Population densities of pack ice seals in the Lasarev Sea, Antarctica. Antarctic Science, 14, 123-127.

Bester MN, Hofmeyr GJG (2007) Ross Seal. In: Encyclopedia of the Antarctic, (Ed) B. Riffenburgh, Taylor & Francis Books Inc., New York, pp 815-816.

Bester MN, Odendaal PN (2000) Abundance and distribution of Antarctic pack ice seals in the Weddell Sea. In: Davison W, Howard-Williams C, Broady P (Eds). Antarctic Ecosystems: Models for Wider Ecological Understanding. Caxton Press, Christchurch, pp 51-55.

Bester MN, Oosthuizen WC, Steinhage D, Bornemann H (2014) Abundance and distribution of seals, pp 116-125 in Knust R, Schröder M (eds) The Expedition PS82 of the Research Vessel POLARSTERN to the southern Weddell Sea in 2013/2014, Berichte zur Polar- und Meeresforschung = Reports on polar and marine research, Bremerhaven, Alfred Wegener Institute for Polar and Marine Research, 680, 155 p.

Bester MN, Skinner JD (1991) South African research on Antarctic seals. South African Journal of Antarctic Research, 21, 165-166.

Bester MN, Wege M, Lübcker N, Postma M, Syndercombe G (2017) Opportunistic ship-based census of pack ice seals in eastern Weddell Sea, Antarctica. Polar Biology (submitted).

Blix AS, Nordøy ES (1998) Ross seal diving behaviour and distribution: A reassessment? New Zealand Natural Scientist, 23(Suppl), 14.

Blix AS, Nordøy ES (2007) Ross seal (*Ommatophoca rossii*) annual distribution, diving behaviour, breeding and moulting, off Queen Maud Land, Antarctica. Polar Biology, 30, 1449-1458.

Boehme L, Lovell P, Biuw M, Roquet F, Nicholson J, Thorpe SE, Meredith MP, Fedak M (2009) Technical note: Animal-borne CTD-Satellite Relay Data Loggers for real-time oceanographic data collection. Ocean Science, 5, 685-695.

Boehme L, Baker A, Fedak M, Årthun M, Nicholls K, Robinson P, Costa D, Biuw M, Photopoulou T (2016) Bimodal winter haul-out patterns of adult Weddell seals (*Leptonychotes weddellii*) in the Southern Weddell Sea. PLoS ONE 11(5): e0155817. doi:10.1371/journal.pone.0155817.

Bornemann H, Mohr E, Plötz J & Krause G (1998) The tide as zeitgeber for Weddell seals. Polar Biology 20:396-403.

Bornemann H & Plötz J (1993) A field method for immobilizing Weddell seals. Wildlife Society Bulletin 21:437-441.

Bornemann H, Bester MN, Oosthuizen WC, Schröder M, Márquez MEI, Mennucci JA, Daneri GA, Rogers T, Eisert R, Dorschel B, Hellmer HH (2014) Foraging behaviour of seals and oceanography, pp 125-135 in Knust R, Schröder M (eds) The Expedition PS82 of the Research Vessel POLARSTERN to the southern Weddell Sea in 2013/2014, Berichte zur Polar- und Meeresforschung = Reports on polar and marine research, Bremerhaven, Alfred Wegener Institute for Polar and Marine Research, 680, 155 p.

Condy PR (1976) Results of the third seal survey in the King Haakon VII Sea, Antarctica. South African Journal of Antarctic Research, 6, 2-8.

Condy PR (1977) Results of the fourth seal survey in the King Haakon VII Sea, Antarctica. South African Journal of Antarctic Research, 7, 10-13.

de Bruyn PJN, Bester MN, Carlini AR & Oosthuizen WR (2009) How to weigh an elephant seal with one finger: a simple three-dimensional photogrammetric application. Aquatic Biology, 5, 31-39

Kooyman MM, Kooyman GL (2009) History of pinniped studies in Antarctica. Aquatic Mammals, 35, 523–556.

Kovacs KM, Lydersen C (2008) Climate change impacts on seals and whales in the North Atlantic Arctic and adjacent shelf seas. Science Progress, 91, 117-150.

Kovacs KM, Aquilar A, Aurioles D, Burkanov V, Campagna C, Gales, N (2012) Global threats to pinnipeds. Marine Mammal Science, 28, 414-436.

Levitus S, Antonov JI, Boyer TP, Stephens C (2000) Warming of the world ocean. Science, 287, 2225-2229.

Lyman JM, Good SA, Gouretski W, Ishii M, Johnson GC, Palmer MD, Smith DM, Willis JK (2010) Robust warming of the global upper ocean. Nature, 465, 334-337.

Nachtsheim DA, Ryan S, Schröder M, Jensen L, Oosthuizen WC, Bester MN, Hagen W, Bornemann H (2018) Winter foraging hotspots of Weddell seals (*Leptonychotes weddellii*) in the southern Weddell Sea. Progress in Oceanography, in prep.

Nordøy ES, Blix AS (2001) The previously pagophilic Ross seal in now rather pelagic. Proceedings of the VIII SCAR International Biology Symposium, Amsterdam, The Netherlands, August 27-September 1, 2001, S5O14.

Nordøy ES, Blix AS (2002) Distribution and food consumption of Ross seals (*Ommatophoca rossii*) and leopard seals (*Hydrurga leptonyx*). In: Report of the Norwegian Antarctic Research Expedition 2000/01, J.G. Winther (ed.). Norsk Polarinstitutt Rapportserie, 120, 55-57.

Øritsland T (1977) Food consumption of seals in the Antarctic pack ice. In: Llano, G.A. (Ed.). Adaptations within Antarctic Ecosystems. Smithsonian Institute, Washington DC, 749-768.

Rau GH, Ainley DG, Bengtson JL, Torres JJ, Hopkins TL (1992) $^{15}N/^{14}N$ and $^{13}C/^{12}C$ in Weddell Sea birds, seals, and fish: implications for diet and trophic structure. Marine Ecology Progress Series, 84, 1-8.

Simmonds MP, Isaac SJ (2007) The impacts of climate change on marine mammals: early signs of significant problems. Oryx, 41, 19-26.

Siniff DB, Garrott RA, Rotella YJ, Fraser WR, Ainley DG (2008) Projecting the effects of environmental change on Antarctic seals. Antarctic Science, 20, 425–435.

Skinner JD, Westlin-van Aarde LM (1989) Aspects of reproduction in female Ross seals (*Ommatophoca rossii*). Journal of Reproduction and Fertility, 87, 67-72.

Skinner, JD, Klages NTW (1994) On some aspects of the biology of the Ross seal *Ommatophoca rossii* from King Haakon VII Sea, Antarctica. Polar Biology 14, 467-472.

Southwell C, Paxton CGM, Borchers D, Boveng P, Nordøy ES, Blix AS (2008) Estimating population status under conditions of uncertainty: the Ross seal in east Antarctica. Antarctic Science, 20, 123-133.

Southwell C (2005) Optimising the timing of visual surveys of crabeater seal abundance: haulout behaviour as a consideration. Wildlife Research, 32, 333-338.

Southwell C, Bengtson J, Bester MN, Blix AS, Bornemann H, Boveng P, Cameron M, Forcada J, Laake J, Nordøy E, Plötz J, Rogers T, Southwell D, Steinhage D, Stewart BS, Trathan P (2012) A review of data on abundance, trends in abundance, habitat use and diet of ice-breeding seals in the Southern Ocean. CCAMLR Science, 19, 49-74.

Teschke K, Bornemann H, Bombosch A, Brey T, Brtnik P, Burkhardt E, Dorschel B, Feindt-Herr H, Gerdes D, Gutt J, Hain S, Herata H, Jerosch K, Knust R, Kock KH, Pehlke H, Schluter M, Schwarzbach W, Siegel V, Strass V, van Opzeeland I, von Nordheim H. 2013. Progress report on the scientific data compilation and analyses in support of the development of a CCAMLR MPA in the Weddell Sea (Antarctica), SC-CCAMLR-XXXII, (BG/07), pp 1-29.

Teschke K, Beaver D, Bester M, Bombosch A, Bornemann H, Brandt A, Brtnik P, De Broyer C, Burkhardt E, Dieckmann G, Douglass L, Flores H, Gerdes D, Griffiths H, Gutt J, Hain S, Hauck J, Hellmer H, Herata H, Hoppema M, Isla E, Jerosch K, Kock KH, Krause R, Kuhn G, Lemke P, Liebschner A, Linse K, Miller H, Mintenbeck K, Nixdorf U, Pehlke H, Petrov A, Schröder M, Shust K, Schwegmann S, Siegel V, Thomisch K, Timmermann R, Trathan P, van de Putte A, van Franeker JA, van Opzeeland I, von Nordheim H & Brey T. 2016. Scientific background document in support of the development of a CCAMLR MPA in the Weddell Sea (Antarctica), Part A: General context of the establishment of MPAs and background information on the Weddell Sea MPA planning area. CCAMLR WG-EMM-15/38, 89 pp.

Trathan PN, Agnew D (2010) Climate change and the Antarctic marine ecosystem: an essay on management implications. Antarctic Science, 22, 387-398.

United Nations (2017) The First Global Integrated Marine Assessment, World Ocean Assessment I. Cambridge University Press, Cambridge, ISBN 9781316510018, 976 pp.

Tab. 9.1: Data on instrumentation of Ross and Weddell seals with satellite tags and sampling during PS111

Event label	Date	Time [UTC]	Latitude	Longitude	Device	Length [mm]	Girth [mm]	Sampling				Photo-grammetry	Duration [min]
								Whisk-ers	Hair	Blood	Biopsy		
PS1112018_ros_a_f_01	2018-01-28	18:00	70°31.500'S	08°05.300'W	Splash	1755	1002.5*	x	x	x	x		00:50
PS1112018_ros_a_m_02	2018-01-31	23:00	71°06.743'S	13°39.208'W	Splash	1720	860*	x	x	x	x		00:45
PS1112018_wed_a_f_01	2018-02-13	16:15	77°02.797'S	50°00.235'W	Spot	2450	1685	x	x			x	01:00
PS1112018_wed_a_f_02	2018-02-22	17:10	77°07.652'S	31°56.468'W	Spot	2480	1790	x	x			x	01:15
PS1112018_wed_a_f_03	2018-02-22	18:10	77°07.562'S	31°56.468'W	Spot	2640	2150	x	x			x	01:30
PS1112018_wed_a_f_04	2018-02-23	18:45	77°42.195'S	34°57.824'W	Spot	2550	1930	x	x			x	01:10
PS1112018_wed_a_m_05	2018-02-24	11:50	77°08.570'S	32°08.809'W	Spot	2560	1890	x	x			x	01:30
							* half circum-ference						

Tab. 9.4: Data on helicopter reconnaissance flights within pack and along fast ice areas to locate Ross and Weddell seals for instrumentation

Flight No	Date	Time start [UTC]	Time end [UTC]	Durat-ion	Primary flight purpose			Location (narrative)	Flight distance [nm]	Observation		
					seal obs	trans-port	ice obs			Ross seal	Weddell seal	Ice type
1	2018-01-29	10:33	11:12	00:39	x			Atka Bay	59			bay fast ice (fragmented)
2	2018-01-31	12:14	13:35	01:21	x			Long inlet	120		x	inlet fast ice
3	2018-02-01	15:14	16:59	01:45	x			Rampen and Christmas Tree inlet	58		x	inlet fast ice
4	2018-02-03	14:24	15:31	01:07			x	Bird flight (ice reconnaissence)	100	x		inlet fast ice (fragmented)
5	2018-02-04	14:48	16:31	01:43	x			Halley Ice	155		x	pack ice floes/inlet fast ice
6	2018-02-08	12:09	12:39	00:30			x	Ice Recce (Horst only)	45	x		pack ice floes
7	2018-02-08	17:12	17:35	00:23			x	Ice Recce (Horst only)	35			
8	2018-02-11	09:10	09:33	00:23			x	Ice Recce (Horst only)	35			
9	2018-02-11	18:15	19:23	01:08	x			Antarctica‘s Armpit	102		x	inlet fast ice
10	2018-08-13	09:28	09:52	00:24	x			Ronne coastal polynja/inlet	36			
11ai	2018-08-13	15:31	15:43	00:12	x			PS1112018_wed_a_f_01 outbound	14		x	inlet fast ice
11aii	2018-08-13	15:49	15:56	00:07		x		Lars inbound	11			
11bi	2018-08-13	17:49	17:57	00:08		x		Lars outbound	12			
11bii	2018-08-13	18:06	18:12	00:06		x		PS1112018_wed_a_f_01 inbound	13		x	inlet fast ice
12ai	2018-08-18	15:45	16:04	00:19	x			Failed Weddell deploy outbound	24		x	pack ice floes
12aii	2018-08-18	16:19	16:31	00:12		x		Michael inbound	23			
12bi	2018-08-18	16:58	17:07	00:09		x		Michael outbound	12			
12bii	2018-08-18	17:21	17:40	00:19		x		Failed Weddell deploy inbound	30		x	pack ice floes
13ai	2018-08-22	15:50	16:24	00:34	x			PS1112018_wed_a_f_02 & 03 outbound	50		x	inlet fast ice
13aii	2018-08-22	16:38	17:08	00:30		x		Michael inbound	50			
13bi	2018-08-22	19:31	20:06	00:35		x		Michael outbound	50			

Flight No	Date	Time start [UTC]	Time end [UTC]	Durat-ion	Primary flight purpose			Location (narrative)	Flight distance [nm]	Observation		
					seal obs	trans-port	ice obs			Ross seal	Weddell seal	Ice type
13bii	2018-08-22	20:23	20:58	00:35		x		PS1112018_wed_a_f_02 & _03 inbound	50		x	inlet fast ice
14ai	2018-08-23	17:50	17:59	00:09	x			PS1112018_wed_a_f_04 outbound	15		x	fast ice
14aii	2018-08-23	18:07	18:10	00:03		x		Lars inbound	5			
14bi	2018-08-23	19:18	19:30	00:12		x		Lars outbound	13			
14bii	2018-08-23	19:43	19:52	00:09		x		PS1112018_wed_a_f_04 inbound	13		x	fast ice
15ai	2018-08-24	11:11	11:25	00:14	x			PS1112018_wed_a_m_05 outbound	17		x	inlet/bay fast ice
15aii	2018-08-24	11:33	11:43	00:10		x		Lars inbound	14			
15bi	2018-08-24	14:18	14:34	00:16		x		Lars outbound	28			
15bii	2018-08-24	14:45	15:03	00:18		x		PS1112018_wed_a_m_05 inbound	28		x	inlet fast ice
16	2018-03-01	18:20	20:08	01:48	x			Last Ross seal scouting flight	162		x	pak ice floes/inlet fast ice
Sum				**16:28**					**1379**			

10. COMBINED EFFECTS OF TEMPERATURE AND ORGANIC MATTER AVAILABILITY ON DEGRADATION ACTIVITY BY ANTARCTIC BACTERIOPLANKTON

Klaus Jürgens[1], Christian Meeske[1] [1]LIO
Judith Piontek[2] (not on board) [2]GEOMAR

Grant-No. AWI_PS111_00

Objectives

Global warming poses new threats to marine ecosystems since rising seawater temperature potentially induces cascading effects in biogeochemical cycles and food webs. In Antarctic marine systems, low seawater temperature, and the availability of labile organic matter are major environmental constraints on bacterial growth and microbial degradation activity. However, temperature and the availability of resources for heterotrophic bacteria are expected to undergo considerable changes induced by climate warming combined with subsequent ice melt and changes in primary productivity. The relevance of these environmental changes for planktonic bacterial communities, organic matter processing and subsequent CO2 release is still unclear. The overarching goals of this project are (1) to assess bacterioplankton communities and their activities at low temperatures in the surface layer of the Weddell Sea, and (2) to explore the synergistic potential of temperature and the availability of labile organic matter in the regulation of heterotrophic bacterial degradation activity. Field sampling of the upper 100 m water column at different stations in the Weddell Sea and neighbouring areas, combined with on-board incubation experiments, were conducted in order to investigate bacterial community composition, bacterial productivity and remineralization activity, and its dependence on temperature and substrate supply. Previous microbiological studies revealed high shares of psychrotolerant bacterial isolates, suggesting a high responsiveness of bacterioplankton in the Weddell Sea to rising temperature (Delille, 1992; Helmke and Weyland, 1995). However, the temperature sensitivity of natural microbial communities, its spatial variability and the potential of increasing temperature to alter organic matter degradation is not fully understood yet (Kirchman et al., 2009).

Work at sea

During PS111, samples for microbiological and biogeochemical analysis were collected at 26 stations (Figure 10.1, Table 10.1). Three stations were along the transit to *Neumayer Station III*, and the others in the southern Weddell Sea in front of the Filchner and the Ronne Ice Shelf, and across an east/west transect through the Filchner Trough (Figure 10.2). The three transit stations in the vicinity of Maud Rise were added to the original station plan as here remnants of deep ocean convection in the water column, caused by the appearance of a large Weddell Polynya during the previous winter, were expected.

Tab. 10.1: CTD rosette stations taken during PS111. Depth indicates maximum bottom depth

Station/CTD cast	Date	Latitude	Longitude	Depth [m]
PS111_140-1	2018-03-01	75° 07.952’ S	026° 37.747’ W	341
PS111_137-2	2018-02-28	75° 28.200’ S	027° 06.720’ W	260
PS111_132-1	2018-02-27	74° 00.410’ S	032° 24.592’ W	1800
PS111_131-1	2018-02-26	74° 36.918’ S	036° 55.590’ W	387
PS111_123-1	2018-02-25	74° 56.646’ S	030° 59.188’ W	566
PS111_101-1	2018-02-18	76° 55.245’ S	043° 48.447’ W	397
PS111_89-1	2018-02-19	77° 49.262’ S	036° 25.266’ W	808
PS111_82-1	2018-02-18	76° 46.909’ S	033° 22.906’ W	556
PS111_74-1	2018-02-17	76° 12.824’ S	029° 40.487’ W	387
PS111_68-1	2018-02-16	76° 03.254’ S	035° 42.526’ W	747
PS111_62-1	2018-02-14	77° 04.111’ S	045° 38.999’ W	312
PS111_58-1	2018-02-13	77° 08.445’ S	048° 24.114’ W	251
PS111_51-1	2018-02-12	75° 08.902’ S	059° 04.747’ W	628
PS111_47-1	2018-02-11	74° 59.009’ S	060° 00.068’ W	661
PS111_40-3	2018-02-10	76° 00.070’ S	054° 14.362’ W	513
PS111_37-2	2018-02-09	76° 28.992’ S	052° 38.241’ W	382
PS111_33-1	2018-02-07	74° 50.493’ S	032° 31.000’ W	595
PS111_28-1	2018-02-05	75° 58.509’ S	028° 25.038’ W	356
PS111_22-1	2018-02-04	75° 53.985’ S	031° 45.446’ W	723
PS111_17-1	2018-02-03	73° 41.983’ S	025° 43.958’ W	3244
PS111_16-1	2018-02-01	72° 23.044’ S	017° 49.030’ W	1419
PS111_14-5	2018-01-31	70° 56.624’ S	010° 31.544’ W	280
PS111_14-1	2018-01-31	70° 56.409’ S	010° 32.416’ W	280
PS111_12-2	2018-01-27	66° 44.323’ S	000° 02.287’ W	4698
PS111_10-2	2018-01-26	65° 23.120’ S	002° 33.989’ E	2092
PS111_9-3	2018-01-26	63° 59.987’ S	005° 00.053’ E	3849

The stations sampled during PS111, with transects from coastal areas to the open sea and from low to high ice coverage, were expected to provide natural gradients in organic matter concentration and possibly also differences in bacterial community compositions and activity. Further, spatial changes in phytoplankton bloom development, as visible for example by distinct differences in the fluorescence profile, were also expected to strongly impact the composition and activity of the bacterioplankton.

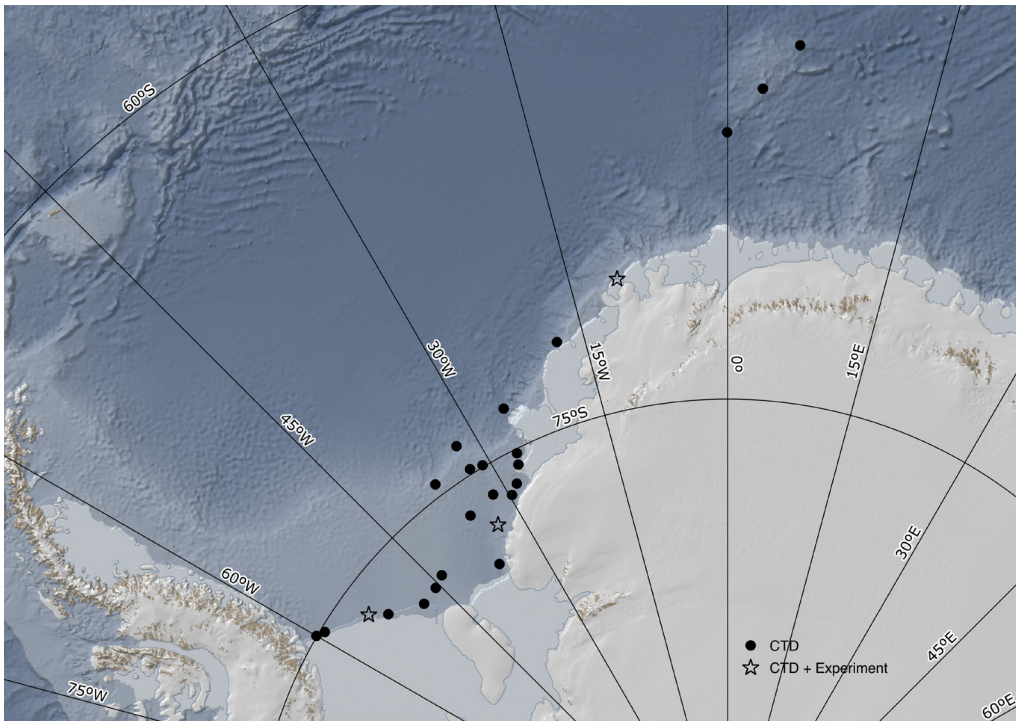

Fig. 10.1: Location of all stations sampled for microbiological and biogeochemical analyses during PS111 in the southern Weddell Sea and along the transect to Neumayer III. Closed circles indicate stations sampled by CTD; stars indicate stations where additionally incubation experiments were started with water collected from one depth. (station map courtesy of M. Diego Feliu).

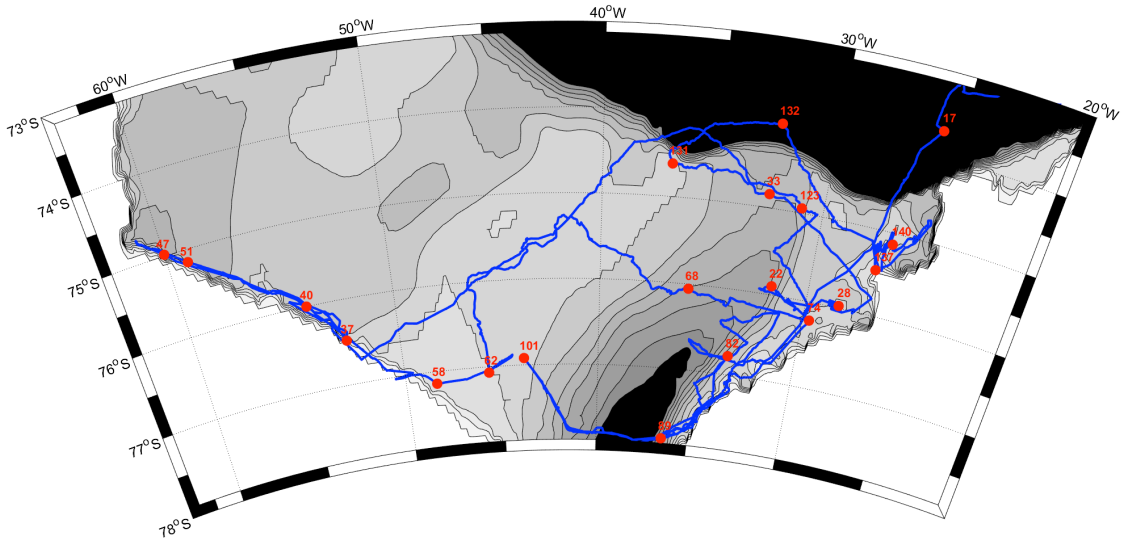

Fig. 10.2: Station map and cruise track during PS111 in the southern Weddell Sea (station map courtesy of M. Janout)

Samples from the CTD rosette were taken from 4-6 depths within the upper 100 m of the water column. This depth range included the peak layer in phytoplankton (if present), and generally also different temperature zones. A range of sampling procedures (with different fixations, filtrations and subsequent storage temperatures) were applied for the later assessment of several microbiological and chemical parameters in the home laboratories (see Table 10.2). The filtered material for nucleic acid extraction (DNA/RNA) will be used for high-throughput sequencing (probably Illumina) of the 16S rRNA and the 16S rRNA gene, for which suitable primer systems are established and which are routinely used for assessing prokaryotic community composition (e.g., Herlemann et al., 2011).

Tab. 10.2: Sampling details for the microbiological and chemical parameters. FCM: flow cytometrie, CARD-FISH: catalyzed reporter deposition fluorescence in-situ hybridisation, P + G: paraformaldehyde/glutaraldehyde mixture

Target parameter	Method	Volume filtered	Replicates per depth	Storage
DNA/RNA	filter, 0.2 µm-filtration	1 L	2	-80°C
CARD-FISH filter	filter, 0.2 µm-filtration	40 ml	1	-20°C
Total prokaryotes (by FCM)	water, P+G fixation	10 ml	2	-80°C
Total prokaryotes and nanoflagellates (by microscopy)	water, formol fixation, DAPI staining	10–30 ml	1	-20°C
Bacterial production	3H-Leucine incorporation	5 ml	3	measurement on board
Dissolved organic carbon (DOC), dissolved organic nitrogen (DON)	filtrate, 0.2 µm-filtration, acidification	20 ml	2	0°C
Dissolved amino acids	filtrate, 0.2 µm-filtration	20 ml	2	-20°C
Dissolved carbohydrates	filtrate, 0.2 µm-filtration	20 ml	2	-20°C
Nutrients	filtrate, 0.2 µm-filtration	50 ml	2	-20°C
Chlorophyll a	filter, whatman GF/F	0.5–1 L	1	-80°C

Bacterial biomass production, assessed by measuring the incorporation of ^{w}H-leucine, was measured also at different incubation temperatures (in situ and +3°C) in order to reveal the short-term response of the bacterioplankton to warming. Two bottle incubation experiments, in which bacterial growth and ^{3}H-leucine incorporation were assessed in parallel for 2-3 days, were conducted in order to determine a conversion factor for calculating bacterial biomass production from leucine incorporation.

For enumeration of prokaryotic cell numbers, samples were taken both for flow cytometry and microscopy (Table 10.2). For the latter, samples were stained with the fluorochrome DAPI and some of them already counted on board with an epifluorescence microscope (Axioskop, Zeiss). In addition to total prokaryotic cell counts, also small protists (nanoflagellates) were enumerated. Of particular importance as bacterial consumers, and probably directly related to bacterial productivity, are heterotrophic nanoflagellates (HNF), which are a taxonomically diverse functional group. In this project the impact of rising temperature will also be examined with regard to the role of protists as bacterivorous grazers and the resulting changes in top-down control on planktonic bacteria.

As indicators for bacterial substrate supply, samples for the analysis of DOC, DON, dissolved carbohydrates and amino acids were taken. The latter two can be considered as a proxy for labile organic matter whereas increased DOC concentrations might be indicative for reduced bacterial substrate utilisation due to low temperature. Samples for determination of chlorophyll-a concentration and, for some selected sites, also lugol-fixed samples for phytoplankton assessments, will give information on the phytoplankton bloom development at the different stations and the different water depths.

Besides the field sampling program, three on-board incubation experiments were conducted, which investigated the combined effects of warming and substrate addition on bacterial production, bacterial composition, and organic matter turnover (Table 10.3). As substrate, dissolved organic material was obtained from freshly collected phytoplankton biomass. The incubations of <20 µm-filtered water took place in a cooling laboratory chamber at two different temperatures (0° and 3°C), for one experiment also at in situ temperature in an incubator, and lasted 3-5 days during which the same parameters as for the field sampling (Table 10.3) were sampled. Additionally, respiration (mainly bacterial) was measured by optodes (Pyroscience). The experiments should allow to link changes in community structure and functioning to warming and substrate supply.

Tab. 10.3: Incubation experiments conducted during PS111. Seawater was taken from the Rosette, incubated at different temperatures and sampled at different time intervals to follow the response in bacterial communities and resulting effects on dissolved organic matter.

Experiment	Start	End	CTD/Rosette	Rosette depth [m]	Temperature [°C]
1	2018-01-31	2018-02-05	PS111_14-1	60	0, 3
2	2018-02-10	2018-02-15	PS111_40-3	60	0, 3
3	2018-02-18	2018-02-23	PS111_82-1	50	-1.6, 0, 3

Preliminary (expected) results

The field programme, with the range of different stations sampled, revealed striking differences in the plankton communities between the stations and a strong stratification of the prokaryotic communities and their activities in the upper water column. One representative example for stations with a pronounced phytoplankton bloom (as evidenced by chl-a fluorescence, measured with a Wetlabs fluorescence sensor) is shown in Fig. 10.3. Thus, bacterial activities, as determined by ^{3}H-leucine incorporation, could differ by a factor of more than 30, comparing the depths of highest and lowest activity. In general, highest bacterial and HNF cell numbers, as well as highest bacterial biomass production was in a depth layer close to the strongest phytoplankton development.

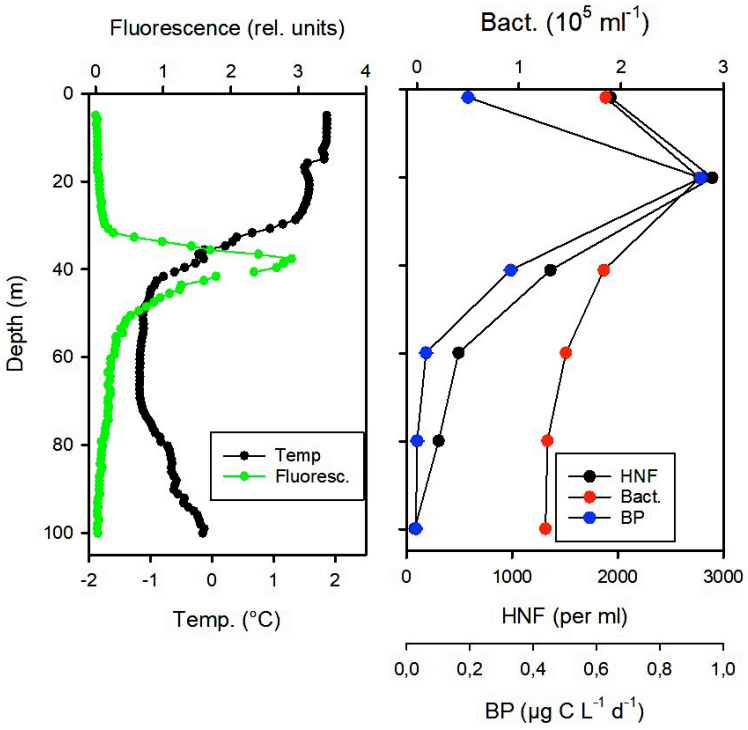

Fig. 10.3: Profiles of temperature and chl-a-fluorescence (left), and bacterial numbers, heterotrophic nanoflagellates (HNF) and bacterial production (BP) (right) for CTD station 9-3. Bacterial and HNF numbers were determined from DAPI-stained preparations, bacterial production from 3H-leucine incorporation.

The analysis of bacterial community composition by high-throughput sequencing will reveal how the communities change in dependence on temperature, phytoplankton bloom development and location.

For some stations the relatively high number of HNF relative to bacteria, as also visible for the example of station 9-3 (Fig. 10.3) indicates that these low water temperatures obviously do not hamper the development of bacterivorous protists which probably exert an efficient top-down control on the bacterioplankton. The complete analysis of all stations will reveal whether this is a common trend.

The incubation experiments showed a strong stimulatory effect of increased temperature on the development of the bacterial communities and their activities whereas the impact of substrate supply was not consistent as could be seen so far. A more detailed analysis of bacterial composition later on will reveal whether the temperature-mediated response is accompanied by community shifts.

Overall, this project, with a combination of field samplings and experimental incubations, will elucidate the modulation of temperature effects on heterotrophic bacterial activity by the availability of reactive organic matter and investigate the synergistic potential of combined effects. Expected results will evaluate the potential of temperature effects on Antarctic bacterioplankton to feedback to the ocean-atmosphere CO_2 exchange in a warming Antarctic.

A better determination of bacterial remineralization and its dependence on substrate concentration and temperature will help to parameterize global models that aim to project the marine carbon cycle under a changing climate.

Data management

All data collected and generated by this project will be submitted to the central PANGAEA database of SPP 1158. DNA and RNA sequence data will be submitted to public databases (Genbank, NCBI).

References

Delille D (1992) Marine bacterioplankton at the Weddell Sea ice edge, distribution of psychrophilic and psychrotrophic populations. Polar Biology, 12, 205-210.

Helmke E, Weyland, H (1995) Bacteria in sea ice and underlying water of the eastern Weddell Sea in midwinter. Marine Ecology Progress Series, 117, 269-287.

Herlemann DPR, Labrenz M, Jürgens K, Bertilsson S, Waniek JJ, Andersson AF (2011) Transitions in bacterial communities along the 2000 km salinity gradient of the Baltic Sea. The ISME Journal 5, 1571–1579.

Kirchman DL, Morán, XAG, Ducklow, HW (2009). Microbial growth in the polar oceans - role of temperature and potential impact of climate change. Nature Reviews Microbiology 7, 451–459.

11. PTEROPODS AS EARLY-WARNING SYSTEM OF OCEAN ACIDIFICATION IN THE WEDDELL SEA

Silke Lischka[1], Jan Michels[2], Stanislav N. Gorb[2]

[1]GEOMAR
[2]Uni Kiel

Grant-No. AWI_PS111_00

Objectives

At high latitudes, thecosome pteropods (marine shell-bearing pelagic mollusks) can dominate zooplankton communities and consequently are important food web components in the pelagial (e.g. Lalli and Gilmer, 1989, Hunt et al., 2008). Due to their calcium carbonate shell made of aragonite, they significantly contribute to ocean carbon flux and are particularly vulnerable to ocean acidification (Berner and Honjo, 1981; Bathmann et al., 1991; Lischka et al., 2011; Bednarsek et al., 2012). Despite their prominent role in the pelagic ecosystem and biogeochemistry, knowledge of the importance of thecosome pteropods for the Weddell Sea zooplankton community is scarce. Recent studies provide evidence for a significant invasion of anthropogenic CO_2 into the Weddell Sea Gyre between 1973 and 2008 having led to a decrease in pH and the saturation state of aragonite (van Heuven et al., 2011). This potentially perils thecosomes by inducing shell dissolution (Lischka et al., 2011, Bednarsek et al., 2012). The present project aims at establishing thecosome pteropods as early-warning organisms of ocean acidification in the Weddell Sea. To this end, the current 'shell dissolution state' will be investigated in relation to the prevailing ocean carbonate chemistry conditions at the main depths of pteropod occurrence to enable the assessment of the present condition of pteropods and to serve as a benchmark for potential future monitoring of ongoing ocean change processes. Samples obtained during this cruise will furthermore serve to describe the ecological (abundance, biomass) and biogeochemical (organic and inorganic carbon contribution) role of thecosome pteropods in the Weddell Sea zooplankton ecosystem.

Our specific objectives are:

- characterizing the current shell dissolution state of thecosome pteropods in detail in relation to prevailing physical and chemical water properties using different light and electron microscopy techniques and methods
- determining the spatial and vertical distribution patterns of thecosome pteropods in relation to prevailing physical and chemical water properties
- assessing the ecological and biogeochemical importance of thecosome pteropods within the mesozooplankton community of the southern Weddell Sea in terms of their organic and inorganic biomass contribution

Work at sea

During PS111, water and zooplankton samples were collected at 19 stations in front of the Filchner and the Ronne Ice Shelf and across an east/west transect that roughly stretched along 76° N through the Filchner Trough (Table 11.1, Fig. 11.1).

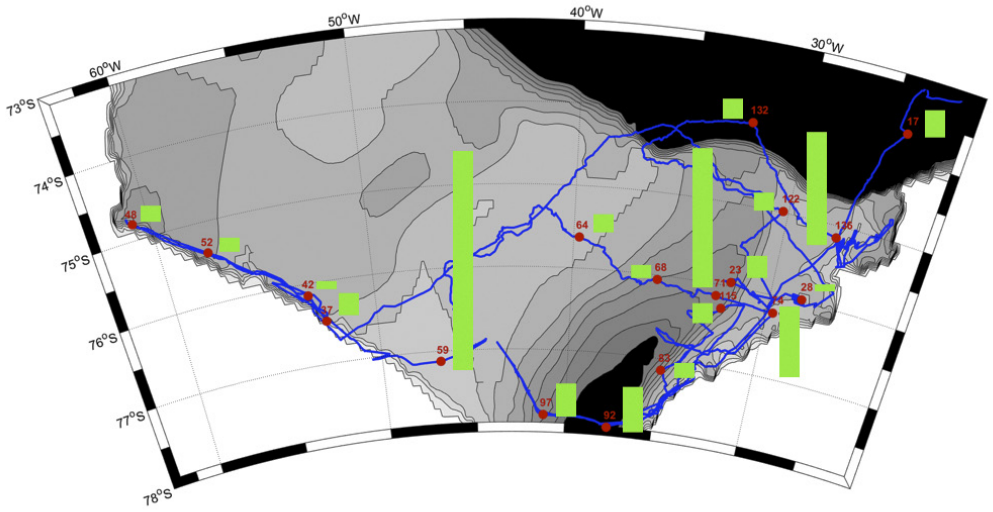

Fig. 11.1: Station map of Bongo Net and MultiNet hauls (red circles) during PS111 with bar charts (green) indicating the mean number of thecosome pteropods per m^{-3} at the different stations. Maximum numbers were found at the station 59 and minimum numbers at the station 28 (see Table 11.2). (Station map courtesy of M. Janout).

Tab. 11.1: CTD rosette, Bongo Net and MultiNet stations during PS111. Maximum sampling depth indicates the depth of the deepest water sample taken at a particular station or the maximum depth of net deployment.

Station	Date	Max. Sampling Depth [m]	Latitude	Longitude	Gear
PS111_17-1	2018-02-03	500	73° 41,983' S	025° 43,960' W	CTD/Rosette
PS111_17-4	2018-02-03	1200	73° 41,986' S	025° 43,692' W	CTD/Rosette
PS111_17-3	2018-02-03	500	73° 41,984' S	025° 43,826' W	Bongonet
PS111_17-5	2018-02-03	500	73° 41,956' S	025° 43,168' W	Multinet
PS111_23-1	2018-02-05	680	75° 57,177' S	032° 02,679' W	CTD/Rosette
PS111_23-2	2018-02-05	500	75° 57,191' S	032° 02,740' W	Bongonet
PS111_23-3	2018-02-05	500	75° 57,226' S	032° 02,650' W	Multinet
PS111_28-1	2018-02-05	300	75° 58,499' S	028° 24,942' W	CTD/Rosette
PS111_28-2	2018-02-05	340	75° 58,514' S	028° 25,041' W	Bongonet
PS111_28-3	2018-02-05	350	75° 58,505' S	028° 25,038' W	Multinet
PS111_19-4	2018-02-04	300	76° 05,369' S	030° 27,849' W	Bongonet
PS111_19-5	2018-02-04	300	76° 05,432' S	030° 28,166' W	Bongonet
PS111_37-2	2018-02-09	350	76° 28,992' S	052° 38,241' W	CTD/Rosette
PS111_37-3	2018-02-09	380	76° 28,986' S	052° 38,370' W	Bongonet
PS111_37-4	2018-02-09	308	76° 29,082' S	052° 38,885' W	Multinet
PS111_42-3	2018-02-10	400	76° 08,681' S	053° 21,393' W	CTD/Rosette

PS111_42-4	2018-02-10	480	76° 08,672' S	053° 21,342' W	Bongonet
PS111_42-5	2018-02-10	480	76° 08,640' S	053° 21,414' W	Bongonet
PS111_48-1	2018-02-11	500	74° 48,030' S	060° 47,955' W	CTD/Rosette
PS111_48-2	2018-02-11	500	74° 48,242' S	060° 47,404' W	Bongonet
PS111_48-3	2018-02-11	500	74° 48,326' S	060° 47,564' W	Bongonet
PS11152-1	2018-02-12	500	75° 22,743' S	057° 44,245' W	CTD/Rosette
PS111_52-2	2018-02-12	500	75° 22,798' S	057° 43,392' W	Bongonet
PS111_52-3	2018-02-12	500	75° 22,882' S	057° 42,327' W	Bongonet
PS111_59-1	2018-02-14	250	77° 07,484' S	046° 52,035' W	CTD/Rosette
PS111_59-2	2018-02-14	250	77° 07,481' S	046° 52,132' W	Bongonet
PS111_59-3	2018-02-14	250	77° 07,490' S	046° 52,133' W	Bongonet
PS111_64-2	2018-02-16	350	75° 37,210' S	039° 42,700' W	CTD/Rosette
PS111_64-3	2018-02-16	370	75° 37,482' S	039° 43,782' W	Bongonet
PS111_64-4	2018-02-16	370	75° 37,500' S	039° 43,745' W	Bongonet
PS111_68-1	2018-02-16	700	76° 03,310' S	035° 42,725' W	CTD/Rosette
PS111_68-2	2018-02-16	500	76° 03,205' S	035° 42,405' W	Bongonet
PS111_68-3	2018-02-16	500	76° 03,153' S	035° 42,107' W	Bongonet
PS111_71-1	2018-02-17	700	76° 08,945' S	032° 40,116' W	CTD/Rosette
PS111_71-2	2018-02-17	500	76° 08,451' S	032° 40,421' W	Bongonet
PS111_71-3	2018-02-17	500	76° 08,311' S	032° 41,110' W	Bongonet
PS111_74-1	2018-02-17	350	76° 12,827' S	029° 40,491' W	CTD/Rosette
PS111_74-2	2018-02-17	360	76° 12,791' S	029° 40,652' W	Bongonet
PS111_74-3	2018-02-17	360	76° 12,829' S	029° 40,515' W	Bongonet
PS111_83-1	2018-02-18	684	77° 08,459' S	034° 55,719' W	CTD/Rosette
PS111_83-2	2018-02-18	500	77° 08,300' S	034° 55,449' W	Bongonet
PS111_83-3	2018-02-18	500	77° 08,263' S	034° 55,219' W	Bongonet
PS111_92-1	2018-02-19	500	77° 53,884' S	037° 35,355' W	Bongonet
PS111_92-2	2018-02-19	500	77° 53,886' S	037° 35,366' W	Bongonet
PS111_92-3	2018-02-19	750	77° 53,881' S	037° 35,189' W	CTD/Rosette
PS111_97-2	2018-02-20	500	77° 47,387' S	041° 14,499' W	Bongonet
PS111_97-3	2018-02-20	500	77° 47,169' S	041° 14,628' W	Bongonet
PS111_115-1	2018-02-22	693	76° 17,037' S	032° 18,591' W	CTD/Rosette
PS111_115-2	2018-02-22	500	76° 16,972' S	032° 18,793' W	Bongonet
PS111_1115-3	2018-02-22	500	76° 16,933' S	032° 18,600' W	Bongonet
PS111_122-1	2018-02-25	750	74° 59,248' S	030° 15,591' W	CTD/Rosette
PS111_122-2	2018-02-25	400	74° 59,082' S	030° 15,260' W	Bongonet
PS111_122-3	2018-02-25	400	74° 58,964' S	030° 15,140' W	Bongonet
PS111_132-1	2018-02-27	750	74° 00,528' S	032° 25,411' W	CTD/Rosette
PS111_132-2	2018-02-27	1500	74° 00,084' S	032° 22,786' W	Multinet
PS111_136-1	2018-02-28	392	75° 08,733' S	027° 32,703' W	CTD/Rosette
PS111_136-2	2018-02-28	380	75° 08,696' S	027° 33,132' W	Bongonet
PS111_136-3	2018-02-28	380	75° 08,748' S	027° 33,622' W	Bongonet

Tab. 11.2: Mean number of thecosome pteropods per m-3 collected by Bongo Net hauls and at the deep MultiNet station 132

Station	Mean	SD
17	0,06	0,01
23	0,05	0,00
28	0,02	0,01
37	0,05	0,02
42	0,02	0,02
48	0,04	0,05
52	0,03	0,03
59	0,50	0,89
64	0,04	0,04
68	0,03	0,04
71	0,32	0,05
74	0,16	0,19
83	0,03	0,05
92	0,10	0,18
97	0,08	0,14
115	0,05	0,04
122	0,04	0,04
132	0,05	–
136	0,26	0,23

To characterize the seawater carbonate system, water samples were obtained from the rosette water sampler attached to the CTD sensor. These included samples for the determination of the pH, dissolved inorganic carbon (DIC), total alkalinity (TA) and inorganic nutrients (phosphate, silicate, nitrate, nitrite). The characterization of the carbonate system conditions is necessary to be able to describe the *in-situ* living conditions of the pteropods and to directly link the pteropod occurrence and distribution patterns to the prevailing oceanographic conditions. The closing depth of the water bottles was dependent on the maximum water depth and always covered the sampling depth to which the zooplankton net was lowered (usually 500 m). To minimize gas exchange, gas samples (pH, DIC, TA) were taken immediately after the CTD rosette was back on deck, usually before any other water was removed from the bottles. In total 206 water samples were taken for pH, TA and nutrient analyses, and 135 for measurements of the DIC concentration. Of the pH samples, voltage readings were performed with a pH Mobile 826 pH meter (Metrohm, Switzerland) onboard immediately after the sampling. These measurements will later serve to calculate the pH on the total seawater scale (SOP6a, Dickson et al. 2007). As standard, certified reference material (CRM) with a known pH calculated from known TA and DIC (Dickson et al., 2007) was measured directly after each set of pH samples from one station had been analyzed. DIC and TA samples were poisoned immediately after collection with a saturated mercuric chloride solution to stop biological activity from changing the carbon distributions in the sample bottles before the analyses back in the home laboratory. Inorganic nutrient samples were frozen immediately after collection at -20 °C and will be analyzed in the home laboratory at GEOMAR in Kiel.

For the determination of the bulk phytoplankton biomass, water samples were taken from the upper 300 m (surface, 25 m, 50 m, 100 m, 200 m, 300 m). In total 114 water samples were collected from the 19 stations, filtered in duplicate through GF/F filters and stored at -20 °C for later determination of the chlorophyll *a* concentration in the home laboratory.

The collection of zooplankton samples to obtain pteropods was conducted with a MultiNet Midi equipped with five nets with a mesh size of 150 µm (depth strata: 0–50 m, 50–100 m, 100–200 m, 200–300 m, 300–500 m) and a Bongo Net with a mesh size of 300 µm (maximum sampling depth: 500 m). At one station, the MultiNet was deployed down to 1,500 m (depth strata: 0–50 m, 50–100 m, 100–500 m, 500–1,000 m, 100–1,500 m). The net hauls were performed in front of the Filchner and Ronne Ice Shelf and in the area of the Filchner Trough. Two stations were situated north of the Filchner Sill. The MultiNet was deployed at 5 of these stations including those north of the sill. Developmental stages of the thecosome pteropod *Limacina helicina antarctica* were picked from the net samples immediately after retrieval on deck and either deep-frozen at -80 °C for later shell surface analyses or preserved in glutardialdehyde for later morphological investigations in the home laboratory at Kiel University. At two stations, also samples for lipid analyses were deep-frozen at -80 °C. The remains of the net samples were preserved in 96 % ethanol or deep-frozen at -80 °C for later determination of species composition, abundance and biomass. In total, 61 zooplankton samples were preserved in 96 % EtOH for the analysis of the community composition and 38 zooplankton samples were deep-frozen for later biomass determination. For shell surface analyses, 1268 individual pteropods of different developmental stages were sorted out from the different stations. For morphological studies and lipid analyses, 113 and 145 individual pteropods of different developmental stages were picked out and preserved in glutardialdehyde and deep-frozen at -80 °C, respectively. These samples will be analyzed in the home laboratories in Kiel.

Preliminary (expected) results

The intention of this project was to provide information about the current shell dissolution state of thecosome pteropods in the Weddell Sea and specify if and to what extent these organisms have already been affected by recent and ongoing anthropogenic CO_2 invasions in the Weddell Sea. Furthermore, the abundance and distribution patterns of thecosome pteropods and their ecological and biogeochemical significance within the mesozooplankton community of the Weddell Sea will be described and assessed. These results will allow establishing pteropods as early-warning organisms for future evaluations of potential global change processes in the Weddell Sea.

The Bongo Net turned out to collect the pteropods more efficiently. For this reason, we mostly conducted Bongo Net hauls to obtain sufficient numbers of organisms for later shell surface analyses. Thecosome pteropods were found at all 19 stations sampled. Except for the northeastern most station (station 17) where we found both one cavolinid species (*Clio pyramidata*) and one limacinid species (*Limacina helicina antarctica*), at all other stations only *L. helicina antarctica* occurred (Fig. 11.2). Highest numbers of *L. helicina antarctica* were found on the continental shelf in front of the northeastern part of the Filchner Shelf at station 136, in the central part of the Filchner Trough at station 71 and in front of the eastern Ronne Ice Shelf at station 59. All developmental stages of *L. helicina antarctica* were recorded during the cruise, from veliger larvae to spawning adult specimens. Developmental stages were spatially separated with the early stages distributed more on the shallow parts of the continental shelf and the older stages preferentially occurring in the deeper parts of the continental shelf. Preliminary mean numbers of pteropods per m^{-3} found in the different nets of the Bongo Net and the MultiNet varied between 0.02 and 0.5 individuals m^{-3} (SD 0.89) individuals (Table 11.2).

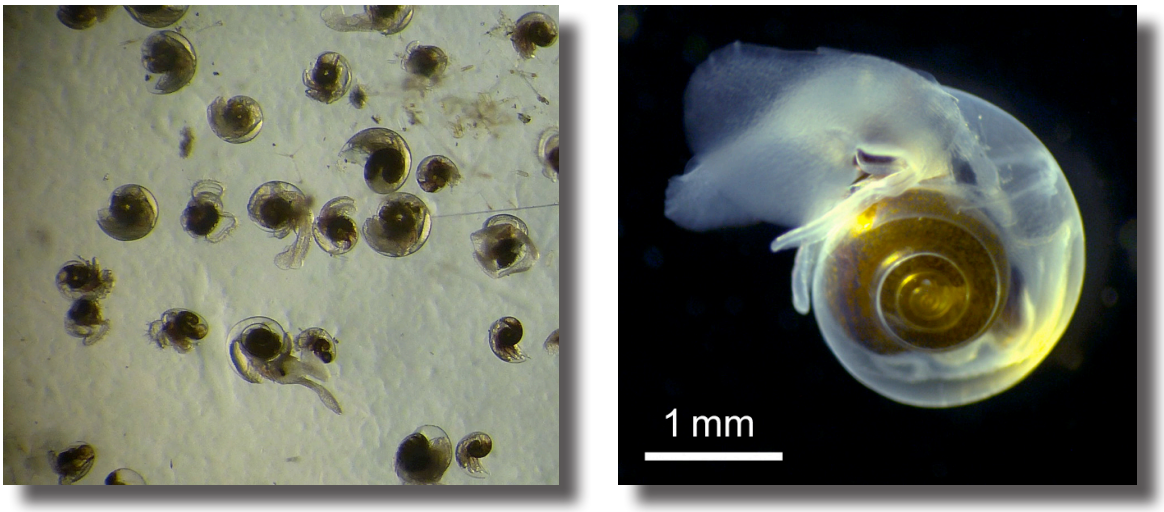

Fig. 11.2: (a) Bongo Net catch with different developmental stages of Limacina helicina antarctica (photo: S. Lischka) (b) Close-up of an individual L. helicina antarctica (photo: S. Gorb)

In the coming months, the outer and inner shell surfaces of the pteropod specimens frozen at -80 °C will be analyzed in detail with different microscopy techniques (stereo microscopy, scanning electron microscopy) to investigate whether signs of shell dissolution are present. If so, the extent of shell dissolution will be quantified with two different methods described by Lischka et al. (2011) and Bednarsek et al. (2012). Both methods classify different levels of degradation/dissolution according to a standardized scheme (spanning from mild surface abrasion of the prismatic layer to dissolution of the deeper crossed-lamellar layer) and allow the use of pteropods as 'early-warning bioindicators' of OA.

Parameters of the carbonate system will be analyzed to determine the *in-situ* conditions at the depths of pteropod occurrence in particular with respect to aragonite saturation and pH. Water samples for the determination of total alkalinity (TA) collected from regular CTD rosette casts will be analyzed directly after the samples arrive at the home laboratories. TA will be measured by microtitration after Dickson et al. (2003), and the accuracy will be determined by measuring certified reference material (CRM) as described above for the pH. DIC concentrations will be quantified by infrared absorption using a LI-COR LI-7000 on an AIRICA system (MARIANDA, Kiel). Furthermore, for a precise determination of the carbonate system, the concentrations of inorganic nutrients (NU) have to be known. Nutrient samples taken onboard *Polarstern* and frozen at -20 °C will be analyzed colourimetrically after Koroleff and Grasshoff (1983) for the biologically influenced dissolved inorganic nutrients phosphate (PO_4^{3-}), nitrite (NO_{2-}), nitrate (NO_{3-}) and silicate ($Si(OH)_2$). Finally, from the measured pH (done onboard, see above), DIC, TA, and dissolved nutrients the remaining carbonate system parameters (most importantly pCO_2, Ω_{ar}, HCO^-, CO_3^{2-}) at the depths of pteropod occurrence will be calculated using CO2SYS.

The results of the shell dissolution analyses will be used to define the current shell dissolution state of thecosome pteropods in the Weddell Sea in relation to the prevailing carbonate chemistry properties.

Of the remaining zooplankton samples preserved in ethanol and at -80 °C, abundance, species composition and vertical/spatial distribution will be analyzed, and the biomass will be determined to estimate the significance of pteropods in the zooplankton community. Furthermore, to assess the biogeochemical importance of thecosomes, subsets of the frozen pteropod samples will be

used for the determination of dry mass (DM), total carbon (TC), total organic (TOC) and total inorganic carbon (TIC). For this purpose, samples will be divided into two batches. One batch will be used for the determination of TC, and the other for the determination of TOC. In case of TOC, the samples will be pre-treated with a sufficient amount of sulphuric acid to remove the inorganic carbon (the shells) prior to analysis. Samples of known DM (measured prior to the carbon content analyses) will then be combusted, and the carbon content will be analyzed. Afterwards, TIC and the calcium carbonate content can be estimated from TC and TOC by applying the following equations:

$$TIC = TC–TOC$$

$$CaCO3 = [TC–TOC] * 8.33$$

(The constant 8.33 is the molecular mass ratio of carbon to calcium carbonate.)

Data management

All data collected and generated by this project will be made publicly available via the World Data Center PANGAEA. All parts of the zooplankton samples not used for analyses will be stored at GEOMAR and be available for potential future analyses.

References

Bathmann U, Noji T, von Bodungen B (1991) Sedimentation of pteropods in the Norwegian Sea in autumn. Deep-Sea Research 38, 1341-1360.

Bednarsek N, Tarling G, Bakker D, Fielding S, Jones E, Venables H, Ward P, Kuzirian A, Lézé B, Feely R, Murphy E (2012) Extensive dissolution of live pteropods in the Southern Ocean. Nature Geoscience, 5, 881-885.

Berner R, Honjo S (1981) Pelagic sedimentation of aragonite: its geochemical significance. Science, 211, 940-942.

Dickson A, Sabine C, Christian J (2007) Guide to best practices for ocean CO_2 measurements. 191 pp.

Heuven van S, Hoppema M, Huhn O, Slagter H, de Baar H (2011) Direct observation of increasing CO2 in the Weddell Gyre along the prime meridian during 1978–2008. Deep-Sea Research II, 58, 2613-2635.

Hun B, Pakhomov E, Hosie G, Siegel V, Ward P, Bernard K (2008) Pteropods in the Southern Ocean ecosystems. Progress in Oceanography, 78, 193-221.

Koroleff F, Grasshoff K (1983) Methods of seawater analysis. Verlag Chemie, Weinheim, Ch. Determination of nutrients, p 419.

Lalli C, Gilmer R (1989) Pelagic snails: the biology of holoplanktonic molluscs. Stanford University Press, Stanford, California.

Lischka S, Büdenbender J, Boxhammer T, Riebesell U (2011) Impact of ocean acidification and elevated temperatures on early juveniles of the polar shelled pteropod *Limacina helicina*: mortality, shell degradation, and shell growth. Biogeosciences, 8, 919-932.

12. QUANTIFYING ELEMENTAL FLUXES WITH RADIUM ISOTOPES ACROSS THE ACC, IN THE WEDDELL GYRE AND IN THE FILCHNER-RONNE REGION

Claudia Hanfland[1], Marc Diego Feliu[2], Walter Geibert[1](not on board)

[1]AWI
[2]UAB

Grant-No. AWI_PS111_00

Background and Objectives

The aim of our investigations during PS111 was a better understanding of the role of upwelling deep water and shelf sources in the process of iron enrichment in surface waters, sea ice and adjoining shelf ice.

While the role of iron in limiting primary productivity has been extensively studied by biologists, possible input paths into the remote waters of the otherwise nutrient-rich Southern Ocean are far from being well understood. Reliable, measured iron concentrations are scarce. In fact, only two sections exist to-date for the Atlantic sector of the Southern Ocean. A section published by Klunder et al. (2011) highlights the role of submarine volcanism (e.g. around Bouvet Island) and gives a first hint for iron release on the Antarctic shelf. A second section across the Weddell Sea (Klunder et al., 2014) confirms relatively low deep iron concentrations in most places, but it also shows a prominent source at the shelf and slope near the Antarctic Peninsula. While iron concentrations are generally very low in Southern Ocean polar waters, they sustain large blooms of phytoplankton that can cover regions up to 600,000 km^2 (Geibert et al., 2010). One hypothesis is input of this trace metal through various input paths (upwelling, melting icebergs that carry terrestrial material, and dust deposition as a minor source) followed by concentration in sea ice. With the onset of the melting season, the iron will be released into surface waters and support plankton growth.

To investigate the origin of iron, radioactive tracers from the U-Th-decay chains provide suitable information on the movement of water masses. ^{226}Ra (half-life 1600 years) is a well-established tracer that is enriched in intermediate and deep waters. High-resolution sampling of this tracer should enable us to identify regions with enhanced upwelling (e.g. Maud Rise).

Surface water activities of ^{226}Ra were investigated by Hanfland (2002). The most salient feature in the distribution of ^{226}Ra is a strong southward increase from approximately 8 dpm/100kg north of the Polar Front to about twice as much in the Weddell Gyre with a mean activity in the southern waters of the Antarctic Circumpolar Current (ACC) and within the Weddell Gyre of about 15.5 dpm/100kg. This gradual increase of the ^{226}Ra activity is closely related to a drop in temperature and displays the effect of upwelling of deeper waters. It can be observed on all transects although the gradients differ in intensity. Highest values coincide with the location of Maud Rise, a topographic feature at 66°S, 3°E. Dissolved silicate has been found to have a similar distribution to ^{226}Ra in this region, with a similar source in deep upwelling as a possible key mechanism. Upwelling is different between the Eastern and Western part of the Weddell Gyre and can be traced by ^{226}Ra. ^{227}Ac, another unstable isotope with a half-life of 22 years, had been investigated intensively by Geibert et al. (2002) and proved to be a suitable tracer to calculate upwelling rates in this area. Given the advancement of modern analytical techniques,

it seemed appropriate to revisit the area and determine ^{226}Ra activities by mass spectrometry on smaller sample volumes. In contrast to former determinations by gamma spectrometry, analytical errors will be smaller and small scale changes in the ^{226}Ra distribution will become detectable.

^{228}Ra (half-life 5.75 years) is a suitable isotope to trace shelf waters off the coast and in the open ocean. It originates mostly from sediments. Due to this specific source and its shorter half-life, it is virtually absent in upwelling deep waters. Instead, it is found enriched near the ocean/continent boundary, and it can be used to trace water masses that have chemically exchanged material with the sea-floor (Charette et al., 2016). The Southwestern boundary of the Weddell Gyre, possibly a substantial source of continental material to the Weddell Gyre, is virtually unsampled for ^{228}Ra (Hanfland, 2002). In addition, ^{228}Ra had never been sampled before in combination with iron in the Weddell Sea. Having similar sources, but a shorter half-life, ^{224}Ra has been used to study sedimentary sources near the Antarctic Peninsula (Annett et al., 2013).

Our objectives during PS111 were to:

- Use improved precision in ^{226}Ra measurements to trace the fate of deep upwelled water in the surface of the Weddell Gyre and its link to macronutrients
- Determine the source strength of the Filchner/Ronne region for ^{228}Ra and Fe in order to estimate the importance of this shelf for productivity in the Weddell Sea
- Determine pore water fluxes and trace metal geochemistry on the shelf areas (in combination with geology)

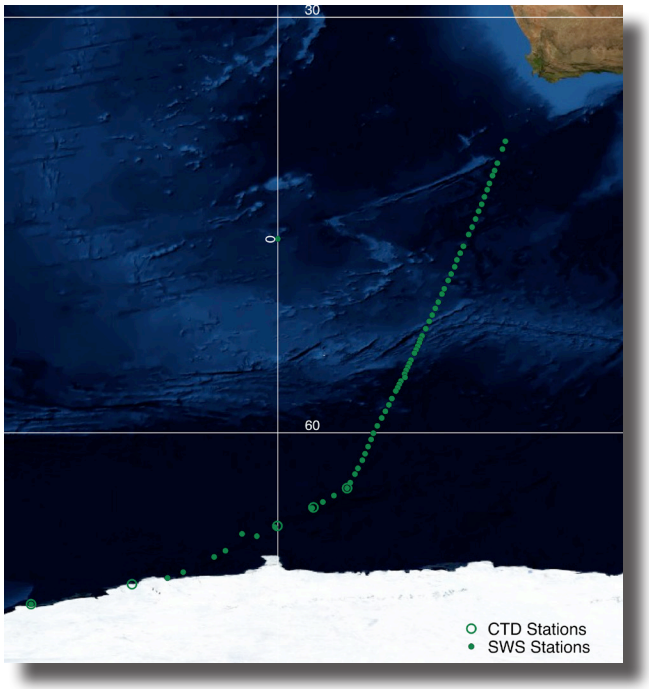

Fig. 12.1: Sampling locations for ^{226}Ra on the transect from Cape Town to Neumayer. Closed circled indicate samples taken from the ship's sea water supply. Open circles indicate station sampling associated with the Polynya over Maud Rise.

Work at sea

^{226}Radium

^{226}Ra has been sampled (1 L) from the ship's sea water intake and from CTD rosette casts. Samples were acidified with 2 ml of 32 % HCl for storage and will be analysed by mass spectrometry (ELEMENT 2) in the home lab. Aliquots of 50 ml have been taken parallel to each radium sample for nutrient analysis, notably silicate. Nutrient aliquots were stored at -20° for further processing at home. In total, we took 159 surface water samples and sampled 57 CTD stations (equalling 189 water column samples) for ^{226}Ra (Figs 12.1 and 12.2).

In addition, regular replicates and blanks have been taken for both ^{226}Ra and nutrient analysis.

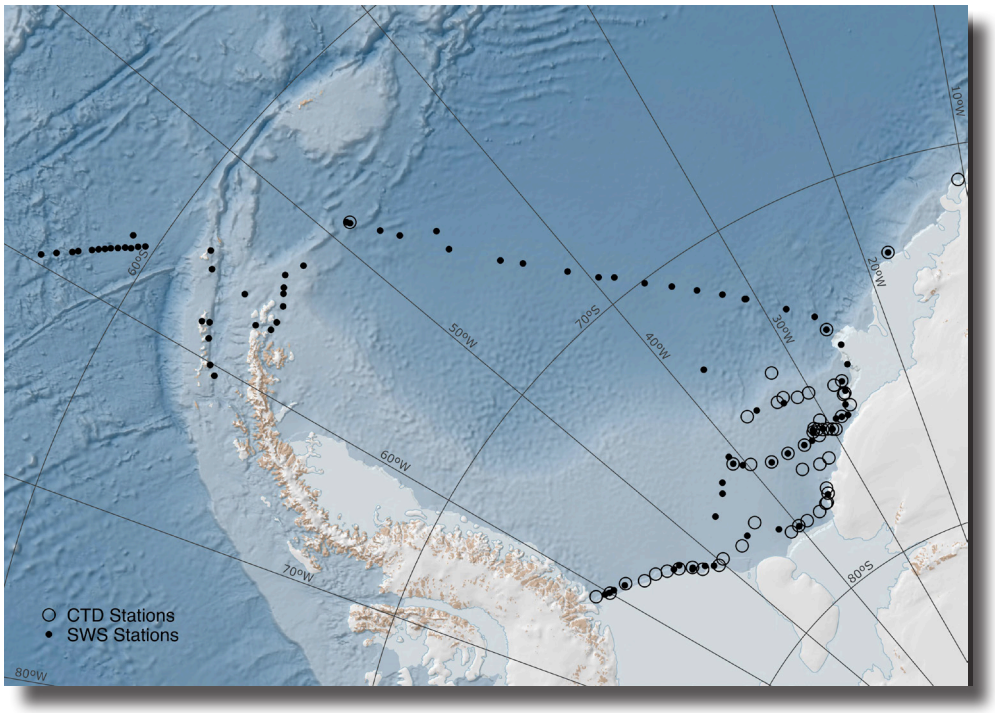

Fig. 12.2: Sampling locations for ^{226}Ra in the Weddell Sea and Drake Passage. Closed circled indicate samples taken from the ship's sea water supply. Open circles indicate station sampling. Red triangles: Sampling during AUV dives underneath Ronne and Filchner shelf ices. Green stars: parallel sampling of iron and ^{228}Ra.

^{228}Radium

^{228}Ra requires larger sample volumes than ^{226}Ra. Hence, activities were concentrated from a large volume of water onto MnO_2-coated fibre. MnO_2 acts as a strong adsorber, thereby enabling the concentration of activities from several hundred litres of sea water onto 40 g of fibre. The fibre is stored wet and cool for transport. Back in the home lab, it will be leached with acid, followed by ion column chemistry to purify the radium fraction. ^{228}Ra activities will then be determined either by gamma-spectrometry or the ^{228}Th ingrowth method (Hanfland 2002) using alpha spectrometry.

^{228}Ra was sampled from surface water by connecting a column filled with MnO_2 fibre to the seawater supply (83 samples). This work started after leaving *Neumayer*, as ^{228}Ra are known to be below the detection limit in the Antarctic Circumpolar Current (Hanfland ,2002). In addition, large volume samples were taken from CTD casts by combining several bottles and pumping the water volume over MnO_2 coated fibre. Here, the focus was on bottom water samples on the continental shelf to constrain the shelf source (Fig. 12.3).

On two occasions, it was possible to sample ^{228}Ra and iron in parallel on the shelf. Iron samples were taken from a rubber boat by clean go-flow bottles several hundred metres distance off *Polarstern*. Analysis of iron and aluminium concentrations will be performed at GEOMAR (co-operation with Marcus Gutjahr). A shallow CTD cast provided 288 L of water from the same depth for ^{228}Ra analysis. This is the first time, that the Fe/^{228}Ra can be constrained for the Weddell Sea. Locations were:

PS111_57	77° 01' S	50° 29' W
PS111_141	75° 27' S	26° 55' W

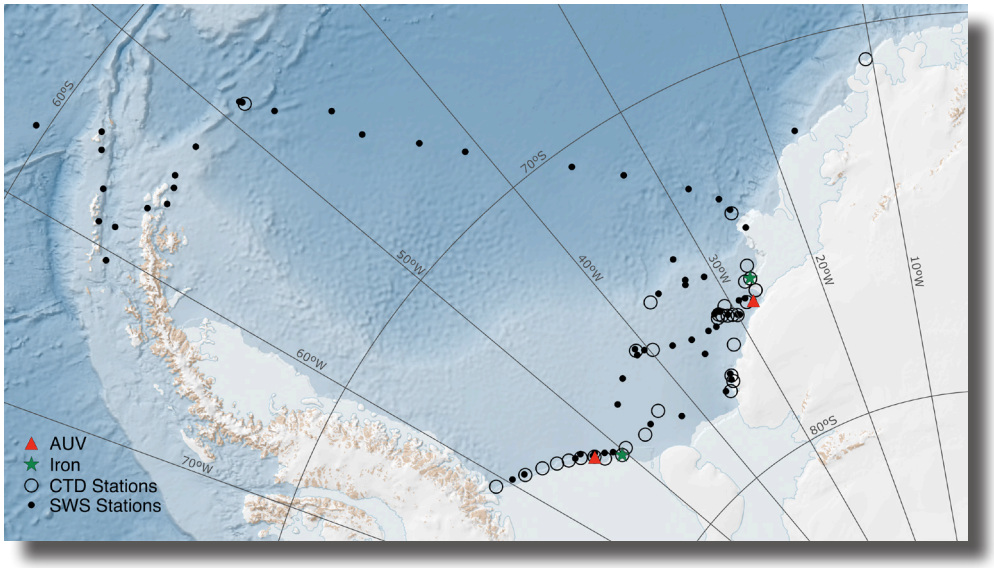

Fig. 12.3: Sampling locations for ^{228}Ra during PS111. Closed circled indicate samples taken from the ship's sea water supply. Open circles indicate large volume sampling from the CTD rosette.

We also deployed a portion of MnO_2 fibre onto the AUV during its journeys underneath the Filchner and Ronne ice shelves. Hosted by a silk net, MnO_2 fibre was attached to the front part of the AUV and was constantly flushed by the waters the AUV was going through. These samples will reveal ^{228}Ra/^{226}Ra ratios and give us an indication whether ^{228}Ra activities are enhanced underneath the ice shelves (environmental permission by NERC). Three samples could be recovered by these means during stations (Fig. 12.3):

PS111_30-1

PS111_37-1

PS111_41-1

Ice cores

For a better understanding of the sources of iron and related trace elements (like aluminium), two ice cores were retrieved by the sea ice physics group for geochemical analysis. Analysis will be carried out at GEOMAR (co-operation with Marcus Gutjahr).

Coring took place at the following locations:

Sea Ice Station	Date	Latitude	Longitude
PS111_SIP_8-7	2018-02-16	75° 59.106' S	36° 28.090' W
PS111_SIP_10-6	2018-02-18	76° 51.647' S	35° 33.265' W

Sediment cores

Sediment cores from the multicorer (MUC) haven been sampled with two aims: first, to better understand the enrichment source of Ra isotopes (^{223}Ra, ^{224}Ra, ^{228}Ra, ^{226}Ra) in bottom waters and to estimate fluxes of pore-water from the sediment to the water column.

To this aim, four sediment cores have been sampled from MUC stations PS111_15-1, PS111_53-3, PS111_60-3 and PS111_80-3 with a recovery of 23, 30, 16, 15 cm respectively. The cores were sliced in 1 cm slides and processed following the $^{224}Ra/^{228}Th$ disequilibrium method (Cai, 2014) and analyzed in a delayed coincidence counter (RaDeCC system; Figure 12.4; Moore, 1996). Each sample has been measured two times; within the first six to twelve hours after sample retrieval to quantify ^{224}Ra and after ten to twelve days when ^{224}Ra achieved secular equilibrium with ^{228}Th to quantify ^{228}Th. A third, final measurement will be conducted in the home-laboratory to more precisely determine ^{228}Th activities.

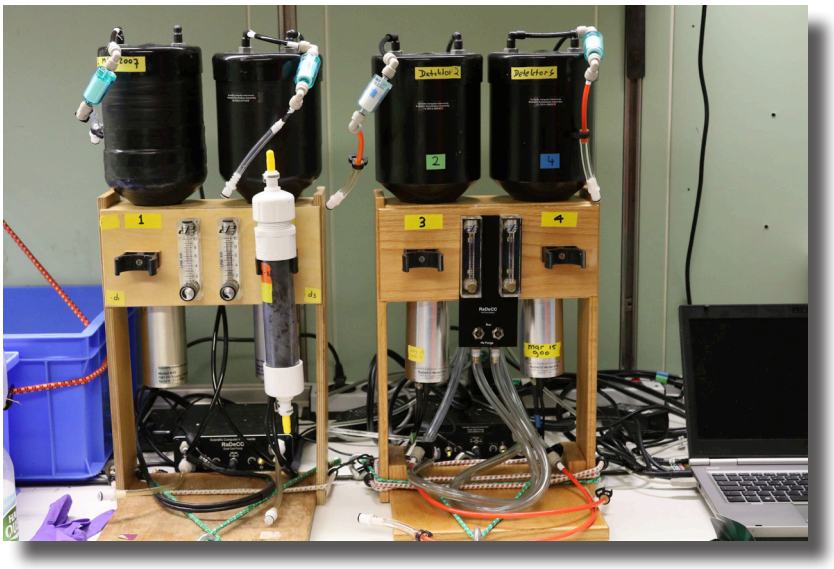

Fig. 12.4: Radium Delayed Coincidence Counter (RaDeCC system after Moore 1996)

Second, twelve sediment cores were taken on MUC stations and sampled for pore water which will be analysed for nutrient and trace metal distribution back in the home lab. Given the presence of drop stones in many cores analysis might prove difficult as some cores were disturbed. Pore water sampling was carried out on the following stations:

PS111_13-2	PS111_42-1	PS111_98-3
PS111_15-1	PS111_53-3	PS111_114-3
PS111_27-1	PS111_70-2	PS111_131-2
PS111_40-2	PS111_80-3	PS111_139-2

Briefly, each MUC contained one core housing with pre-drilled holes at a 1 cm distance. These holes were covered by adhesive tape. Upon retrieval of the core, rhizons were inserted into these holes and pore water collected in syringes (Fig. 12.5). The sample was split in three aliquots for analysis of sulfate, cations and nutrients.

Fig. 12.5: Pore water sampling with rhizons and syringes from a MUC core

Preliminary (expected) results

All chemical analysis will be done in the home lab at AWI or at GEOMAR (iron analysis in clean water samples taken by rubber boat and ice cores).

We expect to get a better idea of the distribution of both ^{226}Ra and ^{228}Ra in the Atlantic sector of the Southern Ocean. ^{226}Ra will indicate areas of upwelling of intermediate and deep waters. In addition, the ^{226}Ra/nutrient relationships will allow a closer look at the interaction between upwelling and particle export across frontal regions.

^{228}Ra will identify possible pathways of shelf waters in to the open ocean. This work will provide the first determination of activities of ^{228}Ra from the Filchner region, possibly a very important source for shelf-derived inputs. Together with existing ^{228}Ra-analyses from other parts of the Weddell Gyre, this will allow to close the budget for ^{228}Ra in the region. Iron analysis in shelf water, sediments, and sea ice will then be linked to ^{228}Ra to determine fluxes.

The sediment work will provide information on trace metal/radium ratios and the role of shelf sediments to provide the necessary iron for phytoplankton blooms.

Data management

All data collected during the expedition will be made available via the Data Publisher for Earth & Environmental Science PANGAEA, hosted by AWI and MARUM. Radium data will be submitted to the Geotraces data base (GDAC).

References

Annett AL, Henley SF, van Beek P, Ganeshram R, Venables HJ, Meredith MP, Geibert W (2013) Use of radium isotopes to estimate mixing rates and trace sediment inputs to surface waters in northern Marguerite Bay (Antarctic Peninsula). Antarctic Science 25 (3), 445-456, doi:10.1017/S0954102012000892.

Cai, P, Shi, X, Moore, WS, Peng, S, Wang, G, Dai, M (2014) ^{224}Ra:^{228}Th disequilibrium in coastal sediments: Implications for solute transfer across the sediment-water interface. Geochimica et Cosmochimica Acta, 125, 68–84.

Charette MA, Lam PJ, Lohan MC, Kwon EY, Hatje V, Jeandel C, Shiller AM, Cutter GA, Thomas AL, Boyd PW, Homoky WB, Milne A, Thomas H, Andersson PS, Porcelli D, Tanaka T, Geibert W, Dehairs F, Garcia-Orellana J (2016) Coastal ocean and shelf-sea biogeochemical cycling of trace elements and isotopes: lessons learned from GEOTRACES. Philosophical Transactions A.

Geibert W, Assmy P, Bakker, DCE, Hanfland C, Hoppema M, Pichevin LE, Schröder M, Schwarz JN, Stimac I, Usbeck R, Webb A (2010) High primary productivity in an ice melting hot spot at the eastern boundary of the Weddell Gyre. Global Biogeochemical Cycles, 24, GB3007. doi:10.1029/2009GB003657.

Hanfland C (2002) ^{226}Radium and ^{228}Radium in the Atlantic sector of the Southern Ocean. Berichte zur Polarforschung, 431, 135 p., hdl:10013/epic.10436.

Klunder MB, Laan P, DeBaar HJW, van Ooijen JC (2011) Dissolved iron in the Southern Ocean (Atlantic sector). DSR II, 58, 2678 – 2694. Doi: http://dx.doi.org/10.1016/j.dsr2.2010.10.042.

Klunder MB, Laan P, DeBaar HJW, Middag R, Neven I van Ooijen JC (2014) Dissolved Fe across the Weddell Sea and Drake Passage: impact of DFe on nutrient uptake. Biogeosciences, 11, 651-669.

Moore, WS, Arnold, R (1996) Ra in coastal waters using a delayed coincidence counter. Journal of Geophysical Research, 101(C1), 1321. https://doi.org/10.1029/95JC03139.

13. BENTHIC COMMUNITIES IN THE SOUTHEASTERN WEDDELL SEA

Claudio Richter[1], Nils Owsianowski[1], Henning Schröder[1], Lena Heins[1], Sandra Maier[2]

[1]AWI
[2]NIOZ

Grant-No. AWI_PS111_00

Objectives

On Antarctic shelves, sponges and other filter-feeders often dominate the megabenthic epifauna (Arntz et al., 1994), but the factors governing their distribution and patchiness are only poorly understood. Food supply and ice-berg scour are believed to be play antagonistic roles in the build-up and removal of benthic biomass, explaining much of the observed patchiness (Clarke et al., 2004). A benthic disturbance experiment (BENDEX) was initiated in 2003/2004 (PS65) to mimic the effect of ice-berg scour on the rich benthic communities in Austasen area and assess the resilience of the benthic community to this physical disturbance (Gerdes et al., 2008). A 1,000 x 100 m area was effectively stripped from its epibenthic cover by trawling and re-visited in later expeditions (PS77 in 2011, PS82 in 2013/14) showing only slow recovery compared to recently shelf-ice exposed areas in the Antarctic Peninsula/western Weddell Sea. Unfortunately, a subsequent attempt to access the BENDEX area during PS96 failed due to fast-ice, but the break-up of the fast-ice in the austral summer of 2017 offered an opportunity to revisit BENDEX in 2018 and assess the state of benthic recovery one and a half decades after initiation of the experiment.

Benthic oxygen uptake rate measurements are important to characterize the various habitats and estimate their demand for organic matter (Glud, 2008). Considering the existing data on fauna abundance for the Weddell Sea shelf, it is timely and highly relevant to investigate the community respiration also as a function of biomass and diversity. The Weddell Sea shelf offers contrasting sites of benthic biomass with high values along its eastern margin and lower values in the western and southern areas (Voß, 1988). It is crucial for our understanding of bentho-pelagic coupling to measure how much the patchy primary production is imprinted on the benthic carbon mineralization below and to supplant current P/B estimates with community respiration measurements.

An exploratory remotely operated vehicle (ROV) survey during the PS96 ice-camp in Drescher Inlet led to the discovery of a community of arcturid isopods living on the underside of the >80 m thick shelf-ice. It is not known so far, how these benthic filter-feeders have populated their peculiar habitat, what role they play in the Antarctic ecosystem and to what extent the measured densities are representative for other parts of the Weddell Sea ice shelf and beyond.

The objectives of this study were three-fold: (i) to repeat the surveys in the BENDEX and control areas to assess the dynamics of Antarctic benthic communities, (ii) to carry out benthic process studies relating benthic biomass to oxygen uptake and remineralization, and (iii) to explore the "hanging gardens" discovered in Drescher Inlet in other parts of the Weddell Sea in relation to potential factors governing the "seeding" of the shelf-ice with benthic organisms (e.g. rising platelet ice) and food supply (e.g. tidal currents).

Particularly, we aimed

- to assess the status of the recovery of benthic communities in the area of the long-term benthic disturbance experiment (BENDEX) started in 2003, in comparison with the natural benthic community dynamics
- to assess the benthic oxygen fluxes and sediment oxygen profiles in relation to benthic biomass and the re-mineralisation of organic matter in sediments
- to identify the abundance and spatial distribution of *Antarcturus spinacoronatus* on the face and underside of the shelf-ice in relation to bottom-up (food concentration, currents) and top-down factors (supply by platelet ice, removal by predators) governing the occurrence of "hanging gardens" at local and regional scales
- to assess the diet and metabolism (respiration, egestion) of *Antarcturus spinacoronatus* on the shelf-ice to assess its ecological role in the Weddell Sea

Work at sea

Work at sea involved (1) seabed imaging for benthic macro- and megafauna abundance and size, (2) the collection of water samples from the water column and near the benthos, (3) an assessment of oxygen consumption in the sediment and consecutive sampling for organic matter/pigment content, (4) the imaging of the ice shelf for macro- and megafauna abundance and size of shelf ice biota. A side aspect included (5) the inspection of the grounding line of the Antarctic ice sheet.

Seabed imaging was carried out with camera systems mounted on inspection and sampling gear including a remotely operated vehicle (ROV), a multicorer (MUC) and a multigrab sampler (MG).

The ROV (Ocean Modules, model V8 Sii) was equipped with two HD video cameras (Kongsberg oe14-502) in front and a standard wide-angle camera (Bowtech L3C-550) to observe the tether in the back. One of the Kongsberg cameras was later replaced by a 4K video camera (SubC Mk6) with the option of taking 16.6 MPx still images. The 4K and HD cameras were equipped with red lasers triplets marking the edges of a reference triangle on the videos (10 cm horizontal, 10 cm vertical). Laser, altimeter and inclination data will allow to scale the images for abundance and size estimates. The lighting was provided by dimmable LED lights (Bowtech LED-2400 aluminium), four in the front and one in the back. ROV navigation was ensured by a compass, an orientation sensor, an altimeter (Tritech Micron Echo Sounder), a Doppler Velocity Log (RDI EXP600-FAM5SC/EXPCP, an obstacle avoidance sonar (Tritech Micron) and an Ultra Short Baseline (USBL) system (IXSea, GAPS) linked to the GPS system of *Polarstern*. A CTD (SeaBird SBE19 plus) equipped with sensors for temperature, conductivity, pressure, pH, oxygen, photosynthetically active radiation, and chlorophyll fluorescence was mounted on the ROV, and the ensemble of video, CTD, navigation and ROV system data recorded on terabyte hard drives.

The ROV was deployed from the starboard side of *Polarstern* using a 550 m cable mounted on a winch (CORMAC 5, MacArtney). A 50 kg depressor weight kept the line taught and out of reach of the vessel's propellers and thrusters. A neutrally buoyant tether was connected to the winch cable allowing the ROV to move freely about a radius of 50 m around the weight.

On one occasion, a ROV transect of a former *Polarstern* expedition (ANT-XV/3) in 1998 (PS48/177) was repeated to assess the change in the seafloor community after a period of

20 years. The start and end position of the former ROV track was imported into the ROV data processing software “Ocean Floor Observation Protocol”, OFOP) along with the bathymetry of the area and the USBL position of the GAPS updated in real-time, to be able to follow the former track as closely as possible. During the transects with the two Kongsberg cameras, one of the cameras was directed perpendicularly towards the ground, whereas the other one was looking forward in an angle of 40-45°. A distance of 1-2 m was kept to the ground, mainly to avoid sediment resuspension caused by the ROV’s thrusters. In the set-up using the SubC Mk6 camera, both cameras were oriented in parallel in the horizontal plane and the ROV oriented level (shelf ice transects) or at an angle of 40-45° to the ground (sea bed transects).

Due to problems with a connector on the telemetry system on board *Polarstern*, initial observations on MUC and GC had to be carried out with a provisional offline camera system consisting of a Git2 camera (2K video mode, GitUp) in an underwater housing (Benthic2, GroupBinc) with custom mounts for MUC and MG. After fixing the connector on the vessel’s deep-sea fibre optics cable, the telemetry and video and camera system (Canon EOS 100D, iSiTEC) was mounted on the MUC. The system allows online video monitoring (but not recording) and automated/manual capture of 16 MP still images.

For the collection of water samples, the CTD-rosette was used. It was operated by the CTD team (see chapter 3) who kindly provided Niskin samples from six standard depths: surface (5 m, 20 m, 40 m, 60 m, 80 m and 5 m.a.b.). Occasionally, depths were adjusted by ± 10 m to account for features apparent in the downcast of the CTD that would have escaped detection by the standard depths (e.g. the chlorophyll fluorescence maximum). The 12 L bottles were released during the upcast, and 2 L aliquots were transferred by silicone tubing to Nalgene bottles, stored in a coolbox and processed without delay.

Samples for suspended organic carbon and nitrogen (POC and PON) were filtered through pre-weighed and pre-combusted GF/F filters and stored frozen at -20°C. Samples for phytoplankton and ice-algae pigments were filtered through GF/F filters and stored frozen at -20°C.

Sediment cores were taken with the MUC in cooperation with the geology team (see chapter 14). Generally, two cores per station were transferred to the temperature-controlled lab container (0°C) in F-Deck, stored in a water bath at near ambient temperature (-1.5 ± -1 °C), and aerated with an air stone (top 5 cm) until initiating the experiment (generally without delay, max. overnight). Initially, a third core was sieved (500 µm) to assess the abundance of dropstones likely interfering with the microsensor measurements. As dropstones were common, a 1000 µm diameter needle was used to puncture the sediment down to 50 mm, before carrying out the microprofile. This precaution, which appeared to have no measurable effect on the oxygen profile in sediments featuring high oxygen penetration depths, allowed us to extend the lifetime of the microoptodes (Bare Fiber Oxygen Sensors, Pyroscience, glued in needles) and to abandon the processing of the third core for drop-stones. Optodes were two-point calibrated in water at 0° ± 0.5°C at 100 % O_2 saturation (air-bubbled MilliQ) and 0 % O_2 saturation (saturated sodium sulfite solution in MilliQ) and mounted on a micromanipulator (MU1, Pyroscience) using an adaptor rod. Profiles (1-3 per core) were carried out in 1 mm steps (17 s per depth step) between the boundary layer (20 mm above the sediment) and 50 mm into the sediment. Profile data (depth, oxygen concentration) were logged electronically using the “Profix” software (Pyroscience). After execution of the microprofiles, the supernatant above the sediment was reduced to 5 to 13 cm using a perforated stopper. A microoptode of the same type was introduced through the stopper into the supernatant and the evolution of the oxygen concentration monitored over time (24 to 71 h, O_2 saturation >80 %) using the software “Pyro Oxygen Logger” (Pyroscience) to assess the respiration of the core biota (microbes and fauna). Stirring (16.5 rpm) was provided by a magnetic stirrer in the stopper. After the end of the incubation experiment, two 24 ml samples of sediment were taken from each core by

means of a cut-off syringe inserted 8.5 cm vertically into the core. Samples were stored frozen at -20°C for later analysis of sediment grain size, porosity, pigments as well as organic carbon and nitrogen content. Finally, the remainder of the core was sieved through 500 µm and the macrofauna (plus larger grains/stones) stored frozen at -20°C for later analysis of biomass and organic C and N content.

The multigrab (MG) was deployed at two stations in the area of the former Benthic Disturbance Experiment during PS65 (ANT-XXI/2, December 2003). Our goal to repeat MG sampling of a formerly disturbed and undisturbed station, respectively, more than 13 years after the experiment was thwarted due to unfortunate circumstances. The failure by the vessel of providing a functioning connector to link the MG's online camera and telemetry system to the fibre-optics deep-sea cable forced us to deploy the MG blindfolded on a hit or miss mission to the only 100 m wide swath of disturbed area. In spite of ideal working conditions (no ice, no wind) the vessel was unable to maintain the prescribed sampling location for the disturbed area ANT-XXI/2-183 so that we very likely ended up with samples from two undisturbed areas. For each of the stations, the sediment from 8 replicate grabs were sieved through 500 µm mesh and stored in 4 % borax-buffered formaline.

Preliminary (expected) results

A total 45 stations were occupied by the benthic communities' team (Table 13.1, Fig. 13.1). Water samples were collected at 19 stations from the CTD. Twelve out of 16 MUC stations sampled yielded sediment cores for microprofiles and incubations. The ROV was deployed at eight stations, the MG at two.

Tab. 13.1: List of stations occupied by the benthic communities' team during PS111 for observations, measurements and samples collected with conductivity temperature depth probe (CTD) mounted on a rosette, multicorer (MUC), multigrab (MG), and Remotely Operated Vehicle (ROV). Failed MUC attempts (mostly due to rocky bottom) are shaded in grey. BENDEX indicates the Benthic Disturbance Experiment carried out in 2003. Two ROV dives with technical difficulties had to be aborted, shelf ice+ indicate shelf ice transects followed by bottom transects, repeat tr followed the PS48/177 ROV transect carried out in 1998.

Gear	Station	Date Time	Latitude	Longitude	Depth [m]	Remarks
CTD	PS111_27-3	05.02.18 18:44	75° 57.288' S	029° 04.928' W	426	
CTD	PS111_29-1	06.02.18 06:22	75° 58.382' S	027° 40.870' W	402	
CTD	PS111_40-3	10.02.18 09:22	76° 00.062' S	054° 14.398' W	513	
CTD	PS111_42-3	10.02.18 20:37	76° 08.680' S	053° 21.396' W	493	
CTD	PS111_47-1	11.02.18 13:17	74° 59.008' S	060° 00.095' W	661	
CTD	PS111_53-1	12.02.18 23:26	76° 01.553' S	054° 07.238' W	497	
CTD	PS111_60-1	14.02.18 04:30	77° 01.202' S	045° 23.820' W	320	
CTD	PS111_70-1	17.02.18 00:55	76° 07.425' S	033° 39.952' W	790	
CTD	PS111_74-1	17.02.18 13:29	76° 12.814' S	029° 40.556' W	387	
CTD	PS111_80-1	18.02.18 08:11	76° 38.705' S	035° 25.848' W	932	
CTD	PS111_86-1	19.02.18 02:26	77° 25.029' S	034° 19.894' W	167	
CTD	PS111_98-1	20.02.18 07:20	77° 47.370' S	040° 27.689' W	926	

Gear	Station	Date Time	Latitude	Longitude	Depth [m]	Remarks
CTD	PS111_109-1	22.02.18 01:14	77° 42.642' S	035° 14.128' W	461	
CTD	PS111_111-1	22.02.18 08:44	77° 00.565' S	033° 56.969' W	453	
CTD	PS111_114-1	22.02.18 18:12	76° 23.246' S	033° 58.359' W	839	
CTD	PS111_121-1	25.02.18 03:01	75° 29.938' S	031° 54.026' W	757	
CTD	PS111_131-1	26.02.18 12:43	74° 37.042' S	036° 55.373' W	387	
CTD	PS111_138-1	28.02.18 22:29	75° 07.767' S	026° 02.664' W	400	
CTD	PS111_140-1	01.03.18 11:26	75° 07.961' S	026° 37.935' W	341	
MUC	PS111_27-1	05.02.18 17:20	76° 06.592' S	033° 39.041' W	794	
MUC	PS111_29-3	06.02.18 07:37	76° 12.817' S	029° 40.546' W	381	
MUC	PS111_40-2	10.02.18 08:49	76° 12.817' S	029° 40.549' W	381	
MUC	PS111_42-1	10.02.18 19:05	76° 12.807' S	029° 40.568' W	382	
MUC	PS111_47-2	11.02.18 14:05	76° 12.788' S	029° 40.565' W	369	
MUC	PS111_53-3	13.02.18 00:45	76° 38.528' S	035° 25.736' W	933	
MUC	PS111_60-3	14.02.18 05:24	76° 38.493' S	035° 25.798' W	932	
MUC	PS111_70-2	17.02.18 01:48	76° 38.460' S	035° 25.889' W	932	
MUC	PS111_74-4	17.02.18 15:29	76° 38.453' S	035° 25.910' W	932	Empty
MUC	PS111_80-3	18.02.18 09:47	77° 25.020' S	034° 19.928' W	167	
MUC	PS111_86-2	19.02.18 03:06	77° 25.006' S	034° 20.000' W	169	Empty
MUC	PS111_98-3	20.02.18 09:06	77° 25.006' S	034° 20.006' W	169	
MUC	PS111_111-3	22.02.18 09:45	77° 25.001' S	034° 20.023' W	170	Empty
MUC	PS111_114-3	22.02.18 19:46	77° 24.997' S	034° 20.036' W	171	Empty
MUC	PS111_131-2	26.02.18 13:30	77° 00.594' S	033° 56.465' W	453	
MUC	PS111_139-2	01.03.18 03:04	77° 00.596' S	033° 56.448' W	453	
MG	PS111_14-3	31.01.18 11:12	70° 56.587' S	010° 32.019' W	302	BENDEX
MG	PS111_14-4	31.01.18 12:20	70° 56.642' S	010° 31.607' W	282	BENDEX
ROV	PS111_14-2	31.01.18 09:42	70° 56.677' S	010° 31.130' W	NA	Aborted
ROV	PS111_3w0-2	06.02.18 18:10	76° 00.952' S	027° 42.641' W	440	Aborted
ROV	PS111_36-2	09.02.18 19:34	76° 30.515' S	052° 48.656' W	401	shelf ice+
ROV	PS111_57-1	13.02.18 13:14	77° 01.638' S	050° 29.897' W	292	shelf ice+
ROV	PS111_63-2	15.02.18 14:30	75° 21.496' S	041° 06.554' W	370	A23A+
ROV	PS111_117-1	23.02.18 14:30	77° 35.069' S	034° 32.573' W	158	ice sheet+
ROV	PS111_137-1	28.02.18 14:51	75° 28.530' S	027° 05.615' W	254	repeat tr
ROV	PS111_141-3	01.03.18 18:19	75° 27.945' S	026° 54.975' W	233	shelf ice

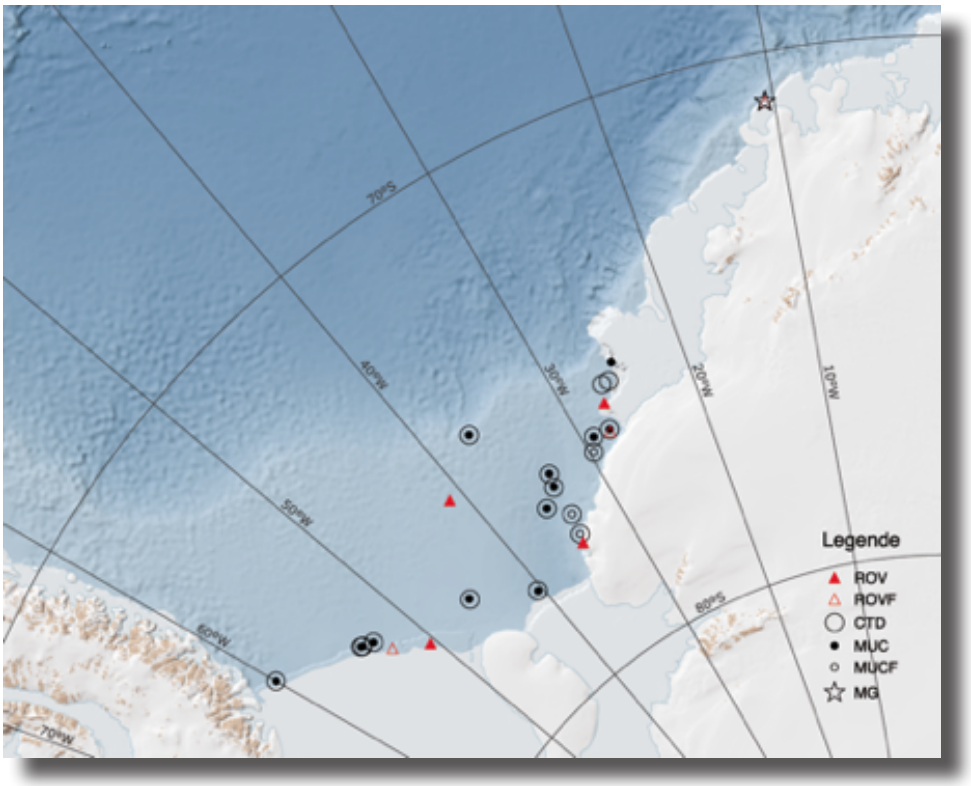

Fig. 13.1: Map of stations occupied by the benthic communities team showing the locations of samples and observations obtained by remotely operated vehicle (ROV, where open triangles ROVF indicate stations that had to be aborted due to technical problems), conductivity-temperature-depth probe and Niskin rosette sampler (CTD), multicorer (MUC, where open circles MUCF indicate stations that yielded empty sediment cores) and multigrab (MG). Map drawn by L. Heins.

Benthic oxygen fluxes

A total of 25 sediment cores were profiled and incubated. The oxygen concentration at 5 cm sediment depth varied between 0 and 64 % saturation. Stations 27_1, 131_2 and 139_2, were characterized by an oxygen penetration depth of less than 5 cm (1.9 to 4.8 cm). Although the analysis of the sediment parameters is still pending, the oxygen fluxes show some relation to the environmental data measured with the CTD; e.g., the shallowest oxygen penetration depth was found where the CTD fluorescence profile indicated a recent phytoplankton bloom. Intense microbial remineralization of the settled organic material is the likely cause for the sharp drop in oxygen levels.

Shelf ice environment and biota

Three ROV dives were carried out down the front of the ice shelf (Ronne, Halley), one down to the bottom of the grounded ice berg A23A, and one at the front of the continental ice sheet down to the grounding line (Coats Land) (Fig. 13.1). Most of the dives showed the typical dimpled “golf ball’ aspect of a melting ice front. The dive in front of the Ronne ice shelf (PS111_36-2), however, showed in addition to the dimpled ice at depth a conspicuously different type of ice aloft: a region of greyish ice with a rough surface with an abrupt transition between the two ice types. The very cold temperature of the water, the occurrence of platelet ice in the water and the salinity data in relation to the ice distribution provide observational support for an ice pump at work (Lewis & Perkin, 1986), with melting of meteoric ice at depth and accretion of marine ice aloft (Foldvik & Kvinge, 1974). Another interesting finding was the

grounding line of the Coats Land ice front (PS111_117-1), where a thin layer of transparent ice was found attached to the underside of the meteoric ice, suggesting re-freezing of meltwater. Shelf-ice biota was limited to microphytobenthic algae growing on the ridges of the dimples (PS111_117-1) down to >60 m and occasional fish perched to the ice (Fig. 13.2), reminiscent of Gutt's (2002) report of *Pagothenia borchgrevinki* associated with the ice shelf at Drescher Inlet. Contrary to Bornemann et al.'s (2016) findings at Drescher Inlet during PS96, we did not find any *Antarcturus spinacoronatus* in any of our dives.

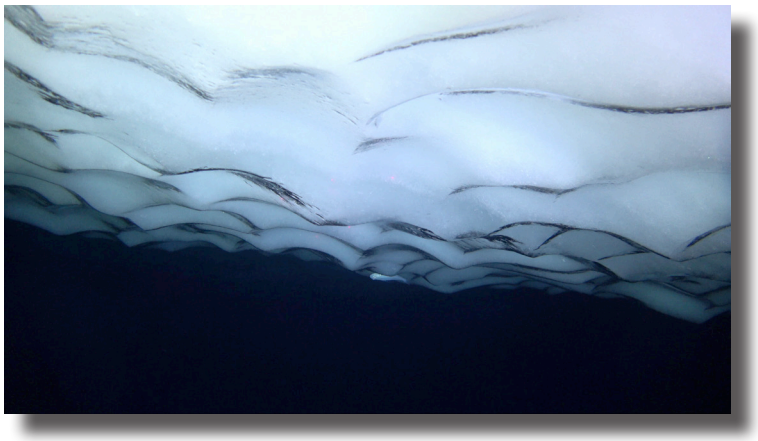

Fig. 13.2: Underside of the Brunt shelf ice near Halley at station PS111_141-3 showing the typical dipled structure of the melting meteoric ice. A fish (likely a juvenile Pagothenia bochgrevinki) can be seen perched to the ice. Video frame taken by N. Owsianowski.

Seafloor biota

Four of the ROV stations included seafloor observations. One surprising finding was the occurrence of a diverse benthic community in the vicinity of the Ronne ice shelf including hexactinellid sponges and a ray (Fig. 13.3). Previous surveys during PS96 had shown a depauperate fauna in the southwestern Weddell Sea and notable absence of glass sponges. Another interesting finding was the observation of moraine-like ridges in the vicinity of the giant iceberg A23A (PS111_63-2), possibly generated by the advance of the now grounded iceberg. Another was the observation of a brachiopod "graveyard" in one of the troughs (Fig. 13.4).

Fig. 13.3: Seafloor image in front of the Ronne ice shelf at station PS111_36-2, showing a rare ray and an unexpected hexactinellid sponge (likely Rossella podagrosa) in the background. Horizonal laser dots are spaced 10 cm apart. Video frame taken by N. Owsianowski.

Fig. 13.4: Aggregation of brachiopod shells near the grounded iceberg A23A (PS111_63-2) providing a substrate for bushy bryozoans. In the left of the image is a feather star (likely Umbellula sp.). Horizontal laser dots are spaced 10 cm apart. Video frame taken by N. Owsianowski.

Data management

Data and related information will be made available in the Data Publisher for Earth and Environmental Science (PANGAEA, www.pangaea.de).

References

Arntz WE, Brey T, Gallardo VA (1994) Antarctic zoobenthos. Oceanography and Marine Biology: an Annual Review, 32, 241-304.

Bornemann H, Held C, Nachtsheim D, Owsianowski N, Richter C, Steinmetz R (2016) Seal research at the Drescher Inlet, 116-129. In: Schröder M, The Expedition PS96 of the Research Vessel POLARSTERN to the southern Weddell Sea in 2015/2016. Berichte zur Polarforschung 700, doi:10.2312/BzPM_0700_2016.

Clarke A, Aronson RB, Crame JA, Gili JM, Blake DB (2004) Evolution and diversity of the benthic fauna of the Southern Ocean continental shelf. Antarctic Science, 16(4), 559-568.

Foldvik A, Kvinge T (1974) Conditional instability of sea water at the freezing point. Deep-sea research, 21, 160-174.

Gerdes D, Isla E, Knust R, Mintenbeck K, Rossi S (2008) Response of Antarctic benthic communities to disturbance: first results from the artificial Benthic Disturbance Experiment on the eastern Weddell Sea Shelf, Antarctica. Polar Biology, 31(12), 1469-1480.

Glud RN (2008) Oxygen dynamics of marine sediments. Marine Biology Research, 4, 243-289.

Lewis EL, Perkin RG (1986) Ice pumps and their rates. Journal of geophysical research, 91, 11756-11762

Voß J (1988) Zoogeographie und Gemeinschaftsanalyse des Makrozoobenthos des Weddellmeeres (Antarktis). Berichte zur Polarforschung, 45.

14. MARINE GEOLOGY

Hannes Grobe[1], Jan-Erik Arndt[1], Marcus Gutjahr[2], Maria-Elena Vorrath[1], Huang Huang[2,3], Juliane Müller[1], Gerhard Kuhn[1], Claus-Dieter Hillenbrand[4] (not on board)

[1]AWI
[2]GEOMAR
[3]Uni Kiel
[4]BAS

Grant-No. AWI_PS111_00

Introduction

Past and ongoing geoscientific and oceanographic research in Antarctica's Weddell Sea sector has highlighted the key role of this area for influencing sea level, thermohaline circulation and climate at a global scale. However, scenarios of the possible contribution of ice-sheet melting to global sea-level rise and of past and future changes in water-mass circulation are mainly based on numerical models or reconstructions from far-field data because proximal evidence from the Weddell Sea embayment is sparse. Geological samples obtained in the study area will provide the base for reconstructing and dating advance/retreat phases of the Ronne and Filchner Ice Shelfs during past climate fluctuations. These sediments further permit the identification of feedbacks between changes in sea ice coverage and the formation of deep-water in the Weddell Sea, which has a significant impact on global ocean circulation patterns. These data help to improve the performance and reliability of climate models. Water column samples will be analysed to obtain a spatially resolved insight into Weddell Sea neodymium (Nd) isotopic variations Rare Earth Element (REE) systematics. Surface sediments will be used for calibration studies for radiogenic isotopic water mass and ice sheet tracers, while longer sediment cores will provide paleoceanographic records. Particular focus is set on two geochemical scientific aspects and one sedimentological investigation including glacial-geomorphological features.

14.1 Biomarker

Objectives

Since Antarctic sea ice is highly variable and its modelling is yet delimited due to paleo records a development of and reliable and stable sea ice proxy is required. Based on an organic geochemical approach the use of specific biomarker lipids (highly branched isoprenoids; IPSO25; Belt et al., 2016) is conducted as a tool for Antarctic sea ice reconstructions. To evaluate the information value of this biomarker a broad data set of short sediment cores from sea ice areas covering the latest climate history shall be used.

Work at sea

Devices deployed for geological sampling were the Multicorer (MUC) and a 1.5 t gravity corer (GC) equipped with a 10 to 3 m core barrels. The MUC was deployed on 22 stations of which 4 had no recovery. The GC was used on 20 stations (see 14.3). The MUC failed four times due to hard ground and presence of dropstones. One time the recovery of sediment from the MUC was so small (2 cm) that the sediment got lost during the tube recovery and a sampling was not possible. Due to the cold conditions (-22°C) the MUC had to be cleaned from frozen sea

water and sediment. A few times the closing mechanisms of the MUC had to be deconstructed and cleaned separately in the lab. The whole construction was kept warm and dry under a Persenning and a heating below to prevent freezing.

Sampling of the MUCs took place onboard into combusted glass vials (biomarker, 1 cm slices) and Whirlpack sampling bags (sedimentology, micropaleontology, 1cm slices, ikaites, 2 cm slice) and aluminium foil with plastic foil (archive core, whole core in one peace). Samples designated for **biomarker** studies at home laboratories at AWI as well as the archivated sediment core needed to be stored frozen (-20°C). Surface sediment samples from areas where ice platelets occur (at ice shelf edges) such as the ikaite samples were stored at 0°C (handled and stored anytime below +4°C!). The samples of sedimentology and micropaleontology were stored at +4°C.

Preliminary (expected) results

No analytical data are available so far. The samples from the multicorer were cut and stored cooled/frozen from different working groups (see Table 14.1). One whole MUC-core was packed in aluminium foil and stored at -20°C for archiving.

Data management

Analytical data will be available latest with publication as supplement related to each publication. All datasets will be made citable including a DOI.

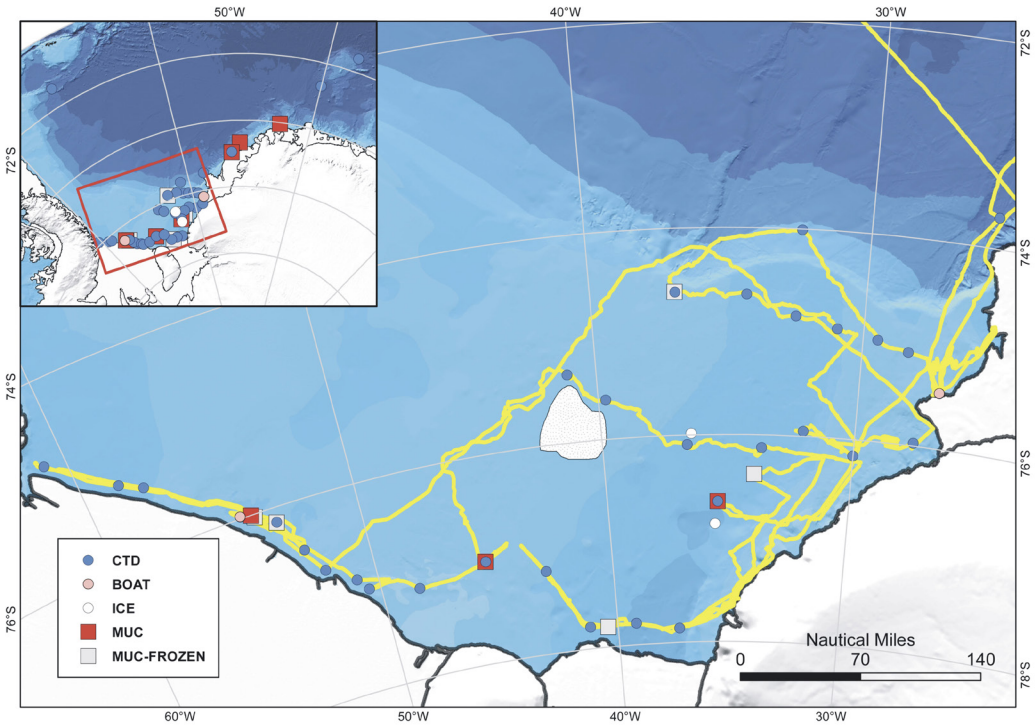

Fig. 14.1: Location of MUC-stations during PS111

Tab. 14.1: This table summarizes all MUC samples of the cruise PS111 with its recovered core length, the purpose of sampling and the amount of samples per working group. For archiving a whole core was frozen at every possible station.

Label	Recov. [cm]	Purpose	No of samples	PI
PS111_13-2	26	Biomarker	24	Juliane Müller
		Micropaleontlogy	27	Oliver Esper
		Sedimentology	23	Gerhard Kuhn
		Archive	1 Core	Curator
		Nd and Pb Isotopes + REE in porewater and sediment	36	Marcus Gutjahr
		Pore Water	17	Claudia Hanfland
		Sediment Radium	5	Claudia Hanfland
PS111_13-3	25	Ikaite	1	Gerhard Kuhn
PS111_15-1	25	Biomarker	24	Juliane Müller
		Micropaleontlogy	24	Oliver Esper
		Sedimentology	21	Gerhard Kuhn
		Archive	1 Core	Curator
		Ikaite	1	Gerhard Kuhn
		Nd and Pb Isotopes + REE in porewater and sediment	55	Marcus Gutjahr
		Pore Water	17	Claudia Hanfland
		Sediment Radium	23	Claudia Hanfland
		Plastic	1	Thomas Mani
PS111_16-3	32	Biomarker	28	Juliane Müller
		Micropaleontlogy	23	Oliver Esper
		Sedimentology	27	Gerhard Kuhn
		Archive	1 Core	Curator
		Ikaite	1	Gerhard Kuhn
		Nd and Pb Isotopes + REE in porewater and sediment	40	Marcus Gutjahr
		Plastic	1	Thomas Mani
PS111_27-1	10	Biomarker	9	Juliane Müller
		Micropaleontlogy	5	Oliver Esper
		Pore Water	7	Claudia Hanfland
		Incubation, Porosity, C and N	4	Claudio Richter
		Plastic	1	Thomas Mani
PS111_29-2	2	no sampling possible		
PS111_29-3	10	Biomarker	7	Juliane Müller
		Incubation	2	Claudio Richter
PS111_40-2	41	Biomarker	39	Juliane Müller
		Micropaleontlogy	39	Oliver Esper
		Sedimentology	37	Gerhard Kuhn
		Archive	1 Core	Curator

Label	Recov. [cm]	Purpose	No of samples	PI
		Ikaite	1	Gerhard Kuhn
		Incubation, Porosity, C and N	4	Claudio Richter
		Nd and Pb Isotopes + REE in porewater and sediment	40	Marcus Gutjahr
		Pore Water	24	Claudia Hanfland
		Plastic	1	Thomas Mani
PS111_42-1	38	Biomarker	33	Juliane Müller
		Micropaleontlogy	35	Oliver Esper
		Sedimentology	34	Gerhard Kuhn
		Archive	1 Core	Curator
		Ikaite	1	Gerhard Kuhn
		Incubation, Porosity, C and N	4	Claudio Richter
		Nd and Pb Isotopes + REE in sediment	1	Marcus Gutjahr
		Pore Water	23	Claudia Hanfland
		Plastic	1	Thomas Mani
PS111_47_2	34	Biomarker	30	Juliane Müller
		Micropaleontlogy	29	Oliver Esper
		Sedimentology	30	Gerhard Kuhn
		Archive	1 Core	Curator
		Ikaite	1	Gerhard Kuhn
		Incubation, Porosity, C and N	4	Claudio Richter
		Plastic	1	Thomas Mani
PS111_53-3	40	Biomarker	38	Juliane Müller
		Micropaleontlogy	40	Oliver Esper
		Sedimentology	39	Gerhard Kuhn
		Archive	1 Core	Curator
		Ikaite	1	Gerhard Kuhn
		Incubation, Porosity, C and N	4	Claudio Richter
		Nd and Pb Isotopes + REE in sediment	1	Marcus Gutjahr
		Pore Water	24	Claudia Hanfland
		Sediment Radium	19	Claudia Hanfland
		Plastic	1	Thomas Mani
PS111_60-2	no recovery			
PS111_60-3	24	Biomarker	38	Juliane Müller
		Micropaleontlogy	22	Oliver Esper
		Sedimentology	23	Gerhard Kuhn
		Archive	1 Core	Curator
		Ikaite	1	Gerhard Kuhn
		Incubation, Porosity, C and N	4	Claudio Richter

Label	Recov. [cm]	Purpose	No of samples	PI
		Nd and Pb Isotopes + REE in porewater and sediment	22	Marcus Gutjahr
		Sediment Radium	16	Claudia Hanfland
		Plastic	1	Thomas Mani
PS111_70-2	34	Biomarker	32	Juliane Müller
		Micropaleontlogy	28	Oliver Esper
		Sedimentology	22	Gerhard Kuhn
		Archive	1 Core	Curator
		Ikaite	1	Gerhard Kuhn
		Incubation, Porosity, C and N	4	Claudio Richter
		Pore Water	23	Claudia Hanfland
		Plastic	1	Thomas Mani
PS111_74-4	no recovery			
PS111_80-3	30	Biomarker	28	Juliane Müller
		Micropaleontlogy	19	Oliver Esper
		Sedimentology	23	Gerhard Kuhn
		Archive	1 Core	Curator
		Ikaite	1	Gerhard Kuhn
		Incubation, Porosity, C and N	4	Claudio Richter
		Nd and Pb Isotopes + REE in porewater and sediment	27	Marcus Gutjahr
		Pore Water	17	Claudia Hanfland
		Sediment Radium	15	Claudia Hanfland
		Plastic	1	Thomas Mani
PS111_86-2	no recovery			
PS111_98-3	41	Biomarker	38	Juliane Müller
		Micropaleontlogy	28	Oliver Esper
		Sedimentology	40	Gerhard Kuhn
		Archive	1 Core	Curator
		Ikaite	1	Gerhard Kuhn
		Incubation, Porosity, C and N	4	Claudio Richter
		Pore Water	24	Claudia Hanfland
		Nd and Pb Isotopes + REE in sediment	1	Marcus Gutjahr
PS111_111-3	no recovery			
PS111_114-3	39	Biomarker	34	Juliane Müller
		Micropaleontlogy	29	Oliver Esper
		Sedimentology	33	Gerhard Kuhn
		Archive	1 Core	Curator
		Ikaite	1	Gerhard Kuhn
		Incubation, Porosity, C and N	4	Claudio Richter
		Pore Water	20	Claudia Hanfland

Label	Recov. [cm]	Purpose	No of samples	PI
		Nd and Pb Isotopes + REE in sediment	1	Marcus Gutjahr
		Plastic	1	Thomas Mani
PS111_131-2	29	Biomarker	23	Juliane Müller
		Micropaleontlogy	16	Oliver Esper
		Sedimentology	24	Gerhard Kuhn
		Archive	1 Core	Curator
		Ikaite	1	Gerhard Kuhn
		Incubation, Porosity, C and N	4	Claudio Richter
		Pore Water	20	Claudia Hanfland
		Nd and Pb Isotopes + REE in sediment	1	Marcus Gutjahr
		Plastic	1	Thomas Mani
PS111_139-2	6	Biomarker	4	Juliane Müller
		Micropaleontlogy	6	Oliver Esper
		Sedimentology	6	Gerhard Kuhn
		Archive	1 Core	Curator
		Ikaite	1	Gerhard Kuhn
		Incubation, Porosity, C and N	4	Claudio Richter
		Pore Water	8	Claudia Hanfland
		Nd and Pb Isotopes + REE in sediment	1	Marcus Gutjahr
		Plastic	1	Thomas Mani

14.2 Isotope geochemistry

Objectives

Within the frame of an ongoing PhD dissertation work (Huang Huang) a deep water and marginal marine neodymium (Nd) and lead (Pb) isotopic reconstruction on the Weddell Sea and Southern Ocean is currently generated extending back to the penultimate glacial termination (~140 ka BP). This dissertation is a collaboration between GEOMAR Kiel and AWI Bremerhaven, co-supervised by Marcus Gutjahr (Kiel), Gerhard Kuhn (Bremerhaven) and Anton Eisenhauer (Kiel). Seawater-derived Nd and Pb isotopes are sensitive indicators of water mass sourcing and mixing. The East Antarctic craton for example is much older than the West Antarctic Peninsula. This distinct geology leads to different Nd and Pb isotopic signatures imparted to water masses circulating through the Weddell Sea as well as meltwater supplied to the Ronne-Filchner Trough area. Dissolved Nd and Pb are incorporated into authigenic Fe-Mn oxyhydroxides in marine sediments and can be extracted using a gentle reductive leaching approach (Gutjahr et al., 2007; Blaser et al., 2016). In fact marine sediments are a mixture of different phases such as carbonates, organic matter, authigenic Fe-Mn oxyhydroxides as well as the terrigenous fraction, each carrying a distinct Nd and Pb isotopic signal. While the two studies mentioned above provided strong support for the reliability of this technique in extracting bottom water Nd and Pb isotope compositions from North Atlantic settings, reductive leaching aiming to extract past bottom water isotope signatures was so far not rigorously

tested for Antarctic sediments. Such sediments are chemically immature since these were largely only physically weathered during sub-glacial erosion. As a result, any freshly ground sediment is chemically relative reactive potentially releasing terrigenous (i.e. non-seawater derived Nd and Pb) during chemical leaching which may ultimately be offsetting extracted bottom water isotopic information.

While first paleo-records look strikingly promising highlighting strong paleocirculation changes over the two last deglaciations, we further want to demonstrate that bottom water Nd and Pb isotopic compositions are indeed reliably archived in Weddell Sea sediments. To this end, sampling for isotope geochemistry (Nd and Pb isotopes as well as Rare Earth Element (REE) concentrations) were done on surface sediments, collected by means of the multicorer (MUC). The Nd and Pb isotopes as well as trace metal concentration of the different sedimentary phases in the MUC samples will be compared. Phases to be assessed comprise (i) the sediment porewater, (ii) authigenic Fe-Mn oxyhydroxides as well as (iii) the residual terrigenous phase. This investigation will also provide crucial information on trace metal cycling in the uppermost few centimetres below the sediment – bottom water interface.

Besides the sedimentary approach described above, the Weddell Sea Nd isotopic as well as its REE composition is for the first time assessed in a comprehensive water sampling campaign led by Marcus Gutjahr. To date previously published southernmost Nd isotopic seawater data exist only from the NE Weddell Sea (Stichel et al., 2012a; Stichel et al., 2012b), despite the fact that the Southern Weddell Sea is the most important AABW formation area (Orsi et al., 1999). Given its unique circulation scheme and hinterland geology, we expect large regional Nd isotopic gradients dependent on water mass sourcing, particularly in the Ronne-Filchner Trough area. Our aim is to provide a water mass Nd isotopic budget for the Southern Weddell Sea area and better constrain the Weddell Sea Deep Water Nd isotope signature exported to Southern Ocean areas further north. A related study was carried out by the investigators during ANT-XXVI/3 along the West Antarctic margin (Rickli et al., 2014).

Work at sea

MUC sampling

Cores for the isotope geochemical studies were taken from identical locations as done for the biomarker studies (section 14.1) with the only difference that not as many core sites were required. Between one and three cores per site were sampled under special trace metal-clean conditions. Fig. 14.IG-1 highlights MUC locations used for the geochemical work as well as those cores frozen at -20°C and taken home for future work. After arrival of the MUC on board *Polarstern* during station work, about three litres of MUC water (i.e. bottom water inside the core liners) of selected cores were collected, filtered (0.2 μm mesh size) and acidified for further Nd and Pb isotopic, as well as REE analyses back at GEOMAR Kiel. MUC sediment sampling was carried out under oxygen-free conditions in glove bags (Fig. 14.IG-2). This setup was chosen to prevent precipitation of certain cations such as Fe under elevated oxygen concentrations. Secondly this approach prevented contamination of trace metal concentrations and isotopic compositions in the sediment- and porewater samples. Sampling was carried out in two centimetre increments, transferring sediments into 50 mL centrifuge vials. Sediments were centrifuged for 60 minutes at 4,000 rpm on board. The separated porewaters, usually between 2 mL to about 25 mL of solution, was filtered (0.2 μm mesh size) and acidified for further Nd and Pb isotopic, as well as REE analyses back at GEOMAR Kiel. For each core filtered but unacidified aliquots were analysed for their alkalinity, its ammonia and phosphate concentrations in the chemistry lab on board *Polarstern*. In total MUC sediments from six

stations were sliced and processed on board, while another five sediment cores were frozen at -20°C for further work at GEOMAR Kiel (Fig. 14.IG-1; Table 14.IG-1).

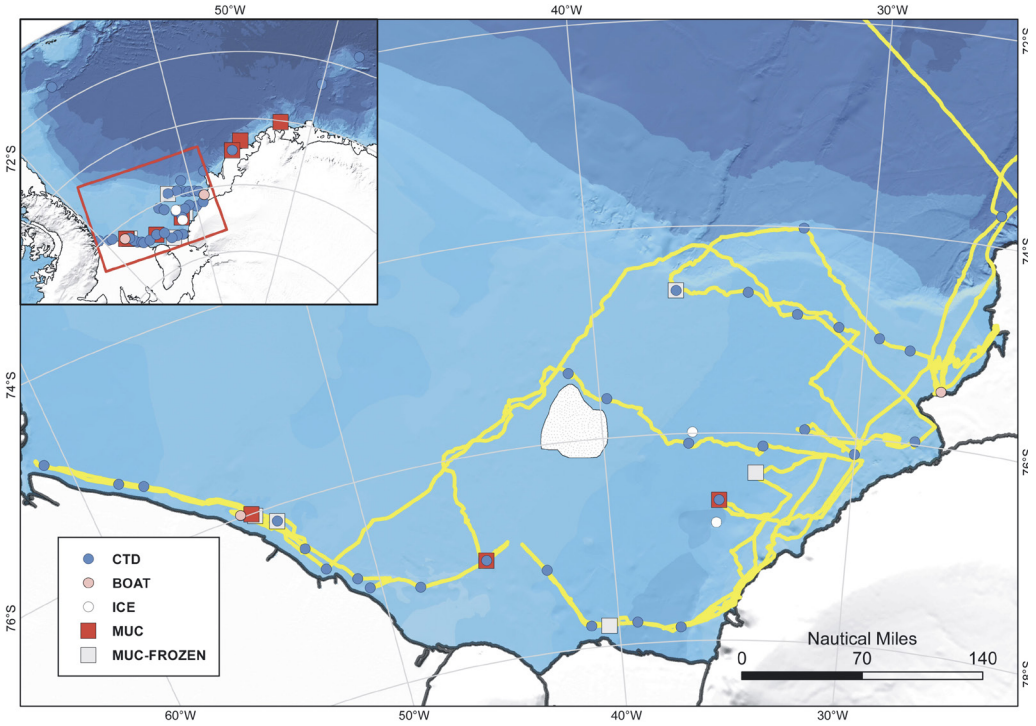

Fig. 14.IG-1: Overview map of all stations covered for the isotope geochemical work of the Marine Geology group on board Polarstern during PS111. Stations within the Ronne-Filcher shelf area are shown in large map. The inset map also shows several CTD and MUC stations occupied during PS111. Bathymetric data following IBCSO (Arndt et al., 2013).

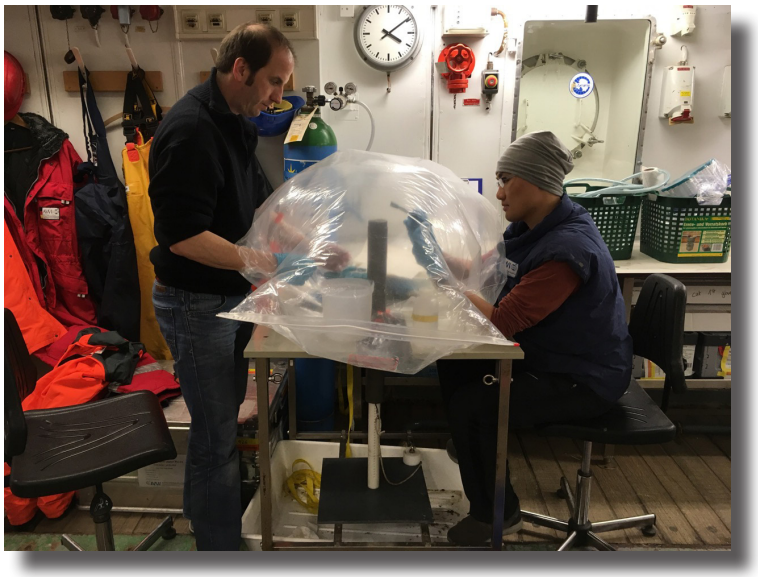

Fig. 14.IG-2: Multi core sediment sampling for porewater extraction was carried out under oxygen-free conditions in an argon atmosphere. This setup also prevented contamination with unwanted trace metals during handling in a non-clean room environment. After centrifugation porewater samples were filtered into pre-cleaned containers in a second oxygen-free glove bag.

Seawater sampling for Nd isotope and REE analyses

The second major aim of the isotope geochemistry group was seawater sampling for Nd isotope and REE concentration analyses. Owing to a fantastic CTD sampling programme carried out by the oceanography group (see chapter 3) we were able to obtain seawater for Nd isotopic analyses from a total of 36 CTD stations (Table 14.IG-1, Fig. 14.IG-1), sampling a total of 134 individual water samples in various locations across the Southern Weddell Sea and Ronne-Filcher Trough area as well as one station at the NW margin of the Weddell Sea near the Antarctic Peninsula, revisiting CTD *Station 253* presented in Schröder et al. (2002). Water depths for seawater samples at each station were usually selected to always include a bottom water sample (usually sampled 5 m above ground), as well as in various water depths marking either water mass end-members (e.g. Ice Shelf Water) or mixtures / transitions of water masses. Since Nd has a rather long residence time in seawater on the order of 200 to 1,000 years (Tachikawa et al., 1999), small-scale variations should only be marginal unless the water masses derived from very different source areas. Besides, a minimum of eight litres of seawater, yet often an entire Niskin bottle (corresponding to twelve litres of seawater) were taken for individual samples since Nd concentrations are in the picomole range requiring large sample sizes. Samples were filtered with 0.2 μm ACROPAC filters directly from the Niskin bottles into acid-cleaned collapsible containers. Samples were acidified to a pH of 2, Fe chloride solution added and left to equilibrate for at least 24 hours, then the seawater pH was raised to >8 with suprapure ammonia. At this high pH, dissolved Fe precipitates also co-precipitating other trace metals such as Nd. After a further three days newly formed Fe oxyhydroxides enriched in REE settle at the base of the collapsible containers, about 80-90 % of the supernatant can be siphoned off and discarded. The pre-concentrated Nd aliquots are transferred into smaller sample containers and packed for shipping and further purification and measurements at GEOMAR Kiel. Before sampling of the Nd isotope aliquot, small (between 50 and 250 mL) aliquots were filtered for REE concentration analyses. These samples were acidified and stored for further analyses at GEOMAR Kiel.

Seawater sampling for Pb isotope analyses

Across the world's oceans, the modern dissolved Pb isotopic composition is more or less entirely controlled by anthropogenic contributions (e.g. Lee et al., 2015). The only places that may potentially still yield a natural Pb isotopic signature are remote near-ice locations such as the Southern Weddell Sea thousands of miles away from anthropogenic sources. The reconstruction of the natural Weddell Sea and Southern Ocean Pb isotopic evolution during the last glacial cycle is an important part of Huang Huang's dissertation work. While a lot of information can be drawn from analyses of the seawater-derived fraction in core-top sediments, we are also interested in comparing sediment-derived (and hence indirect) bottom water information with actual seawater data. This approach is tedious since Pb is easily contaminated either during sampling or on board after sampling. *GoFlo* bottles were used to sample seawater at either 10 m water depth or the surface with a small (metal-free) rubber boat at two locations (see Figs 14.IG-1; 14.IG-3). This approach was chosen since *Polarstern* also constantly releases minor quantities of trace metals including Pb making seawater sampling using a standard CTD approach for Pb isotopic measurements impossible. Two stations were captured for Pb isotopic seawater sampling near the shelf edge, one in front of Ronne Trough and the second close to *Halley VI Base*. If seawater compositions should turn out to be of natural origin we expect large differences between these sites since the geological age and evolution of the hinterland is very different between these two sites. Samples were filtered and acidified on board and immediately packed away to prevent unwanted contamination. All remaining purification steps will be carried out in a clean-room environment at GEOMAR Kiel.

Fig. 14.IG-3: Trace metal-clean seawater sampling for Pb isotopic use with a small rubber boat off Polarstern. ***(a**, left)* *First Pb seawater sampling in front of Ronne Ice Shelf (PS111_57-3) and* ***(b**, right)* *in proximity to Halley Base (PS111_141-1).*

Marine ice sampling

We were able to receive two marine ice cores drilled by Ricarda Winkelmann and Ronja Reese during PS111 (PIK Potsdam; chapter 5) (see Fig. 14.IG-1). This marine ice sampling was realised in cooperation with Claudia Hanfland (AWI Bremerhaven; chapter 12) and the UBA permission for sea ice sampling has been obtained by Claudia Hanfland (all remaining UBA permissions for sampling in chapter 14 were directly granted to Juliane Müller). The aim of the marine ice sampling is to assess the current atmospheric anthropogenic Pb input signal in the remote Southern Weddell Sea if resolvable and compare this signature with direct seawater measurements described above as well as core-top sediment compositions. The two cores were stored in thermo boxes and will be brought back to Bremerhaven and Kiel at -20°C. Under clean-room conditions, the ice will be further processed, sub-sampled and analysed for its major and trace metal concentrations, as well as its Pb isotopic composition.

Fig. 14.IG-4: Inspection flight aiming to sample sediment-containing basal ice from continental ice sequences along the westernmost edge of the Ronne Trough. ***(a**, left)* *While the general setup of the outcrop was excellent, it was unrealistic to land nearby due to hidden glacial crevasses.* ***(b**, right)* *Close-up of exposed rock sequence showing folded highly deformed sequences of unknown age.*

Dirty continental ice sampling

Originally it was planned to also sample dirty continental Antarctic basal ice (i.e. ice containing enclosed sediments). Finding appropriate sampling locations within the study area is very difficult since very few outcrops exist in the Weddell Sea region that could be targeted. We have carried out one attempt to sample ice at the westernmost end of the Ronne Trough (Figure 14.IG-4). While the general setting and outcrop was excellent, it unfortunately was impossible to land with the helicopter at the desired location because of dangers via hidden glacial crevasses. This part of the program therefore had to be abandoned.

Tab. 14.IG-1: Summary of all realised stations during PS111 for which isotope geochemical samples have been sampled for further processing at GEOMAR Kiel.

#	Station - Device Operation	Date time	Device Code	Latitude	Longitude
Summary of all seawater Pb isotope stations					
1	**PS111_57-2**	2018-02-13 15:45	BOAT	77° 01.486' S	050° 29.403' W
2	**PS111_141-1**	2018-03-01 17:22	BOAT	75° 27.857' S	026° 55.067' W
Summary of all seawater Nd isotope and REE stations					
1	**PS111_09-2**	2018-01-26 07:26	CTD	64° 00.021' S	005° 00.108' E
2	**PS111_12-2**	2018-01-27 09:00	CTD	66° 44.331' S	000° 02.320' W
3	**PS111_16-1**	2018-02-01 22:07	CTD	72° 23.048' S	017° 49.026' W
4	**PS111_17-4**	2018-02-03 04:00	CTD	73° 42.019' S	025° 43.428' W
5	**PS111_18-1**	2018-02-04 10:47	CTD	76° 09.471' S	030° 00.846' W
6	**PS111_23-1**	2018-02-04 23:37	CTD	75° 57.174' S	032° 02.629' W
7	**PS111_29-1**	2018-02-06 06:22	CTD	75° 58.382' S	027° 40.870' W
8	**PS111_33-1**	2018-02-07 11:49	CTD	74° 50.603' S	032° 31.102' W
9	**PS111_35-2**	2018-02-09 09:33	CTD	76° 43.903' S	052° 03.437' W
10	**PS111_37-2**	2018-02-09 15:15	CTD	76° 28.977' S	052° 38.226' W
11	**PS111_39-1**	2018-02-10 05:31	CTD	75° 58.938' S	054° 40.057' W
12	**PS111_42-3**	2018-02-10 20:37	CTD	76° 08.680' S	053° 21.396' W
13	**PS111_46-1**	2018-02-11 10:00	CTD	75° 15.966' S	058° 35.320' W
14	**PS111_48-1**	2018-02-11 17:25	CTD	74° 48.031' S	060° 47.939' W
15	**PS111_52-1**	2018-02-12 14:16	CTD	75° 22.732' S	057° 44.615' W
16	**PS111_55-1**	2018-02-13 08:42	CTD	76° 54.488' S	050° 53.916' W
17	**PS111_57-3**	2018-02-13 17:29	CTD	77° 01.450' S	050° 30.325' W
18	**PS111_58-1**	2018-02-13 21:41	CTD	77° 08.446' S	048° 24.105' W
19	**PS111_60-1**	2018-02-14 04:30	CTD	77° 01.202' S	045° 23.820' W
20	**PS111_63-1**	2018-02-15 13:16	CTD	75° 20.567' S	041° 06.395' W

#	Station - Device Operation	Date time	Device Code	Latitude	Longitude
21	**PS111_64-2**	2018-02-16 01:23	CTD	75° 37.201' S	039° 43.701' W
22	**PS111_67-1**	2018-02-16 13:21	CTD	76° 05.589' S	036° 38.045' W
23	**PS111_70-1**	2018-02-17 00:55	CTD	76° 07.425' S	033° 39.952' W
24	**PS111_80-1**	2018-02-18 08:11	CTD	76° 38.705' S	035° 25.848' W
25	**PS111_91-1**	2018-02-19 13:57	CTD	77° 51.854' S	037° 12.719' W
26	**PS111_94-1**	2018-02-19 21:45	CTD	77° 47.666' S	039° 09.716' W
27	**PS111_97-1**	2018-02-20 03:33	CTD	77° 47.515' S	041° 15.265' W
28	**PS111_100-1**	2018-02-20 16:50	CTD	77° 12.257' S	042° 54.084' W
29	**PS111_123-1**	2018-02-25 13:32	CTD	74° 56.690' S	030° 59.163' W
30	**PS111_128-1**	2018-02-26 04:08	CTD	74° 38.676' S	034° 20.004' W
31	**PS111_131-1**	2018-02-26 12:43	CTD	74° 37.042' S	036° 55.373' W
32	**PS111_132-1**	2018-02-27 12:03	CTD	74° 00.529' S	032° 25.412' W
33	**PS111_133-1**	2018-02-28 03:59	CTD	75° 01.242' S	029° 27.639' W
34	**PS111_135-1**	2018-02-28 07:32	CTD	75° 06.458' S	028° 16.805' W
35	**PS111_141-2**	2018-03-01 17:39	CTD	75° 27.821' S	026° 55.131' W
36	**PS111_147-1**	2018-03-06 18:42	CTD	63° 35.227' S	048° 44.659' W
Summary of all processed Multi Core sediment stations					
1	**PS111_13-2**	2018-01-28 08:41	sliced MUC	70° 05.621' S	006° 51.091' W
2	**PS111_15-1**	2018-02-01 11:01	sliced MUC	71° 39.918' S	015° 47.018' W
3	**PS111_16-3**	2018-02-02 00:18	sliced MUC	72° 23.059' S	017° 49.004' W
4	**PS111_40-2**	2018-02-10 08:49	sliced MUC	76° 00.053' S	054° 14.372' W
5	**PS111_60-3**	2018-02-14 05:24	sliced MUC	77° 00.967' S	045° 24.561' W
6	**PS111_80-3**	2018-02-18 09:47	sliced MUC	76° 38.494' S	035° 25.795' W
Summary of all frozen Multi Core sediment stations					
1	**PS111_42-1**	2018-02-10 19:05	frozen MUC	76° 08.698' S	053° 21.397' W
2	**PS111_53-3**	2018-02-13 00:45	frozen MUC	76° 01.554' S	054° 07.256' W
3	**PS111-98-3**	2018-02-20 09:06	frozen MUC	77° 48,070' S	040° 27,276' W

#	Station - Device Operation	Date time	Device Code	Latitude	Longitude
4	**PS111-114-3**	2018-02-22 19:46	frozen MUC	76° 22,614' S	033° 56,035' W
5	**PS111_131-2**	2018-02-26 13:30	frozen MUC	74° 36.666' S	036° 56.217' W
Summary of marine ice coring stations					
1	**PS111_SIP_8-7**	2018-02-16 18:00	marine ice	75° 59.106' S	036° 28.090' W
2	**PS111_SIP_10-6**	2018-02-18 18:00	marine ice	76° 51.647' S	035° 33.265' W

Preliminary (expected) results

No results can as yet be reported for the geochemical part of the Marine Geology group. Samples were only be pre-processed on *Polarstern* for further purification and analyses in mandatory clean-room environments at GEOMAR Kiel. Sediment, seawater and marine ice samples collected within the frame of our project during PS111 will provide a wealth of new insights into Weddell Sea ocean circulation and continental meltwater and sub-glacial input from a radiogenic isotope and dissolved Rare Earth Element perspective. We will produce a first assessment on the regional dissolved Nd isotopic variation in the Weddell Sea region and gauge the Nd isotopic output of Weddell Sea Deep Water into the Southern Ocean further north. The sedimentary analyses will highlight in how far reliable bottom water Nd and Pb isotope reconstructions can be made for paleoceanographic studies. Finally, the marine ice samples will reveal the extent of anthropogenic Pb deposition in remote regions such as the Ronne-Filchner Trough area.

Data management

Analytical data will be available latest with publication as supplement related to each publication. All datasets will be made citable including a DOI.

14.3 Sedimentology

Objectives

For geological studies, bathymetry data can moreover provide valuable information on the glacial history of an area by revealing the geomorphology of the seafloor, i.e. sub- and proglacial bedforms. Supplementing the bathymetric information, high resolution sub-bottom data provide information on the top 10s of meters below the seafloor and the lateral extension of sediment successions. By providing information on the geological architectures, the sub-bottom information can be used for paleoceanograpic and sedimentologic studies. Glacial-induced seabed features such as Mega-Scale Glacial Lineation (MSGL), Grounding Zone Wedges (GZW), moraines, and drumlins provide information on past ice sheet extents and, if dated by sediment cores, valuable data for palaeoclimate reconstructions (Hillenbrand et al., 2014). Main objective is the recovery of core profiles to support the interpretation of the morphological features (see chapter 8) and to find sequences containing a minimum of carbonate for radiocarbon dating.

Work at sea

Sediment cores were obtained using the 1.5t-gravity corer (GC; Kiel/Hydrowerkstätten type, 12 cm Ø). Selection of locations was based on bathymetry (Arndt et al. 2013) with additions of recent cruises (PS96 and this cruise). In addition, sediment echosoundings (Teledyne Parasound System P70) along the cruise track were used to estimate the required core barrel length to be deployed. All data were visualized in the local GIS to select core locations. The GC was deployed on 20 stations with a total recovery of 42.8 m. 5 stations had no recovery due to hard ground (gravely diamicton), on 3 stations the core barrel only contained a few decimeter of sediment for similar reasons.

Each sediment sequence was completed by an undisturbed surface profile recovered with a Multicorer (MUC). One core was sampled in 1 cm slices, one core was completely frozen for archiving.

For the investigation of Biomarker three cores were taken on request of Juliane Müller/AWI as replica on well known and dated core locations. The already existing cores were taken in the late 1980ies and thus fresh material was required for this sensitive geochemical analysis (see first three cores in Table 14.1): PS111_13-4=PS1394-4, PS111_15-2=PS2820-1, PS111_16-2=PS2819-2.

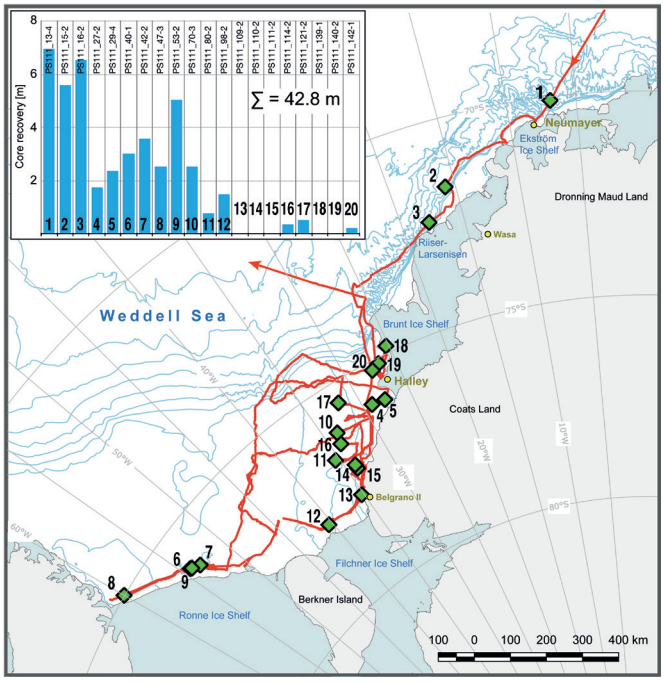

Fig. 14.3.1: Location of gravity cores (green) sampled during PS111. Histogram shows recovery of cores; total recovery is 42.8 m. Eight coring sites had none or almost no recovery due to hard ground. Cruise track (red) and polar stations (yellow) are shown. Bathymetry is given in 500 m depth contours (Arndt et al., 2013). Map produced with QGIS 2.18 and the Quantarctica dataset (Norwegian Polar Institute).

Tab- 14.3.1: Table of gravity cores with penetration and recovery.

Station	Date-Time	Latitude	Longitude	Depth [m]	Pen. [m]	Rec. [m]	Comment
PS111_13-4	2018-01-28 11:32	-70,0936	-6,8501	1776	10.00	6.90	location PS1394-4
PS111_15-2	2018-02-01 12:19	-71,6648	-15,7842	1406	6.50	5.55	location PS2820-1
PS111_16-2	2018-02-01 23:16	-72,3841	-17,8171	1419	8	6.50	location PS2819-2

Station	Date-Time	Latitude	Longitude	Depth [m]	Pen. [m]	Rec. [m]	Comment
PS111_27-2	2018-02-05 18:04	-75,9548	-29,0832	425	2.50	1.72	
PS111_29-4	2018-02-06 08:43	-75,9972	-27,6928	430	2.50	2.33	
PS111_40-1	2018-02-10 08:14	-76,0008	-54,2405	514	4.00	3.00	overpenetration, 20 cm surface loss
PS111_42-2	2018-02-10 19:40	-76,1448	-53,3566	493	5.00	3.53	
PS111_47-3	2018-02-11 14:45	-74,9847	-60,0005	660	3.70	2.52	
PS111_53-2	2018-02-13 00:05	-76,0259	-54,1207	497	7.50	5.00	2.84 to 3 m missing, liner stuck in barrel
PS111_70-3	2018-02-17 02:28	-76,1050	-33,6405	794	3.20	2.50	
PS111_80-2	2018-02-18 09:04	-76,6429	-35,4281	933	1.00	0.75	
PS111_98-2	2018-02-20 08:15	-77,8001	-40,4391	928	4.00	1.46	
PS111_109-2	2018-02-22 08:15	-77,7105	-35,2587	461	0.2	0	Gravel and rock (green shist)
PS111_110-2	2018-02-22 07:25	-77,1119	-33,9369	404	0	0	tilt, till attached to weight
PS111_111-2	2018-02-22 09:14	-77,0100	-33,9410	453	0	0	photo shows rocks and gravel on ground
PS111_114-2	2018-02-22 18:54	-76,3826	-33,9550	840	1.50	0.33	0.5 m loss from base during recovery
PS111_121-2	2018-02-25 03:47	-75,4977	-31,9100	758	1.50	0.5	
PS111_139-1	2018-03-01 02:07	-74,8251	-25,2659	669	1.00	0	6 cm in MUC
PS111_140-2	2018-03-01 11:57	-75,1325	-26,6295	341	0	0	Metall of CC scratched
PS111_142-1	2018-03-01 23:37	-75,2169	-27,4585	373	0.30	0.20	recov in CC only, bag sample

Expected results

No analytical data or documentation is available so far. Gravity cores were cut into 1 m sections and stored at +4°C in the scientific cold store of the ship. Segments will be transferred to the *Polarstern* core repository at AWI/Bremerhaven and are available for sampling on request to curator@awi.de. Priority sampling and analysis will be done by J.-E. Arndt (AWI) and C.-D. Hillenbrand (BAS) according to the *Polarstern*-proposals of Kuhn et al. and Arndt (see chapter 8), also following the work of Arndt et al. 2017. Investigations will include structural and sedimentological analysis. Age dating will be done using the radiocarbon method, as far as carbonate is available. Geological ages mostly younger than about 30 ka are expected.

Data management

Observational and documentary data (Parasound profiles, MUC sampling videos, rock sample images) will be archived in PANGAEA after the cruise, analytical data will be made available latest with publication as supplement related to each paper. All datasets will be made citable including a DOI (see www.pangaea.de).

References

Arndt, et al. (2013)'The International Bathymetric Chart of the Southern Ocean (IBCSO) Version 1.0 - A new bathymetric compilation covering circum-Antarctic waters', Geophysical Research Letters, Vol. 40(9), p. 1-7, doi:10.1002/grl.50413.

Arndt JE, Hillenbrand CD, Grobe H, Kuhn G, Wacker, L (2017) Evidence for a dynamic groundig line in outer Filchner Trough, Antarctica, unit the early Holocen. Geology, 45(11), 1035-1038.

Belt ST, Smik L, Brown TA, Kim JH, Rowland SJ, Allen CS, Gal JK, Shin KH, Lee JI, Taylor KWR (2016) Source identification and distribution reveals the potential of the geochemical Antarctic sea ice proxy IPSO25. Nature Communications, 7, p. 12655.

Blaser P, Lippold J, Gutjahr M, Frank N, Link JM, Frank M (2016) Extracting foraminiferal seawater Nd isotope signatures from bulk deep sea sediment by chemical leaching. Chemical Geology 439, 189-204.

Gutjahr M, Frank M, Stirling, CH, Klemm V, van de Flierdt T, Halliday AN (2007) Reliable extraction of a deepwater trace metal isotope signal from Fe-Mn oxyhydroxide coatings of marine sediments. Chemical Geology 242, 351-370.

Hillenbrand C-D, Bentley MJ, Stolldorf TD, Hein AS, Kuhn G, Graham AGC, Fogwill CJ, Kristoffersen Y, Smith JA, Anderson JB, Larter RD, Melles M, Hodgson DA, Mulvaney R, Sugden DE (2014) Reconstruction of changes in the Weddell Sea sector of the Antarctic Ice Sheet since the Last Glacial Maximum. Quaternary Science Reviews 100, 111-136.

Lee J-ML, Boyle EA, Gamob T, Obata H, Norisuye K, Echegoyen Y (2015) Impact of anthropogenic Pb and ocean circulation on the recent distribution of Pb isotopes in the Indian Ocean. Geochimica et Cosmochimica Acta 170, 126-144.

Orsi AH, Johnson GC, Bullister JL (1999) Circulation, mixing, and production of Antarctic Bottom Water. Progress in Oceanography 43, 55-109.

Rickli J, Gutjahr M, Vance D, Fischer-Gödde M, Hillenbrand C-D, Kuhn G (2014) Neodymium and hafnium boundary contributions to seawater along the West Antarctic continental margin. Earth and Planetary Science Letters 394, 99-110.

Schröder M, Hellmer HH, Absy JM (2002) On the near-bottom variability in the northwestern Weddell Sea. Deep-Sea Research II 49, 4767-4790.

Stichel T, Frank M, Rickli J, Haley BA (2012a) The hafnium and neodymium isotope composition of seawater in the Atlantic sector of the Southern Ocean. Earth and Planetary Science Letters 317-318, 282-294.

Stichel T, Frank M, Rickli J, Hathorne EC, Haley BA, Jeandel C, Pradoux C (2012b) Sources and input mechanisms of hafnium and neodymium in surface waters of the Atlantic sector of the Southern Ocean. Geochimica et Cosmochimica Acta 94, 22-37.

Tachikawa K, Jeandel C, Roy-Barman M (1999) A new approach to the Nd residence time in the ocean: the role of atmospheric inputs. Earth and Planetary Science Letters 170, 433-446.

van de Flierdt T, Griffiths AM, Lambelet M, Little SH, Stichel T, Wilson DJ (2016) Neodymium in the oceans: a global database, a regional comparison and implications for palaeoceanographic research. Philosophical Transactions of the Royal Society A: Mathematical, Physical and Engineering Sciences, 374.

15. MICROPLASTICS - A POTENTIAL THREAT TO THE REMOTE AND PRISTINE ECOSYSTEMS OF THE ANTARCTIC SEAS?

Thomas Mani[1],
Patricia Burkhardt-Holm[1], Helmut Segner[2],
Markus Zennegg[3], Linda Amaral-Zettler[4] (not on board)

[1]Uni Basel
[2]University of Bern
[3]EMPA
[4]NIOZ

Grant-No. AWI_PS111_00

Objectives

Microplastics (MP) pose an emerging threat to the global environment. Wherever one searches, MP is found, albeit in differing concentrations and constitutions. The Southern Ocean around Antarctica is thought to be an exception because it is considered beyond the reach of human impact (apart from scientific and leisure tourism). Furthermore, the major current systems of the Southern Ocean are thought to provide an effective barrier against the transfer of MP from lower latitudes to the Antarctic Ocean. However, very recent studies indicate that MP is present in the Southern Ocean (Cincinelli et al., 2017). This highlights an urgent need for investigations into the possible origin and fate of MP: concentrations and distributions in the Southern Ocean, sources originating in Antarctica, and, finally, potential transfer into Antarctic food webs. The conducted microplastic studies should furthermore provide a baseline for future research on the topic.

This project will explore MP occurrence and distribution in water and biota such as zooplankton and fish. To obtain insights into the origins and impacts of MP, we will study the microbial community composition on the plastic particles, as well as the persistent organic pollutant (POP) load of MP. To structure the research, we address these hypotheses: (1) The concentration of MP is higher in the more anthropogenically-exposed Western Antarctic Peninsula (WAP) and Scotia Sea than in the Weddell Sea (WS); (2) MP in the Southern Ocean around Antarctica originates from outside the ACC, i.e. north of the Polar front; (3) MP from local sources, i.e. research stations, and research and cruise vessels, contribute detectably to the MP load; (4) Microbial colonization of MP can inform MP origins; (5) The abiotic polymer characteristics (particle morphology, polymer type) and the POP profile of MP in the Southern Ocean around Antarctica reflect the characteristics of their sources; and, (6) Microplastic particles will enter Antarctic food webs. To reach the goals, we will sample MP in the water column, in filter-feeding zooplankton and fish of the different sites in the Southern Ocean (WS, WAP, Scotia Sea) and compare them with selected samples from subtropical southern gyres; we will characterize the MP particles with respect to their morphology, their polymer composition, the profile of adsorbed POPs and of the resident microbial communities. The microbiome work will include molecular analyses, as well as novel microscopic characterization using multiple probes combined with spectral analysis to unravel the spatial organization of the microbial communities. The polymer analysis will comprise ATR-FT–IR and microscopic FT–IR. Both approaches will contribute to assessing the importance of local sources (e.g. waste water treatment plants) and their potential origin from sites outside the ACC. The results will provide critical empirical data for ocean circulation transport models to backtrack the origin of floating MP based on probabilistic

models of surface flow in the Southern Ocean. Our ultimate goal is to answer questions on the concentration and distribution of MP in the Southern Ocean, its potential sources and its uptake into the food web.

Work at sea

Surface water was sampled for MP with a Manta Trawl (floating neuston net towed to on-board crane for trawling; *n* = 10, Figure and Table 15.1). Sub-surface water was sampled by filtering pumped seawater from beneath the vessel at approximately 11.2 m depth (*n* = 27, Figure and Table 15.2). MP collected will be analysed for polymer type, particle morphology and size, POP and Plastisphere (inhabiting microbial community characterizations). 13 sediment samples were taken with a multicorer (MUC, Table 15.3).

Suspended surface solids sampled by Manta Trawl

15 trawls were attempted during PS111, 10 were completed successfully (Fig. 15.3, Table 15.1). Two trawls were aborted due to grease ice accumulation in the mesh after 15 and 20 minutes when air temperatures surpassed –13.2° C with winds of >5.4 m s^{-1} and water temperatures below –1.7° C (MT Nr. 12); two were cancelled pre-sampling due to ice conditions and 1 was cancelled pre-sampling due to too strong winds for launching (38 knots, 8 Beaufort). The Manta Trawl (MT) (aperture: 60 cm x 18 cm) is equipped with a mechanical flowmeter and a 300 µm mesh with a removable cod end. The MT (total weight ≈ 15 kg) was deployed by an on-board crane adding an 8 kg steel weight to improve stability against dynamic forces such as wind and waves (Fig. 15.1). The steel rope was released long enough to allow for a flat sampling angle (≤ 30°) approximately 20 m behind the crane at 5–8 m away from the side of the hull (depending on wind, current and vessel course) at starboard. The tows were performed at a vessel speed of 3 knots during a target trawling duration of 30 minutes (in case the cod end filled up with plankton or ice the sampling time was reduced, see Table 15.1). This resulted in an average (± SD) of approximately 306 ± 92 m^3 of filtered seawater per successful sample and a total of 3,064 m^3. After every tow the MT was hauled from the water and the content of the removable cod and subsequently transferred into a Bogorov counting chamber for visual inspection (*n* = 7, using a stereomicroscope (Olympus SZ61) equipped with a camera (Olympus SC50) and connected to the imaging software CellSens Entry (Version 1.17.16030.0; three samples will need purification treatment at the mainland laboratory prior to visual inspection due to the high abundance of biological residue). Putative anthropogenic particles were sorted and characterized microscopically. Samples for microbial DNA-analysis were fixed in 2 mL PureGene lysis buffer, samples for microscopy via FISH and CLASI-FISH were fixed in paraformaldehyde (for less than 24 hours) then transferred to 50 % ethanol in PBS for storage at –20°C. To compare free-living microbial communities with those on MP, 2 L of seawater were drawn with

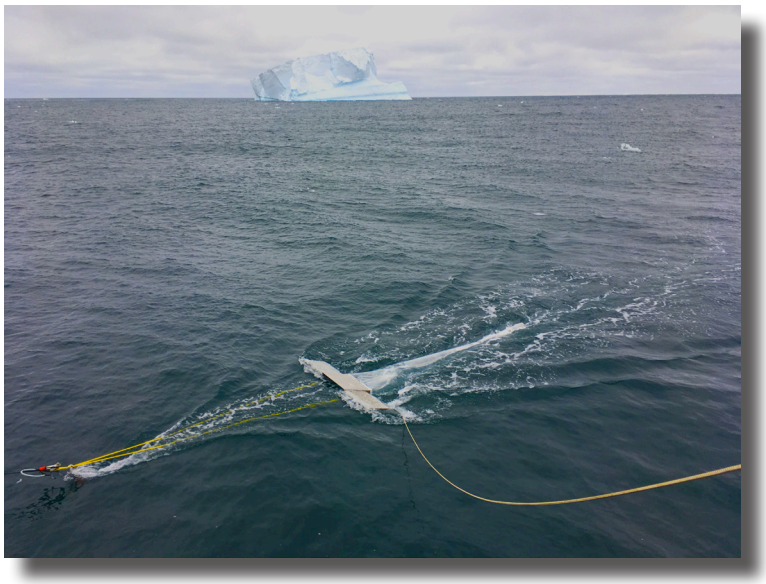

Fig. 15.1: Manta Trawl deployed in the Southern Ocean

a plastic bucket during MT trawling and subsequently filtered through a 0.2 µm Sterivex™ cartridge filter (Millipore). Cartridges were subsequently flooded with 2 mL of PureGene lysis buffer. If particles conspicuously appear to be plastic as determined by eye (e.g. based on color, texture and shape; Noren et al., 2007), these will be analysed for microbial community composition first and subsequently identified using FT–IR. 7 particles from the Trawls 1, 3, 7, 9 and 10 were saved for this purpose.

Sub-surface suspended solids sampled by on-board sea water pump

To address the MP load in the sub-surface water layer, 32 samples were taken from pumped seawater intake in the on-board wet lab. A Klaus Union Sealex Centrifugal Pump (Bochum, Germany) delivered seawater from approx. 11.2 m depth to the laboratory via stainless steel pipes (first described by Lusher et al., 2014). The water was filtered through a stack of geological sieves. 14 samples were taken using a 20 µm sieve (combined with 100 µm and 300 µm sieves) and 18 samples were taken using a 100 µm sieve as the lower mesh boundary (combined with a 300 µm sieve). Sieves were protected from airborne contamination by a dimension-tailored solid wooden construction additionally sealed off with aluminium foil (Fig. 15.2, adapted from Kanhai et al., 2016). A mean (± SD) water flow duration of 10.3 ± 9.5 hours at 0.05 ± 0.02 L s^{-1} resulted in an average of 2.35 ± 2.36 m^3 filtered seawater per sample. After every filtration process residues of all involved sieves were pooled in a pre-rinsed glass jar using pumped seawater from the stainless steel wet lab pipe system and a PTFE squirt bottle as a rinsing agent. Samples were sealed with metal lids, labelled by the lowest applied mesh size and stored in v:v 50:50 suspended sample:EtoH at 4° C.

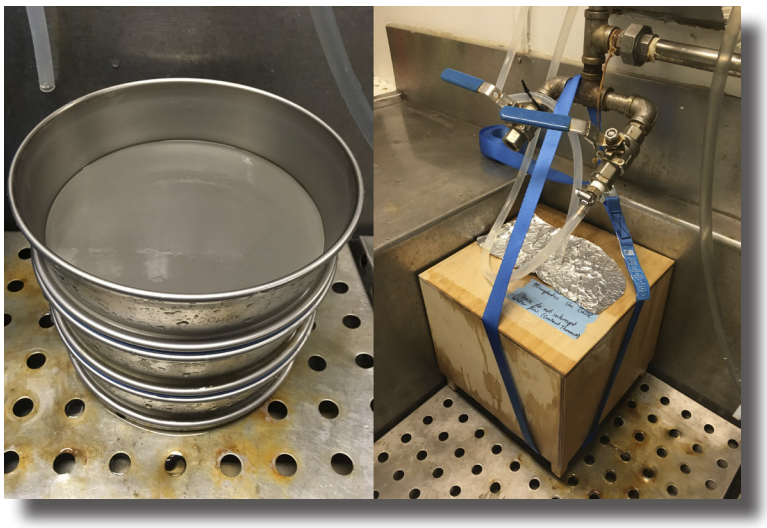

Fig. 15.2: Stack of geological sieves (20, 100 and 300 µm, left). Covered sieve stack with wooden protection, sealed, fastened, and connected to the seawater intake system (right).

Sediment samples

13 sediment samples were taken by multicorer (MUC, Chapter 14) from the Weddell Sea at depths ranging from 332–1,418 m (Table 15. 3). For the purpose of MP investigation the top 3 cm of the kindly provided MUC cores (inner diameter: 6.2 cm) were sub-sampled using a Mili-Q rinsed steel pipe (inner diameter: 2.7 cm) to a depth of approx. 3 cm resulting in approximately 17 cm^3 each. Samples were transferred into pre-combusted (12 h at 400° C) glass vials (40 ml) and stored at 4° C. The sediment samples will be further processed by a ZnCl density separation (Imhof et al., 2012), a Fenton's reagent purification (Tagg et al., 2017) and analysed with focal plane array (FPA) micro Fourier transform infrared spectroscopy (FT–IR) (Löder et al., 2015).

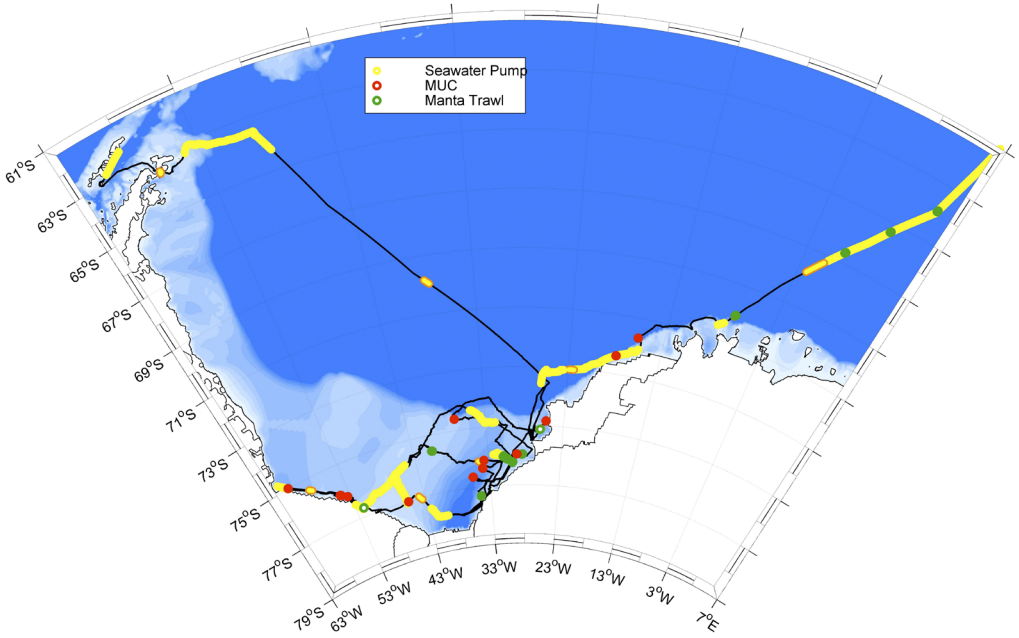

Fig. 15.3: Sampling locations. Yellow transects represent 0.1 mm mesh. Yellow transects bordered by an orange line represent 0.02 mm mesh. Red and green marks indicate multicorer and Manta Trawl samples, respectively. The black line indicates the Polarstern track on the cruise PS111.

Tab. 15.1: Summary of Manta Trawl samples for microplastics on PS111

Sample ID	Station Name	Date	Coordinates Start	Coordinates End	Transect [m]	Filtered Vol. [m3]
Manta Trawl (MT) 1	PS111_9-1	2018-01-26	-63.905159; 5.053958	-63.936306; 5.036211	3,483.9	376.3
MT 2	PS111_10-1	2018-01-26	-65.306004; 2.70799	-65.331941; 2.663314	3,551.1	383.5
MT 3	PS111_12-1	2018-01-27	-66.632579; 0.189451	-66.657449; 0.135565	3,299.1	356.3
MT 4	PS111_13-1	2018-01-28	-70.040489; -6.74798	-70.061082; -6.820045	3,561.3	384.6
MT 5	PS111_19-1	2018-02-04	-76.104748; -30.370666	-76.120101; -30.440141	2,577.6	278.4
MT 6	PS111_20-1	2018-02-04	-76.0127; -30.884445	-76.03348; -30.95367	3,104.1	335.2
MT 7	PS111_28-4	2018-02-05	-75.973637; -28.406722	-75.961511; -28.300494	3,105.3	335.4

Sample ID	Station Name	Date	Coordinates Start	Coordinates End	Transect [m]	Filtered Vol. [m3]
MT 8ab	PS111_35-1	2018-02-09	-76.707562; -51.845019	-76.711764; -51.893151	98.4	10.6
MT 9	PS111_64-1	2018-02-15	-75.548026; -40.44837	-75.544617; -40.54514	2,772.0	299.4
MT 10	PS111_74-5	2018-02-17	-76.214619; -29.683427	-76.236688; -29.720002	2,085.6	225.2
MT 11c	PS111_85-2	2018-02-19	-77.308448; -34.520721	-77.316982; -34.564203	831.0	89.7
MT 12a	PS111_138-2	2018-02-28	-75.126413; -26.038154	-75.11979; -25.960787	1,433.1	154.8

[a]Aborted due to grease ice accumulation in Manta Trawl

[b]Defect of flowmeter due to freezing

[c]Hoisting of Manta Trawl after 15 minutes due to phytoplankton accumulation in the cod end

Tab. 15.2: Summary seawater pump samples for microplastics on PS111

Sample ID	Coordinates Start	Coordinates End	Filtered Vol. [L]	Mesh Size [µm]
Seawater Pump (SP) 1	-43.310596; 14.789067	-45.873514; 13.714196	4,762.8	20
SP 2	-46.295037; 13.517873	-48.338984; 12.609975	2,829.0	100
SP 3	-48.386536; 12.587699	-51.529018; 11.144197	4,766.0	100
SP 4	-51.566922; 11.126238	-55.276444; 9.378046	5,651.0	100
SP 5	-55.325263; 9.35429	-60.391373; 6.767601	8,017.1	100
SP 6	-60.435814; 6.752008	-65.385393; 2.566424	8,099.0	100
SP 7	-65.385256; 2.567096	-67.142484; 0.856763	3,952.0	100
SP 8	-67.264469; -1.106756	-67.795751 -2.210384	297.0	20

Sample ID	Coordinates Start	Coordinates End	Filtered Vol. [L]	Mesh Size [µm]
SP 9	-70.093846; -6.85067	-70.093689; -6.850199	114.9	20
SP 10	-70.40211; -7.624916	-70.546071; -8.142461	4,363.1	100
SP 11	-72.041787; -15.520476	-72.995041; -21.430651	4,075.1	100
SP 12	-73.008257; -21.640274	-73.04826; -22.900553	217.0	20
SP 13	-73.075024; -23.532446	-73.568687; -26.071103	2,194.0	100
SP 14	-76.044146; -30.987383	-76.087175; -30.452237	4,685.9	100
SP 15	-75.975035; -28.416919	-75.963451; -28.315971	181.1	20
SP 16	-74.860296; -31.814451	-74.37882; -34.858545	2,408.1	100
SP 17	-75.788026; -44.511445	-76.505807; -52.811142	3,168.0	100
SP 18	-74.983358; -60.000768	-74.731947; -61.026099	1,164.9	100
SP 19	-75.381265; -57.707349	-75.440777; -57.341792	99.0	20
SP 20	-77.068797; -45.64848	-76.201814; -46.084503	2,283.0	100
SP 21	-76.106115; -34.6476	-76.196562; -33.885373	153.0	20
SP 22	-76.213615; -29.675775	-76.237923; -29.71535	89.0	20
SP 23	-77.308453; -34.519384	-77.335053; -34.582502	101.9	20
SP 24	-77.794927; -40.00413	-77.439638; -42.348412	3,467.0	100
SP 25	-76.943152; -43.734653	-77.070112; -43.341808	160.0	20

Sample ID	Coordinates Start	Coordinates End	Filtered Vol. [L]	Mesh Size [µm]
SP 26	-75.131051; -26.038469	-75.091618; -25.849534	269.0	20
SP 27	-69.972507; -37.418955	-69.830417; -37.864793	186.0	20
SP 28	-64.294352; -47.924158	-63.330227; -54.137903	2,792.0	100
SP 29	-63.608203; -56.437342	-63.513015; -56.394712	133.0	20
SP 30	-62.768051; -60.033051	-62.021279 -57.275862	2,505.0	100
SP 31	-59.417025; -57.03486	-59.296198; -57.209862	148.0	20
SP 32	-58.966349; -57.684771	-56.796928; -60.647233	4,244.0	100

Tab. 15.3: Summary of sediment samples for microplastics on PS111

Sample ID	Station Name	Coordinates	Depth
Sediment Core (SC) 1	PS111_15-1	-71.665894; -15.783055	1,402 m
SC 2	PS111_16-3	-72.384301; -17.816957	1,418 m
SC 3	PS111_27-1	-75.954850; -29.084043	425 m
SC 4	PS111_40-2	-76.000968; -54.239456	513 m
SC 5	PS111_42-1	-76.144926; -53.356988	493 m
SC 6	PS111_47-2	-74.984737; -60.001606	660 m
SC 7	PS111_53-3	-76.025914; -54.120589	496 m
SC 8	PS111_60-3	-77.019015; -45.400304	332 m
SC 9	PS111_70-2	-76.114507; -33.658977	796 m
SC 10	PS111_80-3	-76.642137; -35.428931	933 m
SC 11	PS111_114-3	-76.379052; -33.942022	839 m
SC 12	PS111_131-2	-74.612930; -36.931811	386 m
SC 13	PS111_139-2	-74.825079; -25.271639	665 m

Preliminary (expected) results

All of the visually inspected Manta Trawl samples (*n* = 7) yielded conspicuous coloured fragments (mean concentration 0.02 ± 0.02 SD m^{-3}) and fibres (0.04 ± 0.05 m^{-3}; Fig. 15.4). However, it was not yet possible to conclusively determine the origin of these particles. A first estimate of the vessel activity-related contamination potential suggests that the fragments likely constitute ship paint fragments (Figs 15.5 and 15.6) while the fibres likely stem from

textiles present in the launching and hauling area of the Manta Trawl as well as in the on-board laboratories. All Manta Trawl samples will undergo further visual and chemical investigation (FT–IR) for the final assessment of the oceanic microplastics load.

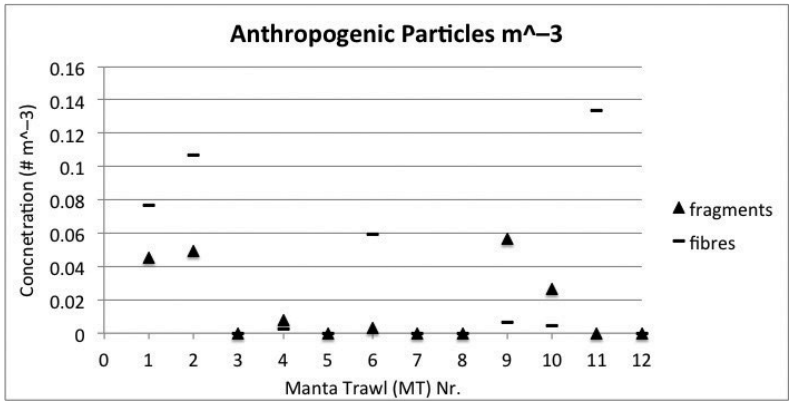

Fig. 15.4: Frequency distribution of putative anthropogenic residue m^{-3} in the Manta Trawl (MT) samples 1–12 of sampled surface seawater. MT Samples 3, 5, 7 were not yet assessed due to excess biogenic material. MT samples 8 and 12 were aborted mid-sampling due to grease ice accumulation in the mesh (Table 15.1). All putative anthropogenic particles will be analysed using Fourier transform infrared spectroscopy (FT–IR).

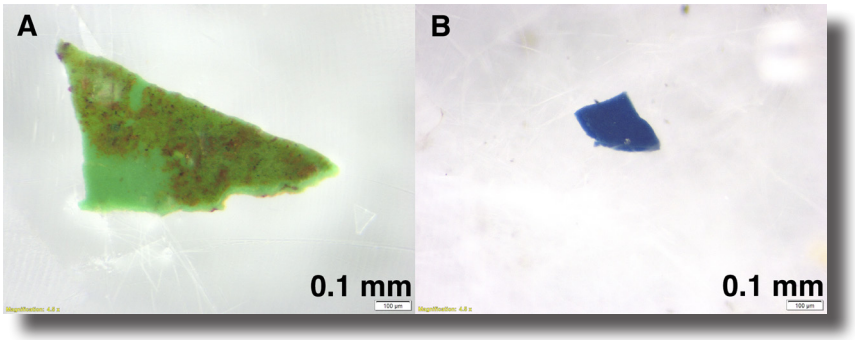

Fig. 15.5: Green and blue potentially anthropogenic fragment from MT 2 (A) and MT 1 (B) respectively. Initially assessed as putative microplastic particles due to colouring and homogenous, non-cellular texture they will now be subject to chemical analysis (FT–IR) in the mainland laboratory. Visual similarity (e.g. colour) suggests that the particles might originate from Polarstern vessel paint.

Quality control and contamination protection

The Manta Trawl (MT) aperture was sealed with a cotton cloth for transport to the launching area on the working deck (E-deck). Any rinsing activity on the working deck which could result in anthropogenic particles being washed into the surrounding waters of *Polarstern* were halted prior to MT trawling. The continuously running seawater hose on the working deck was pulled out of the drain and hung directly over the reling to avoid additional washing of particles into the surrounding waters (e.g. ship paint or plastic fragments from scientific devices such as the multicorer, etc.). The grey water outlet of the on-board waste water treatment plant (WWTP, outlet located on the opposite hull side on portside) was interrupted at least 30 minutes prior to MT trawling starting from MT Nr. 7. Whenever possible sampling was conducted with winds facing starboard to avoid lining up *Polarstern* between wind origin and MT. White lab coats

(100 % cotton) and blue nitrile gloves were worn in the laboratory when handling and inspecting samples. Glassware was used as far as possible. If the use of synthetic polymer material (e.g. pipe for seawater sampling) was necessary, items were rinsed before use thoroughly.

Procedural blanks were run in the dry lab where MT samples were inspected (*n* = 4). For this purpose two petri dishes at a time (diameter: 6 cm, first set 17 hours [assessment yielded 39 and 34 fibres, respectively], second set 26 hours) were placed on the lab bench and subsequently filtered onto glass microfiber paper (GF/C); Whatman: 47 mm, pore size: 1.2 µm, using a Buchner funnel and a vacuum flask. Filters were subsequently folded, sealed in aluminium foil and stored in glass petri dishes. Following the same filtration and storing procedure background samples were furthermore taken from the work-passage on E-deck (0.4 L glass jars, 24 hours, *n* = 2) dry lab freshwater supply (2 L, *n* = 3), lab ethanol supply for sample conservation (100 mL, *n* = 3), freshwater hose working deck for externally rinsing the MT mesh pre and post trawling (2 L, *n* = 3) and seawater for Sterivex filtration (1 L, *n* = 3).

Procedural blanks were run for the seawater pump sampling by rinsing the sieve stack upon exposure into a pre-rinsed (Mili-Q) glass jar and fixating with v:v 50% EtoH (*n* = 3).

For later (forensic) referencing, material samples from the yellow synthetic MT bridle, orange synthetic AWI work deck jackets, red synthetic AWI Tempex suits, blue synthetic fastening straps in the lab and a shaving of the multicorer (MUC) tube ware preserved and sealed seperately in colourless polypropylene (PP) tubes (cf. Fig. 7 and 8). The same was done with fragments of ship paint (green, blue, red/orange and white – the main paint colours on *Polarstern*, cf. Fig. 15.6).

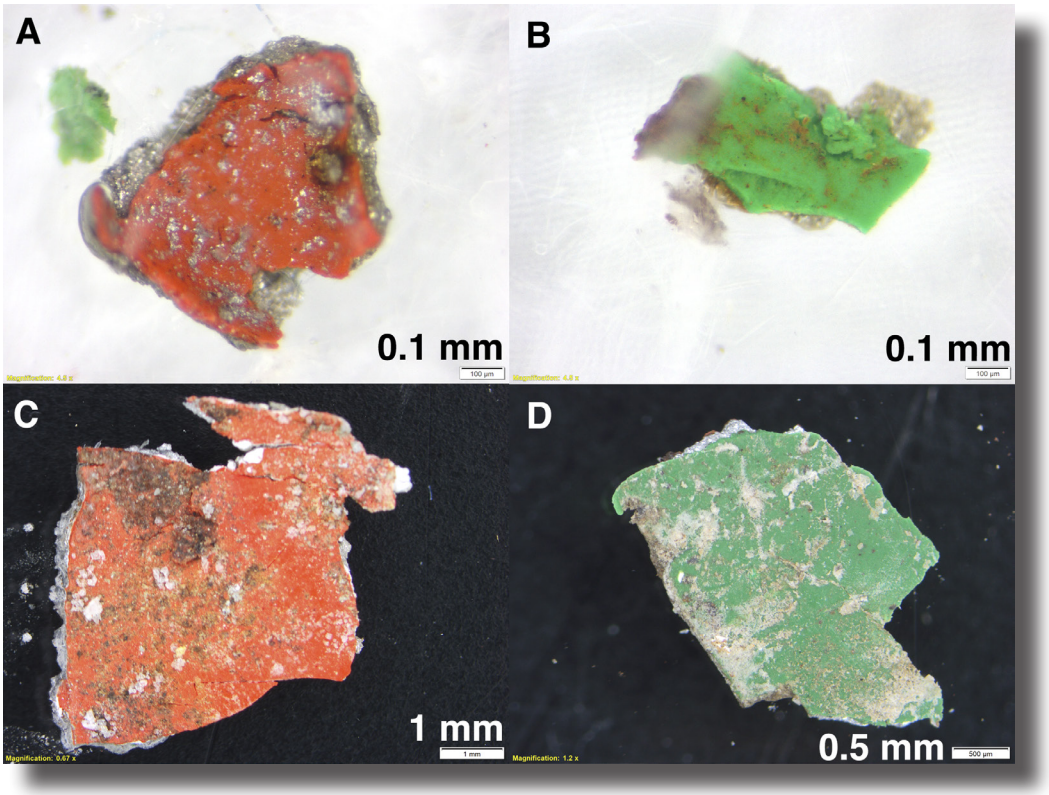

Fig. 15.6: Red/orange and green likely vessel paint fragment from MT 2 (A) and MT 1 (B) respectively. For comparison ship paint fragments deliberately collected from the working deck (E-deck) red/orange (C) and green (D).

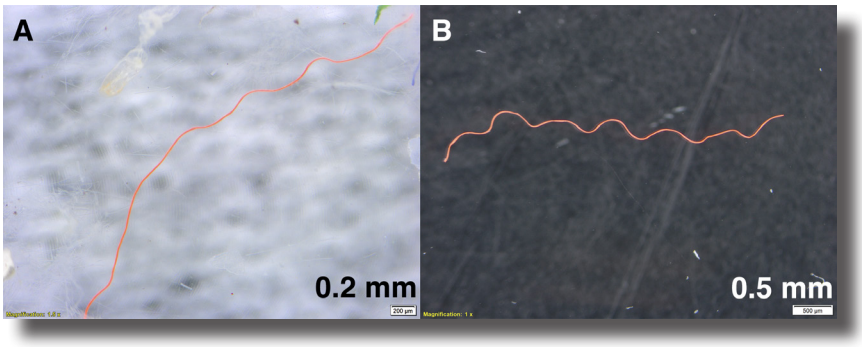

Fig. 15.7: Orange fibre from sample MT 1 (A) and reference sample taken from an orange AWI working jacket (B).

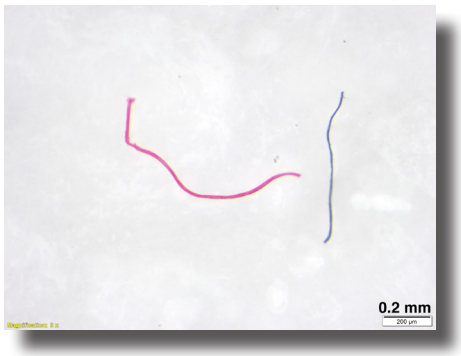

Fig. 15.8: Red and blue fibre from the lab bench procedural blank 1 (petri dish diameter 6 cm exposed to dry lab atmosphere for 17 hours, yielding 39 fibres).

Proposed developments for future microplastic research from Polarstern

Investigating an anthropogenic contaminant, such as microplastics, in a pristine and remote environment like Antarctic seas from a research vessel e.g. *Polarstern*, requires rigid measures against research activity and vessel-induced contamination potential. While sampling on the seafloor may offer a relatively undisturbed compartment (despite the synthetic MUC coring tubes), sampling immediately below the vessel hull (seawater pump) or a few metres away from the hull on the water surface (MT) constitutes a great challenge for avoiding anthropogenic contamination of samples. In an ideal scenario sampling for microplastics would be conducted independently from the vessel as much as possible. Many of the previously described precautionary measures were developed during PS111 in cooperation with fellow scientists. Some further, cooperatively established, optimisation ideas for the deployment of the MT or similar neuston net devices shall be listed here:

- Installing of shutter-mechanism which can be released immediately when device reaches the water surface
- Deployment of MT from crane in front of vessel bow
- Elastic trawling component for buffering wave and current induced tugging and “flying” of MT in rough conditions
- Installing of outward steering rudders for creating more distance to the hull and working deck (E-deck on *Polarstern*)
- Development of sampling protocol for trawling far behind the vessel (>500 m)
- Deployment of MT or similar device by helicopter or drone

Data management

Microplastic samples will either be destroyed by analysis or those not analysed will be stored at the home laboratory at University of Basel. All sequence data will be deposited in EBI's European Nucleotide Archive and will conform to the minimum information standards recommended by the Genomics Standards Consortium (http://gensc.org/projects/mixs-gscproject/). Metadata and results will be stored at data servers of the University of Basel. After a thorough quality control, processing and publication in a peer reviewed journal, the processed data will be stored in the PANGAEA data base.

References

Cincinelli A, Scopetani C, Chelazzi D, Lombardini E, Martellini T, Katsoyiannis A, Fossi MC, Corsolini S (2017) Microplastic in the surface waters of the Ross Sea (Antarctica): Occurrence, distribution and characterization by FTIR, 175, 391-400.

Imhof HK, Schmid J, Niessner R, Ivleva NP, Laforsch C (2012) A novel, highly efficient method for the separation and quantification of plastic particles in sediments of aquatic environments. Limnol. Oceanogr. Methods, 10, 524−537.

Kanhai LDK, Officer R, Lyashevska O, Thompson RC, O'Connor I (2016) Microplastic abundance, distribution and composition along a latitudinal gradient in the Atlantic Ocean. Marine Pollution Bulletin, 115, 307-314.

Löder MGJ, Kuczera M, Mintenig S, Lorenz C, Gerdts G (2015) Focal plane array detector-based micro-Fourier-transform infrared imaging for the analysis of microplastics in environmental samples. Environ. Chem., 12, 563-581.

Lusher AL, Burke A, O'Connor I, Officer R (2014) Microplastic pollution in the Northeast Atlantic Ocean: Validated and opportunistic sampling. Marine Pollution Bulletin, 88, 325-333.

Noren F (2007) Small Plastic Particles in Coastal Swedish Waters. N-research, Sweden.

Tagg AS, Harrison JP, Ju-Nam Y, Sapp M, Bradley EL, Sinclair CJ, Ojeda JJ (2017) Fenton's reagent for the rapid and efficient isolation of microplastics from wastewater. Chem. Commun., 53, 372-375.

APPENDIX

A.1 TEILNEHMENDE INSTITUTE / PARTICIPATING INSTITUTIONS

A.2 FAHRTTEILNEHMER / CRUISE PARTICIPANTS

A.3 SCHIFFSMANNSCHAFT / SHIP'S CREW

A.4 STATIONSLISTE / STATION LIST

A.1 TEILNEHMENDEINSTITUTE/PARTICIPATINGINSTITUTIONS

	Address
AWI	Alfred-Wegener-Institut Helmholtz-Zentrum für Polar- und Meeresforschung Postfach 120161 27515 Bremerhaven Germany
BAS	British Antarctic Survey Cambridge High Cross, Madingley Road Cambridge, CB3 0ET UK
DWD	Deutscher Wetterdienst Geschäftsbereich Wettervorhersage Seeschifffahrtsberatung Bernhard Nocht Str. 76 20359 Hamburg Germany
GEOMAR	GEOMAR Helmholtz-Zentrum für Ozeanforschung Wischhofstr. 1-3 24148 Kiel Germany
LIO	Leibniz Institut für Ostseeforschung Säestr. 15 18199 Rostock Germany
MGU	Universität Basel, MGU Vesalgasse 1 4051 Basel Switzerland
MRI	Mammal Research Institute Dept. of Zoology & Entomology University of Pretoria Private Bay X20, Hatfield 0028 Gauteng South Africa
NIOZ	NIOZ Royal Netherlands Institute for Sea Research Korringa Weg 7 4401 NT Yerseke The Netherlands
NOC	National Oceanographic Centre Southampton European Way Southampton, SO14 3ZH UK

	Address
PIK	Potsdam-Institut für Klimafolgenforschung Telegrafenberg A62 14473 Potsdam Germany
UAB	Facultat de Ciencias Environmental Sciences Universita Autonoma de Barcelona Barcelona, Bellaterra Spain
Uni Bergen	Uni Research Climate P.O. Box 7810 5020 Bergen Norway
Uni Bremen, GEO	Universität Bremen Geowissenschaften Bibliotheksstr. 1 28359 Bremen Germany
Uni Bremen, IU	Universität Bremen Institut für Umweltphysik Otto-Hahn-Allee 28359 Bremen Germany
Uni Kiel	Universität Kiel Zoologisches Institut Am Botanischen Garten 1-9 24118 Kiel Germany
Uni Trier	Universität Trier Fachbereich VI - Raum- und Umweltwissenschaften Fach Umweltmeteorologie 54286 Trier Germany

A.2 FAHRTTEILNEHMER / CRUISE PARTICIPANTS

Name/ Last name	Vorname/ First name	Institut/ Institute	Beruf/ Profession	Fachbereich/ Discipline
Arndt	Jan Erik	AWI	Scientist	Geophysics
Arndt	Stefanie	AWI	Scientist	Sea ice physics
Bartsch*	Christine	AWI	Physician	Logistics
Bester	Marthán	MRI	Scientist	Biology, zoology
Bornemann	Horst	AWI	Scientist	Biology, zoology
Braakmann-Folgmann	Anne	AWI	Student	Geophysics
Diego Feliu	Marc	UAB	Phd student	Environmental science
Geilen	Johanna	AWI	Student	Environmental Physics
Grobe	Hannes	AWI	Scientist	Geology
Gutjahr	Marcus	GEOMAR	Scientist	Geochemistry
Hanfland	Claudia	AWI	Scientist	Geochemistry
Heins	Lena	AWI	Student	Biology
Hellmer	Hartmut	AWI	Scientist	Oceanography
Hirsekorn*	Marius	AWI	Engineer	Logistics
Horb	Stanislav	Uni Kiel	Scientist	Zoology
Huang	Huang	Uni Kiel	Phd student	Geochemistry
Huntemann	Marcus	Uni Bremen, AWI	Scientist	Sea ice physics
Janout	Markus	AWI	Scientist	Oceanography
Jenkins	Adrian	BAS	Scientist	Geophysics
Jürgens	Klaus	LIO	Scientist	MicroBiology
Kern	Yannick	AWI, Uni Bergen	Student	Oceanography
Lischka	Silke	GEOMAR	Scientist	Biology
Maier	Sandra	NIOZ	Phd student	Biology
Mani	Thomas	MGU	Phd student	Geography
McPhail	Stephen	NOC	Engineer	Electronics, AUV
Meeske	Christian	LIO	Engineer	Biology
Michels	Jan	Uni Kiel,	Scientist	Biology, zoology
Østerhus	Svein	Uni Bergen	Scientist	Oceanography
Owsianowski	Nils	AWI	Engineer	Biology, ROV
Reese	Ronja	PIK	Phd student	Sea ice physics
Reiser	Fabian	Uni Trier	Phd student	Meteorology
Richter	Claudio	AWI	Scientist	Biology
Schnaase	Frank	Uni Trier	Phd student	Oceanography
Schröder	Henning	AWI	Engineer	Biology, ROV
Schröder	Michael	AWI	C**hief scientist**	Oceanography,
Slabon	Patricia	AWI	Phd student	geosphysics
Stoll	Nicolas Angelo	AWI	Student	Sea ice physics
Stolle	Clara	AWI	Student	Oceanography
Sültenfuß	Jürgen	Uni Bremen	Scientist	Physics
Sültenfuß	Pia	Uni Bremen	Student	Geoscience

Name/ Last name	**Vorname/ First name**	**Institut/ Institute**	**Beruf/ Profession**	**Fachbereich/ Discipline**
Templeton	Robert	NOC, Southampton, UK	Engineer	Mechanics, AUV
Vorrath	Maria-Elena	AWI	Phd student	Geology
Wege	Mia	MRI, Uni Pretoria, RSA	Scientist	Biology, zoology
Werner*	Martin	AWI	Scientist	Physics
Winkelmann	Ricarda	PIK, Potsdam	Scientist	Sea ice physics
Wischnewski	Fanny	Uni Bremen	Student	Physics
Wisotzki	Andreas	AWI	Scientist	Oceanography
Wurr*	Karsten	AWI	Scientist	Director
Vaupel	Lars	Heli Service Int.	Chief pilot	
Gischler	Michael	Heli Service Int.	Pilot	
Richter	Roland	Heli Service Int.	Technician	Certifying staff
Rothenburg	Mark	Heli Service Int.	Technician	
Schaaf	Tobias	DWD	Scientist	Meteorology
Rohleder	Christian	DWD	Technician	Meteorology
Barker**	Richard	BAS	Technician	Logistics
Barningham**	Simon	BAS	Observer	Logistics
Carp**	Octavian	BAS	Engineer	Logistics
Dubois**	Andre	BAS	Scientist	
Gillies**	Ross	BAS	Engineer	Logistics
Gregory**	Elliot	BAS	Technician	Logistics
Harvey**	Alexander	BAS	Technician	Logistics
Hume**	Thomas	BAS	Technician	Logistics
Jacobs**	Sarah	BAS	Engineer	Logistics
Porter**	Mark	BAS	Engineer	Logistics
Riley**	Stewart	BAS	Engineer	Logistics
Stevenson-Jones**	Ralph	BAS	Engineer	Logistics
Stewart**	Donald	BAS	Engineer	Logistics
Truckel**	Paul	BAS	Technician	Logistics
Warren**	Richard	BAS	Scientist	
Wild**	Lynsay	BAS	Technician	Logistics

* Christine Bartsch Cape Town - *Neumayer Station III*
* Martin Werner Cape Town - *Neumayer Station III*
* Karsten Wurr Cape Town - *Neumayer Station III*
* Marius Hirsekorn *Neumayer Station III* - Punta Arenas

** BAS Halley VI Team *Halley Station VI* - Punta Arenas

A.3 SCHIFFSBESATZUNG / SHIP'S CREW

No.	Name	Rank
01.	Schwarze, Stefan	Master
02.	Langhinrichs, Moritz	1. Offc.
03.	Farysch, Bernd	Ch. Eng.
04.	Kentges, Felix	2. Offc.Lad.
05.	Fallei, Holger	2. Offc.
06.	Neumann, Ralph Peter	2. Offc.
07.	Rudde-Teufel, Claus	Doctor
08.	Christian, Boris	R. Offc.
09.	Grafe, Jens	2. Eng.
10.	Krinfeld, Oleksandr	2. Eng.
11.	Haack, Michael	2. Eng.
12.	Redmer, Jens Dirk	Elec. Eng.
13.	Ganter, Armin	ELO
14.	Hüttebräucker, Olaf	ELO
15.	Nasis, Ilias	ELO
16.	Himmel, Frank	ELO
17.	Loidl, Rainer	Boatsw.
18.	Reise, Lutz	Carpenter
19.	Hagemann, Manfred	A.B.
20.	Winkler, Michael	A.B.
21.	Scheel, Sebastian	A.B.
22.	Bäcker, Andreas	A.B.
23.	Brück, Sebastian	A.B.
24.	Wende, Uwe	A.B.
25.	Klee, Philipp	A.B.
26.	Löscher, Steffen Andreas	A.B.
27.	Preußner, Jörg	Storek.
28.	Teichert, Uwe	Mot-man
29.	Rhau, Lars-Peter	Mot-man
30.	Lamm, Gerd	Mot-man
31.	Schünemann, Mario	Mot-man
32.	Schwarz, Uwe	Mot-man
33.	Schnieder, Sven	Cook
34.	Silinski, Frank	Cooksmate
35.	Möller, Wolfgang	Cooksmate
36.	Czyborra, Bärbel	1. Stwdess
37.	Wöckener, Martina	Stwdess/N.
38.	Dibenau, Torsten	2. Steward
39.	Silinski, Carmen	2. Stwdess
40.	Golla, Gerald	2. Steward
41.	Arendt, Rene	2. Steward
42.	Sun, Yong Shen	2. Steward
43.	Chen, Dan Sheng	Laundrym.

A4. STATIONSLISTE / STATION LIST

Station	Date	Time	Latitude	Longitude	Depth [m]	Gear	Action
PS111_0_Underway-1	2018-01-19	12:00	-33.90982	18.43591	NA	WST	profile start
PS111_0_Underway-2	2018-01-19	13:06	-34.15136	18.16149	171	ADCP_150	profile start
PS111_0_Underway-2	2018-03-12	11:40	-56.75096	-60.70964	4000	ADCP_150	profile end
PS111_0_Underway-3	2018-01-19	13:08	-34.15712	18.15955	173	FBOX	profile start
PS111_0_Underway-3	2018-03-12	11:40	-56.75133	-60.70918	4000	FBOX	profile end
PS111_0_Underway-4	2018-01-19	13:09	-34.15779	18.15933	175	PCO2_GO	profile start
PS111_0_Underway-4	2018-03-12	11:39	-56.75174	-60.70866	3997	PCO2_GO	profile end
PS111_0_Underway-5	2018-01-19	13:09	-34.15852	18.15908	176	PCO2_SUB	profile start
PS111_0_Underway-5	2018-03-12	11:39	-56.75228	-60.70798	3996	PCO2_SUB	profile end
PS111_0_Underway-6	2018-01-19	13:09	-34.16007	18.15853	176	TSG_KEEL	profile start
PS111_0_Underway-6	2018-03-12	11:39	-56.75270	-60.70745	3996	TSG_KEEL	profile end
PS111_0_Underway-7	2018-01-19	13:10	-34.16076	18.15828	177	TSG_ KEEL_2	profile start
PS111_0_Underway-7	2018-03-12	11:39	-56.75331	-60.70667	3995	TSG_ KEEL_2	profile end
PS111_0_Underway-8	2018-01-20	12:00	-37.82389	16.85833	4575	HSPS	profile start
PS111_0_Underway-8	2018-03-12	11:38	-56.75465	-60.70492	3994	HSPS	profile end
PS111_1-1	2018-01-20	23:01	-39.99996	16.06304	4879	FLOAT	station start
PS111_2-1	2018-01-22	01:03	-44.99672	14.11767	4495	FLOAT	station start
PS111_2-2	2018-01-22	01:05	-44.99851	14.11777	4497	SVP_B	station start
PS111_3-1	2018-01-22	22:44	-48.99728	12.29959	4247	FLOAT	station start
PS111_4-1	2018-01-23	17:27	-52.49935	10.68395	3691	SVP_B	station start
PS111_5-1	2018-01-25	01:53	-58.49965	7.74218	4745	FLOAT	station start
PS111_5-2	2018-01-25	01:55	-58.50126	7.74159	4749	SVP_B	station start
PS111_6-1	2018-01-25	09:26	-59.99406	6.91125	5233	UCTD	station start
PS111_6-1	2018-01-25	09:54	-60.08396	6.87507	5319	UCTD	station end
PS111_6-2	2018-01-25	11:27	-60.39242	6.76724	5331	UCTD	station start
PS111_6-2	2018-01-25	11:51	-60.47602	6.73718	5299	UCTD	station end
PS111_7-1	2018-01-25	11:58	-60.49892	6.72863	5327	SVP_B	station start
PS111_6-3	2018-01-25	13:24	-60.78155	6.61281	5262	UCTD	station start
PS111_6-3	2018-01-25	13:54	-60.87873	6.57257	5251	UCTD	station end
PS111_6-4	2018-01-25	15:24	-61.17364	6.45012	5326	UCTD	station start
PS111_6-4	2018-01-25	15:55	-61.27554	6.40686	5097	UCTD	station end
PS111_6-5	2018-01-25	17:22	-61.56777	6.28424	5329	UCTD	station start
PS111_6-5	2018-01-25	17:47	-61.65215	6.24846	5327	UCTD	station end

Station	Date	Time	Latitude	Longitude	Depth [m]	Gear	Action
PS111_6-6	2018-01-25	19:10	-61.92588	6.13143	5304	UCTD	station start
PS111_6-6	2018-01-25	19:59	-62.04727	6.07221	5314	UCTD	station end
PS111_8-1	2018-01-25	19:38	-62.01430	6.09250	5313	SVP_B	station start
PS111_6-7	2018-01-25	21:20	-62.30392	5.94416	5308	UCTD	station start
PS111_6-7	2018-01-25	21:45	-62.38364	5.89428	5312	UCTD	station end
PS111_6-8	2018-01-25	23:28	-62.72139	5.71184	5320	UCTD	station start
PS111_6-8	2018-01-25	23:52	-62.80075	5.66826	5318	UCTD	station end
PS111_6-9	2018-01-26	01:33	-63.12841	5.48852	5141	UCTD	station start
PS111_6-9	2018-01-26	01:55	-63.20149	5.44848	5108	UCTD	station end
PS111_6-10	2018-01-26	03:23	-63.49240	5.28586	4895	UCTD	station start
PS111_6-10	2018-01-26	03:52	-63.58976	5.23188	4739	UCTD	station end
PS111_6-11	2018-01-26	04:49	-63.77754	5.12598	4538	UCTD	station start
PS111_6-11	2018-01-26	05:17	-63.86976	5.07406	4376	UCTD	station end
PS111_9-1	2018-01-26	05:33	-63.90911	5.05253	4244	MT	station start
PS111_9-1	2018-01-26	06:06	-63.94142	5.03332	4054	MT	station end
PS111_9-2	2018-01-26	07:07	-64.00056	4.99901	NA	CTDOZE	station start
PS111_9-2	2018-01-26	07:26	-64.00035	5.00180	NA	CTDOZE	at depth
PS111_9-2	2018-01-26	07:45	-64.00047	5.00070	NA	CTDOZE	station end
PS111_9-3	2018-01-26	08:30	-63.99964	5.00139	NA	CTDOZE	station start
PS111_9-3	2018-01-26	09:46	-63.99976	4.99987	3849	CTDOZE	at depth
PS111_9-3	2018-01-26	11:06	-63.99977	5.00088	3851	CTDOZE	station end
PS111_9-4	2018-01-26	11:18	-64.00304	4.99791	3845	FLOAT	station start
PS111_6-12	2018-01-26	12:41	-64.21352	4.63125	3143	UCTD	station start
PS111_6-12	2018-01-26	13:06	-64.27857	4.51698	2952	UCTD	station end
PS111_6-13	2018-01-26	14:51	-64.56463	4.02463	2537	UCTD	station start
PS111_6-13	2018-01-26	15:14	-64.62776	3.91602	2477	UCTD	station end
PS111_6-14	2018-01-26	17:19	-64.96264	3.32191	2489	UCTD	station start
PS111_6-14	2018-01-26	17:47	-65.03846	3.18761	2441	UCTD	station end
PS111_10-1	2018-01-26	19:30	-65.30620	2.70774	1510	MT	station start
PS111_10-1	2018-01-26	20:01	-65.33293	2.66146	1600	MT	station end
PS111_10-2	2018-01-26	20:36	-65.38581	2.56414	2156	CTDOZE	station start
PS111_10-2	2018-01-26	21:22	-65.38526	2.56711	2092	CTDOZE	at depth
PS111_10-2	2018-01-26	22:10	-65.38533	2.56648	2105	CTDOZE	station end
PS111_10-3	2018-01-26	22:16	-65.38549	2.56639	2097	FLOAT	station start
PS111_6-15	2018-01-27	00:21	-65.71990	1.99592	2590	UCTD	station start
PS111_6-15	2018-01-27	00:45	-65.78713	1.88095	2621	UCTD	station end
PS111_11-1	2018-01-27	02:08	-66.01559	1.48330	2668	FLOAT	station start
PS111_6-16	2018-01-27	02:27	-66.06051	1.39190	3203	UCTD	station start

Station	Date	Time	Latitude	Longitude	Depth [m]	Gear	Action
PS111_6-16	2018-01-27	02:51	-66.12232	1.26015	3134	UCTD	station end
PS111_6-17	2018-01-27	04:30	-66.38036	0.72221	4090	UCTD	station start
PS111_6-17	2018-01-27	04:59	-66.45591	0.56352	4297	UCTD	station end
PS111_12-1	2018-01-27	06:13	-66.63583	0.18167	4632	MT	station start
PS111_12-1	2018-01-27	06:46	-66.66308	0.12291	4647	MT	station end
PS111_12-2	2018-01-27	07:26	-66.73833	-0.03681	4699	CTDOZE	station start
PS111_12-2	2018-01-27	09:00	-66.73885	-0.03867	4698	CTDOZE	at depth
PS111_12-2	2018-01-27	10:36	-66.73871	-0.03811	4699	CTDOZE	station end
PS111_12-3	2018-01-27	10:46	-66.73923	-0.04757	4665	FLOAT	station start
PS111_12-4	2018-01-27	11:07	-66.77669	-0.11518	4673	SVP_B	station start
PS111_6-18	2018-01-27	12:38	-67.02561	-0.61837	4678	UCTD	station start
PS111_6-18	2018-01-27	12:59	-67.08531	-0.74020	4664	UCTD	station end
PS111_6-19	2018-01-27	14:32	-67.34327	-1.26888	4591	UCTD	station start
PS111_6-19	2018-01-27	14:55	-67.40641	-1.39926	4567	UCTD	station end
PS111_6-20	2018-01-27	16:31	-67.67671	-1.96099	4502	UCTD	station start
PS111_6-20	2018-01-27	16:56	-67.74453	-2.10290	4365	UCTD	station end
PS111_6-21	2018-01-27	18:32	-68.00901	-2.66031	3950	UCTD	station start
PS111_6-21	2018-01-27	18:59	-68.08395	-2.81954	3927	UCTD	station end
PS111_6-22	2018-01-27	20:26	-68.32306	-3.33079	3684	UCTD	station start
PS111_6-22	2018-01-27	20:51	-68.39177	-3.47885	3732	UCTD	station end
PS111_6-23	2018-01-27	22:19	-68.63976	-3.97807	3765	UCTD	station start
PS111_6-23	2018-01-27	22:43	-68.71291	-4.11334	3511	UCTD	station end
PS111_13-1	2018-01-28	07:00	-70.03965	-6.74429	1944	MT	station start
PS111_13-1	2018-01-28	07:34	-70.06309	-6.82680	1885	MT	station end
PS111_13-2	2018-01-28	08:13	-70.09333	-6.84936	1775	MUC	station start
PS111_13-2	2018-01-28	08:41	-70.09368	-6.85151	1775	MUC	at depth
PS111_13-2	2018-01-28	09:20	-70.09394	-6.85023	1777	MUC	station end
PS111_13-3	2018-01-28	09:35	-70.09390	-6.85162	1776	MUC	station start
PS111_13-3	2018-01-28	10:04	-70.09358	-6.85035	1775	MUC	at depth
PS111_13-3	2018-01-28	10:42	-70.09379	-6.85063	1776	MUC	station end
PS111_13-4	2018-01-28	11:11	-70.09377	-6.84987	1776	GC	station start
PS111_13-4	2018-01-28	11:32	-70.09363	-6.85011	1776	GC	at depth
PS111_13-4	2018-01-28	12:00	-70.09400	-6.85121	1777	GC	station end
PS111_0_Underway-9	2018-01-28	12:00	-70.09400	-6.85121	1777	LIDAR	profile start
PS111_0_Underway-9	2018-03-02	12:30	-75.46016	-26.82656	NA	LIDAR	profile end
PS111_14-1	2018-01-31	08:19	-70.94003	-10.54040	NA	CTDOZE	station start
PS111_14-1	2018-01-31	08:25	-70.94027	-10.54078	NA	CTDOZE	at depth
PS111_14-1	2018-01-31	08:32	-70.94016	-10.54026	NA	CTDOZE	station end

Station	Date	Time	Latitude	Longitude	Depth [m]	Gear	Action
PS111_14-2	2018-01-31	09:39	-70.94484	-10.51901	NA	ROV	station start
PS111_14-2	2018-01-31	10:19	-70.94449	-10.52041	NA	ROV	station end
PS111_14-3	2018-01-31	11:01	-70.94314	-10.53361	NA	MG	station start
PS111_14-3	2018-01-31	11:12	-70.94311	-10.53365	NA	MG	at depth
PS111_14-3	2018-01-31	11:24	-70.94289	-10.53050	291	MG	station end
PS111_14-4	2018-01-31	12:09	-70.94376	-10.52725	282	MG	station start
PS111_14-4	2018-01-31	12:20	-70.94403	-10.52678	282	MG	at depth
PS111_14-4	2018-01-31	12:33	-70.94408	-10.52649	279	MG	station end
PS111_14-5	2018-01-31	12:51	-70.94421	-10.52643	280	CTDOZE	station start
PS111_14-5	2018-01-31	13:01	-70.94400	-10.52665	280	CTDOZE	at depth
PS111_14-5	2018-01-31	13:12	-70.94373	-10.52574	277	CTDOZE	station end
PS111_15-1	2018-02-01	10:40	-71.66589	-15.78303	1403	MUC	station start
PS111_15-1	2018-02-01	11:01	-71.66531	-15.78363	1405	MUC	at depth
PS111_15-1	2018-02-01	11:23	-71.66296	-15.78415	1411	MUC	station end
PS111_15-2	2018-02-01	12:02	-71.66533	-15.78309	1404	GC	station start
PS111_15-2	2018-02-01	12:19	-71.66480	-15.78421	1406	GC	at depth
PS111_15-2	2018-02-01	12:48	-71.66388	-15.78595	1371	GC	station end
PS111_16-1	2018-02-01	21:35	-72.38376	-17.81884	1420	CTDOZE	station start
PS111_16-1	2018-02-01	22:07	-72.38414	-17.81709	1419	CTDOZE	at depth
PS111_16-1	2018-02-01	22:44	-72.38407	-17.81716	1419	CTDOZE	station end
PS111_16-2	2018-02-01	22:58	-72.38404	-17.81713	1419	GC	station start
PS111_16-2	2018-02-01	23:16	-72.38407	-17.81708	1419	GC	at depth
PS111_16-2	2018-02-01	23:40	-72.38409	-17.81711	1419	GC	station end
PS111_16-3	2018-02-01	23:59	-72.38430	-17.81696	1418	MUC	station start
PS111_16-3	2018-02-02	00:18	-72.38431	-17.81674	1418	MUC	at depth
PS111_16-3	2018-02-02	00:43	-72.38428	-17.81678	1418	MUC	station end
PS111_17-1	2018-02-03	00:03	-73.70046	-25.73200	3242	CTDOZE	station start
PS111_17-1	2018-02-03	00:18	-73.69998	-25.73312	3244	CTDOZE	at depth
PS111_17-1	2018-02-03	00:37	-73.69971	-25.73263	3243	CTDOZE	station end
PS111_17-2	2018-02-03	01:38	-73.69963	-25.73185	3241	CTDOZE	station start
PS111_17-2	2018-02-03	01:44	-73.69953	-25.73141	3241	CTDOZE	at depth
PS111_17-2	2018-02-03	01:51	-73.69961	-25.73068	3240	CTDOZE	station end
PS111_17-3	2018-02-03	02:07	-73.69973	-25.73044	3240	BONGO	station start
PS111_17-3	2018-02-03	02:24	-73.69974	-25.72941	3239	BONGO	at depth
PS111_17-3	2018-02-03	02:46	-73.69992	-25.72797	3233	BONGO	station end
PS111_17-4	2018-02-03	02:55	-73.69976	-25.72820	3235	CTDOZE	station start
PS111_17-4	2018-02-03	04:00	-73.70032	-25.72380	3219	CTDOZE	at depth
PS111_17-4	2018-02-03	05:11	-73.69953	-25.71977	3216	CTDOZE	station end

Station	Date	Time	Latitude	Longitude	Depth [m]	Gear	Action
PS111_17-5	2018-02-03	05:25	-73.69927	-25.71946	3216	MN_S5	station start
PS111_17-5	2018-02-03	05:44	-73.69913	-25.71909	3216	MN_S5	at depth
PS111_17-5	2018-02-03	06:08	-73.69885	-25.71828	3216	MN_S5	station end
PS111_17-6	2018-02-03	08:53	-73.71618	-25.77007	3223	MOOR	station end
PS111_17-7	2018-02-03	14:29	-73.72137	-25.78389	3212	MOOR	station start
PS111_18-1	2018-02-04	10:34	-76.15848	-30.00938	410	CTDOZE	station start
PS111_18-1	2018-02-04	10:47	-76.15786	-30.01409	410	CTDOZE	at depth
PS111_18-1	2018-02-04	11:06	-76.15596	-30.00258	405	CTDOZE	station end
PS111_19-1	2018-02-04	11:51	-76.10814	-30.38306	464	MT	station start
PS111_19-1	2018-02-04	12:26	-76.12716	-30.47481	461	MT	station end
PS111_19-2	2018-02-04	12:47	-76.08860	-30.46173	443	MOOR	at depth
PS111_19-2	2018-02-04	13:09	-76.09151	-30.46839	466	MOOR	station end
PS111_20-1	2018-02-04	14:18	-76.01481	-30.88771	449	MT	station start
PS111_20-1	2018-02-04	14:20	-76.01618	-30.89122	449	MT	at depth
PS111_20-1	2018-02-04	14:50	-76.03772	-30.96811	452	MT	station end
PS111_20-2	2018-02-04	14:57	-76.04386	-30.98774	454	MOOR	at depth
PS111_20-2	2018-02-04	15:17	-76.04517	-30.99029	470	MOOR	station end
PS111_21-1	2018-02-04	17:02	-75.95780	-31.47186	595	MOOR	station end
PS111_21-2	2018-02-04	18:07	-75.96118	-31.48289	597	MOOR	station start
PS111_21-3	2018-02-04	19:15	-75.95950	-31.46940	595	CTDOZE	station start
PS111_21-3	2018-02-04	19:35	-75.95981	-31.47025	595	CTDOZE	at depth
PS111_21-3	2018-02-04	19:59	-75.95987	-31.47075	595	CTDOZE	station end
PS111_22-1	2018-02-04	21:15	-75.90268	-31.75995	723	CTDOZE	station start
PS111_22-1	2018-02-04	21:30	-75.90153	-31.75851	723	CTDOZE	at depth
PS111_22-1	2018-02-04	21:56	-75.89975	-31.75744	725	CTDOZE	station end
PS111_23-1	2018-02-04	23:17	-75.95389	-32.04423	724	CTDOZE	station start
PS111_23-1	2018-02-04	23:37	-75.95289	-32.04382	747	CTDOZE	at depth
PS111_23-1	2018-02-05	00:05	-75.95303	-32.04517	748	CTDOZE	station end
PS111_23-2	2018-02-05	00:12	-75.95318	-32.04567	748	BONGO	station start
PS111_23-2	2018-02-05	00:31	-75.95354	-32.04474	749	BONGO	at depth
PS111_23-2	2018-02-05	00:51	-75.95378	-32.04419	750	BONGO	station end
PS111_23-3	2018-02-05	01:00	-75.95377	-32.04416	750	MN_S5	station start
PS111_23-3	2018-02-05	01:18	-75.95373	-32.04317	751	MN_S5	at depth
PS111_23-3	2018-02-05	01:40	-75.95394	-32.04367	751	MN_S5	station end
PS111_24-1	2018-02-05	02:23	-75.94873	-32.32744	770	CTDOZE	station start
PS111_24-1	2018-02-05	02:42	-75.94817	-32.32747	770	CTDOZE	at depth
PS111_24-1	2018-02-05	03:05	-75.94766	-32.32878	770	CTDOZE	station end
PS111_25-1	2018-02-05	05:27	-75.99875	-31.23178	495	CTDOZE	station start

Station	Date	Time	Latitude	Longitude	Depth [m]	Gear	Action
PS111_25-1	2018-02-05	05:43	-75.99879	-31.23332	NA	CTDOZE	at depth
PS111_25-1	2018-02-05	06:01	-75.99807	-31.23320	NA	CTDOZE	station end
PS111_20-3	2018-02-05	06:50	-76.04521	-30.99741	471	CTDOZE	station start
PS111_20-3	2018-02-05	07:05	-76.04523	-30.99770	472	CTDOZE	at depth
PS111_20-3	2018-02-05	07:24	-76.04426	-30.99546	471	CTDOZE	station end
PS111_26-1	2018-02-05	08:16	-76.06930	-30.74533	462	CTDOZE	station start
PS111_26-1	2018-02-05	08:30	-76.06931	-30.74608	462	CTDOZE	at depth
PS111_26-1	2018-02-05	08:43	-76.06925	-30.74609	461	CTDOZE	station end
PS111_19-3	2018-02-05	09:27	-76.08618	-30.44956	448	CTDOZE	station start
PS111_19-3	2018-02-05	09:41	-76.08746	-30.45501	461	CTDOZE	at depth
PS111_19-3	2018-02-05	09:58	-76.08860	-30.46118	465	CTDOZE	station end
PS111_19-4	2018-02-05	10:06	-76.08948	-30.46414	466	BONGO	station start
PS111_19-4	2018-02-05	10:18	-76.09061	-30.46828	466	BONGO	at depth
PS111_19-4	2018-02-05	10:30	-76.08992	-30.47010	467	BONGO	station end
PS111_19-5	2018-02-05	10:33	-76.09002	-30.46975	467	BONGO	station start
PS111_19-5	2018-02-05	10:44	-76.09044	-30.46933	467	BONGO	at depth
PS111_19-5	2018-02-05	10:59	-76.09081	-30.47006	467	BONGO	station end
PS111_19-6	2018-02-05	11:17	-76.09112	-30.47085	467	MOOR	station start
PS111_20-4	2018-02-05	12:56	-76.04576	-31.00952	474	MOOR	station start
PS111_27-1	2018-02-05	17:12	-75.95519	-29.08283	410	MUC	station start
PS111_27-1	2018-02-05	17:20	-75.95488	-29.08226	425	MUC	at depth
PS111_27-1	2018-02-05	17:31	-75.95485	-29.08404	425	MUC	station end
PS111_27-2	2018-02-05	17:55	-75.95497	-29.08320	426	GC	station start
PS111_27-2	2018-02-05	18:04	-75.95482	-29.08319	425	GC	at depth
PS111_27-2	2018-02-05	18:17	-75.95462	-29.08261	425	GC	station end
PS111_27-3	2018-02-05	18:29	-75.95487	-29.08148	426	CTDOZE	station start
PS111_27-3	2018-02-05	18:44	-75.95480	-29.08213	426	CTDOZE	at depth
PS111_27-3	2018-02-05	19:01	-75.95427	-29.08280	426	CTDOZE	station end
PS111_28-1	2018-02-05	20:19	-75.97498	-28.41569	357	CTDOZE	station start
PS111_28-1	2018-02-05	20:32	-75.97510	-28.41655	356	CTDOZE	at depth
PS111_28-1	2018-02-05	20:47	-75.97515	-28.41730	356	CTDOZE	station end
PS111_28-2	2018-02-05	20:57	-75.97524	-28.41735	355	BONGO	station start
PS111_28-2	2018-02-05	21:09	-75.97513	-28.41744	356	BONGO	at depth
PS111_28-2	2018-02-05	21:25	-75.97509	-28.41715	357	BONGO	station end
PS111_28-3	2018-02-05	21:33	-75.97509	-28.41731	357	MN_S5	station start
PS111_28-3	2018-02-05	21:45	-75.97520	-28.41722	356	MN_S5	at depth
PS111_28-3	2018-02-05	22:02	-75.97520	-28.41686	356	MN_S5	station end
PS111_28-4	2018-02-05	22:15	-75.97451	-28.41405	351	MT	station start

Station	Date	Time	Latitude	Longitude	Depth [m]	Gear	Action
PS111_28-4	2018-02-05	22:47	-75.96248	-28.30837	404	MT	station end
PS111_29-1	2018-02-06	06:09	-75.97307	-27.68194	403	CTDOZE	station start
PS111_29-1	2018-02-06	06:22	-75.97303	-27.68117	402	CTDOZE	at depth
PS111_29-1	2018-02-06	06:37	-75.97305	-27.68080	401	CTDOZE	station end
PS111_29-2	2018-02-06	06:51	-75.97312	-27.68120	401	MUC	station start
PS111_29-2	2018-02-06	06:59	-75.97305	-27.68048	401	MUC	at depth
PS111_29-2	2018-02-06	07:10	-75.97305	-27.68077	401	MUC	station end
PS111_29-3	2018-02-06	07:30	-75.97165	-27.67967	411	MUC	station start
PS111_29-3	2018-02-06	07:37	-75.97174	-27.68034	411	MUC	at depth
PS111_29-3	2018-02-06	07:48	-75.97147	-27.68045	414	MUC	station end
PS111_29-4	2018-02-06	08:37	-75.99756	-27.69330	415	GC	station start
PS111_29-4	2018-02-06	08:43	-75.99725	-27.69284	430	GC	at depth
PS111_29-4	2018-02-06	08:52	-75.99723	-27.69424	429	GC	station end
PS111_30-1	2018-02-06	10:28	-76.01705	-27.70409	455	AUV	station start
PS111_30-1	2018-02-06	16:17	-76.02298	-27.70711	436	AUV	station end
PS111_30-2	2018-02-06	17:26	-76.01546	-27.70945	427	ROV	station start
PS111_30-2	2018-02-06	17:41	-76.01583	-27.71041	436	ROV	station end
PS111_30-2	2018-02-06	17:47	-76.01568	-27.71029	433	ROV	station start
PS111_30-2	2018-02-06	18:10	-76.01586	-27.71068	440	ROV	at depth
PS111_30-2	2018-02-06	18:34	-76.01588	-27.71204	437	ROV	station end
PS111_31-1	2018-02-06	21:18	-75.80534	-26.96985	319	CTDOZE	station start
PS111_31-1	2018-02-06	21:29	-75.80535	-26.97003	318	CTDOZE	at depth
PS111_31-1	2018-02-06	21:40	-75.80535	-26.96991	318	CTDOZE	station end
PS111_32-1	2018-02-07	08:48	-74.86059	-31.81423	635	CTDOZE	station start
PS111_32-1	2018-02-07	09:05	-74.86034	-31.81506	637	CTDOZE	at depth
PS111_32-1	2018-02-07	09:29	-74.85875	-31.81591	635	CTDOZE	station end
PS111_32-2	2018-02-07	09:53	-74.85359	-31.81912	637	MOOR	station start
PS111_33-1	2018-02-07	11:32	-74.84406	-32.52000	599	CTDOZE	station start
PS111_33-1	2018-02-07	11:49	-74.84338	-32.51837	595	CTDOZE	at depth
PS111_33-1	2018-02-07	12:11	-74.84155	-32.51667	598	CTDOZE	station end
PS111_33-2	2018-02-07	12:17	-74.84063	-32.51666	598	MOOR	station start
PS111_34-1	2018-02-07	14:21	-74.85866	-33.01654	571	CTDOZE	station start
PS111_34-1	2018-02-07	14:36	-74.85849	-33.01587	592	CTDOZE	at depth
PS111_34-1	2018-02-07	14:55	-74.85660	-33.01002	596	CTDOZE	station end
PS111_34-2	2018-02-07	14:59	-74.85624	-33.00696	598	MOOR	station start
PS111_35-1	2018-02-09	08:35	-76.70899	-51.85760	283	MT	station start
PS111_35-1	2018-02-09	08:50	-76.71314	-51.90771	291	MT	station end
PS111_35-2	2018-02-09	09:33	-76.73169	-52.05738	295	CTDOZE	station start

Station	Date	Time	Latitude	Longitude	Depth [m]	Gear	Action
PS111_35-2	2018-02-09	09:33	-76.73172	-52.05729	295	CTDOZE	at depth
PS111_35-2	2018-02-09	09:58	-76.73401	-52.06768	602	CTDOZE	station end
PS111_36-1	2018-02-09	12:43	-76.50597	-52.81465	404	CTDOZE	station start
PS111_36-1	2018-02-09	12:54	-76.50598	-52.81477	404	CTDOZE	at depth
PS111_36-1	2018-02-09	13:08	-76.50611	-52.81529	404	CTDOZE	station end
PS111_37-1	2018-02-09	14:07	-76.48280	-52.63596	396	AUV	station start
PS111_37-1	2018-02-09	14:25	-76.48307	-52.63603	NA	AUV	profile start
PS111_37-1	2018-02-09	18:32	-76.48466	-52.64479	398	AUV	station end
PS111_37-2	2018-02-09	15:02	-76.48296	-52.63668	NA	CTDOZE	station start
PS111_37-2	2018-02-09	15:15	-76.48295	-52.63710	NA	CTDOZE	at depth
PS111_37-2	2018-02-09	15:34	-76.48320	-52.63735	NA	CTDOZE	station end
PS111_37-3	2018-02-09	15:59	-76.48252	-52.63799	NA	BONGO	station start
PS111_37-3	2018-02-09	16:15	-76.48307	-52.63925	396	BONGO	at depth
PS111_37-3	2018-02-09	16:29	-76.48307	-52.63952	396	BONGO	station end
PS111_37-4	2018-02-09	16:44	-76.48330	-52.64021	396	MN_M7	station start
PS111_37-4	2018-02-09	16:50	-76.48328	-52.64084	397	MN_M7	station end
PS111_37-4	2018-02-09	17:20	-76.48349	-52.65002	397	MN_M7	station start
PS111_37-4	2018-02-09	17:33	-76.48460	-52.64917	397	MN_M7	at depth
PS111_37-4	2018-02-09	17:52	-76.48468	-52.64809	397	MN_M7	station end
PS111_36-2	2018-02-09	19:27	-76.50851	-52.81180	401	ROV	station start
PS111_36-2	2018-02-09	22:49	-76.50748	-52.80750	401	ROV	station end
PS111_38-1	2018-02-10	02:21	-76.19810	-53.67824	459	CTDOZE	station start
PS111_38-1	2018-02-10	02:34	-76.19777	-53.67878	459	CTDOZE	at depth
PS111_38-1	2018-02-10	02:53	-76.19797	-53.68039	463	CTDOZE	station end
PS111_39-1	2018-02-10	05:14	-75.98280	-54.66594	485	CTDOZE	station start
PS111_39-1	2018-02-10	05:31	-75.98230	-54.66761	505	CTDOZE	at depth
PS111_39-1	2018-02-10	05:52	-75.98305	-54.66566	NA	CTDOZE	station end
PS111_40-1	2018-02-10	08:06	-76.00048	-54.24045	NA	GC	station start
PS111_40-1	2018-02-10	08:14	-76.00077	-54.24046	514	GC	at depth
PS111_40-1	2018-02-10	08:24	-76.00085	-54.23979	513	GC	station end
PS111_40-2	2018-02-10	08:40	-76.00104	-54.24018	514	MUC	station start
PS111_40-2	2018-02-10	08:49	-76.00088	-54.23953	513	MUC	at depth
PS111_40-2	2018-02-10	09:00	-76.00097	-54.23946	513	MUC	station end
PS111_40-3	2018-02-10	09:16	-76.00109	-54.24035	514	CTDOZE	station start
PS111_40-3	2018-02-10	09:22	-76.00103	-54.23996	513	CTDOZE	at depth
PS111_40-3	2018-02-10	09:31	-76.00116	-54.23937	514	CTDOZE	station end
PS111_41-1	2018-02-10	14:56	-76.48390	-52.63218	399	AUV	station start
PS111_41-1	2018-02-10	15:58	-76.48300	-52.63037	399	AUV	station end

Station	Date	Time	Latitude	Longitude	Depth [m]	Gear	Action
PS111_41-1	2018-02-10	16:08	-76.48319	-52.64343	398	AUV	profile end
PS111_41-1	2018-02-10	16:13	-76.48340	-52.64735	397	AUV	station end
PS111_42-1	2018-02-10	18:58	-76.14493	-53.35699	495	MUC	station start
PS111_42-1	2018-02-10	19:05	-76.14498	-53.35662	493	MUC	at depth
PS111_42-1	2018-02-10	19:18	-76.14484	-53.35677	493	MUC	station end
PS111_42-2	2018-02-10	19:34	-76.14460	-53.35652	493	GC	station start
PS111_42-2	2018-02-10	19:40	-76.14483	-53.35660	493	GC	at depth
PS111_42-2	2018-02-10	19:51	-76.14522	-53.35675	494	GC	station end
PS111_42-3	2018-02-10	20:21	-76.14464	-53.35622	493	CTDOZE	station start
PS111_42-3	2018-02-10	20:37	-76.14467	-53.35659	493	CTDOZE	at depth
PS111_42-3	2018-02-10	20:54	-76.14472	-53.35577	494	CTDOZE	station end
PS111_42-4	2018-02-10	21:03	-76.14485	-53.35630	493	BONGO	station start
PS111_42-4	2018-02-10	21:23	-76.14453	-53.35571	493	BONGO	at depth
PS111_42-4	2018-02-10	21:39	-76.14468	-53.35590	493	BONGO	station end
PS111_42-5	2018-02-10	21:43	-76.14458	-53.35601	493	BONGO	station start
PS111_42-5	2018-02-10	22:10	-76.14400	-53.35692	496	BONGO	at depth
PS111_42-5	2018-02-10	22:28	-76.14399	-53.35809	495	BONGO	station end
PS111_43-1	2018-02-11	02:14	-75.76732	-55.67144	474	CTDOZE	station start
PS111_43-1	2018-02-11	02:27	-75.76728	-55.67151	474	CTDOZE	at depth
PS111_43-1	2018-02-11	02:44	-75.76673	-55.67178	475	CTDOZE	station end
PS111_44-1	2018-02-11	04:42	-75.60047	-56.57865	NA	CTDOZE	station start
PS111_44-1	2018-02-11	04:57	-75.60054	-56.57886	363	CTDOZE	at depth
PS111_44-1	2018-02-11	05:10	-75.60104	-56.57622	361	CTDOZE	station end
PS111_45-1	2018-02-11	06:14	-75.51747	-56.94097	445	CTDOZE	station start
PS111_45-1	2018-02-11	06:29	-75.51791	-56.93358	445	CTDOZE	at depth
PS111_45-1	2018-02-11	06:46	-75.51837	-56.92426	442	CTDOZE	station end
PS111_46-1	2018-02-11	09:41	-75.26613	-58.58908	NA	CTDOZE	station start
PS111_46-1	2018-02-11	10:00	-75.26610	-58.58867	627	CTDOZE	at depth
PS111_46-1	2018-02-11	10:19	-75.26646	-58.58837	627	CTDOZE	station end
PS111_47-1	2018-02-11	13:01	-74.98363	-60.00206	662	CTDOZE	station start
PS111_47-1	2018-02-11	13:17	-74.98346	-60.00158	661	CTDOZE	at depth
PS111_47-1	2018-02-11	13:41	-74.98349	-60.00113	661	CTDOZE	station end
PS111_47-2	2018-02-11	13:53	-74.98474	-60.00161	NA	MUC	station start
PS111_47-2	2018-02-11	14:05	-74.98473	-60.00099	660	MUC	at depth
PS111_47-2	2018-02-11	14:18	-74.98450	-60.00034	660	MUC	station end
PS111_47-3	2018-02-11	14:36	-74.98455	-60.00013	660	GC	station start
PS111_47-3	2018-02-11	14:45	-74.98471	-60.00053	660	GC	at depth
PS111_47-3	2018-02-11	15:00	-74.98467	-59.99904	659	GC	station end

Station	Date	Time	Latitude	Longitude	Depth [m]	Gear	Action
PS111_48-1	2018-02-11	17:06	-74.80089	-60.79844	NA	CTDOZE	station start
PS111_48-1	2018-02-11	17:25	-74.80052	-60.79898	NA	CTDOZE	at depth
PS111_48-1	2018-02-11	17:46	-74.80072	-60.79764	NA	CTDOZE	station end
PS111_48-2	2018-02-11	17:53	-74.80085	-60.79568	NA	BONGO	station start
PS111_48-2	2018-02-11	18:13	-74.80188	-60.79603	NA	BONGO	at depth
PS111_48-2	2018-02-11	18:33	-74.80415	-60.78966	NA	BONGO	station end
PS111_48-3	2018-02-11	18:38	-74.80423	-60.78906	NA	BONGO	station start
PS111_48-3	2018-02-11	18:57	-74.80472	-60.78921	NA	BONGO	at depth
PS111_48-3	2018-02-11	19:20	-74.80563	-60.79283	NA	BONGO	station end
PS111_49-1	2018-02-11	20:40	-74.73105	-61.02529	638	CTDOZE	station start
PS111_49-1	2018-02-11	20:57	-74.73189	-61.02587	633	CTDOZE	at depth
PS111_49-1	2018-02-11	21:16	-74.73250	-61.02745	634	CTDOZE	station end
PS111_50-1	2018-02-12	06:25	-74.88510	-60.33480	661	CTDOZE	station start
PS111_50-1	2018-02-12	06:43	-74.88350	-60.32844	660	CTDOZE	at depth
PS111_50-1	2018-02-12	07:00	-74.88362	-60.32562	660	CTDOZE	station end
PS111_51-1	2018-02-12	10:22	-75.14776	-59.07870	628	CTDOZE	station start
PS111_51-1	2018-02-12	10:39	-75.14846	-59.07877	628	CTDOZE	at depth
PS111_51-1	2018-02-12	10:57	-75.14836	-59.07912	628	CTDOZE	station end
PS111_52-1	2018-02-12	14:00	-75.37883	-57.74945	557	CTDOZE	station start
PS111_52-1	2018-02-12	14:16	-75.37887	-57.74359	555	CTDOZE	at depth
PS111_52-1	2018-02-12	14:35	-75.37905	-57.73720	556	CTDOZE	station end
PS111_52-2	2018-02-12	14:44	-75.37911	-57.73443	556	BONGO	station start
PS111_52-2	2018-02-12	15:03	-75.37972	-57.72852	553	BONGO	at depth
PS111_52-2	2018-02-12	15:23	-75.37996	-57.72241	554	BONGO	station end
PS111_52-3	2018-02-12	15:24	-75.37994	-57.72180	554	BONGO	station start
PS111_52-3	2018-02-12	15:44	-75.38031	-57.71352	553	BONGO	at depth
PS111_52-3	2018-02-12	16:04	-75.38138	-57.70518	552	BONGO	station end
PS111_53-1	2018-02-12	23:11	-76.02610	-54.11941	496	CTDOZE	station start
PS111_53-1	2018-02-12	23:26	-76.02589	-54.12064	497	CTDOZE	at depth
PS111_53-1	2018-02-12	23:42	-76.02580	-54.12045	497	CTDOZE	station end
PS111_53-2	2018-02-12	23:58	-76.02580	-54.12019	497	GC	station start
PS111_53-2	2018-02-13	00:05	-76.02589	-54.12074	497	GC	at depth
PS111_53-2	2018-02-13	00:18	-76.02581	-54.12081	497	GC	station end
PS111_53-3	2018-02-13	00:37	-76.02591	-54.12059	497	MUC	station start
PS111_53-3	2018-02-13	00:45	-76.02590	-54.12093	497	MUC	at depth
PS111_53-3	2018-02-13	00:58	-76.02557	-54.12011	480	MUC	station end
PS111_55-1	2018-02-13	08:30	-76.90684	-50.89897	287	CTDOZE	station start
PS111_55-1	2018-02-13	08:42	-76.90813	-50.89860	289	CTDOZE	at depth

Station	Date	Time	Latitude	Longitude	Depth [m]	Gear	Action
PS111_55-1	2018-02-13	08:53	-76.90992	-50.89993	290	CTDOZE	station end
PS111_56-1	2018-02-13	10:50	-76.97876	-49.58629	230	CTDOZE	station start
PS111_56-1	2018-02-13	10:59	-76.97883	-49.58535	230	CTDOZE	at depth
PS111_56-1	2018-02-13	11:08	-76.97868	-49.58632	230	CTDOZE	station end
PS111_57-1	2018-02-13	13:05	-77.02735	-50.49829	292	ROV	station start
PS111_57-1	2018-02-13	15:17	-77.02461	-50.48996	289	ROV	station end
PS111_57-2	2018-02-13	15:45	-77.02476	-50.49005	289	BOAT	station start
PS111_57-2	2018-02-13	16:14	-77.02347	-50.50072	287	BOAT	station end
PS111_57-3	2018-02-13	17:17	-77.02419	-50.50470	288	CTDOZE	station start
PS111_57-3	2018-02-13	17:29	-77.02416	-50.50542	288	CTDOZE	at depth
PS111_57-3	2018-02-13	17:39	-77.02440	-50.50549	288	CTDOZE	station end
PS111_58-1	2018-02-13	21:32	-77.14070	-48.40191	251	CTDOZE	station start
PS111_58-1	2018-02-13	21:41	-77.14077	-48.40175	251	CTDOZE	at depth
PS111_58-1	2018-02-13	21:52	-77.14075	-48.40190	251	CTDOZE	station end
PS111_59-1	2018-02-14	00:27	-77.12510	-46.87206	259	CTDOZE	station start
PS111_59-1	2018-02-14	00:37	-77.12478	-46.87033	268	CTDOZE	at depth
PS111_59-1	2018-02-14	00:51	-77.12481	-46.86728	268	CTDOZE	station end
PS111_59-2	2018-02-14	00:59	-77.12483	-46.86907	268	BONGO	station start
PS111_59-2	2018-02-14	01:09	-77.12472	-46.86947	268	BONGO	at depth
PS111_59-2	2018-02-14	01:20	-77.12472	-46.86906	268	BONGO	station end
PS111_59-3	2018-02-14	01:22	-77.12477	-46.86956	268	BONGO	station start
PS111_59-3	2018-02-14	01:32	-77.12491	-46.86968	268	BONGO	at depth
PS111_59-3	2018-02-14	01:45	-77.12490	-46.86906	258	BONGO	station end
PS111_60-1	2018-02-14	04:18	-77.02120	-45.39529	321	CTDOZE	station start
PS111_60-1	2018-02-14	04:30	-77.02003	-45.39700	NA	CTDOZE	at depth
PS111_60-1	2018-02-14	04:43	-77.01908	-45.40007	NA	CTDOZE	station end
PS111_60-2	2018-02-14	04:44	-77.01901	-45.40030	NA	MUC	station start
PS111_60-2	2018-02-14	05:04	-77.01722	-45.40425	332	MUC	at depth
PS111_60-2	2018-02-14	05:16	-77.01664	-45.40696	333	MUC	station end
PS111_60-3	2018-02-14	05:18	-77.01649	-45.40770	332	MUC	station start
PS111_60-3	2018-02-14	05:24	-77.01612	-45.40935	332	MUC	at depth
PS111_60-3	2018-02-14	05:34	-77.01547	-45.41064	331	MUC	station end
PS111_61-1	2018-02-14	07:31	-76.87541	-44.39556	358	CTDOZE	station start
PS111_61-1	2018-02-14	07:43	-76.87641	-44.39697	357	CTDOZE	at depth
PS111_61-1	2018-02-14	07:54	-76.87696	-44.39911	358	CTDOZE	station end
PS111_62-1	2018-02-14	13:53	-77.06854	-45.64968	312	CTDOZE	station start
PS111_62-1	2018-02-14	14:03	-77.06851	-45.64998	312	CTDOZE	at depth
PS111_62-1	2018-02-14	14:15	-77.06851	-45.64998	312	CTDOZE	station end

Station	Date	Time	Latitude	Longitude	Depth [m]	Gear	Action
PS111_63-1	2018-02-15	13:05	-75.34293	-41.10910	367	CTDOZE	station start
PS111_63-1	2018-02-15	13:16	-75.34278	-41.10659	369	CTDOZE	at depth
PS111_63-1	2018-02-15	13:31	-75.34309	-41.10285	368	CTDOZE	station end
PS111_63-2	2018-02-15	14:30	-75.35826	-41.10923	370	ROV	station start
PS111_63-2	2018-02-15	17:46	-75.35902	-41.10545	371	ROV	station end
PS111_63-3	2018-02-15	18:13	-75.35962	-41.09157	371	LIDAR	station start
PS111_63-3	2018-02-15	20:46	-75.35016	-40.91849	359	LIDAR	station end
PS111_64-1	2018-02-15	23:07	-75.54853	-40.42909	367	MT	station start
PS111_64-1	2018-02-15	23:38	-75.54576	-40.52908	364	MT	station end
PS111_64-2	2018-02-16	01:12	-75.61999	-39.73721	370	CTDOZE	station start
PS111_64-2	2018-02-16	01:23	-75.62002	-39.72835	NA	CTDOZE	at depth
PS111_64-2	2018-02-16	01:40	-75.62018	-39.71032	384	CTDOZE	station end
PS111_64-3	2018-02-16	02:04	-75.62463	-39.72948	384	BONGO	at depth
PS111_64-3	2018-02-16	02:20	-75.62468	-39.73008	384	BONGO	station end
PS111_64-4	2018-02-16	02:21	-75.62465	-39.73025	384	BONGO	station start
PS111_64-4	2018-02-16	02:36	-75.62464	-39.72894	384	BONGO	at depth
PS111_64-4	2018-02-16	02:54	-75.62462	-39.72859	370	BONGO	station end
PS111_65-1	2018-02-16	05:07	-75.73299	-38.58078	NA	CTDOZE	station start
PS111_65-1	2018-02-16	05:21	-75.73123	-38.57870	NA	CTDOZE	at depth
PS111_65-1	2018-02-16	05:35	-75.72889	-38.57744	NA	CTDOZE	station end
PS111_66-1	2018-02-16	09:37	-75.97776	-37.75988	NA	CTDOZE	station start
PS111_66-1	2018-02-16	09:53	-75.97721	-37.76283	516	CTDOZE	at depth
PS111_66-1	2018-02-16	10:09	-75.97638	-37.76621	517	CTDOZE	station end
PS111_67-1	2018-02-16	13:04	-76.09462	-36.63706	NA	CTDOZE	station start
PS111_67-1	2018-02-16	13:21	-76.09315	-36.63408	680	CTDOZE	at depth
PS111_67-1	2018-02-16	13:44	-76.09232	-36.63803	678	CTDOZE	station end
PS111_68-1	2018-02-16	16:08	-76.05607	-35.71653	NA	CTDOZE	station start
PS111_68-1	2018-02-16	16:26	-76.05524	-35.71255	747	CTDOZE	at depth
PS111_68-1	2018-02-16	16:51	-76.05423	-35.70877	746	CTDOZE	station end
PS111_68-2	2018-02-16	16:56	-76.05414	-35.70850	747	BONGO	station start
PS111_68-2	2018-02-16	17:15	-76.05399	-35.70841	747	BONGO	at depth
PS111_68-2	2018-02-16	17:35	-76.05337	-35.70650	747	BONGO	station end
PS111_68-3	2018-02-16	17:36	-76.05331	-35.70623	747	BONGO	station start
PS111_68-3	2018-02-16	17:56	-76.05259	-35.70198	747	BONGO	at depth
PS111_68-3	2018-02-16	18:17	-76.05149	-35.69719	747	BONGO	station end
PS111_69-1	2018-02-16	20:31	-76.10470	-34.65992	NA	CTDOZE	station start
PS111_69-1	2018-02-16	20:52	-76.10496	-34.65437	766	CTDOZE	at depth
PS111_69-1	2018-02-16	21:12	-76.10586	-34.64780	766	CTDOZE	station end

Station	Date	Time	Latitude	Longitude	Depth [m]	Gear	Action
PS111_70-1	2018-02-17	00:35	-76.12552	-33.66908	789	CTDOZE	station start
PS111_70-1	2018-02-17	00:55	-76.12374	-33.66586	790	CTDOZE	at depth
PS111_70-1	2018-02-17	01:21	-76.11813	-33.65913	798	CTDOZE	station end
PS111_70-2	2018-02-17	01:35	-76.11451	-33.65898	796	MUC	station start
PS111_70-2	2018-02-17	01:48	-76.11253	-33.65489	794	MUC	at depth
PS111_70-2	2018-02-17	02:04	-76.10987	-33.65069	794	MUC	station end
PS111_70-3	2018-02-17	02:17	-76.10615	-33.64223	794	GC	station start
PS111_70-3	2018-02-17	02:28	-76.10500	-33.64049	794	GC	at depth
PS111_70-3	2018-02-17	02:42	-76.10305	-33.63927	767	GC	station end
PS111_71-1	2018-02-17	04:35	-76.14975	-32.66626	NA	CTDOZE	station start
PS111_71-1	2018-02-17	04:54	-76.14912	-32.66855	797	CTDOZE	at depth
PS111_71-1	2018-02-17	05:20	-76.14486	-32.67112	797	CTDOZE	station end
PS111_71-2	2018-02-17	05:27	-76.14360	-32.67258	799	BONGO	station start
PS111_71-2	2018-02-17	05:48	-76.14160	-32.67428	801	BONGO	at depth
PS111_71-2	2018-02-17	06:07	-76.14079	-32.67383	801	BONGO	station end
PS111_71-3	2018-02-17	06:10	-76.14054	-32.67469	801	BONGO	station start
PS111_71-3	2018-02-17	06:31	-76.13867	-32.67810	801	BONGO	at depth
PS111_71-3	2018-02-17	06:52	-76.13846	-32.68632	797	BONGO	station end
PS111_72-1	2018-02-17	08:43	-76.17417	-31.66713	536	CTDOZE	station start
PS111_72-1	2018-02-17	08:58	-76.17151	-31.66312	540	CTDOZE	at depth
PS111_72-1	2018-02-17	09:15	-76.17078	-31.66308	541	CTDOZE	station end
PS111_73-1	2018-02-17	11:10	-76.19541	-30.67221	450	CTDOZE	station start
PS111_73-1	2018-02-17	11:24	-76.19497	-30.67396	447	CTDOZE	at depth
PS111_73-1	2018-02-17	11:38	-76.19457	-30.67541	448	CTDOZE	station end
PS111_74-1	2018-02-17	13:17	-76.21383	-29.67477	371	CTDOZE	station start
PS111_74-1	2018-02-17	13:29	-76.21357	-29.67593	387	CTDOZE	at depth
PS111_74-1	2018-02-17	13:46	-76.21374	-29.67478	383	CTDOZE	station end
PS111_74-2	2018-02-17	14:10	-76.21259	-29.68066	384	BONGO	station start
PS111_74-2	2018-02-17	14:23	-76.21326	-29.67936	382	BONGO	at depth
PS111_74-2	2018-02-17	14:38	-76.21319	-29.67741	383	BONGO	station end
PS111_74-3	2018-02-17	14:40	-76.21322	-29.67714	383	BONGO	station start
PS111_74-3	2018-02-17	14:55	-76.21389	-29.67613	380	BONGO	at depth
PS111_74-3	2018-02-17	15:11	-76.21382	-29.67525	381	BONGO	station end
PS111_74-4	2018-02-17	15:22	-76.21376	-29.67558	381	MUC	station start
PS111_74-4	2018-02-17	15:29	-76.21362	-29.67577	381	MUC	at depth
PS111_74-4	2018-02-17	15:41	-76.21314	-29.67609	369	MUC	station end
PS111_74-5	2018-02-17	15:55	-76.21789	-29.69324	356	MT	station start
PS111_74-5	2018-02-17	15:57	-76.21880	-29.69658	360	MT	at depth

Station	Date	Time	Latitude	Longitude	Depth [m]	Gear	Action
PS111_74-5	2018-02-17	16:23	-76.23730	-29.72008	320	MT	station end
PS111_75-1	2018-02-17	20:32	-76.78238	-31.15991	463	CTDOZE	station start
PS111_75-1	2018-02-17	20:47	-76.78296	-31.16164	460	CTDOZE	at depth
PS111_75-1	2018-02-17	21:00	-76.78313	-31.16169	460	CTDOZE	station end
PS111_76-1	2018-02-17	22:49	-76.77578	-32.09777	246	CTDOZE	station start
PS111_76-1	2018-02-17	23:00	-76.77621	-32.09964	248	CTDOZE	at depth
PS111_76-1	2018-02-17	23:11	-76.77632	-32.10093	247	CTDOZE	station end
PS111_77-1	2018-02-18	01:11	-76.83464	-33.03920	426	CTDOZE	station start
PS111_77-1	2018-02-18	01:23	-76.83481	-33.03712	439	CTDOZE	at depth
PS111_77-1	2018-02-18	01:35	-76.83450	-33.03796	457	CTDOZE	station end
PS111_78-1	2018-02-18	03:08	-76.79983	-33.95908	742	CTDOZE	station start
PS111_78-1	2018-02-18	03:26	-76.79991	-33.95209	740	CTDOZE	at depth
PS111_78-1	2018-02-18	03:46	-76.79995	-33.94796	738	CTDOZE	station end
PS111_79-1	2018-02-18	05:19	-76.77903	-34.89206	970	CTDOZE	station start
PS111_79-1	2018-02-18	05:43	-76.77832	-34.89212	971	CTDOZE	at depth
PS111_79-1	2018-02-18	06:06	-76.77876	-34.89111	970	CTDOZE	station end
PS111_80-1	2018-02-18	07:48	-76.64589	-35.43304	932	CTDOZE	station start
PS111_80-1	2018-02-18	08:11	-76.64509	-35.43080	932	CTDOZE	at depth
PS111_80-1	2018-02-18	08:41	-76.64379	-35.42883	934	CTDOZE	station end
PS111_80-2	2018-02-18	08:51	-76.64335	-35.42840	934	GC	station start
PS111_80-2	2018-02-18	09:04	-76.64288	-35.42813	933	GC	at depth
PS111_80-2	2018-02-18	09:23	-76.64236	-35.42855	933	GC	station end
PS111_80-3	2018-02-18	09:31	-76.64214	-35.42893	933	MUC	station start
PS111_80-3	2018-02-18	09:47	-76.64158	-35.42991	932	MUC	at depth
PS111_80-3	2018-02-18	10:06	-76.64089	-35.43183	932	MUC	station end
PS111_81-1	2018-02-18	13:07	-76.79140	-34.32496	885	CTDOZE	station start
PS111_81-1	2018-02-18	13:27	-76.79251	-34.32464	879	CTDOZE	at depth
PS111_81-1	2018-02-18	13:46	-76.79318	-34.32538	934	CTDOZE	station end
PS111_82-1	2018-02-18	15:31	-76.78280	-33.38715	557	CTDOZE	station start
PS111_82-1	2018-02-18	15:46	-76.78203	-33.38414	556	CTDOZE	at depth
PS111_82-1	2018-02-18	16:05	-76.78182	-33.38176	556	CTDOZE	station end
PS111_83-1	2018-02-18	20:06	-77.14101	-34.92871	NA	CTDOZE	at depth
PS111_83-1	2018-02-18	20:27	-77.14036	-34.92979	NA	CTDOZE	station end
PS111_83-2	2018-02-18	20:35	-77.13940	-34.92548	NA	BONGO	station start
PS111_83-2	2018-02-18	20:55	-77.13860	-34.92399	NA	BONGO	at depth
PS111_83-3	2018-02-18	21:16	-77.13833	-34.92424	NA	BONGO	station start
PS111_83-3	2018-02-18	21:37	-77.13777	-34.92091	NA	BONGO	at depth
PS111_83-3	2018-02-18	21:58	-77.13761	-34.91962	711	BONGO	station end

Station	Date	Time	Latitude	Longitude	Depth [m]	Gear	Action
PS111_84-1	2018-02-18	22:59	-77.21254	-34.73198	551	CTDOZE	station start
PS111_84-1	2018-02-18	23:15	-77.21289	-34.73173	550	CTDOZE	at depth
PS111_84-1	2018-02-18	23:28	-77.21312	-34.73298	549	CTDOZE	station end
PS111_85-1	2018-02-19	00:28	-77.30840	-34.52113	453	CTDOZE	station start
PS111_85-1	2018-02-19	00:42	-77.30831	-34.51919	453	CTDOZE	at depth
PS111_85-1	2018-02-19	00:53	-77.30834	-34.51809	452	CTDOZE	station end
PS111_85-2	2018-02-19	01:05	-77.31181	-34.53925	441	MT	station start
PS111_85-2	2018-02-19	01:07	-77.31259	-34.54286	439	MT	at depth
PS111_85-2	2018-02-19	01:20	-77.32013	-34.57631	432	MT	station end
PS111_86-1	2018-02-19	02:19	-77.41710	-34.33137	162	CTDOZE	station start
PS111_86-1	2018-02-19	02:26	-77.41715	-34.33157	167	CTDOZE	at depth
PS111_86-1	2018-02-19	02:36	-77.41694	-34.33172	167	CTDOZE	station end
PS111_86-2	2018-02-19	02:48	-77.41701	-34.33214	167	MUC	station start
PS111_86-2	2018-02-19	03:06	-77.41677	-34.33333	169	MUC	at depth
PS111_86-2	2018-02-19	03:16	-77.41662	-34.33394	171	MUC	station end
PS111_87-1	2018-02-19	07:08	-77.74948	-35.51355	NA	CTDOZE	station start
PS111_87-1	2018-02-19	07:23	-77.74956	-35.51065	NA	CTDOZE	at depth
PS111_87-1	2018-02-19	07:35	-77.74932	-35.50867	NA	CTDOZE	station end
PS111_88-1	2018-02-19	08:37	-77.79497	-36.01366	NA	CTDOZE	station start
PS111_88-1	2018-02-19	08:38	-77.79498	-36.01366	NA	CTDOZE	at depth
PS111_88-1	2018-02-19	09:10	-77.79569	-36.00896	NA	CTDOZE	station end
PS111_89-1	2018-02-19	10:21	-77.82068	-36.42269	808	CTDOZE	station start
PS111_89-1	2018-02-19	10:41	-77.82084	-36.42211	808	CTDOZE	at depth
PS111_89-1	2018-02-19	11:03	-77.82103	-36.42109	807	CTDOZE	station end
PS111_90-1	2018-02-19	11:51	-77.84436	-36.77899	1103	CTDOZE	station start
PS111_90-1	2018-02-19	12:18	-77.84479	-36.77914	1120	CTDOZE	at depth
PS111_90-1	2018-02-19	12:45	-77.84487	-36.77969	1117	CTDOZE	station end
PS111_91-1	2018-02-19	13:33	-77.86438	-37.21192	1122	CTDOZE	station start
PS111_91-1	2018-02-19	13:57	-77.86424	-37.21199	1121	CTDOZE	at depth
PS111_91-1	2018-02-19	14:24	-77.86417	-37.21281	1120	CTDOZE	station end
PS111_92-1	2018-02-19	15:14	-77.89828	-37.58935	1156	BONGO	station start
PS111_92-1	2018-02-19	15:33	-77.89809	-37.58904	1156	BONGO	at depth
PS111_92-1	2018-02-19	15:52	-77.89809	-37.58927	1155	BONGO	station end
PS111_92-2	2018-02-19	15:54	-77.89813	-37.58922	1155	BONGO	station start
PS111_92-2	2018-02-19	16:14	-77.89808	-37.58903	1155	BONGO	at depth
PS111_92-2	2018-02-19	16:34	-77.89809	-37.58958	1156	BONGO	station end
PS111_92-3	2018-02-19	16:45	-77.89803	-37.58960	1155	CTDOZE	station start
PS111_92-3	2018-02-19	17:12	-77.89802	-37.58648	1155	CTDOZE	at depth

Station	Date	Time	Latitude	Longitude	Depth [m]	Gear	Action
PS111_92-3	2018-02-19	17:44	-77.89718	-37.59618	1156	CTDOZE	station end
PS111_93-1	2018-02-19	19:02	-77.82760	-38.33749	1198	CTDOZE	station start
PS111_93-1	2018-02-19	19:29	-77.82764	-38.33678	1198	CTDOZE	at depth
PS111_93-1	2018-02-19	19:58	-77.82807	-38.33276	1198	CTDOZE	station end
PS111_94-1	2018-02-19	21:19	-77.79439	-39.16363	1122	CTDOZE	station start
PS111_94-1	2018-02-19	21:45	-77.79443	-39.16194	1123	CTDOZE	at depth
PS111_94-1	2018-02-19	22:13	-77.79436	-39.15731	1122	CTDOZE	station end
PS111_95-1	2018-02-19	23:40	-77.79490	-40.00614	966	CTDOZE	station start
PS111_95-1	2018-02-20	00:04	-77.79491	-40.00636	966	CTDOZE	at depth
PS111_95-1	2018-02-20	00:26	-77.79494	-40.00408	968	CTDOZE	station end
PS111_96-1	2018-02-20	01:42	-77.79103	-40.84253	856	CTDOZE	station start
PS111_96-1	2018-02-20	02:03	-77.79062	-40.84508	888	CTDOZE	at depth
PS111_96-1	2018-02-20	02:26	-77.79032	-40.84819	887	CTDOZE	station end
PS111_97-1	2018-02-20	03:14	-77.79135	-41.24796	843	CTDOZE	station start
PS111_97-1	2018-02-20	03:33	-77.79191	-41.25442	842	CTDOZE	at depth
PS111_97-1	2018-02-20	03:58	-77.79151	-41.24046	842	CTDOZE	station end
PS111_97-2	2018-02-20	04:05	-77.79145	-41.24085	842	BONGO	station start
PS111_97-2	2018-02-20	04:23	-77.79132	-41.24070	842	BONGO	at depth
PS111_97-2	2018-02-20	04:42	-77.78959	-41.24177	842	BONGO	station end
PS111_97-3	2018-02-20	04:44	-77.78931	-41.24189	842	BONGO	station start
PS111_97-3	2018-02-20	05:03	-77.78618	-41.24388	842	BONGO	at depth
PS111_97-3	2018-02-20	05:25	-77.78994	-41.24584	NA	BONGO	station end
PS111_98-1	2018-02-20	06:58	-77.79474	-40.44226	926	CTDOZE	station start
PS111_98-1	2018-02-20	07:20	-77.78950	-40.46149	926	CTDOZE	at depth
PS111_98-1	2018-02-20	07:47	-77.78880	-40.44928	922	CTDOZE	station end
PS111_98-2	2018-02-20	08:15	-77.80006	-40.43913	928	GC	at depth
PS111_98-2	2018-02-20	08:30	-77.79753	-40.46294	928	GC	station end
PS111_98-3	2018-02-20	08:46	-77.79827	-40.47721	928	TVMUC	station start
PS111_98-3	2018-02-20	09:06	-77.80116	-40.45460	928	TVMUC	at depth
PS111_98-3	2018-02-20	09:27	-77.80344	-40.42717	928	TVMUC	station end
PS111_99-1	2018-02-20	13:08	-77.50706	-42.05420	604	CTDOZE	station start
PS111_99-1	2018-02-20	13:22	-77.50963	-42.04951	604	CTDOZE	at depth
PS111_99-1	2018-02-20	13:37	-77.51171	-42.04658	604	CTDOZE	station end
PS111_100-1	2018-02-20	16:50	-77.20428	-42.90141	473	CTDOZE	at depth
PS111_100-1	2018-02-20	17:04	-77.20372	-42.90387	470	CTDOZE	station end
PS111_101-1	2018-02-20	19:31	-76.92107	-43.80591	397	CTDOZE	station start
PS111_101-1	2018-02-20	19:43	-76.92088	-43.80644	397	CTDOZE	at depth
PS111_101-1	2018-02-20	20:00	-76.92074	-43.80746	397	CTDOZE	station end

Station	Date	Time	Latitude	Longitude	Depth [m]	Gear	Action
PS111_102-1	2018-02-20	21:29	-77.07010	-43.34117	NA	CTDOZE	station start
PS111_102-1	2018-02-20	21:44	-77.07011	-43.34164	NA	CTDOZE	at depth
PS111_102-1	2018-02-20	21:59	-77.07011	-43.34317	446	CTDOZE	station end
PS111_103-1	2018-02-21	00:33	-77.36102	-42.48344	556	CTDOZE	station start
PS111_103-1	2018-02-21	00:52	-77.36068	-42.48448	557	CTDOZE	at depth
PS111_103-1	2018-02-21	01:06	-77.36046	-42.48584	557	CTDOZE	station end
PS111_104-1	2018-02-21	03:37	-77.68501	-41.69760	727	CTDOZE	station start
PS111_104-1	2018-02-21	03:54	-77.68455	-41.69874	726	CTDOZE	at depth
PS111_104-1	2018-02-21	04:09	-77.68403	-41.69943	725	CTDOZE	station end
PS111_105-1	2018-02-21	07:51	-77.79020	-39.58266	1062	CTDOZE	station start
PS111_105-1	2018-02-21	08:16	-77.78980	-39.58082	1062	CTDOZE	at depth
PS111_105-1	2018-02-21	08:41	-77.79010	-39.58085	1062	CTDOZE	station end
PS111_106-1	2018-02-21	10:06	-77.81391	-38.75926	1182	CTDOZE	station start
PS111_106-1	2018-02-21	10:31	-77.81411	-38.75829	1182	CTDOZE	at depth
PS111_106-1	2018-02-21	10:58	-77.81432	-38.75623	1181	CTDOZE	station end
PS111_107-1	2018-02-21	12:16	-77.86777	-37.98423	1199	CTDOZE	station start
PS111_107-1	2018-02-21	12:44	-77.86786	-37.98358	1198	CTDOZE	at depth
PS111_107-1	2018-02-21	13:10	-77.86854	-37.98486	1199	CTDOZE	station end
PS111_108-1	2018-02-21	15:31	-77.82599	-36.72743	997	AUV	station start
PS111_108-1	2018-02-21	21:41	-77.81938	-36.70071	NA	AUV	station end
PS111_109-1	2018-02-22	01:02	-77.71033	-35.23472	461	CTDOZE	station start
PS111_109-1	2018-02-22	01:14	-77.71071	-35.23547	461	CTDOZE	at depth
PS111_109-1	2018-02-22	01:27	-77.71089	-35.23604	461	CTDOZE	station end
PS111_109-2	2018-02-22	01:47	-77.71055	-35.25875	461	GC	station start
PS111_109-2	2018-02-22	01:53	-77.71053	-35.25869	461	GC	at depth
PS111_109-2	2018-02-22	02:03	-77.71096	-35.26002	461	GC	station end
PS111_110-1	2018-02-22	06:42	-77.11301	-33.93708	392	CTDOZE	station start
PS111_110-1	2018-02-22	06:55	-77.11316	-33.93696	NA	CTDOZE	at depth
PS111_110-1	2018-02-22	07:10	-77.11230	-33.93214	NA	CTDOZE	station end
PS111_110-2	2018-02-22	07:19	-77.11187	-33.93561	404	GC	station start
PS111_110-2	2018-02-22	07:25	-77.11193	-33.93686	404	GC	at depth
PS111_110-2	2018-02-22	07:32	-77.11174	-33.93663	404	GC	station end
PS111_110-3	2018-02-22	07:38	-77.11177	-33.93643	404	LAND	station start
PS111_111-1	2018-02-22	08:44	-77.00941	-33.94948	453	CTDOZE	at depth
PS111_111-1	2018-02-22	08:58	-77.00985	-33.94364	452	CTDOZE	station end
PS111_111-2	2018-02-22	09:08	-77.00993	-33.94158	453	GC	station start
PS111_111-2	2018-02-22	09:14	-77.00998	-33.94103	453	GC	at depth
PS111_111-2	2018-02-22	09:24	-77.00995	-33.94076	453	GC	station end

Station	Date	Time	Latitude	Longitude	Depth [m]	Gear	Action
PS111_111-3	2018-02-22	09:45	-77.00994	-33.94080	453	MUC	at depth
PS111_111-3	2018-02-22	10:14	-77.01004	-33.94407	453	MUC	station end
PS111_112-1	2018-02-22	13:49	-76.58800	-32.50099	478	CTDOZE	station start
PS111_112-1	2018-02-22	14:02	-76.58804	-32.50056	478	CTDOZE	at depth
PS111_112-1	2018-02-22	14:12	-76.58812	-32.50015	478	CTDOZE	station end
PS111_113-1	2018-02-22	15:19	-76.52050	-33.05056	717	CTDOZE	station start
PS111_113-1	2018-02-22	15:36	-76.51827	-33.04330	716	CTDOZE	at depth
PS111_113-1	2018-02-22	15:53	-76.51601	-33.03554	718	CTDOZE	station end
PS111_114-1	2018-02-22	18:12	-76.38743	-33.97264	839	CTDOZE	at depth
PS111_114-1	2018-02-22	18:37	-76.38435	-33.95853	839	CTDOZE	station end
PS111_114-2	2018-02-22	18:43	-76.38369	-33.95643	840	GC	station start
PS111_114-2	2018-02-22	18:54	-76.38258	-33.95497	840	GC	at depth
PS111_114-2	2018-02-22	19:08	-76.38064	-33.94551	839	GC	station end
PS111_114-3	2018-02-22	19:23	-76.37905	-33.94202	839	TVMUC	station start
PS111_114-3	2018-02-22	19:46	-76.37691	-33.93392	839	TVMUC	at depth
PS111_114-3	2018-02-22	20:04	-76.37415	-33.92493	839	TVMUC	station end
PS111_115-1	2018-02-22	23:18	-76.28504	-32.31144	NA	CTDOZE	station start
PS111_115-1	2018-02-22	23:37	-76.28393	-32.30996	NA	CTDOZE	at depth
PS111_115-1	2018-02-22	23:58	-76.28368	-32.31118	725	CTDOZE	station end
PS111_115-2	2018-02-23	00:07	-76.28337	-32.31231	723	BONGO	station start
PS111_115-2	2018-02-23	00:27	-76.28288	-32.31330	723	BONGO	at depth
PS111_115-2	2018-02-23	00:46	-76.28216	-32.31322	725	BONGO	station end
PS111_115-3	2018-02-23	00:50	-76.28221	-32.31368	725	BONGO	station start
PS111_115-3	2018-02-23	01:10	-76.28173	-32.31045	727	BONGO	at depth
PS111_115-3	2018-02-23	01:33	-76.28219	-32.31010	725	BONGO	station end
PS111_116-1	2018-02-23	03:20	-76.19861	-31.16708	474	CTDOZE	station start
PS111_116-1	2018-02-23	03:33	-76.19855	-31.16653	474	CTDOZE	at depth
PS111_116-1	2018-02-23	03:45	-76.19872	-31.16568	473	CTDOZE	station end
PS111_117-1	2018-02-23	14:30	-77.58449	-34.54288	158	ROV	station start
PS111_117-1	2018-02-23	16:36	-77.58308	-34.54960	162	ROV	station end
PS111_117-2	2018-02-23	16:54	-77.58290	-34.54924	162	CTDOZE	station start
PS111_117-2	2018-02-23	17:02	-77.58283	-34.54957	161	CTDOZE	at depth
PS111_117-2	2018-02-23	17:09	-77.58268	-34.55000	161	CTDOZE	station end
PS111_118-1	2018-02-23	21:01	-77.82162	-36.70702	1014	AUV	station start
PS111_118-1	2018-02-23	22:14	-77.82178	-36.70707	1018	AUV	station end
PS111_118-1	2018-02-23	23:18	-77.82831	-36.70951	969	AUV	station start
PS111_118-1	2018-02-24	00:56	-77.82818	-36.70964	970	AUV	station end
PS111_119-1	2018-02-24	21:55	-75.78180	-30.74877	NA	CTDOZE	station start

Station	Date	Time	Latitude	Longitude	Depth [m]	Gear	Action
PS111_119-1	2018-02-24	22:10	-75.78131	-30.74736	464	CTDOZE	at depth
PS111_119-1	2018-02-24	22:24	-75.78078	-30.74630	464	CTDOZE	station end
PS111_120-1	2018-02-25	00:10	-75.64011	-31.23320	623	CTDOZE	station start
PS111_120-1	2018-02-25	00:29	-75.63927	-31.23821	626	CTDOZE	at depth
PS111_120-1	2018-02-25	00:48	-75.63836	-31.24355	629	CTDOZE	station end
PS111_121-1	2018-02-25	02:43	-75.49912	-31.89535	760	CTDOZE	station start
PS111_121-1	2018-02-25	03:01	-75.49896	-31.90044	757	CTDOZE	at depth
PS111_121-1	2018-02-25	03:20	-75.49855	-31.90555	759	CTDOZE	station end
PS111_121-2	2018-02-25	03:37	-75.49792	-31.90768	758	GC	station start
PS111_121-2	2018-02-25	03:47	-75.49766	-31.90998	758	GC	at depth
PS111_121-2	2018-02-25	03:59	-75.49723	-31.91277	757	GC	station end
PS111_122-1	2018-02-25	09:08	-74.98792	-30.26244	NA	CTDOZE	station start
PS111_122-1	2018-02-25	09:22	-74.98752	-30.26007	NA	CTDOZE	at depth
PS111_122-1	2018-02-25	09:37	-74.98673	-30.25788	NA	CTDOZE	station end
PS111_122-2	2018-02-25	09:45	-74.98593	-30.25676	NA	BONGO	station start
PS111_122-2	2018-02-25	10:01	-74.98544	-30.25534	NA	BONGO	at depth
PS111_122-2	2018-02-25	10:19	-74.98453	-30.25403	NA	BONGO	station end
PS111_122-3	2018-02-25	10:21	-74.98443	-30.25384	NA	BONGO	station start
PS111_122-3	2018-02-25	10:36	-74.98356	-30.25283	NA	BONGO	at depth
PS111_122-3	2018-02-25	10:53	-74.98256	-30.25228	NA	BONGO	station end
PS111_123-1	2018-02-25	13:16	-74.94564	-30.98465	568	CTDOZE	station start
PS111_123-1	2018-02-25	13:32	-74.94483	-30.98604	566	CTDOZE	at depth
PS111_123-1	2018-02-25	13:53	-74.94410	-30.98647	566	CTDOZE	station end
PS111_124-1	2018-02-25	15:58	-74.80595	-31.52382	604	CTDOZE	station start
PS111_124-1	2018-02-25	16:13	-74.80578	-31.52312	604	CTDOZE	at depth
PS111_124-1	2018-02-25	16:31	-74.80517	-31.52148	605	CTDOZE	station end
PS111_125-1	2018-02-25	18:32	-74.79860	-32.26534	NA	CTDOZE	station start
PS111_125-1	2018-02-25	18:50	-74.79773	-32.26153	NA	CTDOZE	at depth
PS111_125-1	2018-02-25	19:05	-74.79856	-32.26415	NA	CTDOZE	station end
PS111_126-1	2018-02-25	20:48	-74.73888	-32.76956	597	CTDOZE	station start
PS111_126-1	2018-02-25	21:05	-74.73807	-32.76560	595	CTDOZE	at depth
PS111_126-1	2018-02-25	21:24	-74.73701	-32.76302	598	CTDOZE	station end
PS111_127-1	2018-02-26	01:42	-74.76033	-33.53273	589	CTDOZE	station start
PS111_127-1	2018-02-26	01:58	-74.75885	-33.53264	591	CTDOZE	at depth
PS111_127-1	2018-02-26	02:16	-74.75742	-33.53206	591	CTDOZE	station end
PS111_128-1	2018-02-26	03:54	-74.64523	-34.33335	555	CTDOZE	station start
PS111_128-1	2018-02-26	04:08	-74.64460	-34.33340	553	CTDOZE	at depth
PS111_128-1	2018-02-26	04:24	-74.64331	-34.33271	552	CTDOZE	station end

Station	Date	Time	Latitude	Longitude	Depth [m]	Gear	Action
PS111_129-1	2018-02-26	06:06	-74.66638	-35.06905	506	CTDOZE	station start
PS111_129-1	2018-02-26	06:21	-74.66526	-35.06945	506	CTDOZE	at depth
PS111_129-1	2018-02-26	06:35	-74.66433	-35.06981	506	CTDOZE	station end
PS111_130-1	2018-02-26	09:40	-74.64977	-35.87454	439	CTDOZE	station start
PS111_130-1	2018-02-26	09:53	-74.64806	-35.87638	439	CTDOZE	at depth
PS111_130-1	2018-02-26	10:08	-74.64614	-35.87866	438	CTDOZE	station end
PS111_131-1	2018-02-26	12:30	-74.61844	-36.92004	386	CTDOZE	station start
PS111_131-1	2018-02-26	12:43	-74.61736	-36.92288	387	CTDOZE	at depth
PS111_131-1	2018-02-26	12:59	-74.61529	-36.92651	386	CTDOZE	station end
PS111_131-2	2018-02-26	13:14	-74.61293	-36.93181	387	MUC	station start
PS111_131-2	2018-02-26	13:30	-74.61110	-36.93695	387	MUC	at depth
PS111_131-2	2018-02-26	13:40	-74.61015	-36.94050	387	MUC	station end
PS111_132-1	2018-02-27	11:25	-74.01111	-32.43337	1790	CTDOZE	station start
PS111_132-1	2018-02-27	12:03	-74.00882	-32.42354	1800	CTDOZE	at depth
PS111_132-1	2018-02-27	12:52	-74.00683	-32.40987	1807	CTDOZE	station end
PS111_132-2	2018-02-27	13:07	-74.00610	-32.40588	1810	MN_S5	station start
PS111_132-2	2018-02-27	14:02	-74.00338	-32.39055	1815	MN_S5	at depth
PS111_132-2	2018-02-27	14:56	-74.00135	-32.37960	1817	MN_S5	station end
PS111_132-3	2018-02-27	15:10	-74.00078	-32.37821	1820	MOOR	station start
PS111_133-1	2018-02-28	03:59	-75.02070	-29.46064	408	CTDOZE	at depth
PS111_133-1	2018-02-28	04:12	-75.01951	-29.45706	407	CTDOZE	station end
PS111_134-1	2018-02-28	05:35	-75.07959	-28.88033	401	CTDOZE	station start
PS111_134-1	2018-02-28	05:47	-75.08086	-28.88499	405	CTDOZE	at depth
PS111_134-1	2018-02-28	05:58	-75.08168	-28.89335	404	CTDOZE	station end
PS111_135-1	2018-02-28	07:16	-75.10843	-28.27761	467	CTDOZE	station start
PS111_135-1	2018-02-28	07:32	-75.10763	-28.28008	NA	CTDOZE	at depth
PS111_135-1	2018-02-28	07:45	-75.10687	-28.28680	NA	CTDOZE	station end
PS111_136-1	2018-02-28	09:17	-75.14567	-27.54634	389	CTDOZE	station start
PS111_136-1	2018-02-28	09:30	-75.14554	-27.54515	NA	CTDOZE	at depth
PS111_136-1	2018-02-28	09:44	-75.14461	-27.54797	NA	CTDOZE	station end
PS111_136-2	2018-02-28	09:50	-75.14477	-27.55049	NA	BONGO	station start
PS111_136-2	2018-02-28	10:05	-75.14502	-27.55030	413	BONGO	at depth
PS111_136-2	2018-02-28	10:20	-75.14486	-27.55237	410	BONGO	station end
PS111_136-3	2018-02-28	10:22	-75.14473	-27.55318	410	BONGO	station start
PS111_136-3	2018-02-28	10:23	-75.14473	-27.55326	410	BONGO	at depth
PS111_136-3	2018-02-28	11:14	-75.14572	-27.56013	413	BONGO	station end
PS111_137-1	2018-02-28	14:51	-75.47550	-27.09359	254	ROV	station start
PS111_137-1	2018-02-28	17:51	-75.46795	-27.11282	259	ROV	station end

Station	Date	Time	Latitude	Longitude	Depth [m]	Gear	Action
PS111_137-2	2018-02-28	18:14	-75.46855	-27.11416	260	CTDOZE	station start
PS111_137-2	2018-02-28	18:25	-75.46916	-27.11297	260	CTDOZE	at depth
PS111_137-2	2018-02-28	18:37	-75.46999	-27.11199	259	CTDOZE	station end
PS111_138-1	2018-02-28	22:15	-75.13051	-26.03731	389	CTDOZE	station start
PS111_138-1	2018-02-28	22:29	-75.12945	-26.04440	400	CTDOZE	at depth
PS111_138-1	2018-02-28	22:43	-75.12841	-26.04849	398	CTDOZE	station end
PS111_138-2	2018-02-28	23:02	-75.12641	-26.03815	381	MT	station start
PS111_138-2	2018-02-28	23:21	-75.12117	-25.98007	376	MT	station end
PS111_139-1	2018-03-01	02:07	-74.82506	-25.26585	669	GC	station start
PS111_139-1	2018-03-01	02:07	-74.82506	-25.26587	669	GC	at depth
PS111_139-1	2018-03-01	02:29	-74.82447	-25.26820	668	GC	station end
PS111_139-2	2018-03-01	02:43	-74.82508	-25.27164	666	MUC	station start
PS111_139-2	2018-03-01	03:04	-74.82480	-25.27717	663	MUC	at depth
PS111_139-2	2018-03-01	03:19	-74.82491	-25.28168	661	MUC	station end
PS111_140-1	2018-03-01	11:13	-75.13276	-26.63356	341	CTDOZE	station start
PS111_140-1	2018-03-01	11:26	-75.13268	-26.63225	341	CTDOZE	at depth
PS111_140-1	2018-03-01	11:42	-75.13253	-26.62912	342	CTDOZE	station end
PS111_140-2	2018-03-01	11:52	-75.13261	-26.63106	341	GC	station start
PS111_140-2	2018-03-01	11:57	-75.13245	-26.62949	341	GC	at depth
PS111_140-2	2018-03-01	12:06	-75.13255	-26.62791	342	GC	station end
PS111_141-1	2018-03-01	17:22	-75.46429	-26.91778	234	BOAT	station start
PS111_141-1	2018-03-01	17:46	-75.46394	-26.91922	235	BOAT	station end
PS111_141-2	2018-03-01	17:30	-75.46409	-26.91848	234	CTDOZE	station start
PS111_141-2	2018-03-01	17:39	-75.46368	-26.91886	235	CTDOZE	at depth
PS111_141-2	2018-03-01	17:48	-75.46432	-26.91935	234	CTDOZE	station end
PS111_141-3	2018-03-01	18:19	-75.46576	-26.91624	233	ROV	station start
PS111_141-3	2018-03-01	20:51	-75.46501	-26.91683	234	ROV	station end
PS111_142-1	2018-03-01	23:31	-75.21646	-27.45983	376	GC	station start
PS111_142-1	2018-03-01	23:37	-75.21693	-27.45845	373	GC	at depth
PS111_142-1	2018-03-01	23:46	-75.21722	-27.45862	373	GC	station end
PS111_147-1	2018-03-06	17:35	-63.59853	-48.75924	3323	CTDOZE	station start
PS111_147-1	2018-03-06	18:42	-63.58712	-48.74432	3342	CTDOZE	at depth
PS111_147-1	2018-03-06	19:57	-63.56543	-48.73723	3360	CTDOZE	station end
PS111_147-2	2018-03-06	19:28	-63.57520	-48.73746	3354	HN	station start
PS111_147-2	2018-03-06	20:11	-63.56080	-48.73734	3360	HN	station end
PS111_147-3	2018-03-06	22:07	-63.52464	-48.77062	3341	HN	station start
PS111_147-3	2018-03-06	22:23	-63.52057	-48.77777	3334	HN	station end

Gear abbreviations	Gear
ADCP_150	ADCP 150kHz
AUV	Autonomous Underwater Vehicle
BOAT	Boat
BONGO	Bongo Net
CTDOZE	CTD AWI-OZE
FBOX	FerryBox
FLOAT	Float
GC	Gravity Corer
HN	Hand Net
HSPS	Hydrosweep-Parasound
ICEOBS	Ice Observation
LAND	Lander
LIDAR	Doppler-Wind LIDAR
MG	Multigrab / Multibox corer
MN_M7	Multinet Medium 7 Nets
MN_S5	Multinet Small 5 Nets
MOOR	Mooring
MT	Manta Trawl
MUC	Multi Corer
PCO2_GO	pCO2 GO
PCO2_SUB	pCO2 Subctech
ROV	Remotely Operated Vehicle
SVP_B	Surface Velocity Profiler
TSG_KEEL	Thermosalinograph Keel
TSG_KEEL_2	Thermosalinograph Keel 2
TVMUC	Video Multi Corer
UCTD	Underway CTD
WST	Weatherstation

Die **Berichte zur Polar- und Meeresforschung** (ISSN 1866-3192) werden beginnend mit dem Band 569 (2008) als Open-Access-Publikation herausgegeben. Ein Verzeichnis aller Bände einschließlich der Druckausgaben (ISSN 1618-3193, Band 377-568, von 2000 bis 2008) sowie der früheren **Berichte zur Polarforschung** (ISSN 0176-5027, Band 1-376, von 1981 bis 2000) befindet sich im electronic Publication Information Center **(ePIC)** des Alfred-Wegener-Instituts, Helmholtz-Zentrum für Polar- und Meeresforschung (AWI); see http://epic.awi.de. Durch Auswahl “Reports on Polar- and Marine Research“ (via “browse”/”type”) wird eine Liste der Publikationen, sortiert nach Bandnummer, innerhalb der absteigenden chronologischen Reihenfolge der Jahrgänge mit Verweis auf das jeweilige pdf-Symbol zum Herunterladen angezeigt.

The **Reports on Polar and Marine Research** (ISSN 1866-3192) are available as open access publications since 2008. A table of all volumes including the printed issues (ISSN 1618-3193, Vol. 377-568, from 2000 until 2008), as well as the earlier **Reports on Polar Research** (ISSN 0176-5027, Vol. 1-376, from 1981 until 2000) is provided by the electronic Publication Information Center **(ePIC)** of the Alfred Wegener Institute, Helmholtz Centre for Polar and Marine Research (AWI); see URL http://epic.awi.de. To generate a list of all Reports, use the URL http://epic.awi.de and select “browse”/ ”type” to browse ”Reports on Polar and Marine Research”. A chronological list in declining order will be presented, and pdf-icons displayed for downloading.

Zuletzt erschienene Ausgaben:

Recently published issues:

718 (2018) The Expedition PS111 of the Research Vessel POLARSTERN to the southern Weddell Sea in 2018, edited by Michael Schröder

717 (2018) The Expedition PS107 of the Research Vessel POLARSTERN to the Fram Strait and the AWI-HAUSGARTEN in 2017, edited by Ingo Schewe

716 (2018) Polar Systems under Pressure, 27th International Polar Conference, Rostock, 25 - 29 March 2018, German Society for Polar Research, edited by H. Kassens, D. Damaske, B. Diekmann, D. Fütterer, G. Heinemann, U. Karsten, E.M. Pfeiffer, J. Regnery, M. Scheinert, J. Thiede, R. Tiedemann & D. Wagner

715 (2018) The Expedition PS109 of the Research Vessel POLARSTERN to the Nordic Seas in 2017, edited by Torsten Kanzow

714 (2017) The Expedition SO258/2 of the Research Vessel SONNE to the central Indian Ocean in 2017, edited by Wolfram Geissler

713 (2017) The Expedition PS102 of the Research Vessel POLARSTERN to the Atlantic Ocean in 2016, edited by Karen Wiltshire, Eva-Maria Brodte, Annette Wilson and Peter Lemke

712 (2017) The Expedition PS104 of the Research Vessel POLARSTERN to the Amundsen Sea in 2017, edited by Karsten Gohl

711 (2017) Mid-Range forecasting of the German Waterways streamflow based on hydrologic, atmospheric and oceanic data by Monica Ionita

710 (2017) The Expedition PS103 of the Research Vessel POLARSTERN to the Weddell Sea in 2016/2017, edited by Olaf Boebel

709 (2017) Russian-German Cooperation: Expeditions to Siberia in 2016, edited by Pier Paul Overduin, Franziska Blender, Dmitry Y. Bolshiyanov, Mikhail N. Grigoriev, Anne Morgenstern, Hanno Meyer

708 (2017) The role of atmospheric circulation patterns on the variability of ice core constitutents in coastal Dronning Maud Land, Antarctica by Kerstin Schmidt

ALFRED-WEGENER-INSTITUT
HELMHOLTZ-ZENTRUM FÜR POLAR-
UND MEERESFORSCHUNG

BREMERHAVEN

Am Handelshafen 12
27570 Bremerhaven
Telefon 0471 4831-0
Telefax 0471 4831-1149
www.awi.de

HELMHOLTZ
GEMEINSCHAFT